Allgemeine Relativitätstheorie mit dem Computer

PC-POOL RAUM 01.120
JOHANN WOLFGANG GOETHE UNIVERSITÄT
26. JUNI, 2020

Aufgrund der Corona Krise findet die Vorlesung und die freiwilligen Übungstermine in diesem Semester nur Online statt.

MATTHIAS HANAUSKE

FRANKFURT INSTITUTE FOR ADVANCED STUDIES
JOHANN WOLFGANG GOETHE UNIVERSITÄT
INSTITUT FÜR THEORETISCHE PHYSIK
ARBEITSGRUPPE RELATIVISTISCHE ASTROPHYSIK
D-60438 FRANKFURT AM MAIN
GERMANY

9. Vorlesung

Grundlagen der Allgemeinen Relativitätstheorie

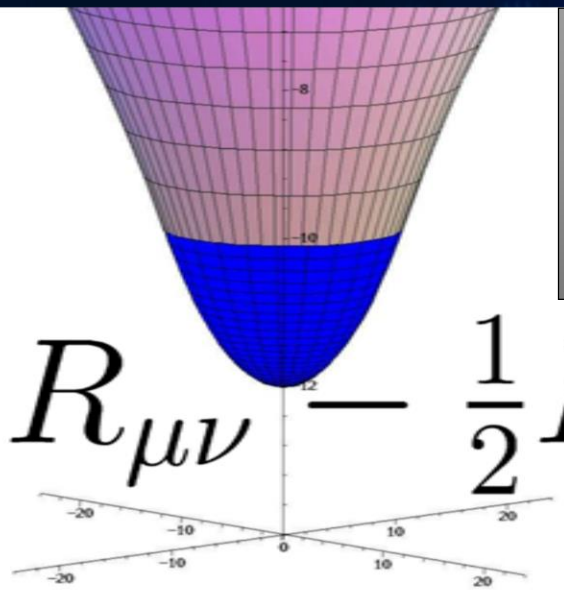

Vor etwa hundert Jahren (1915) stellte Albert Einstein seine „Allgemeine Relativitätstheorie“ (ART) der Öffentlichkeit vor.

$$R_{\mu\nu} - \frac{1}{2} R\, g_{\mu\nu} = \frac{8\pi G}{c^4} T_{\mu\nu}$$

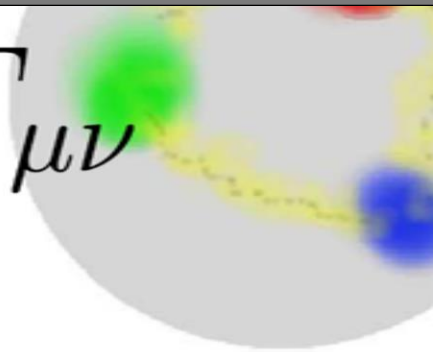

Die ART ist eine sehr revolutionäre Theorie. Sie besagt, dass jegliche Energieformen (z.B. Masse eines Körpers) die „Raumzeit“ verbiegen und durch diese Krümmung des Raumes und der Zeit die Gravitation (Schwerkraft) resultiert. -> Raumzeit-Krümmung = Energie

Teil III
Computersimulationen mit dem Einstein-Toolkit

In diesem Teil wird ein Einblick in die allgemeinrelativistische Simulation auf Supercomputern gegeben. Unter Zuhilfenahme des Einstein-Toolkits werden unterschiedliche, realistische Systeme betrachtet (z.B. Neutronenstern-Kollisionen mit Aussendung von Gravitationswellen)

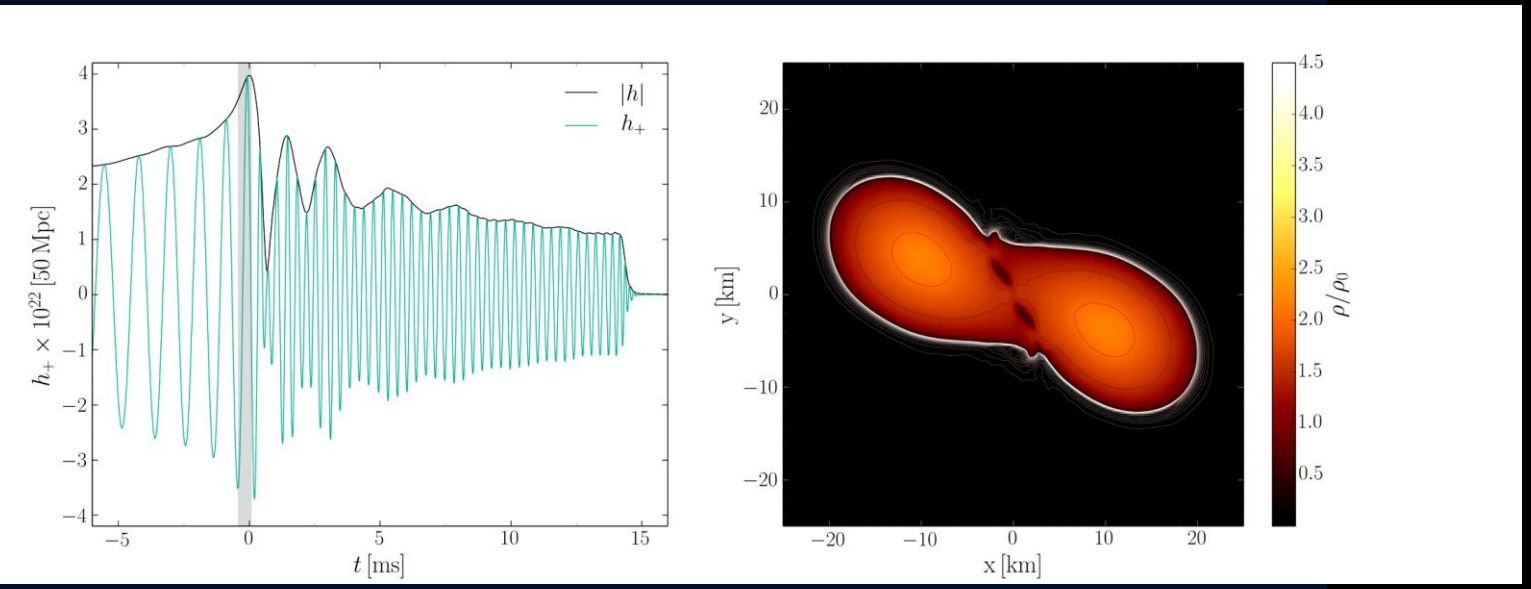

Broadbrush picture

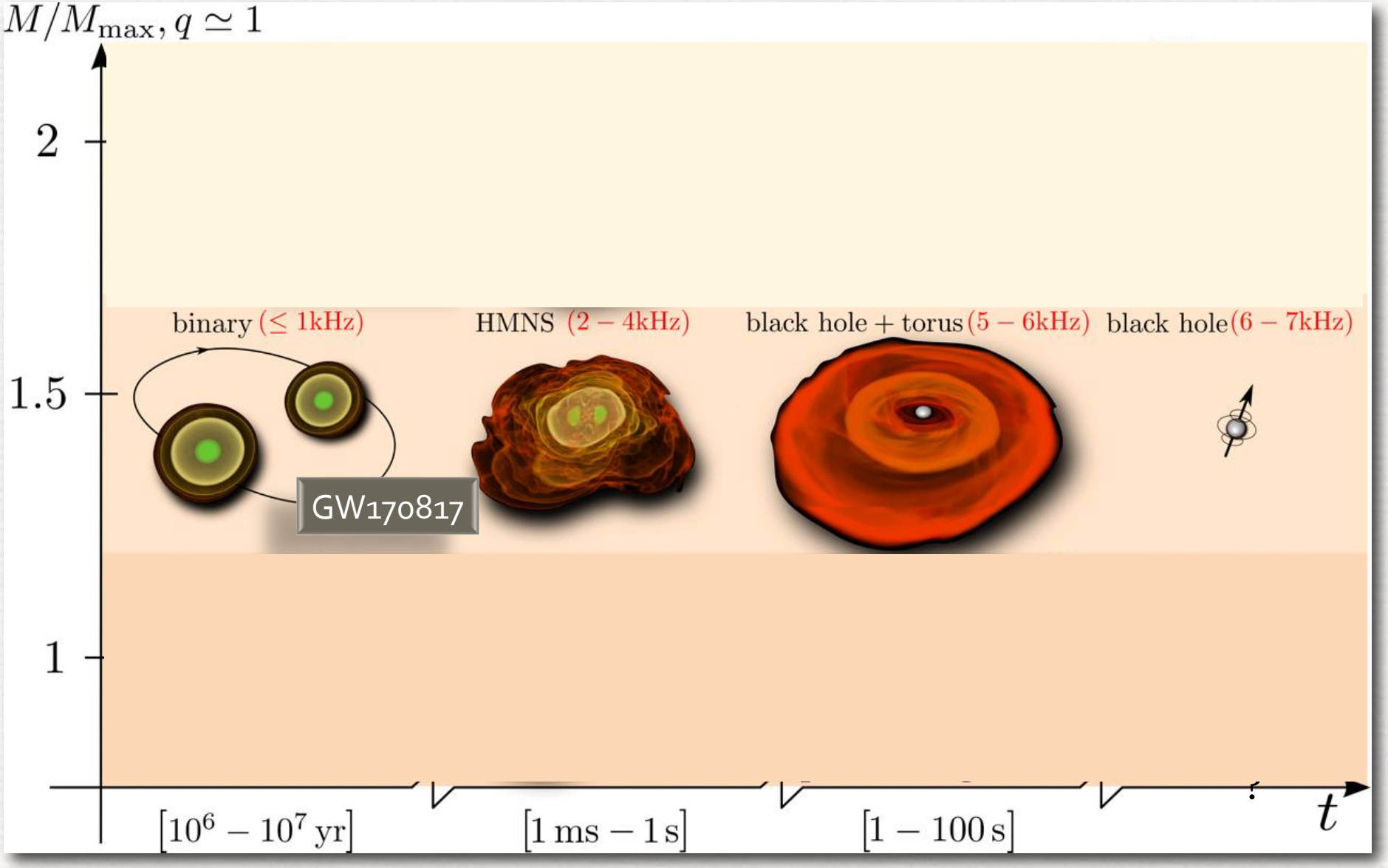

The Einstein Equation and the EOS of Compact Stars

ART	Yang-Mills-Theories
$D_\beta v^\alpha = \partial_\beta v^\alpha + \Gamma^\alpha_{\sigma\beta} v^\sigma$	$D_{\beta a}{}^b = \partial_\beta 1_a{}^b + ig A_{\beta a}{}^b$
$R^\delta{}_{\mu\alpha\beta} v^\mu = [D_\alpha, D_\beta] v^\delta$	$F_{\alpha\beta a}{}^b = \frac{1}{ig}\left[D_{\alpha a}{}^c, D_{\beta c}{}^b\right]$
$R^\delta{}_{\mu\alpha\beta} = \Gamma^\delta_{\mu\alpha\|\beta} - \Gamma^\delta_{\mu\beta\|\alpha}$	$= A_{\beta a}{}^b{}_{\|\alpha} - A_{\alpha a}{}^b{}_{\|\beta}$
$+\Gamma^\delta_{\nu\beta}\Gamma^\nu_{\mu\alpha} + \Gamma^\delta_{\nu\alpha}\Gamma^\nu_{\mu\beta}$	$+\frac{1}{ig}\left[A_{\alpha a}{}^c, A_{\beta c}{}^b\right]$
$\mathcal{L}_G = R + \underbrace{(c_1 R_{\mu\nu}R^{\mu\nu} + \ldots)}_{\equiv 0 \text{ for ART}}$	$\mathcal{L}_{YM} = \frac{1}{4} F_{\mu\nu a}{}^b F^{\mu\nu}{}_a{}^b$

QuantumCromoDynamic:

$(SU(3)_{(c)}$- Color Yang-Mills-Gauge Theory)

$$D_{\beta A}{}^B = \partial_\beta 1_A{}^B + ig G_{\beta A}{}^B$$

$_A{}^B$ =red, green, blue

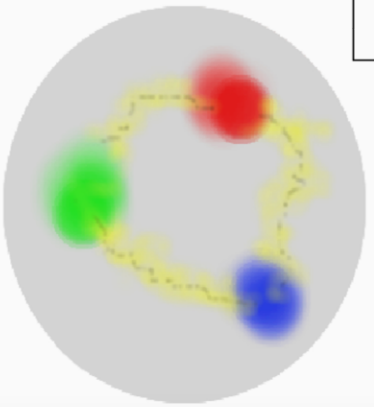

$$\psi^f_A = \begin{pmatrix} \psi^f_r \\ \psi^f_g \\ \psi^f_b \end{pmatrix}$$

Confinement

chiral symmetry, ...

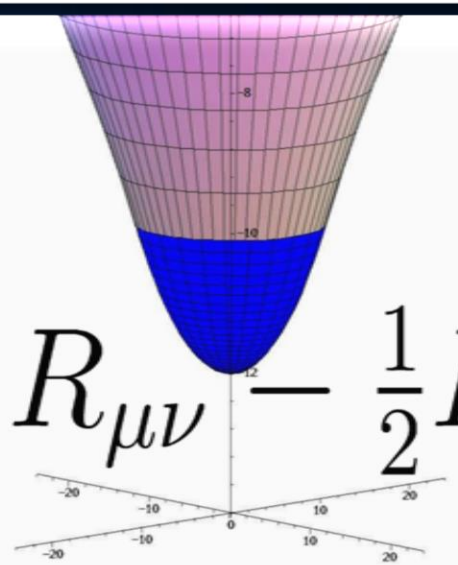

$$R_{\mu\nu} - \frac{1}{2} R\, g_{\mu\nu} = \frac{8\pi G}{c^4} T_{\mu\nu}$$

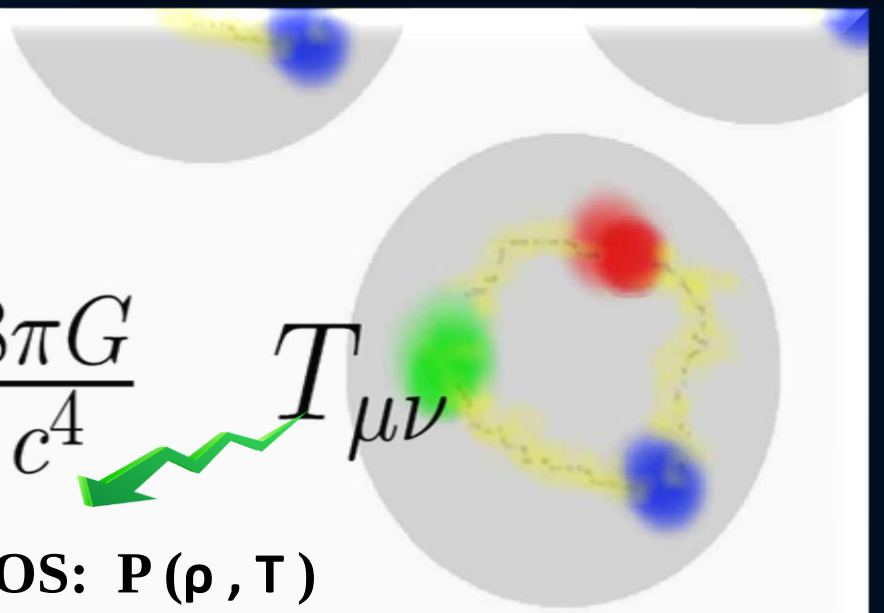

EOS: P(ρ, T)

The Hadron-Quark Phase Transition

The QCD Phase Diagram

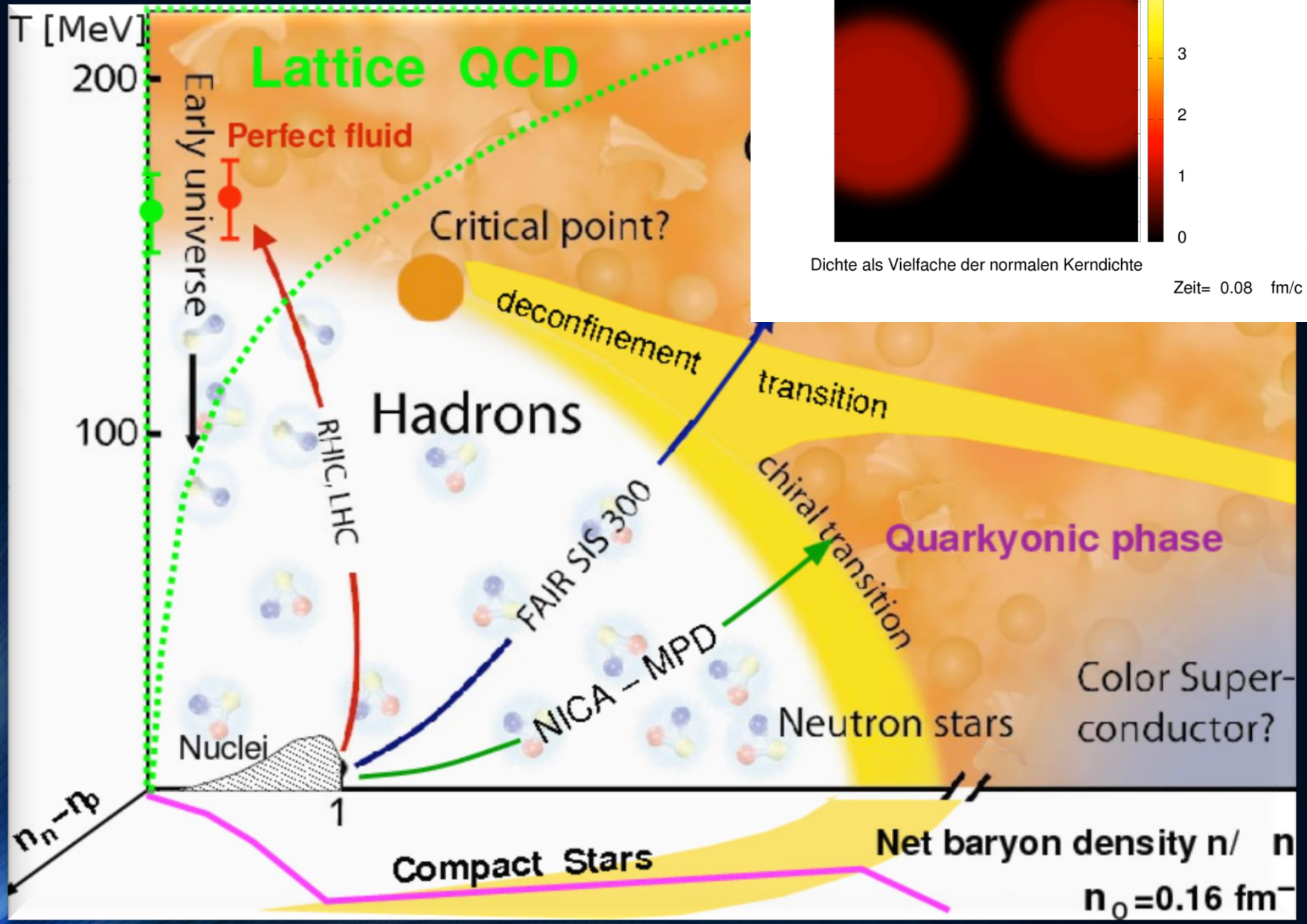

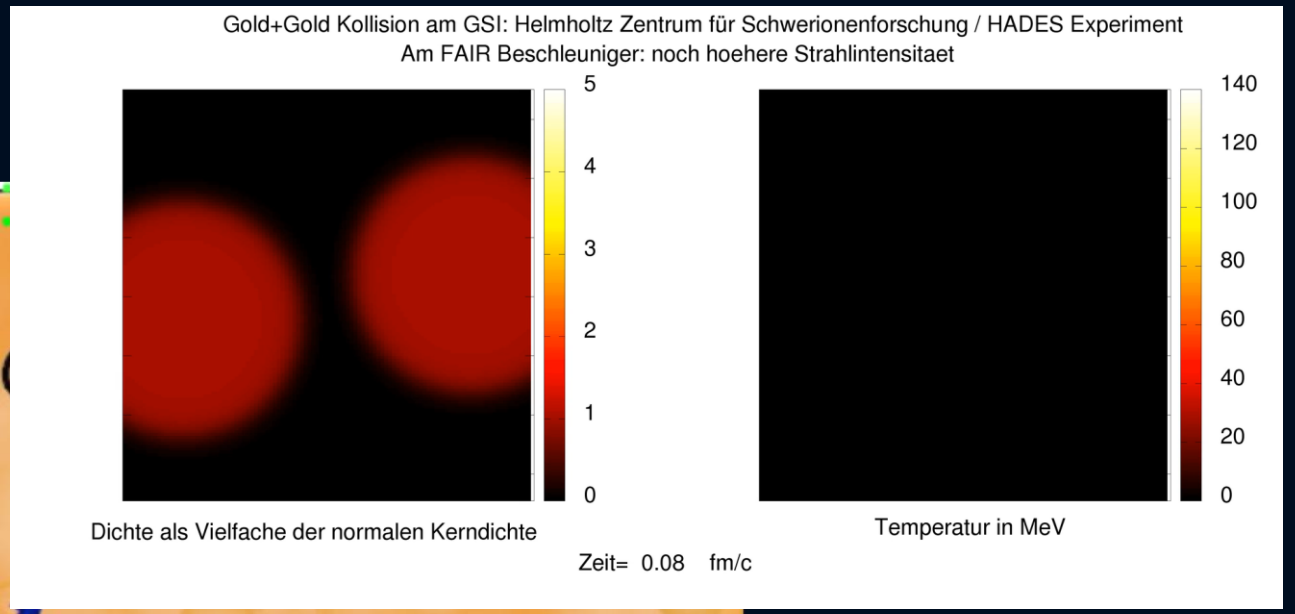

Credits:
Jan Steinheimer

Neutron Proton

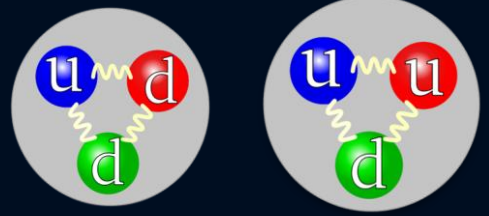

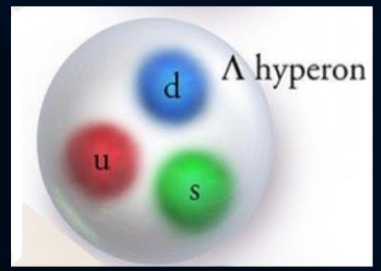

The QCD – Phase Transition and the Interior of a Hybrid Star

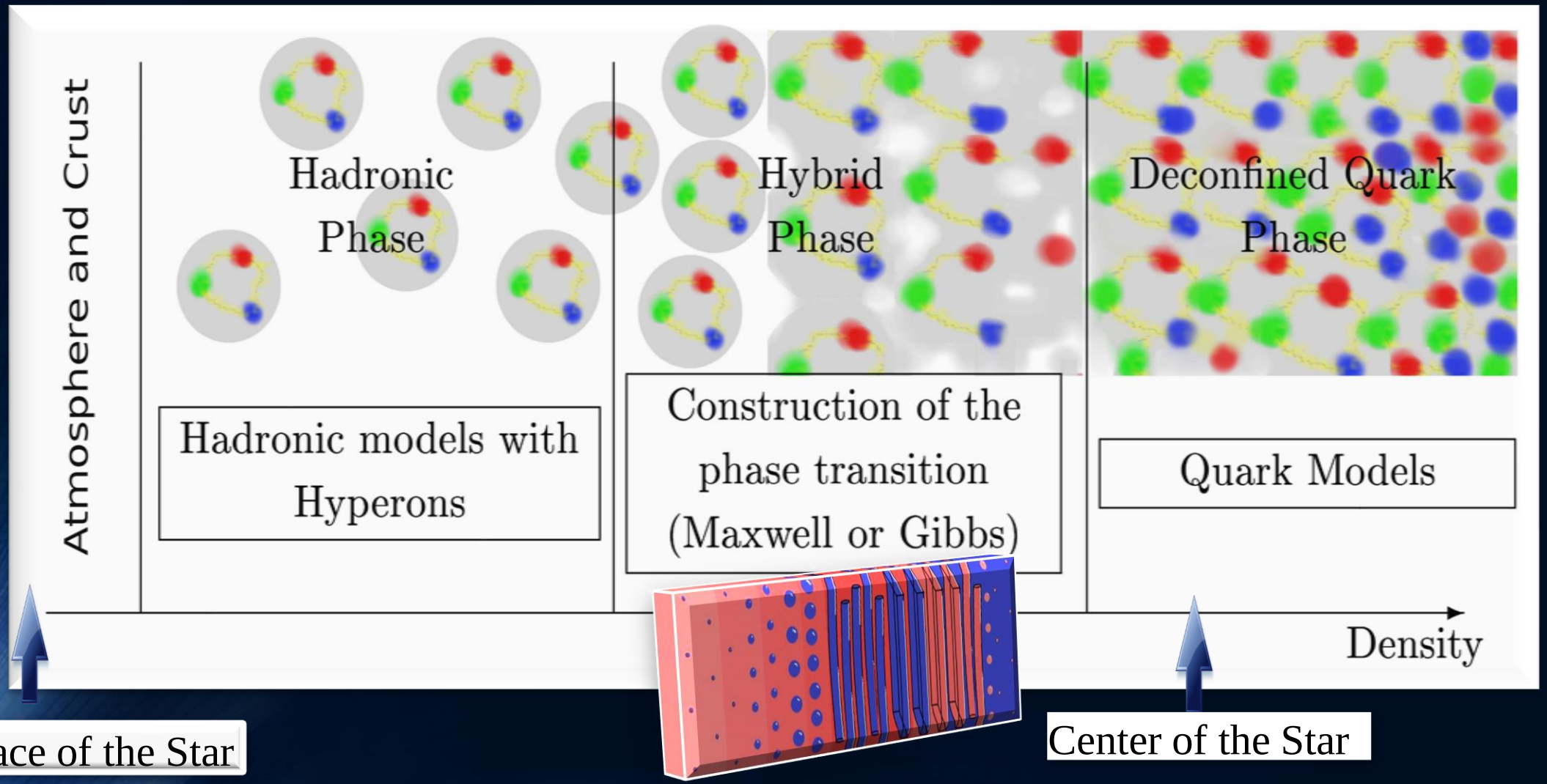

Matthias Hanauske; Doctoral Thesis:
Properties of Compact Stars within QCD-motivated Models; University Library Publication Frankfurt (2004)

The Gibbs Construction

Hadronic and quark surface:

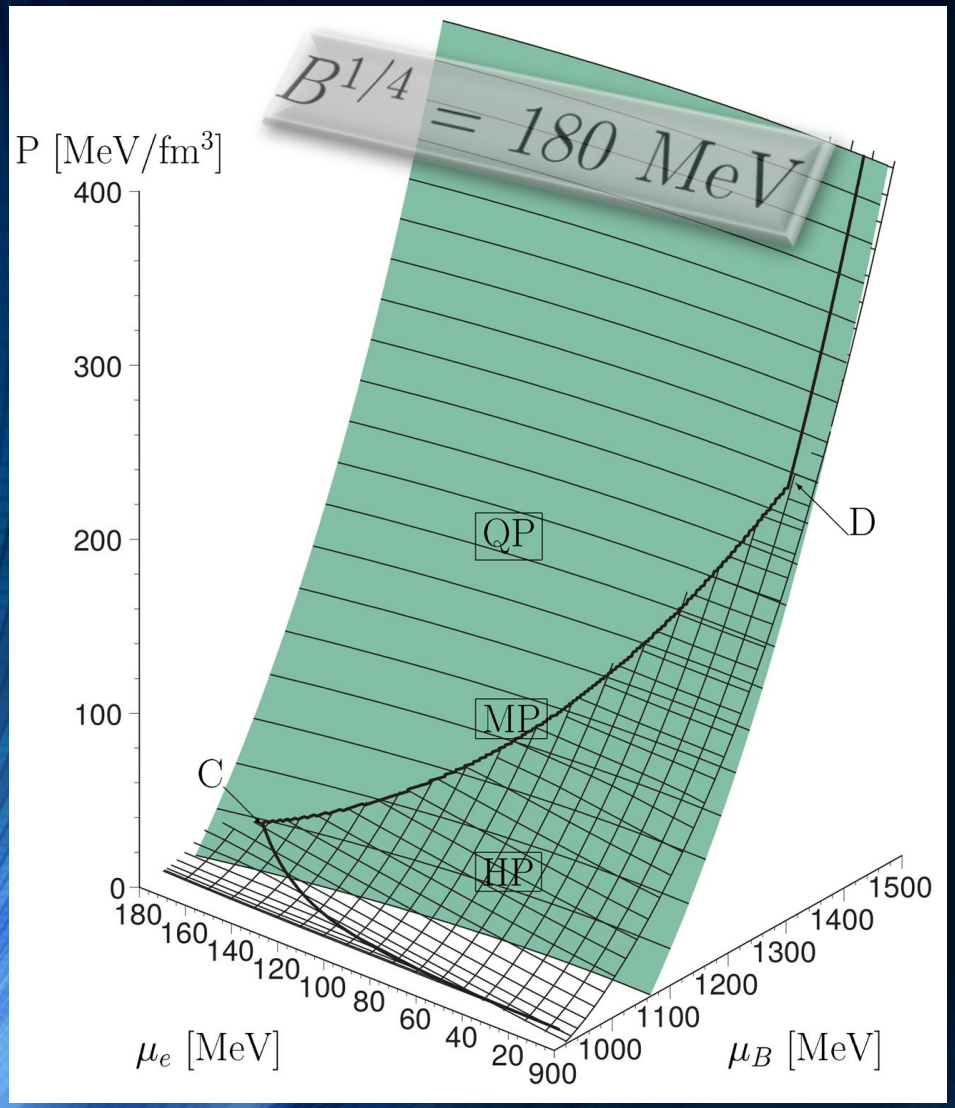

Charge neutrality condition is only globally realized

$$\rho_e := (1-\chi)\,\rho_e^H(\mu_B,\mu_e) + \chi\,\rho_e^Q(\mu_B,\mu_e) = 0\,.$$

The pressure in the mixed phase depends on two independent chemical potentials

$$\begin{aligned} P^H(\mu_B,\mu_e) &= P^Q(\mu_B,\mu_e)\,, \\ \mu_B = \mu_B^H &= \mu_B^Q\,, \\ \mu_e = \mu_e^H &= \mu_e^Q \end{aligned}$$

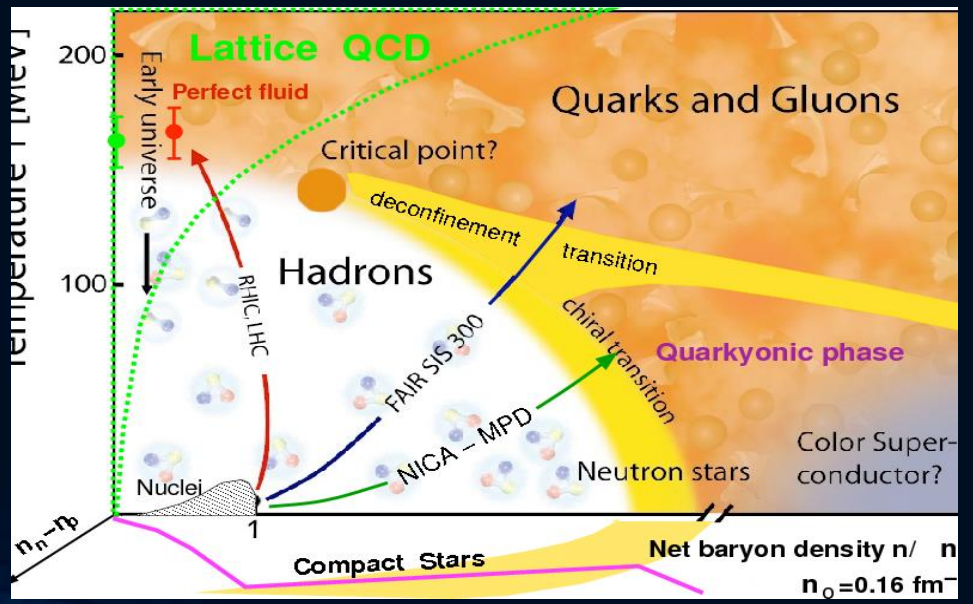

The Gibbs Construction

Hadronic and quark surface:

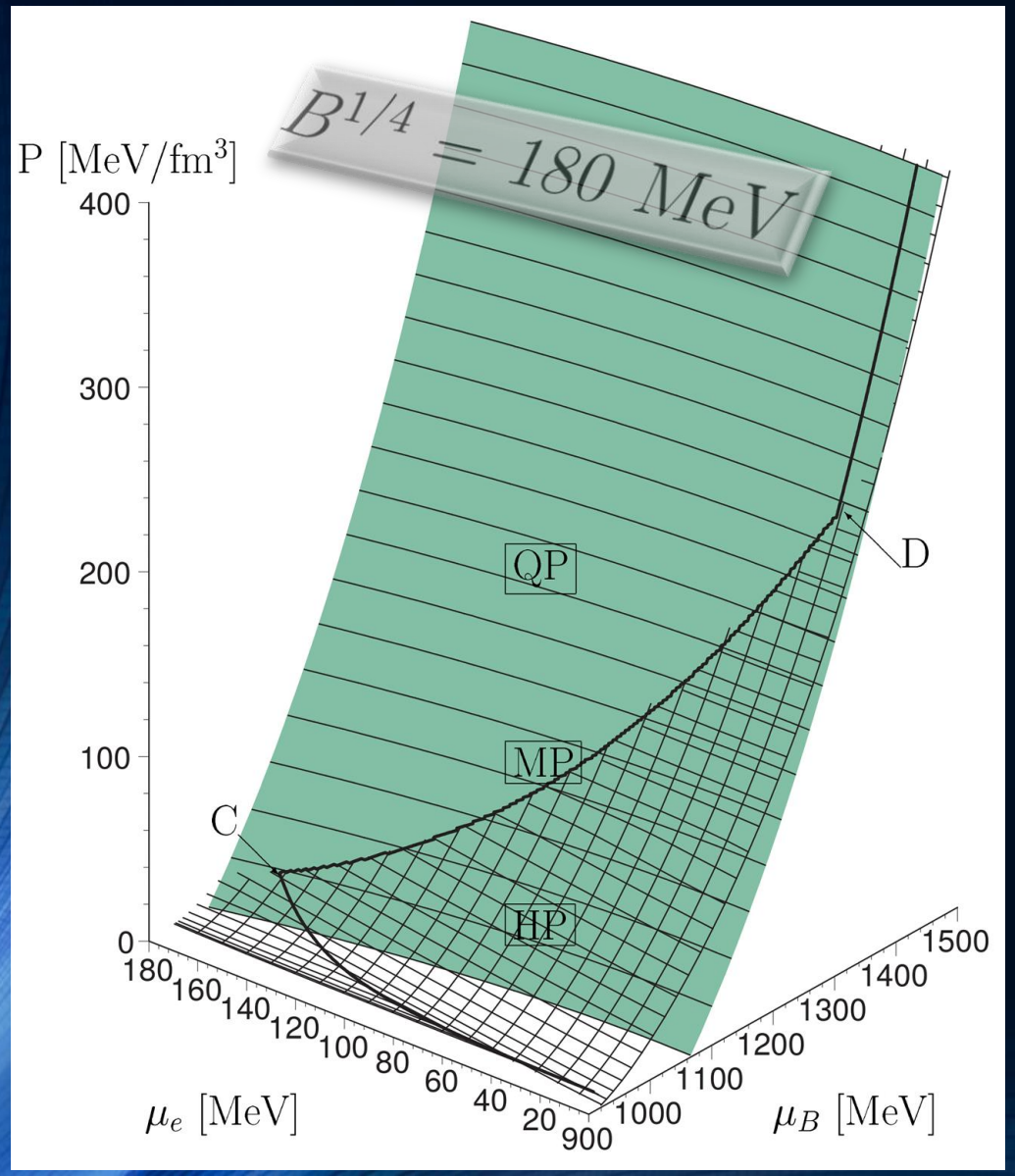

Charge neutrality condition is only globally realized

$$\rho_e := (1-\chi)\,\rho_e^H(\mu_B,\mu_e) + \chi\,\rho_e^Q(\mu_B,\mu_e) = 0\,.$$

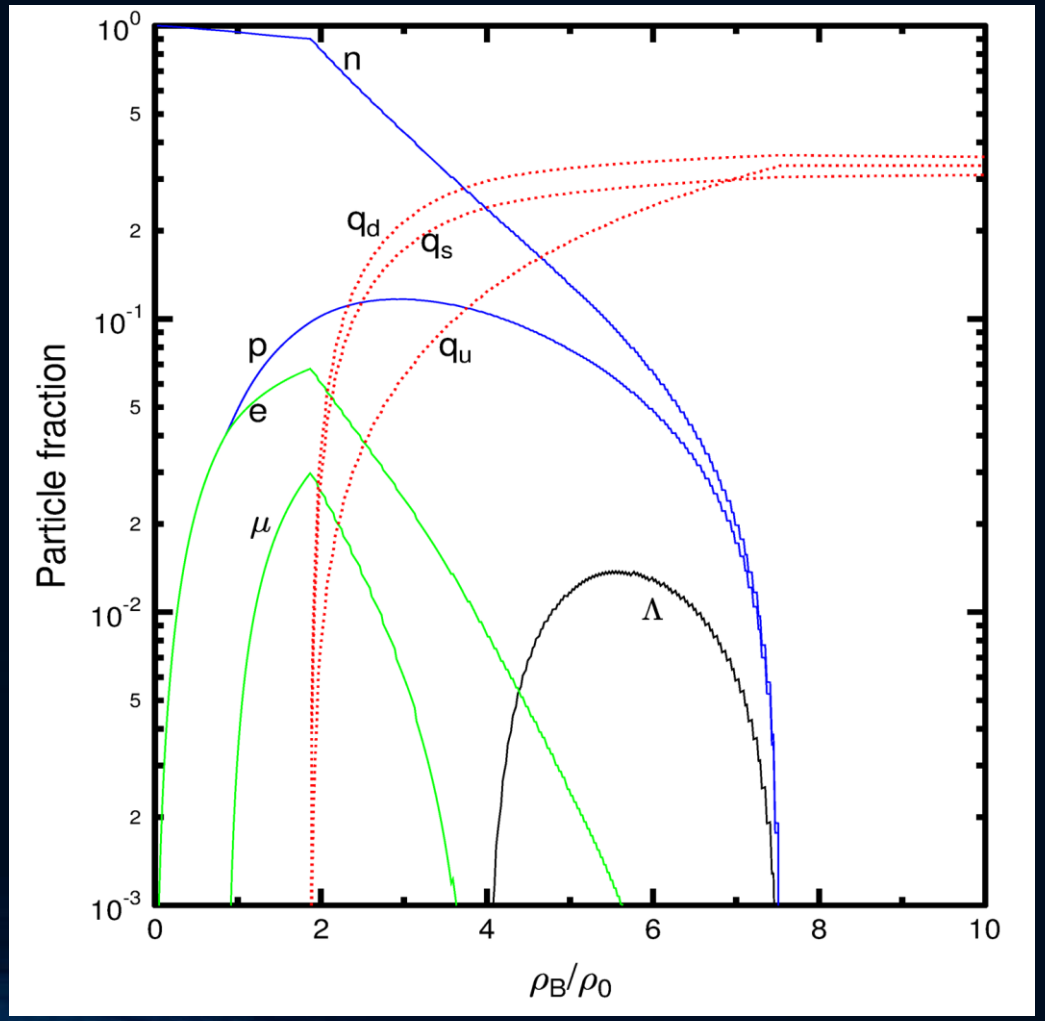

The Gibbs Construction

Hadronic and quark surface:

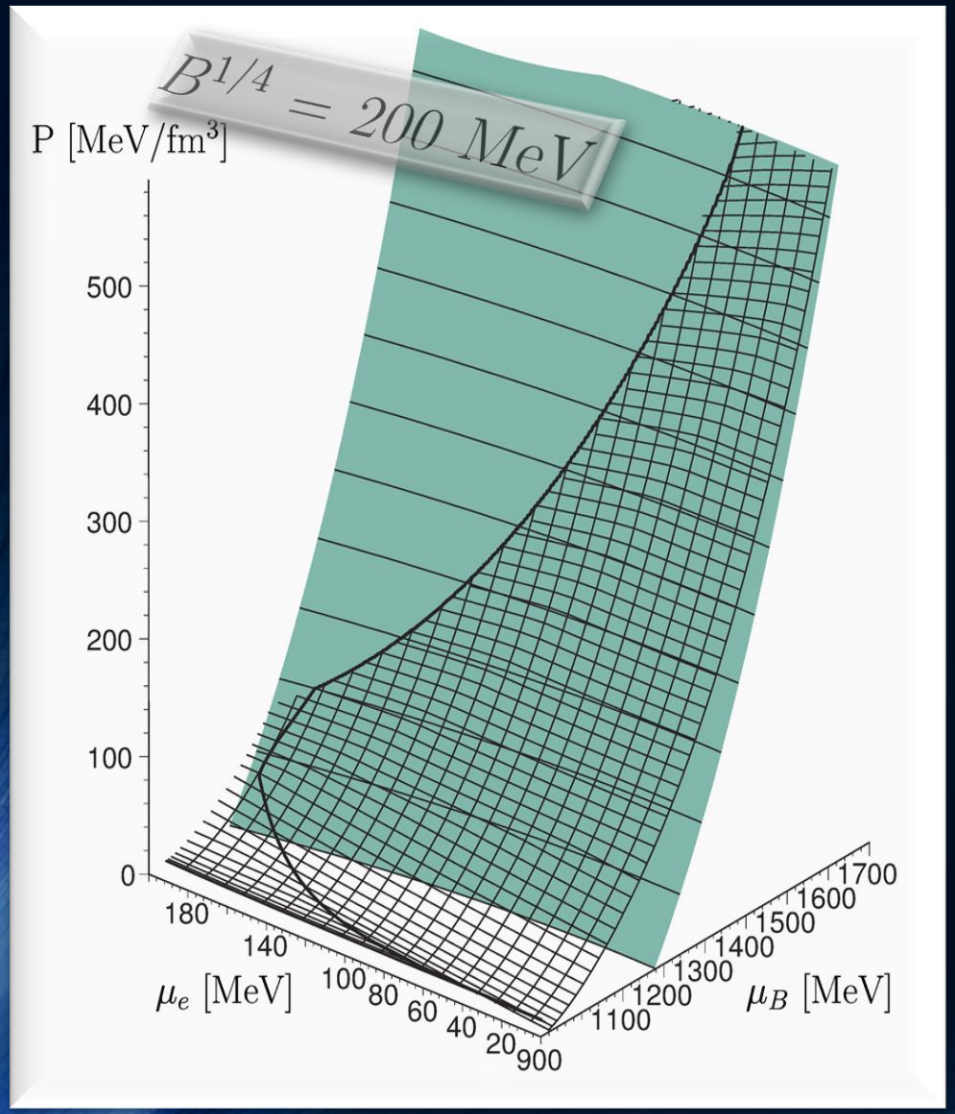

Particle composition:

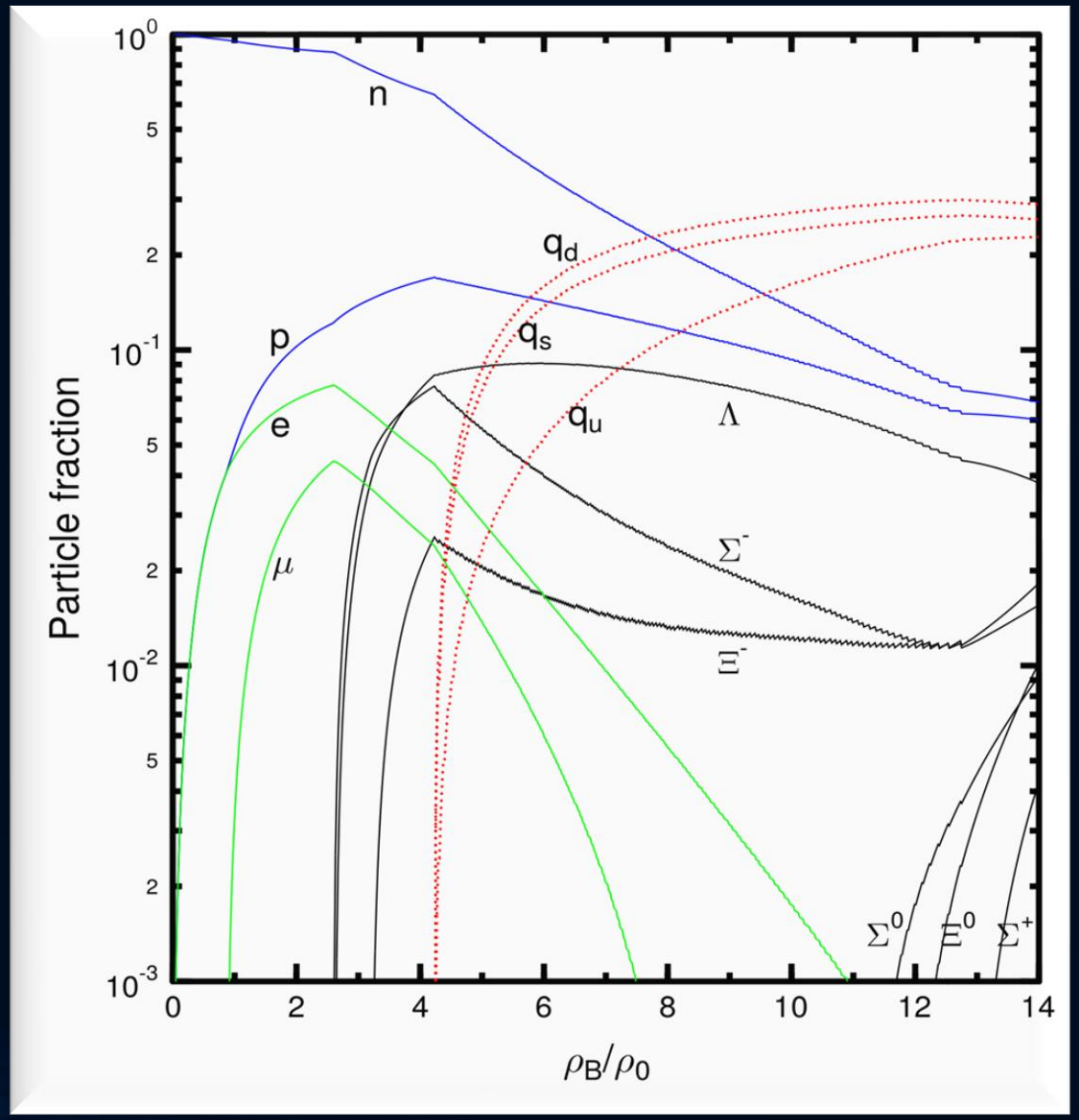

M. Hanauske, Dissertation, "Properties of Compact Stars within QCD-motivated Models"

Neutron Stars, Hybrid Stars, Quark Stars and Black Holes

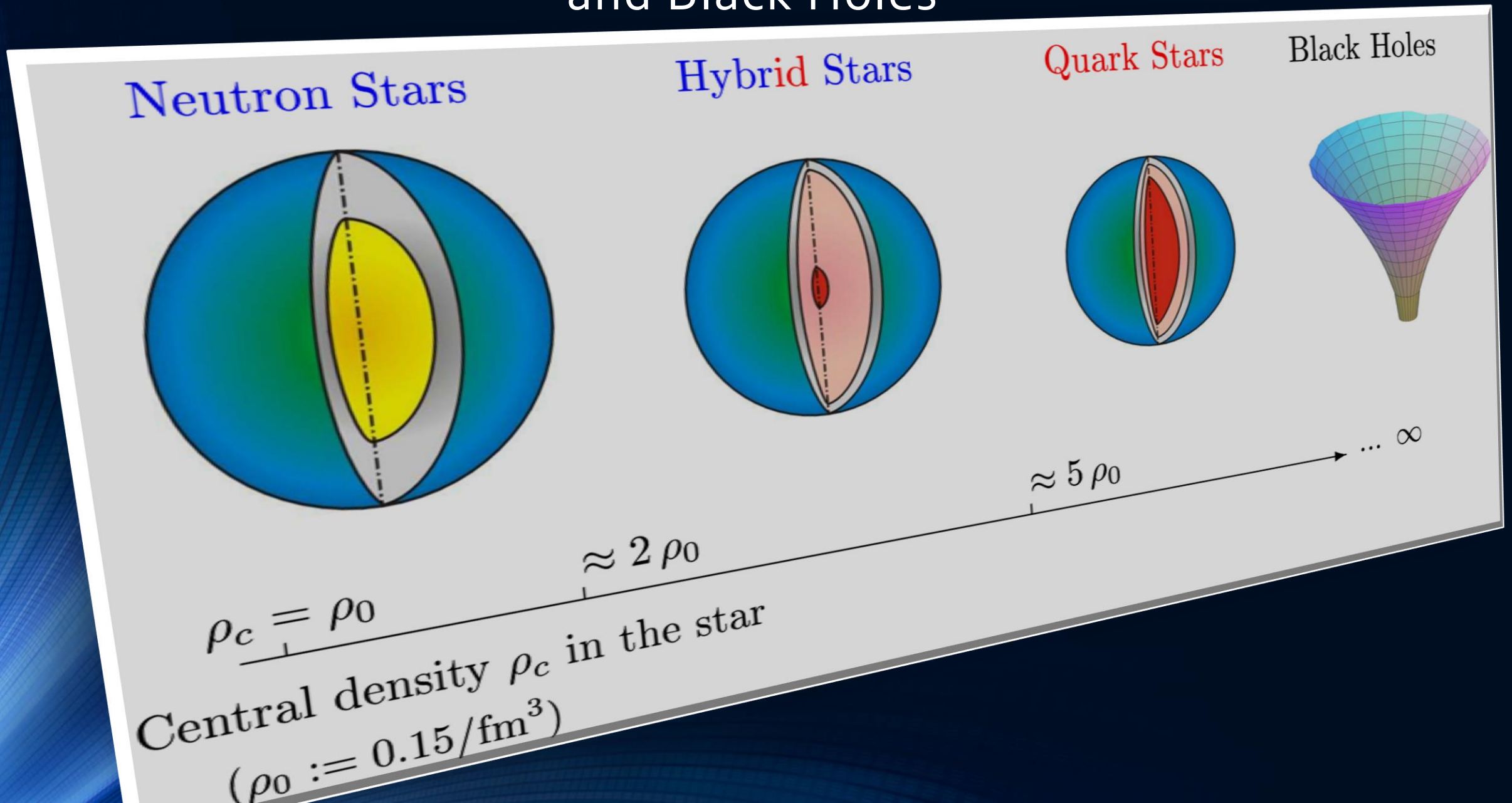

Constraining the Equation of State by Multimessenger Gravitational Wave Astronomy

DPG Meeting 2002 (17 years ago !)

Über die Möglichkeit mittels Gravitationswellen-Detektion etwas über die starke Wechselwirkung zu lernen

Matthias Hanauske, Walter Greiner und Horst Stöcker

1. Einführung
   - ART ⇔ QCD
   - Confinement
   - Quark-Gluon-Plasma
2. Kompakte Sterne
   - Theoretische Vorhersagen
   - Beobachtbare Größen
3. Emission von Gravitationswellen
   - In welchen Systemen können die von kompakten Sternen emittierten Gravitationswellen von den Eigenschaften der QCD abhängen

ART ⇔ QCD

ART	Yang-Mills-Theorien
$D_\beta v^\alpha = \partial_\beta v^\alpha + \Gamma^\alpha_{\sigma\beta} v^\sigma$	$D_{\beta a}{}^b = \partial_\beta 1_a{}^b + ig A_{\beta a}{}^b$
$R^\delta{}_{\mu\alpha\beta} v^\mu = [D_\alpha, D_\beta] v^\delta$	$F_{\alpha\beta a}{}^b = \frac{1}{ig}\left[D_{\alpha a}{}^c, D_{\beta c}{}^b\right]$
$R^\delta{}_{\mu\alpha\beta} = \Gamma^\delta_{\mu\alpha\|\beta} - \Gamma^\delta_{\mu\beta\|\alpha}$	$= A_{\beta a}{}^b{}_{\|\alpha} - A_{\alpha a}{}^b{}_{\|\beta}$
$+\Gamma^\delta_{\nu\beta}\Gamma^\nu_{\mu\alpha} + \Gamma^\delta_{\nu\alpha}\Gamma^\nu_{\mu\beta}$	$+\frac{1}{ig}\left[A_{\alpha a}{}^c, A_{\beta c}{}^b\right]$
$\mathcal{L}_G = R + \underbrace{(c_1 R_{\mu\nu}R^{\mu\nu} + ...)}_{\equiv 0 \text{ for ART}}$	$\mathcal{L}_{YM} = \frac{1}{4} F_{\mu\nu a}{}^b F^{\mu\nu}{}_a{}^b$

QuantenCromoDynamik:
$(SU(3)_{(c)}$ Yang-Mills-Theorie der Farbe)

$$D_{\beta A}{}^B = \partial_\beta 1_A{}^B + ig G_{\beta A}{}^B$$

${}_A{}^B$ =rot, grün, blau

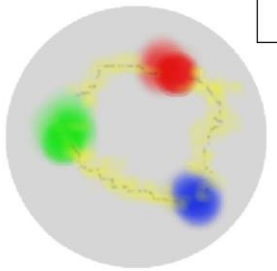

$$\psi^f_A = \begin{pmatrix} \psi^f_r \\ \psi^f_g \\ \psi^f_b \end{pmatrix}$$

Confinement
chirale Symmetrie, ...

Entstehung und Beobachtungsmöglichkeiten von kompakten Sternen

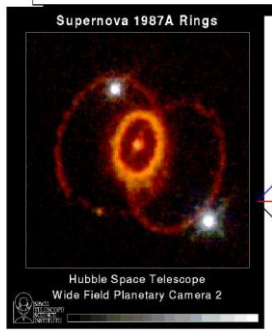

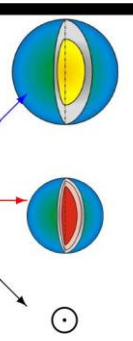

- Neutronen Stern
- Quark- oder Hyperstern
- Schwarzes Loch

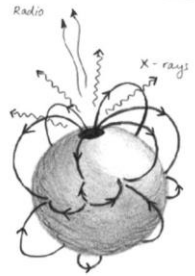

- Radiowellen Teleskope(ca. 1400)
- Optische Teleskope (3)
- Röntgen Detektoren (ca. 30)
- Gravitationswellen Detektoren

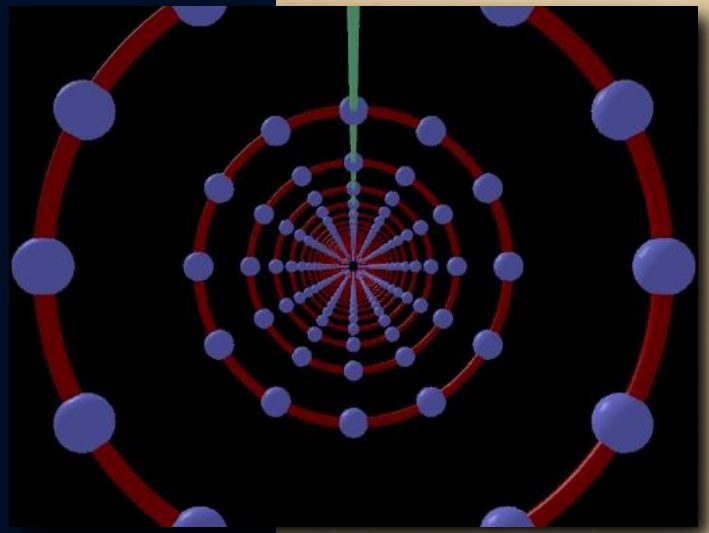

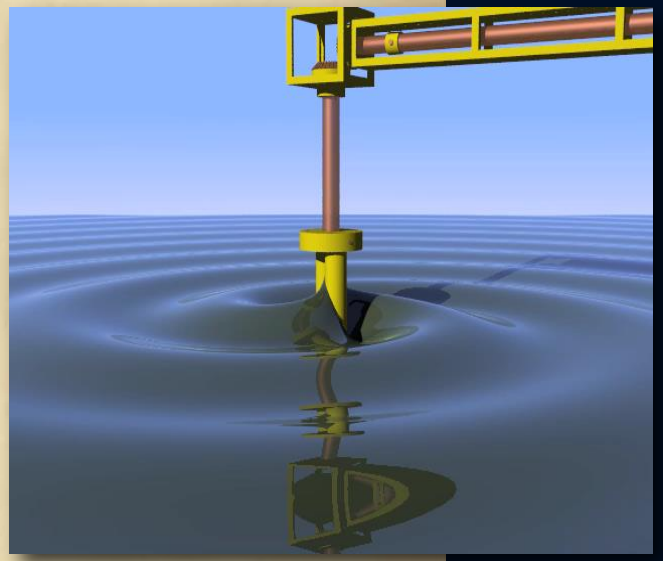

Über Gravitationswellen.

Von A. Einstein.

(Vorgelegt am 31. Januar 1918 [s. oben S. 79].)

Die wichtige Frage, wie die Ausbreitung der Gravitationsfelder erfolgt, ist schon vor anderthalb Jahren in einer Akademiearbeit von mir behandelt worden[1]. Da aber meine damalige Darstellung des Gegenstandes nicht genügend durchsichtig und außerdem durch einen bedauerlichen Rechenfehler verunstaltet ist, muß ich hier nochmals auf die Angelegenheit zurückkommen.

Einsteins erste Arbeit über Gravitationswellen, Juni 1916, war leider falsch ...

Sitzungsberichte der Königlich-Preußischen Akademie der Wissenschaften

100 Jahre später LIGO:
LIGO: **Laser Interferometer Gravitational-Wave Observatory**

PRL **116,** 061102 (2016)

Selected for a Viewpoint in *Physics*
PHYSICAL REVIEW LETTERS

week ending
12 FEBRUARY 2016

Observation of Gravitational Waves from a Binary Black Hole Merger

B. P. Abbott *et al.*[*]
(LIGO Scientific Collaboration and Virgo Collaboration)
(Received 21 January 2016; published 11 February 2016)

On September 14, 2015 at 09:50:45 UTC the two detectors of the Laser Interferometer Gravitational-Wave Observatory simultaneously observed a transient gravitational-wave signal. The signal sweeps upwards in frequency from 35 to 250 Hz with a peak gravitational-wave strain of 1.0×10^{-21}. It matches the waveform predicted by general relativity for the inspiral and merger of a pair of black holes and the ringdown of the resulting single black hole. The signal was observed with a matched-filter signal-to-noise ratio of 24 and a false alarm rate estimated to be less than 1 event per 203 000 years, equivalent to a significance greater than 5.1σ. The source lies at a luminosity distance of 410^{+160}_{-180} Mpc corresponding to a redshift $z = 0.09^{+0.03}_{-0.04}$. In the source frame, the initial black hole masses are $36^{+5}_{-4} M_\odot$ and $29^{+4}_{-4} M_\odot$, and the final black hole mass is $62^{+4}_{-4} M_\odot$, with $3.0^{+0.5}_{-0.5} M_\odot c^2$ radiated in gravitational waves. All uncertainties define 90% credible intervals. These observations demonstrate the existence of binary stellar-mass black hole systems. This is the first direct detection of gravitational waves and the first observation of a binary black hole merger.

1. Direkter Nachweis von Gravitationswellen
Signalform: Verschmelzung von zwei **schwarzen** Löchern

Gravitationswellen gefunden: LIGO!!!

Kollision zweier Schwarzer Löcher GW150914

Massen: 36 & 29 Sonnenmassen

Abstand zur Erde 410 Mpc (1.34 Milliarden Lichtjahre)

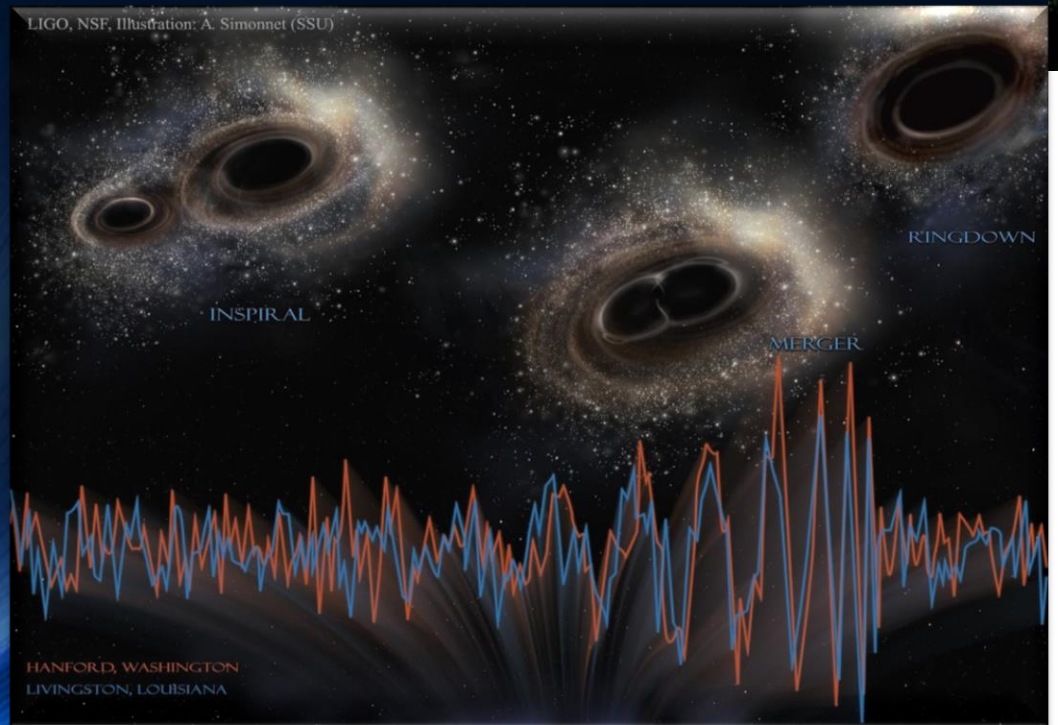

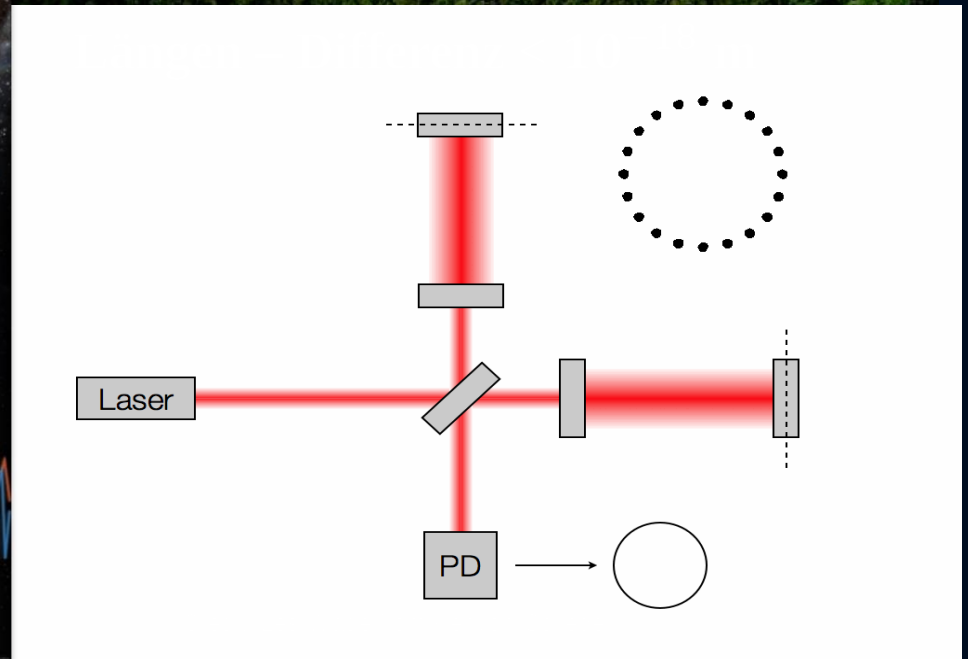

Gravitationswellen von Neutronenstern Kollisionen

Neutronenstern Kollision (Simulation)

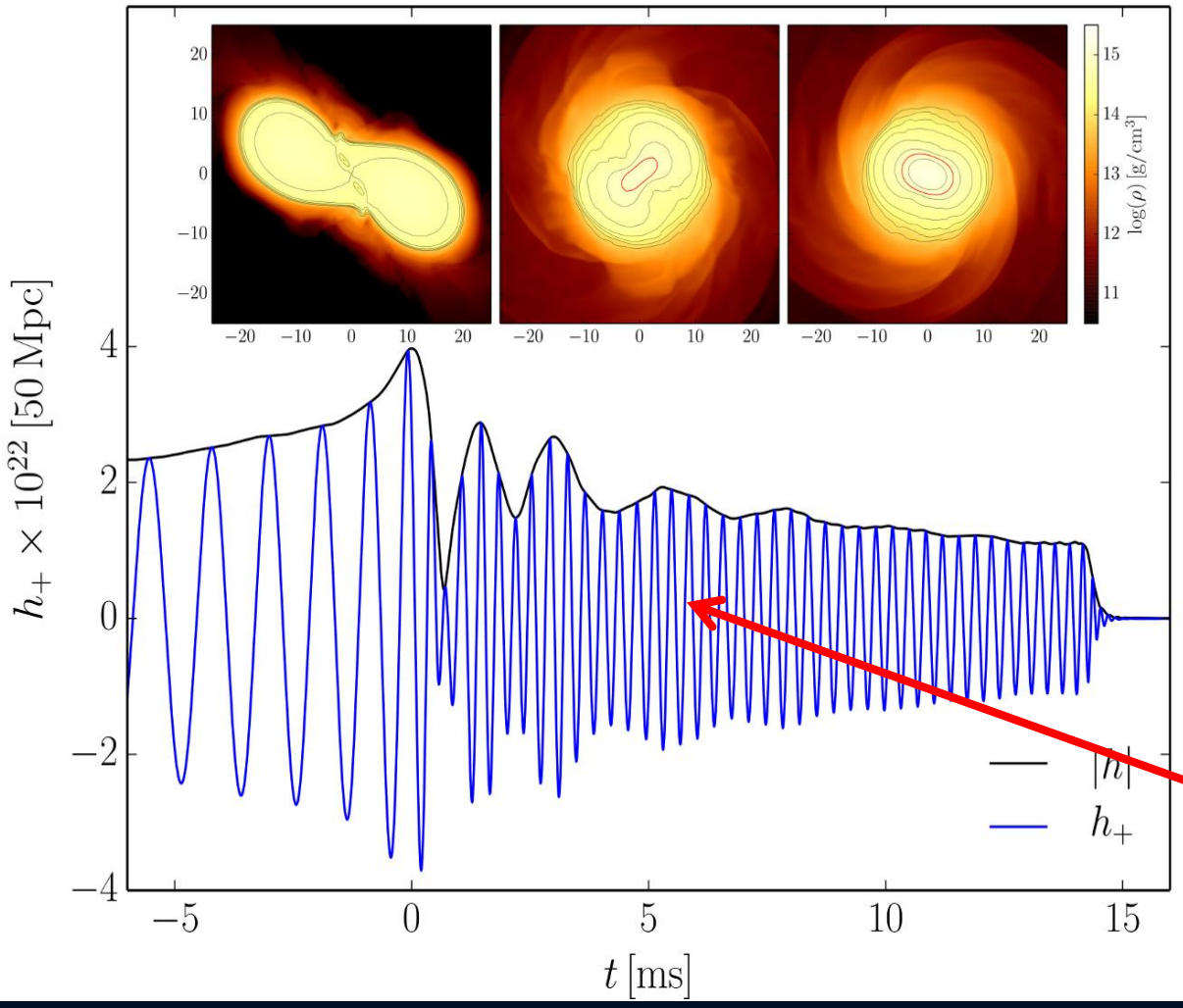

Kollision zweier schwarzer Löcher

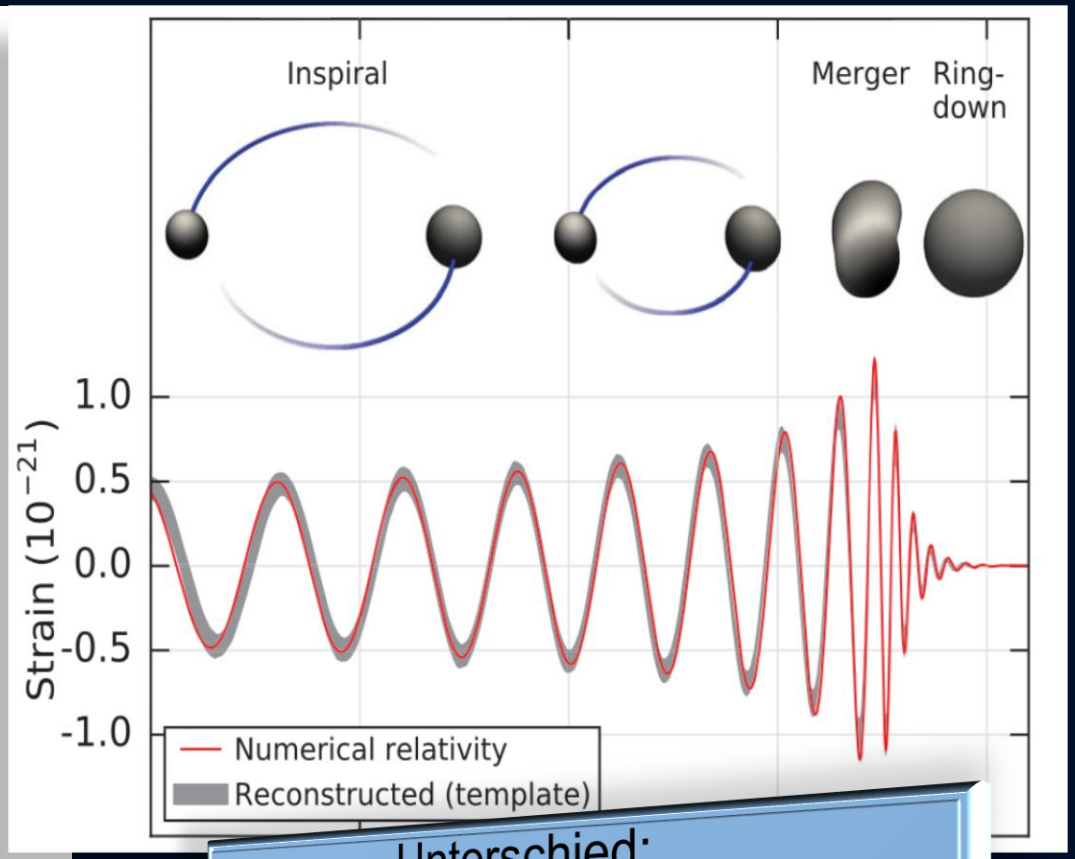

Unterschied:
Bei Neutronenstern Kollisionen gibt es meistens eine ***Post-Kollisionsphase***

Allgemeine Relativitätstheorie einfach dargestellt

14. Mai 2018: Vortrag in der Denkbar
www.denkbar-frankfurt.de

Allgemeine Relativitätstheorie
Einsteins schönster Geniestreich auf dem Prüfstand

Als Albert Einstein im Jahre 1915 die Allgemeine Relativitätstheorie (ART) an der Königlich Preußischen Akademie der Wissenschaften vorstellte, glaubten noch wenige Physiker an seine neue, revolutionäre Theorie. Die ART besagt, dass die Ursache der Gravitationskraft in einer Verformung der raumzeitlichen Struktur begründet ist und heutzutage bezeichnen viele Physiker Einsteins mathematisch elegant formulierte Idee als "die schönste Gleichung der Physik". Während einer Sonnenfinsternis im Jahre 1919 gelang es die Ablenkung von Licht in der gekrümmten Raumzeit der Sonnenumgebung zu beobachten und Einstein wurde schlagartig berühmt. Weitere Vorhersagen der ART konnten in den folgenden Jahrzehnten überprüft und bestätigt werden, wobei eine der grundlegenden Folgerungen der ART, die Existenz von Raumzeit-Wellen (Gravitationswellen), lange Zeit nicht direkt nachgewiesen werden konnte. Schließlich, im Jahre 2015 konnte die erste Raumzeit-Welle mittels zweier hochempfindlicher Gravitationswellendetektoren nachgewiesen werden und im Jahre 2017 wurde diese Sensation mit dem Nobelpreis für Physik geehrt. Die grundlegenden Konzepte und Folgerungen der ART sollen in diesem Vortrag in allgemeinverständlicher, unterhaltsamer Weise illustriert werden. So werden z.B. die einzelnen Phasen einer Gravitationswellen erzeugende Neutronensterne-Kollision anhand eines Sammelsuriums einzelner Gesellschaftstänze veranschaulicht und die Eigenschaften von schwarzen Löchern mittels des Reichstagsgebäudes illustriert.

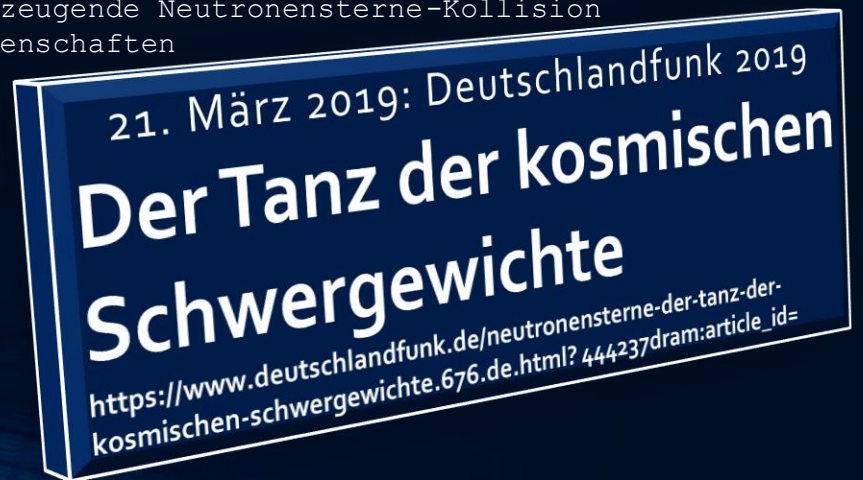

Pulsars

Rotating Neutronstars with large Magnetic Fields

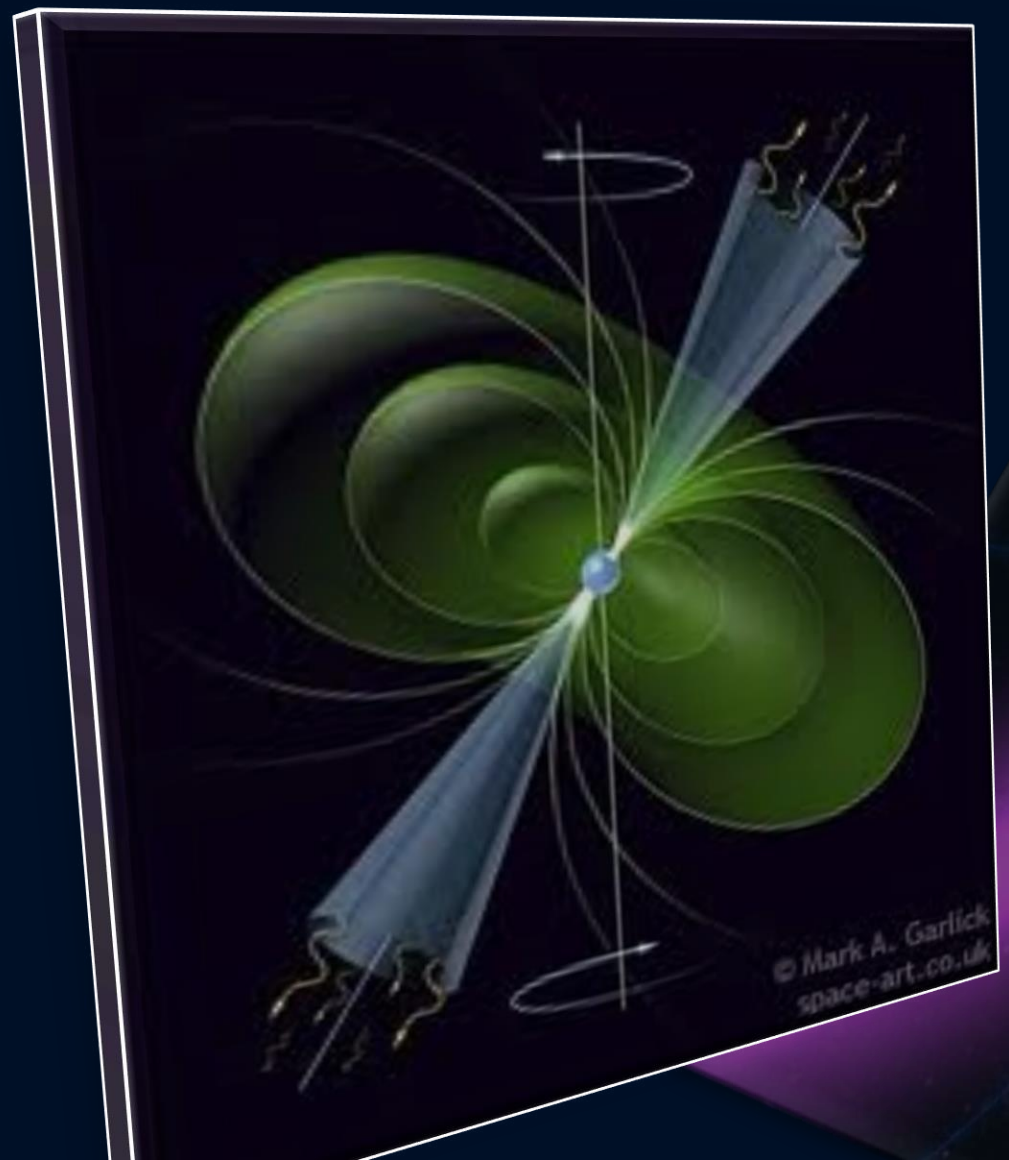

Binary Neutron Star Systems

Kramer, Wex, Class. Quantum Grav. 2009

The **Double Pulsar** (PSR J0737-3039A/B):
Observed in 2003
Eccentricity: 0.088
Pulsar A: P=23 ms, M=1.3381(7)
Pulsar B: P=2.7 s, M=1.2489(7)
Only separated 800,000 km from each other
Orbital period: 147 Minuten
Pulsar A is eclipsed by Pulsar B
(30 s for each orbit)

Distance shrinks
due to Gravitational Wave emission
→ They will collide in 85 Million Years!

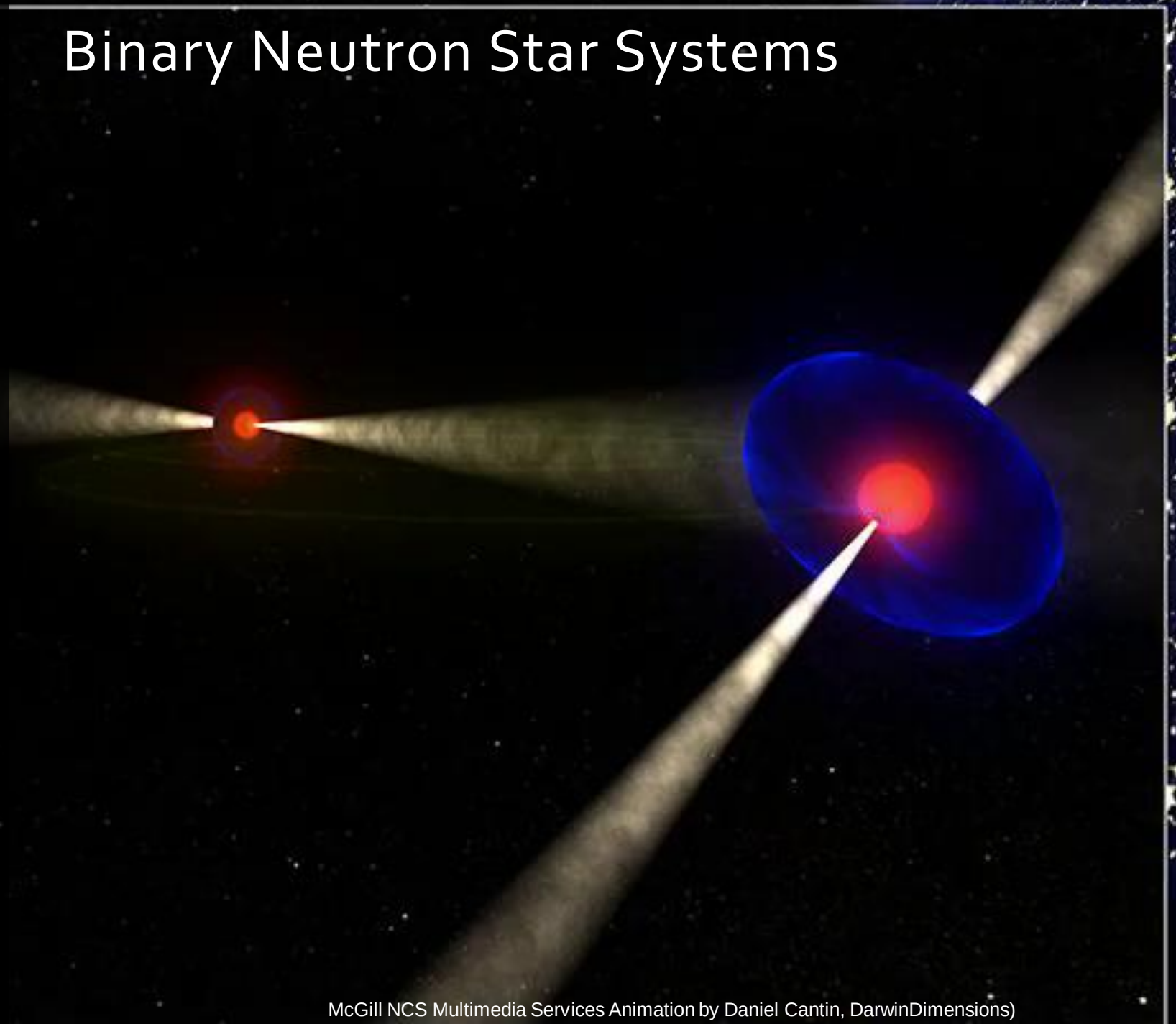

McGill NCS Multimedia Services Animation by Daniel Cantin, DarwinDimensions)

The different Phases of a Binary Compact Star Merger Event

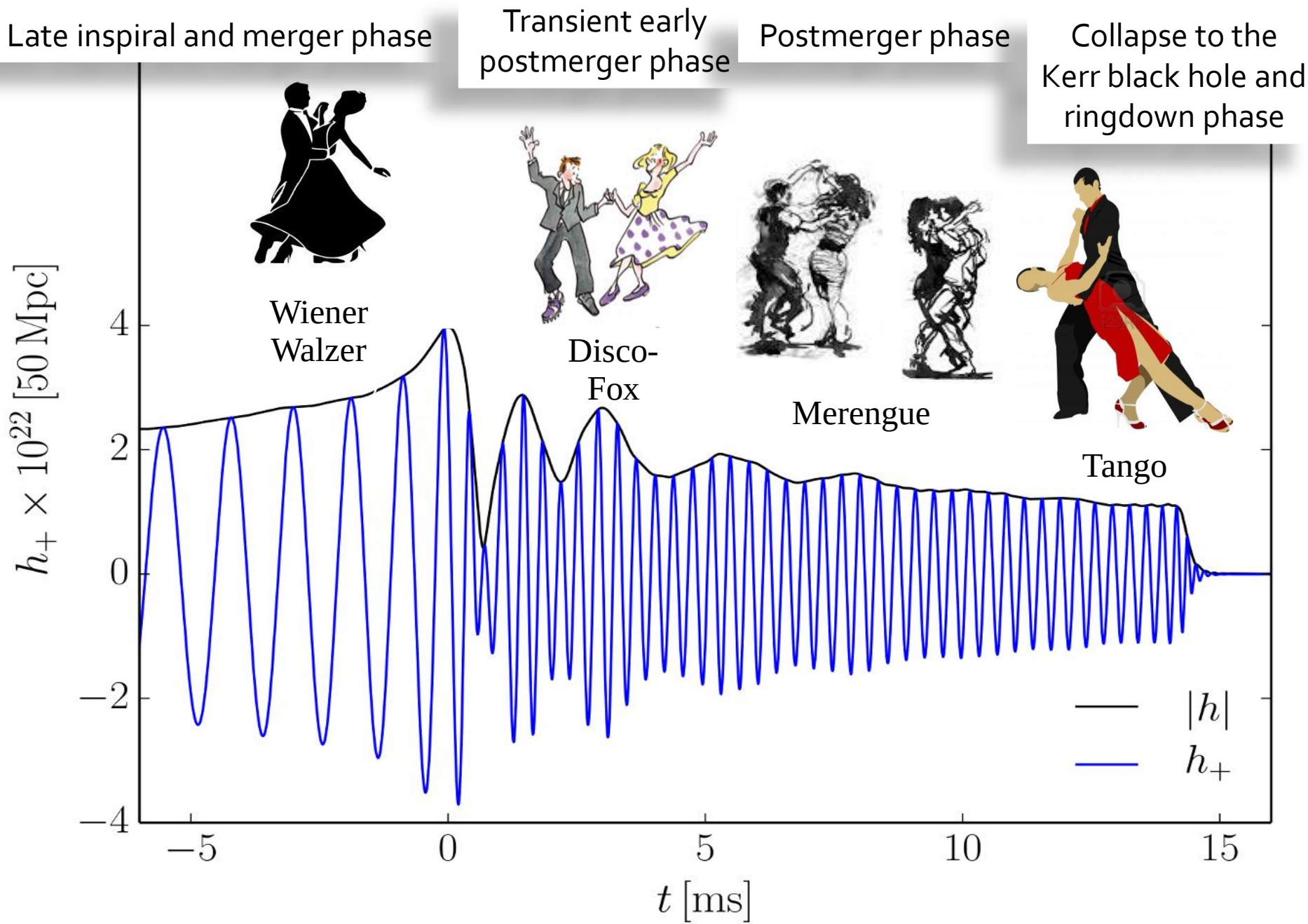

Raumzeit-Diagramm eines schwarzen Loches

Sichtweise ruhender Beobachter im Unendlichen

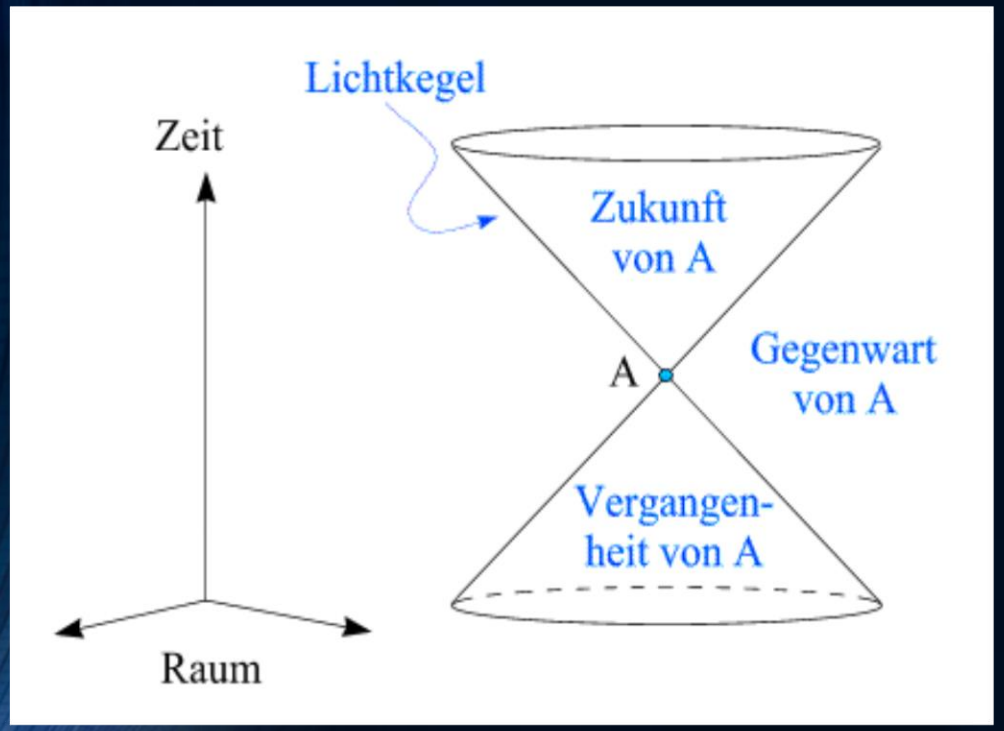

Raumzeit-Struktur
im flachen Raum

Ereignis-
horizont

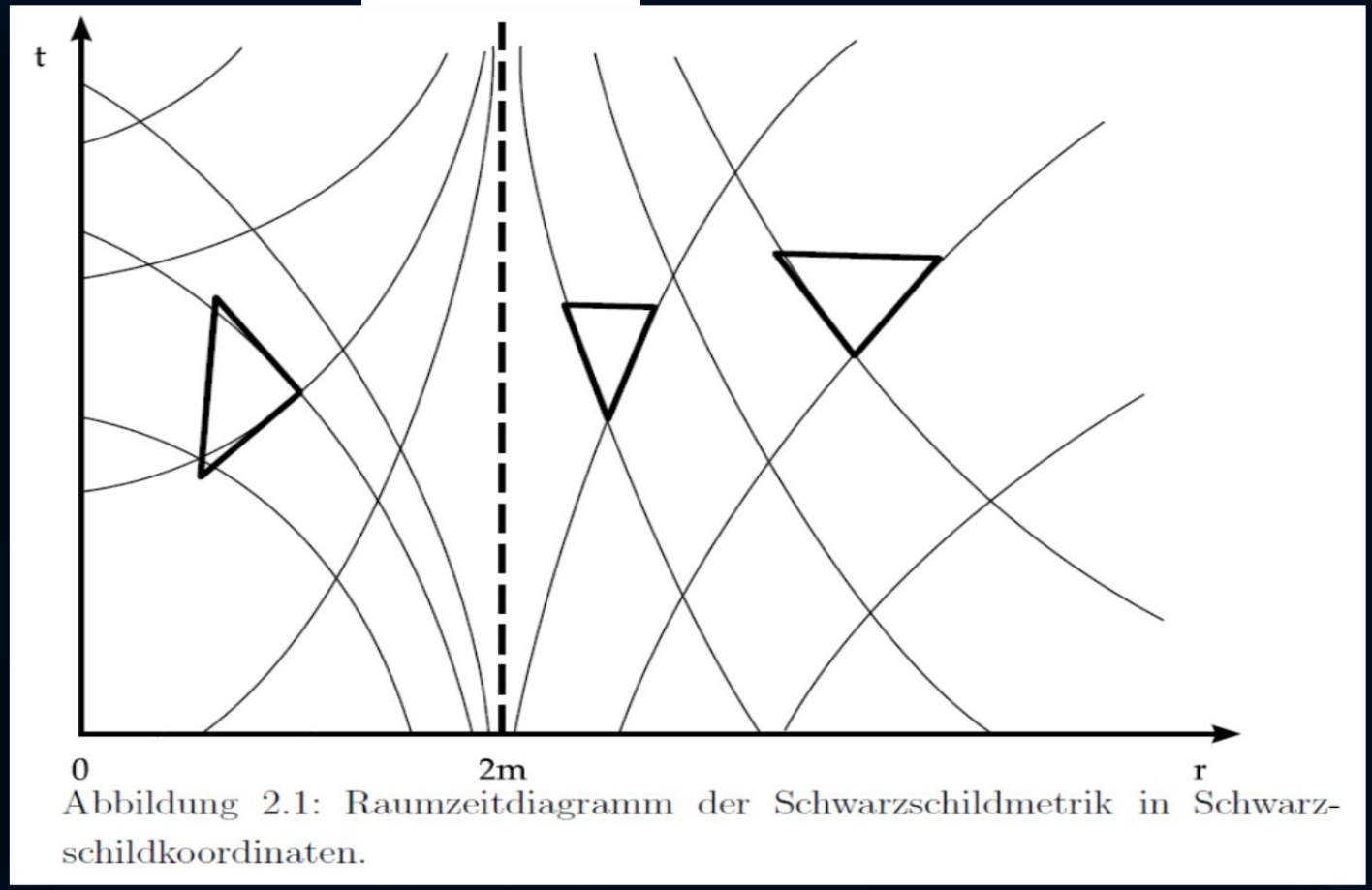

Abbildung 2.1: Raumzeitdiagramm der Schwarzschildmetrik in Schwarzschildkoordinaten.

Raumzeit-Struktur um ein schwarzes Loch

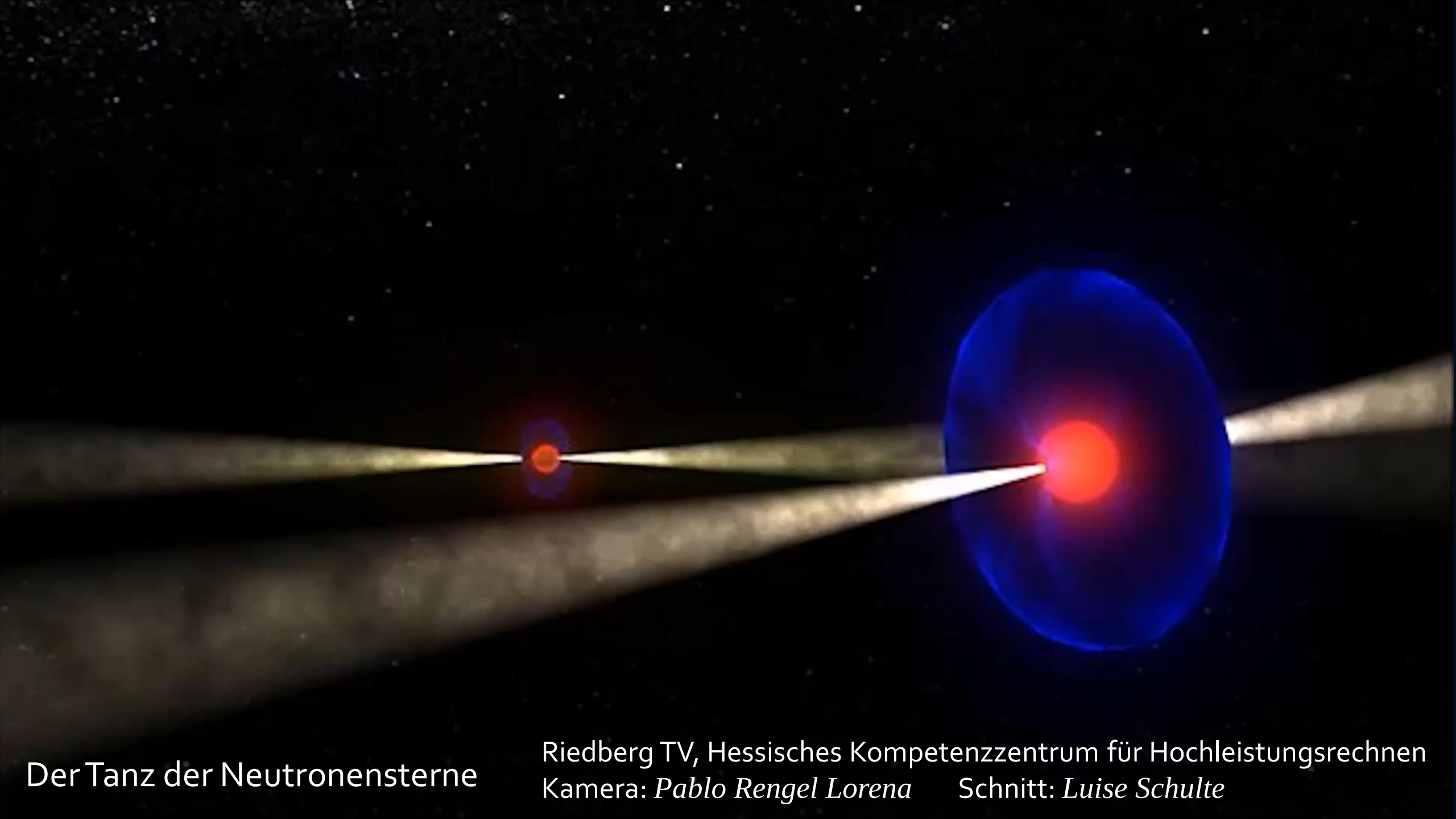

Der Tanz der Neutronensterne

Riedberg TV, Hessisches Kompetenzzentrum für Hochleistungsrechnen
Kamera: *Pablo Rengel Lorena* Schnitt: *Luise Schulte*

Postmerger gravitational-wave signatures of phase transitions in binary compact star mergers

- Introduction
- Numerical general relativity of compact star mergers
- The equation of state of compact star matter and the hadron-quark phase transition
- **The different phases of a binary compact star merger event**
- Gravitational-wave signatures of the hadron-quark phase transition in binary compact star mergers
  - The inspiral and merger phase (premerger signals)
  - Hypermassive hybrid stars (HMHS) within the prompt phase transition scenario (PPT)
  - HMHS within the delayed phase transition scenario (DPT)
  - HMHS within the phase transition triggered collapse scenario (PTTC)
- Summary and Outlook

The different Phases during the Postmergerphase of the HMNS

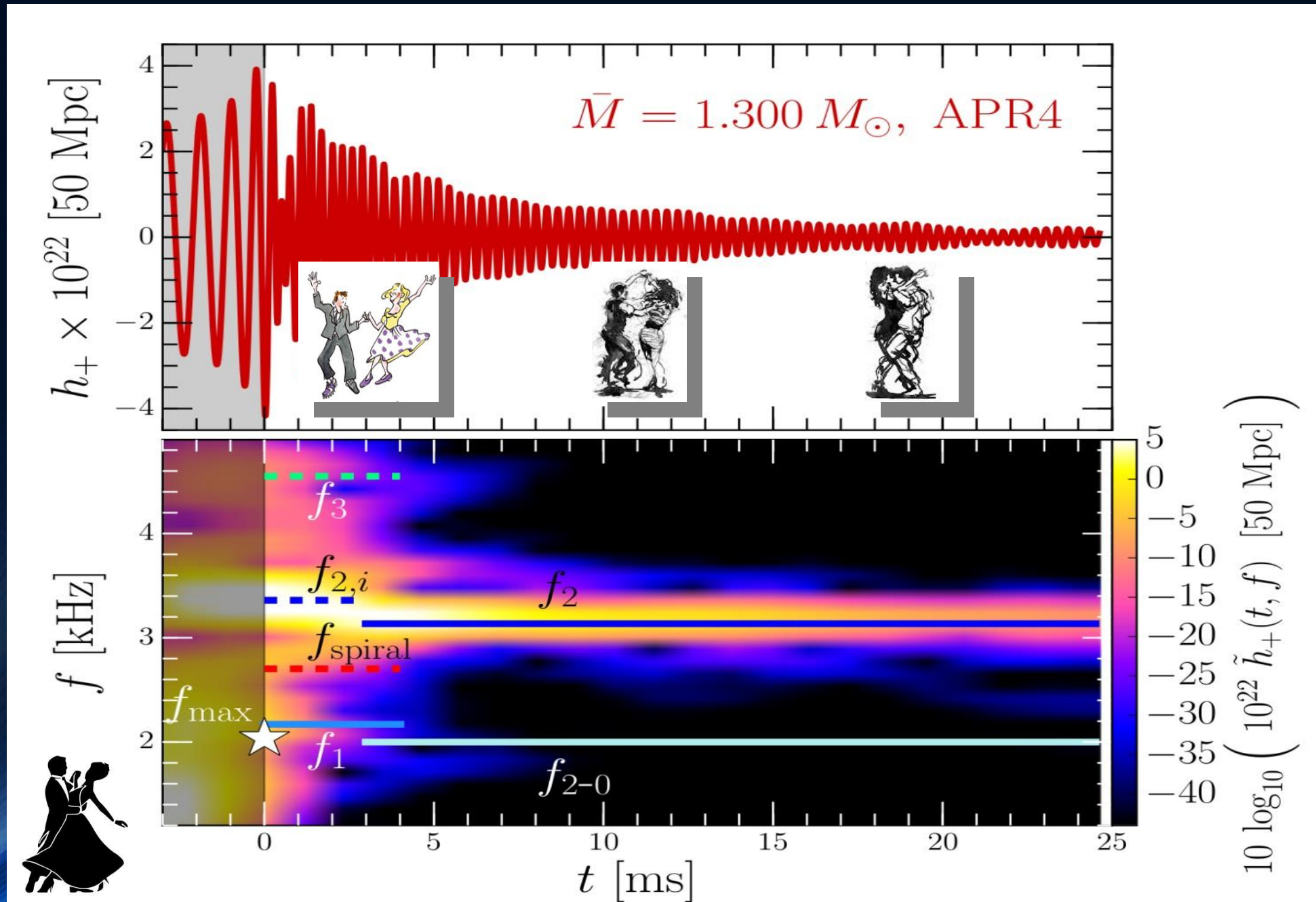

Time Evolution of the GW-Spectrum

The power spectral density profile of the post-merger emission is characterized by several distinct frequencies. Approximately 5 ms after merger, the only remaining dominant frequency is the f_2-frequency (see e.g. L.Rezzolla and K.Takami, PRD, 93(12), 124051 (2016))

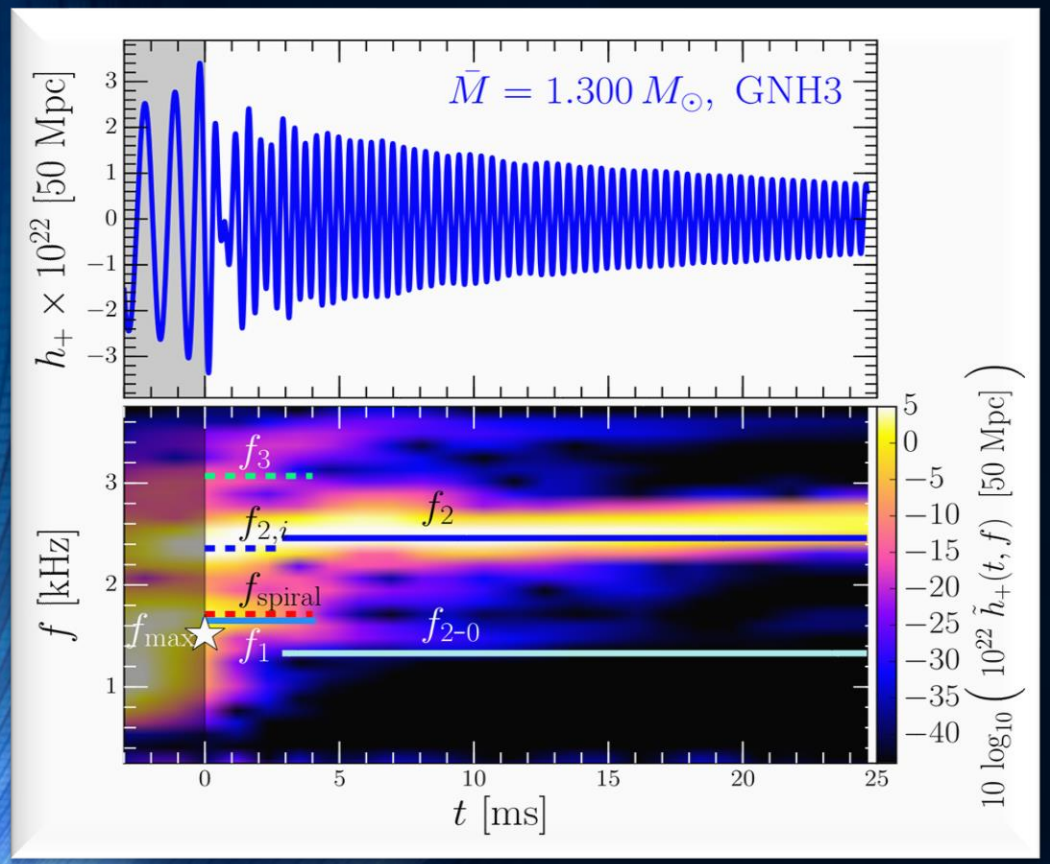

Stiff EOS

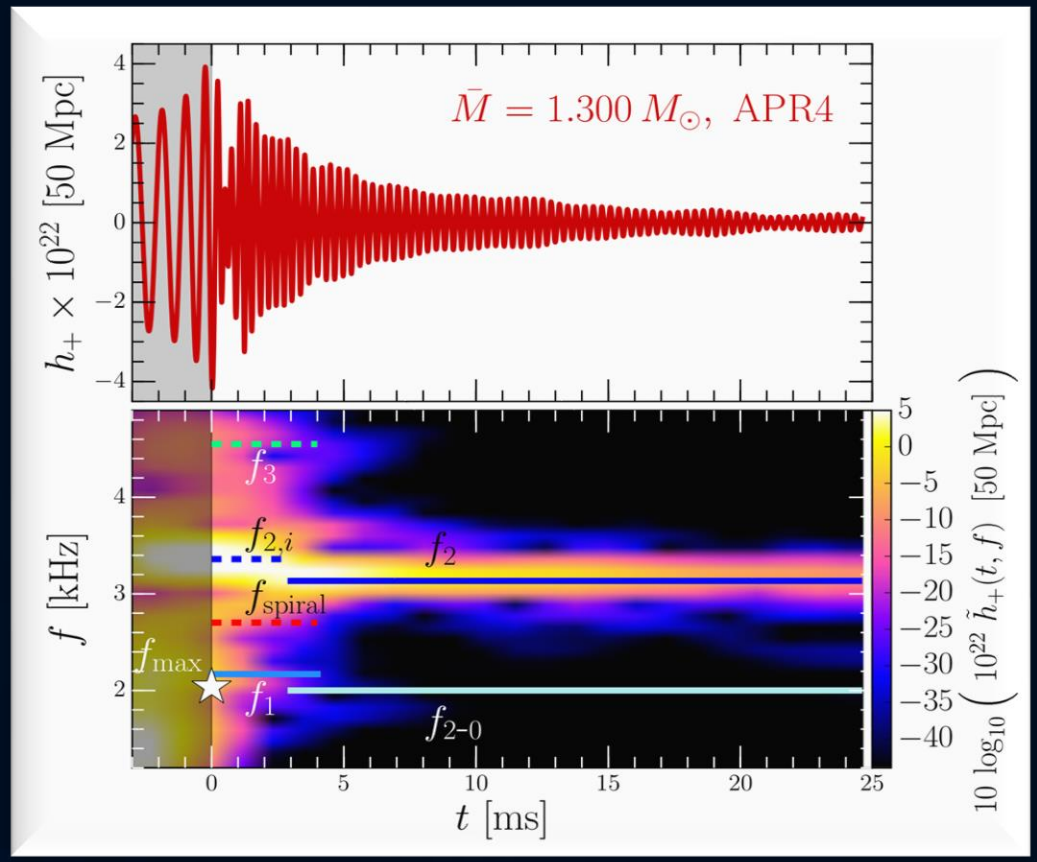

Soft EOS

Unfortunately, clow sensitivity at high gravitational wave frequencies, no post-merger signal has been found in GW170817.

But advanced detectors / next-generation detectors might be able to detect!!?

Evolution of the frequency spectrum of the emitted gravitational waves for the stiff GNH3 (left) and soft APR4 (right) EOS.

A new approach to constrain the EOS

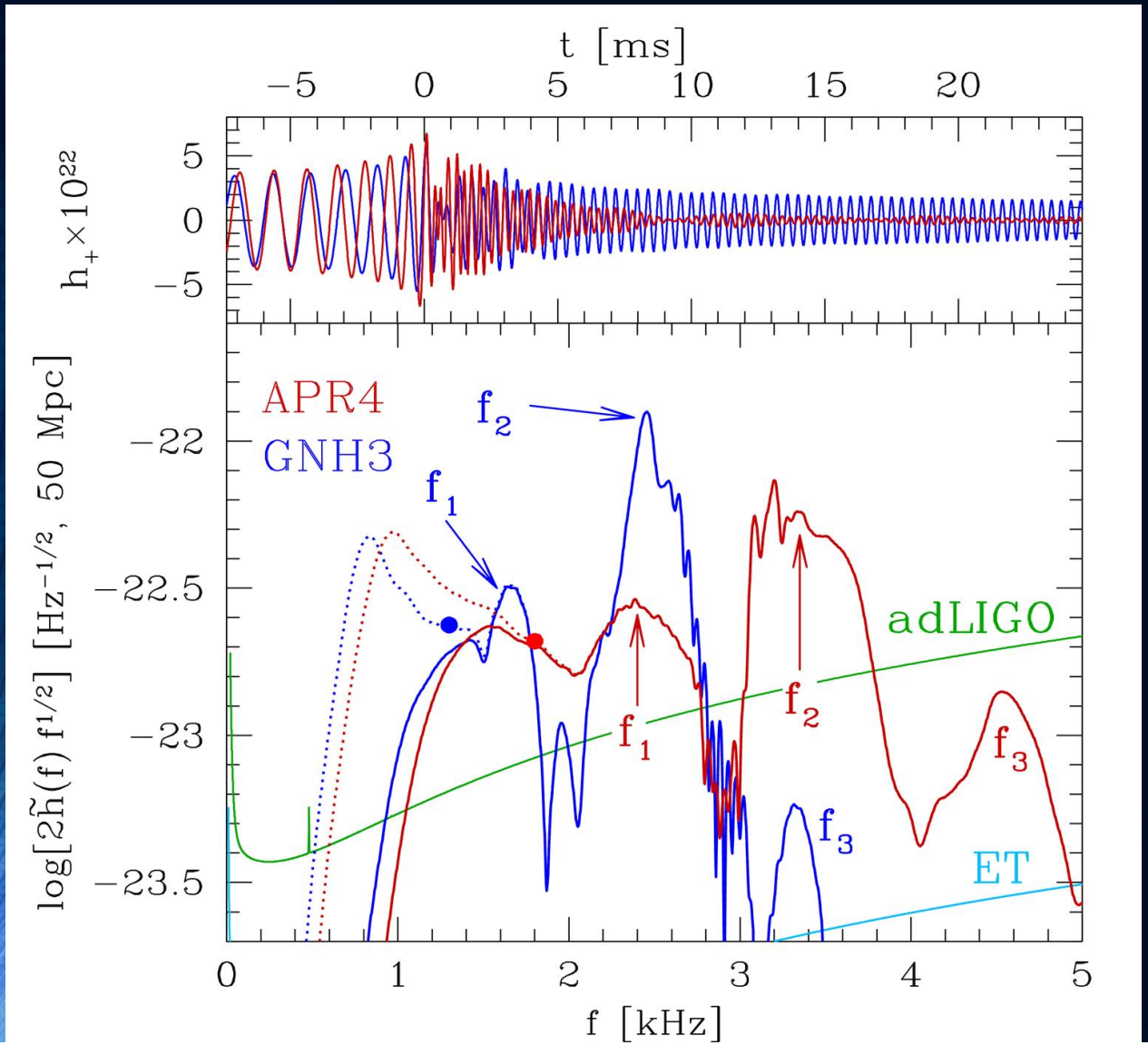

Kentaro Takami, Luciano Rezzolla, and Luca Baiotti, Physical Review D 91, 064001 (2015)

Hotokezaka, K., Kiuchi, K., Kyutoku, K., Muranushi, T., Sekiguchi, Y. I., Shibata, M., & Taniguchi, K. (2013). Physical Review D, 88(4), 044026.

Bauswein, A., & Janka, H. T. (2012). Physical review letters, 108(1), 011101.

Clark, J. A., Bauswein, A., Stergioulas, N., & Shoemaker, D. (2015). arXiv:1509.08522.

Bernuzzi, S., Dietrich, T., & Nagar, A. (2015). Physical review letters, 115(9), 091101.

Oechslin+2007, Baiotti+2008, Bauswein+ 2011, 2012, Stergioulas+ 2011, Hotokezaka+ 2013, Takami 2014, 2015, Bernuzzi 2014, 2015, Bauswein+ 2015, Clark+ 2016, Rezzolla+2016, de Pietri+ 2016, Feo+ 2017, Bose+ 2017 …

Evolution of the density in the post merger phase

ALF2-EOS: Mixed phase region starts at $3\rho_0$ (see red curve), initial NS mass: 1.35 M_{solar}

Hanauske, et.al. PRD, 96(4), 043004 (2017)

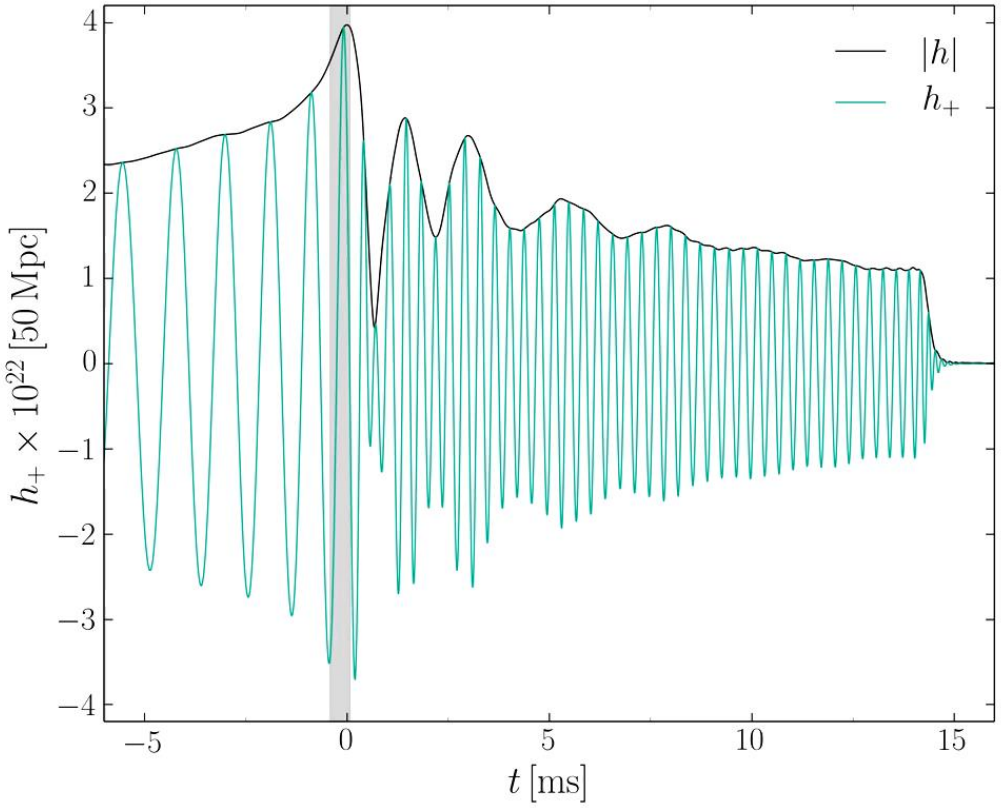

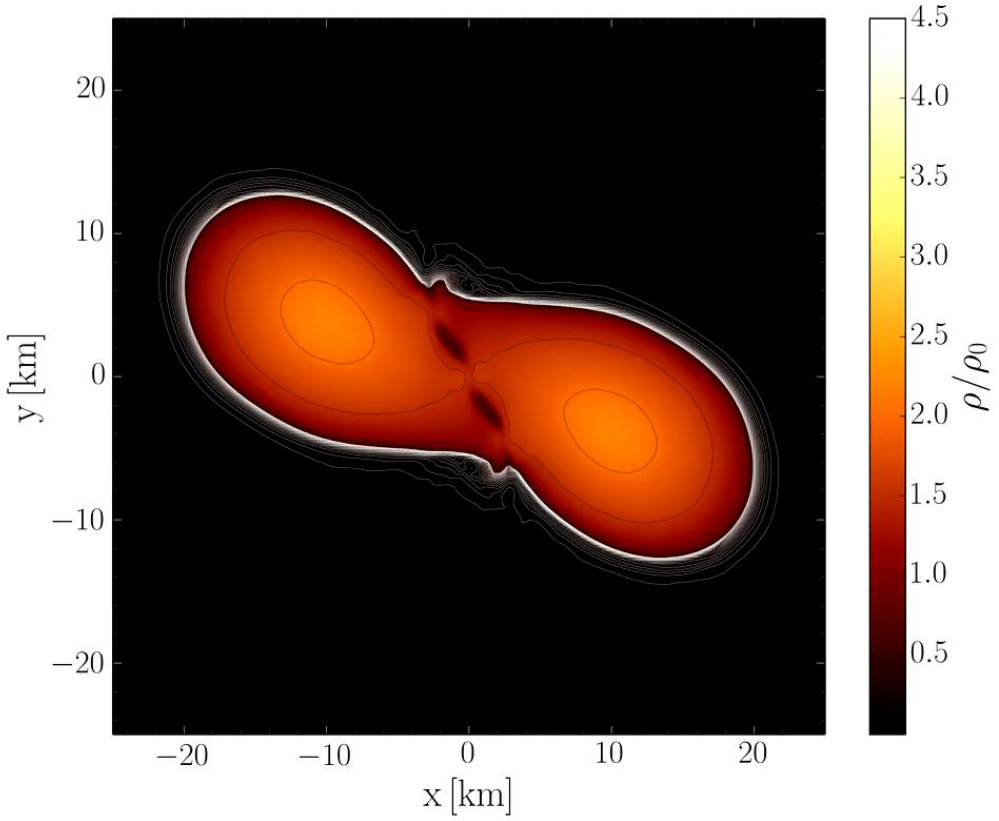

Gravitational wave amplitude
at a distance of 50 Mpc

Rest mass density distribution ρ(x,y)
in the equatorial plane

in units of the nuclear matter density ρ_0

Hypermassive Neutron Stars in the QCD Phase Diagram

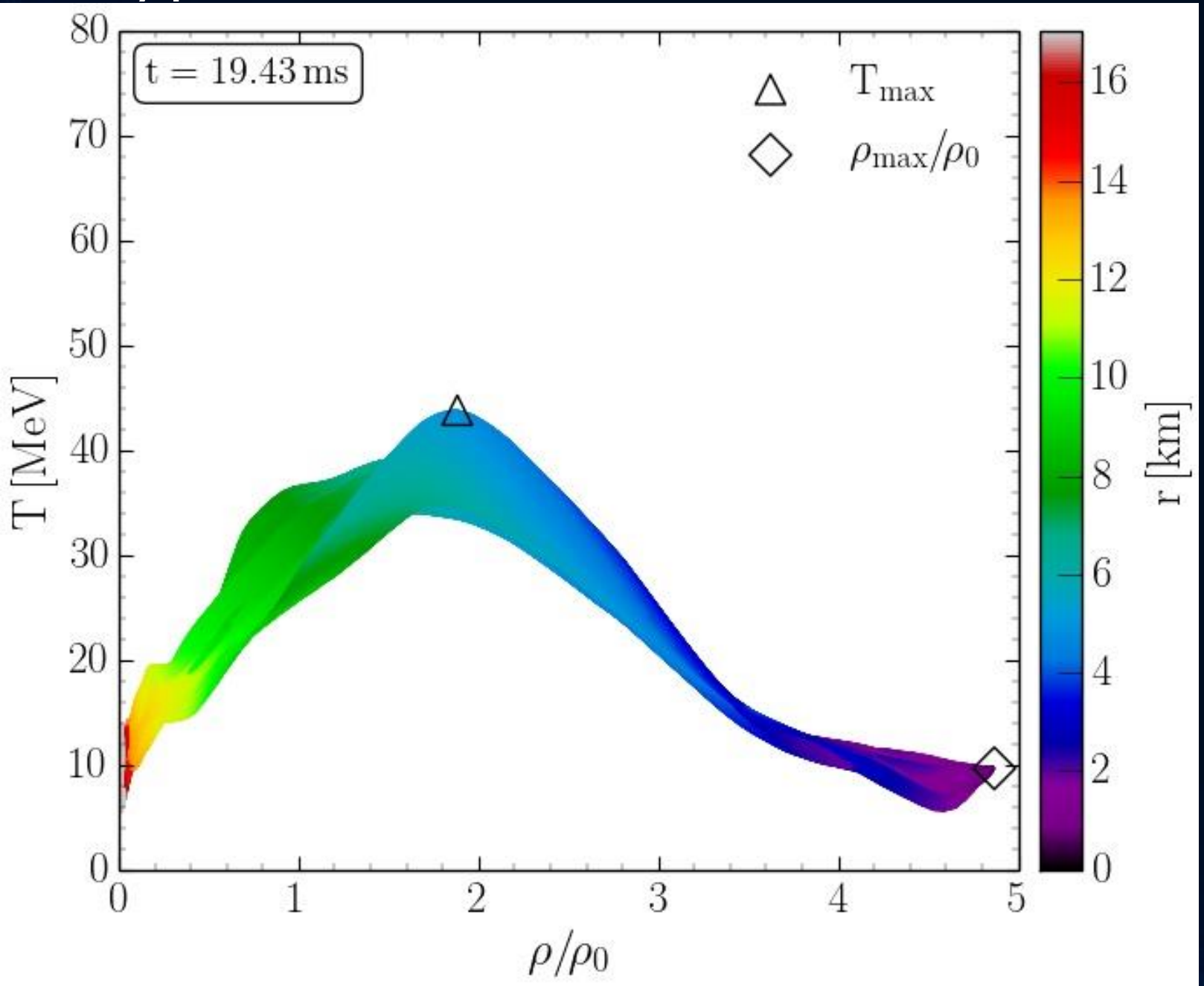

Density-temperature profiles inside the inner area of a hypermassive neutron star simulated within the LS220 EOS with a total mass of $M_{total}=2.7\ M_{solar}$ in the style of a (T-ρ) QCD phase diagram plot at t=19.43 ms after the merger.

The color-coding indicate the radial position r of the corresponding (T- ρ) fluid element measured from the origin of the simulation (x , y) = (0 , 0) on the equatorial plane at z = 0.

The open triangle marks the maximum value of the temperature while the open diamond indicates the maximum of the density.

QCD Phase Diagram: The Late Inspiral Phase

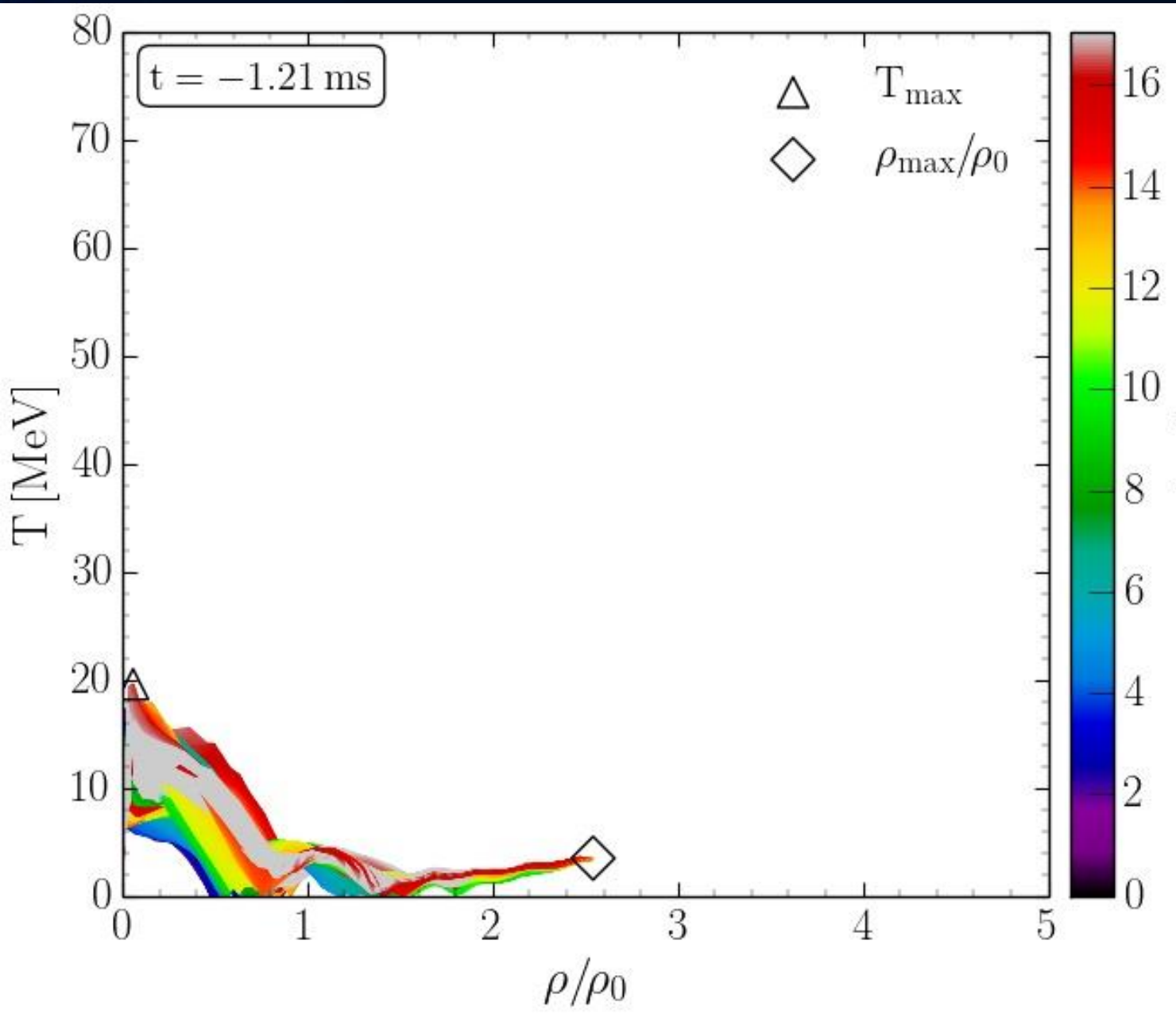

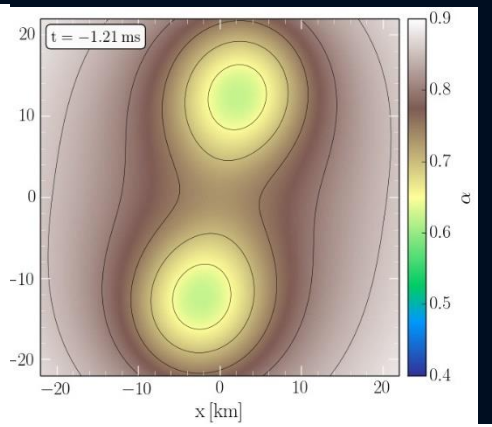

Lapse function α (left)

rest mass density ρ

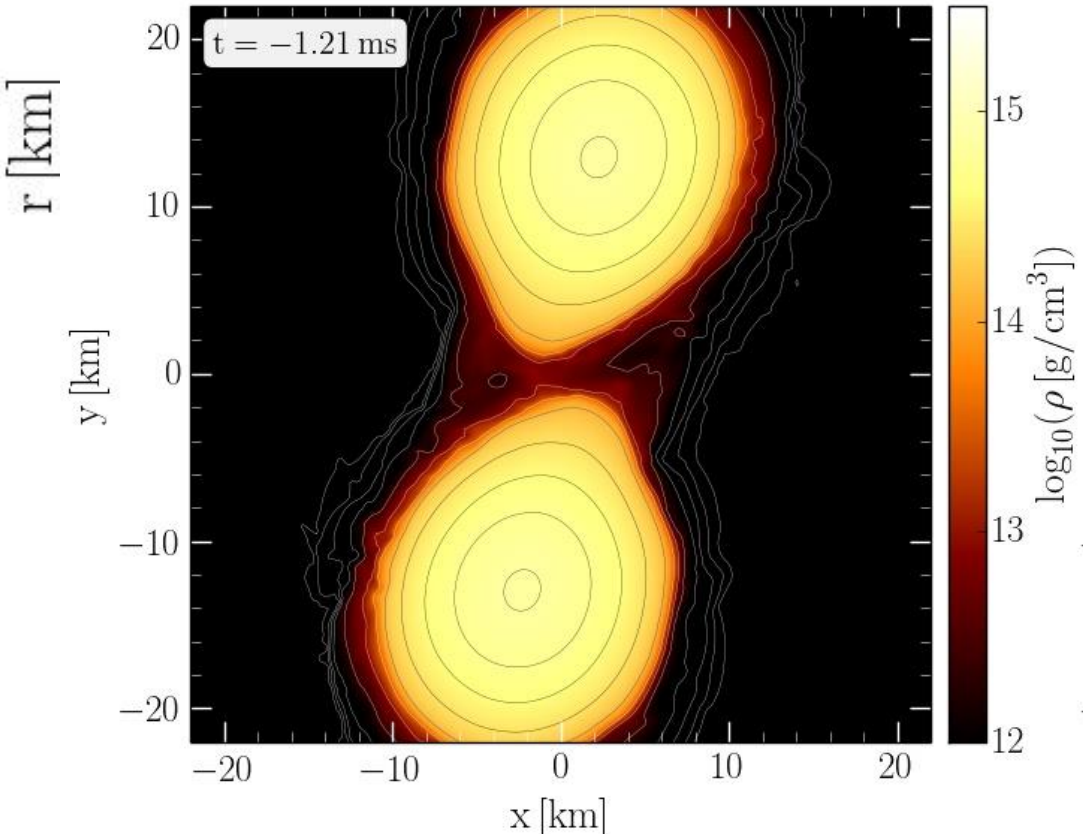

QCD Phase Diagram: The Late Inspiral Phase

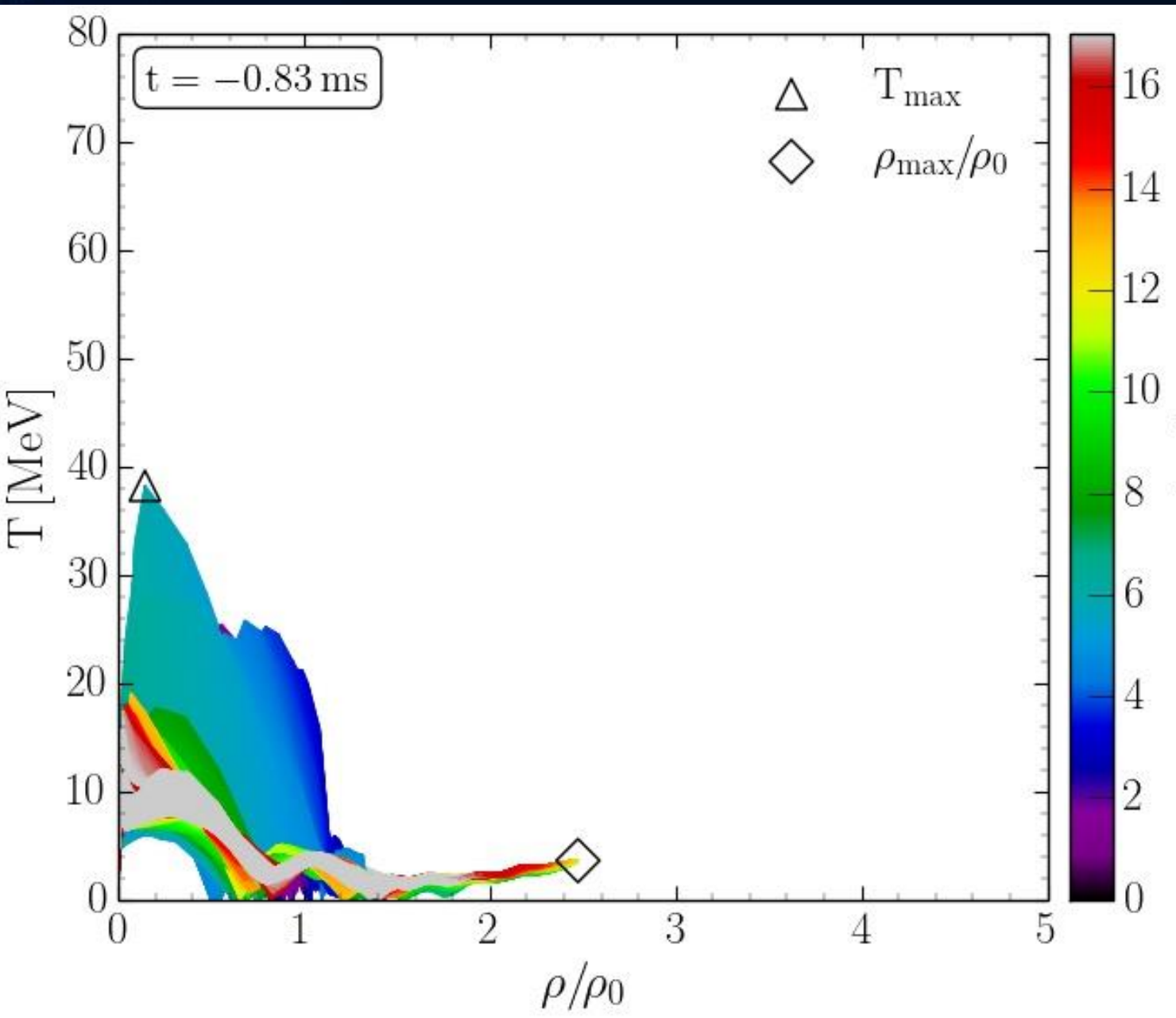

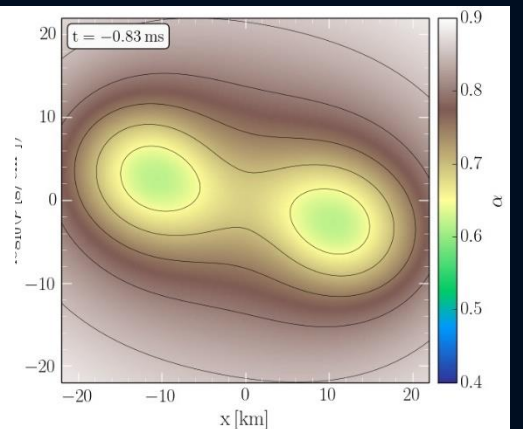

Lapse function α (left)

rest mass density ρ

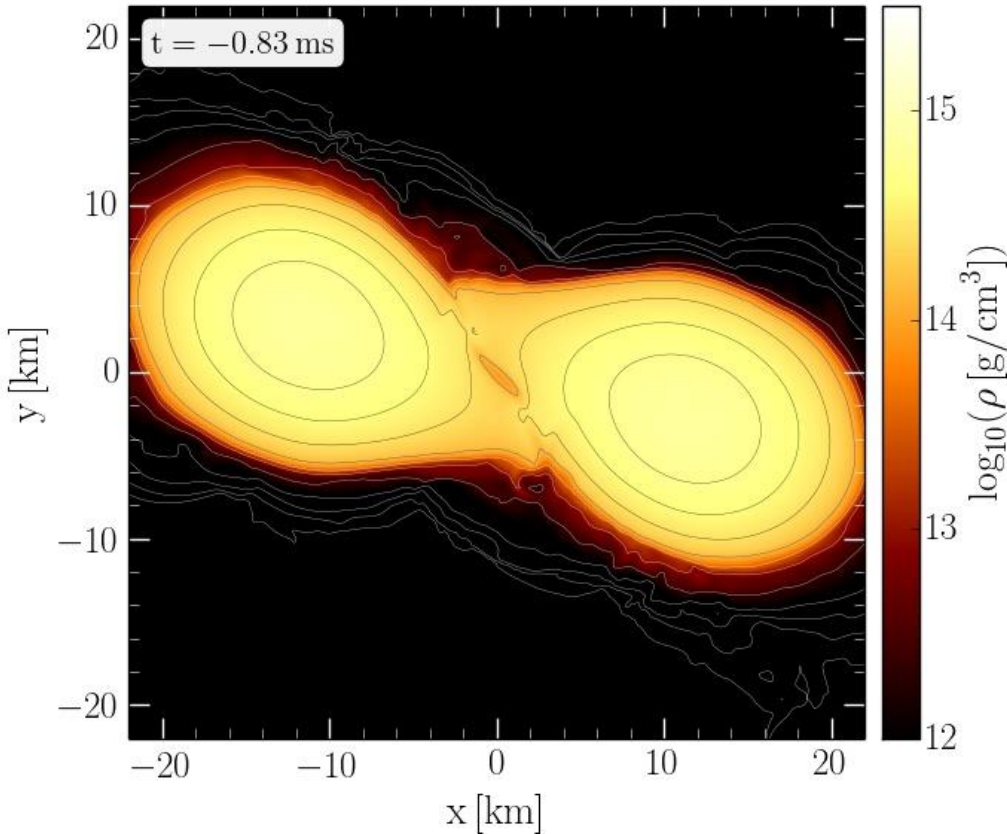

QCD Phase Diagram: The Late Inspiral Phase

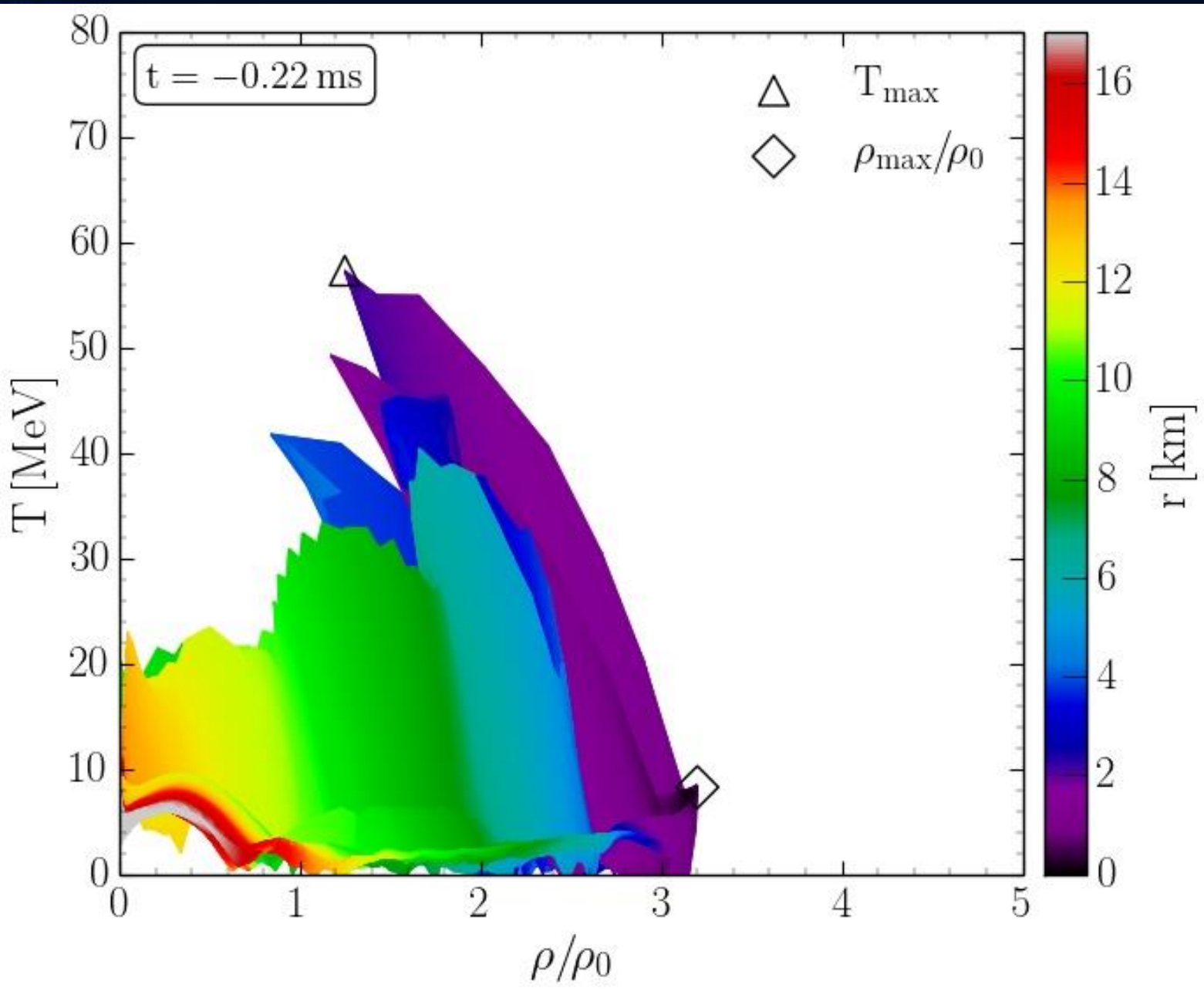

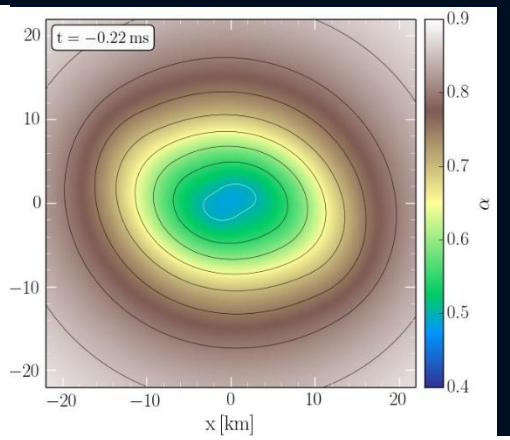

Lapse function α (left)

rest mass density ρ

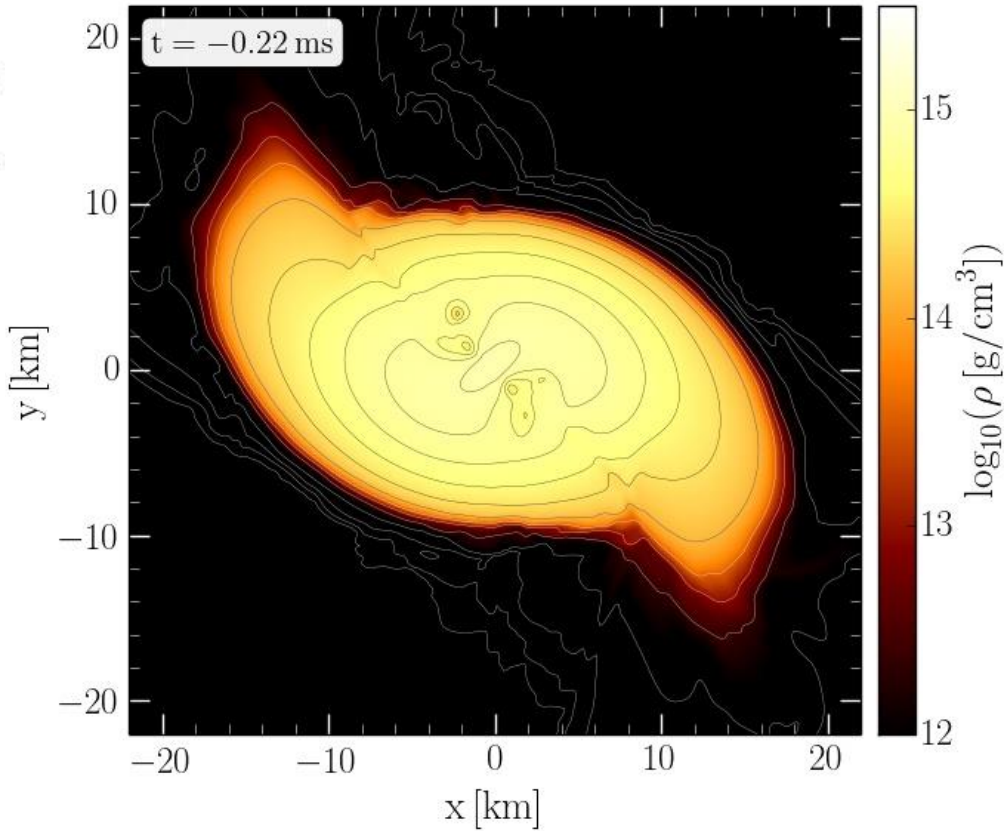

Binary Neutron Star Mergers in the QCD Phase Diagram

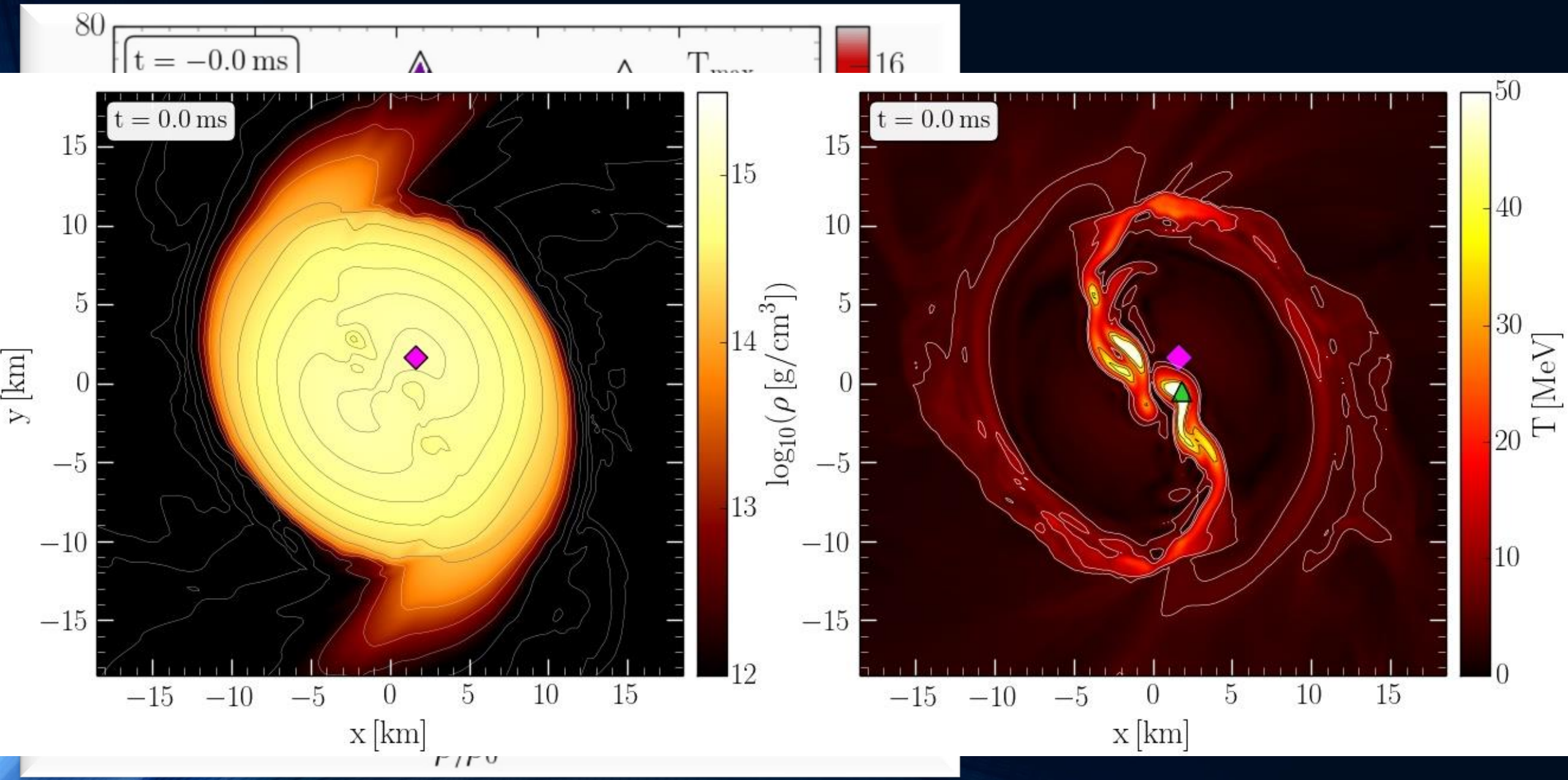

The Co-Rotating Frame

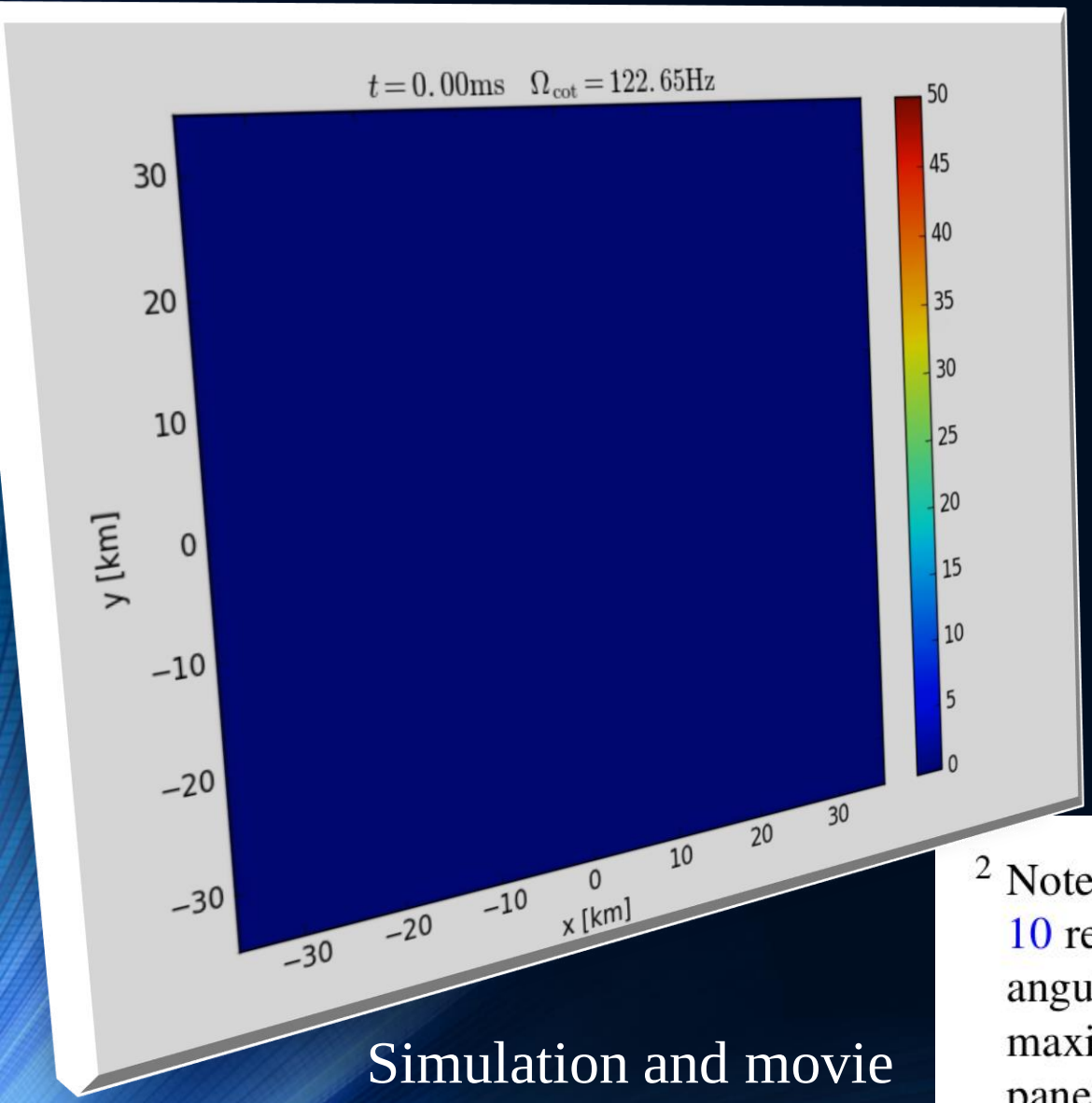

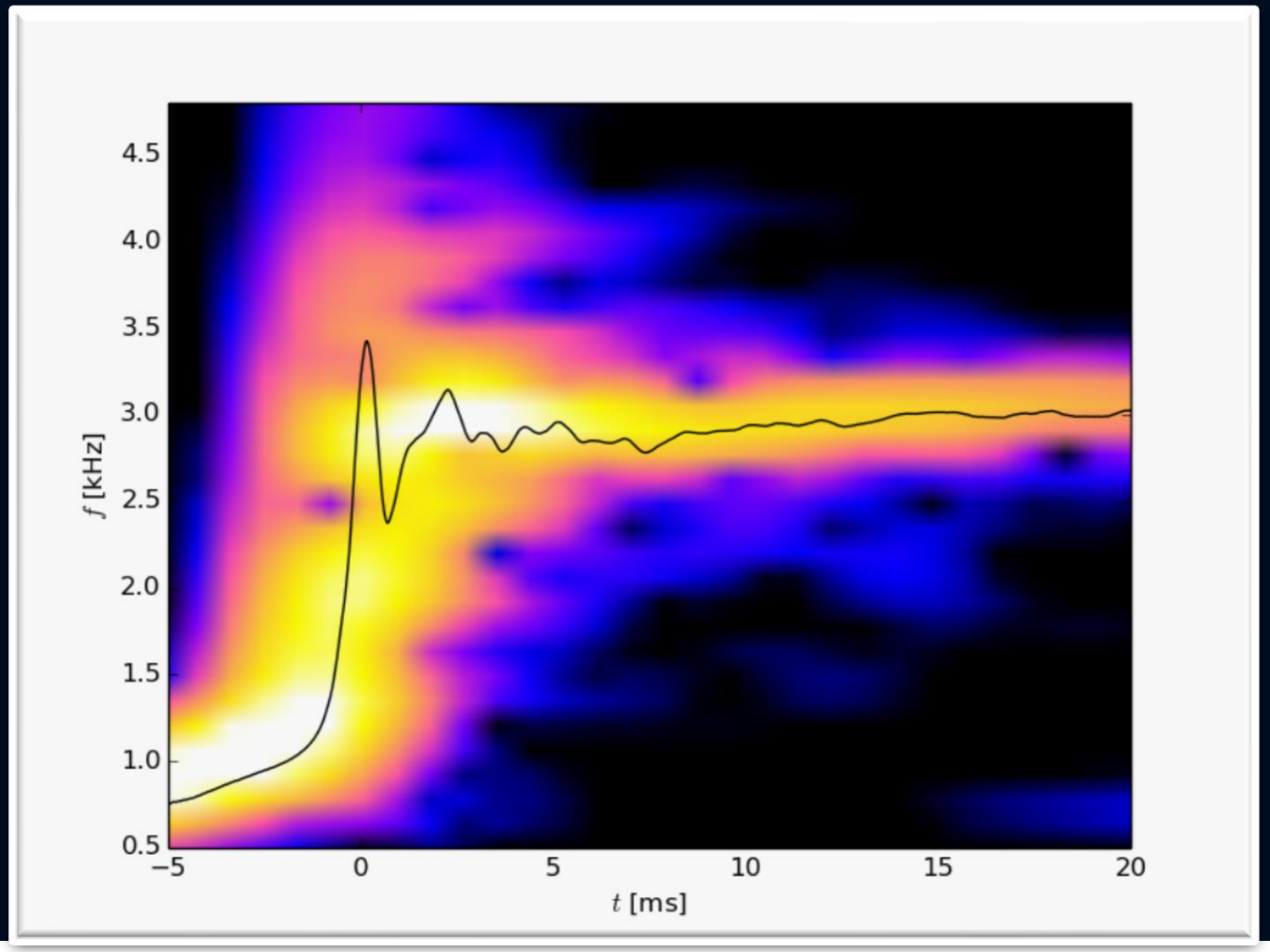

Simulation and movie has been produced by Luke Bovard

[2] Note that the angular-velocity distribution in the lower central panel of Fig. 10 refers to the corotating frame and that this frame is rotating at half the angular frequency of the emitted gravitational waves, $\Omega_{\rm GW}$. Because the maximum of the angular velocity $\Omega_{\rm max}$ is of the order of $\Omega_{\rm GW}/2$ (cf. left panel of Fig. 12), the ring structure in this panel is approximately at zero angular velocity.

Density and Temperature Evolution inside the HMNS

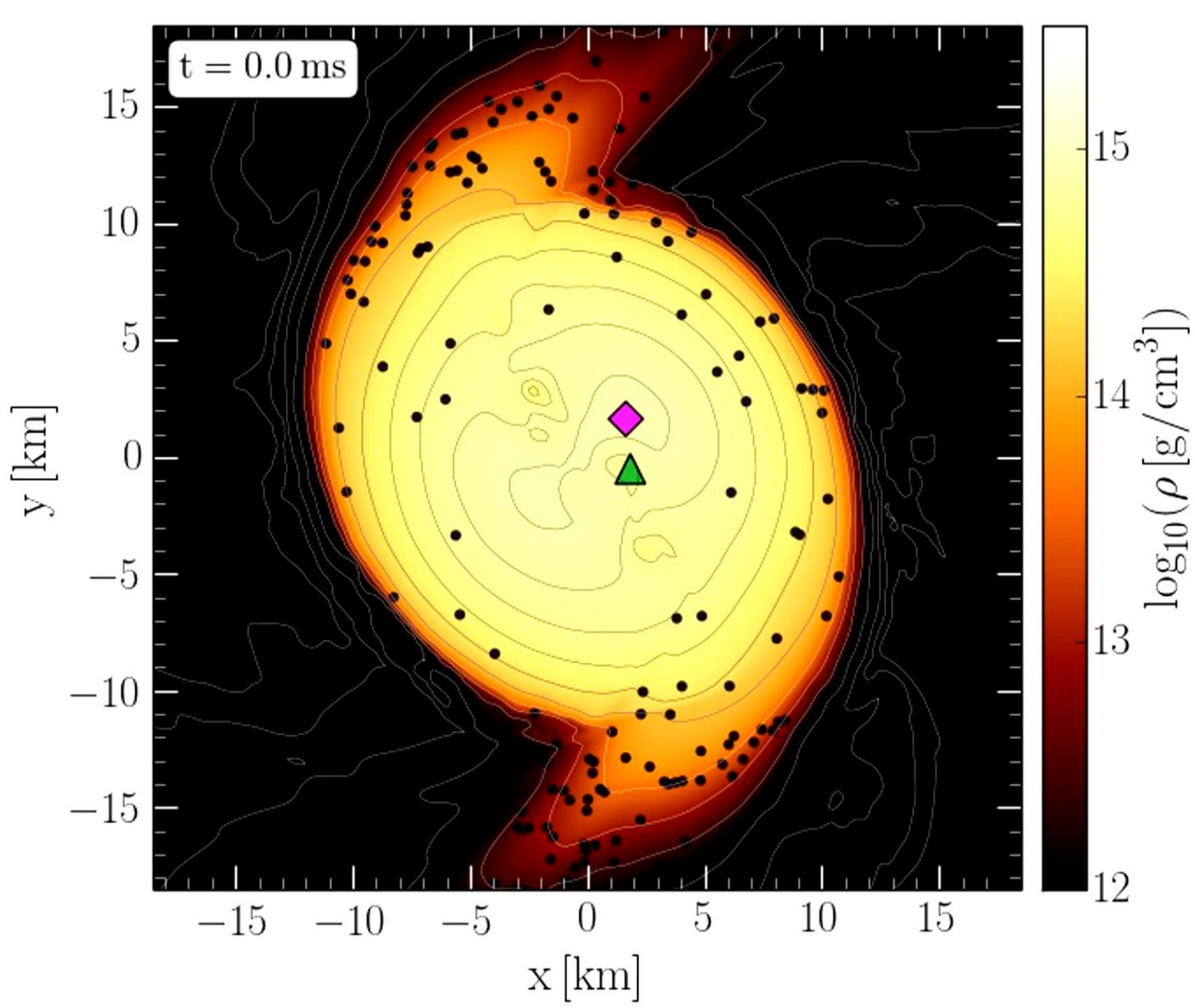

Rest mass density on the equatorial plane

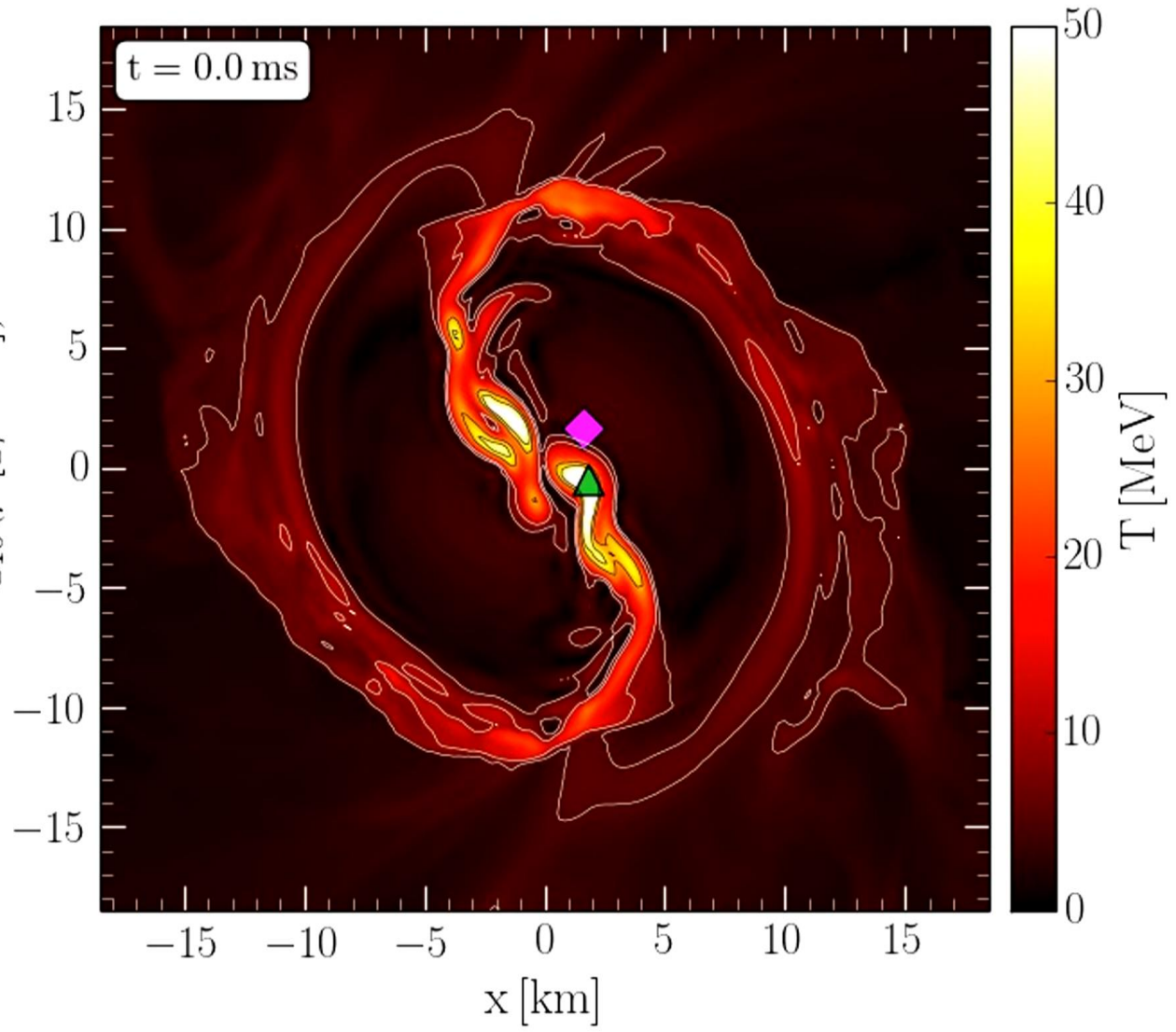

Temperature on the equatorial plane

Binary Neutron Star Mergers in the QCD Phase Diagram

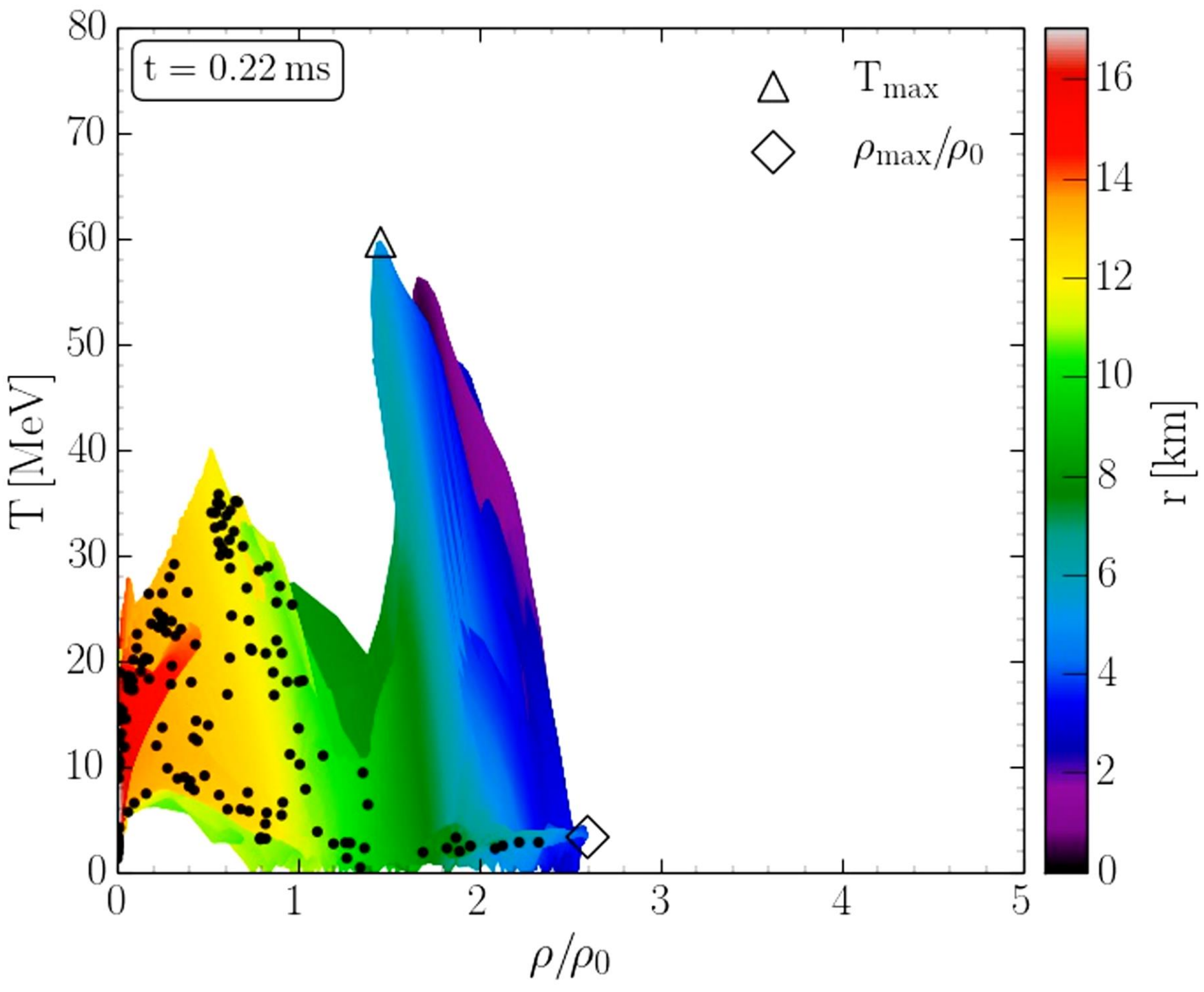

Evolution of hot and dense matter inside the inner area of a hypermassive neutron star simulated within the LS220 EOS with a total mass of $M_{total}=2.7\ M_{solar}$ in the style of a (T- ρ) QCD phase diagram plot

The color-coding indicate the radial position r of the corresponding (T- ρ) fluid element measured from the origin of the simulation (x , y) = (0 , 0) on the equatorial plane at z = 0.

The open triangle marks the maximum value of the temperature while the open diamond indicates the maximum of the density.

The Angular Velocity in the (3+1)-Split

The angular velocity Ω in the (3+1)-Split is a combination of the lapse function α , the ϕ-component of the shift vector β^{ϕ} and the 3-velocity v^{ϕ} of the fluid (spatial projection of the 4-velocity **u**):

$$\Omega(x,y,z,t) = \frac{u^{\phi}}{u^{t}} = \alpha\, v^{\phi} - \beta^{\phi}$$

Angular velocity Ω

Lapse function α

Φ-component of 3-velocity v^{φ}

Frame-dragging β^{φ}

(3+1)-decomposition of spacetime:

$$g_{\mu\nu} = \begin{pmatrix} -\alpha^2 + \beta_i \beta^i & \beta_i \\ \beta_i & \gamma_{ij} \end{pmatrix}$$

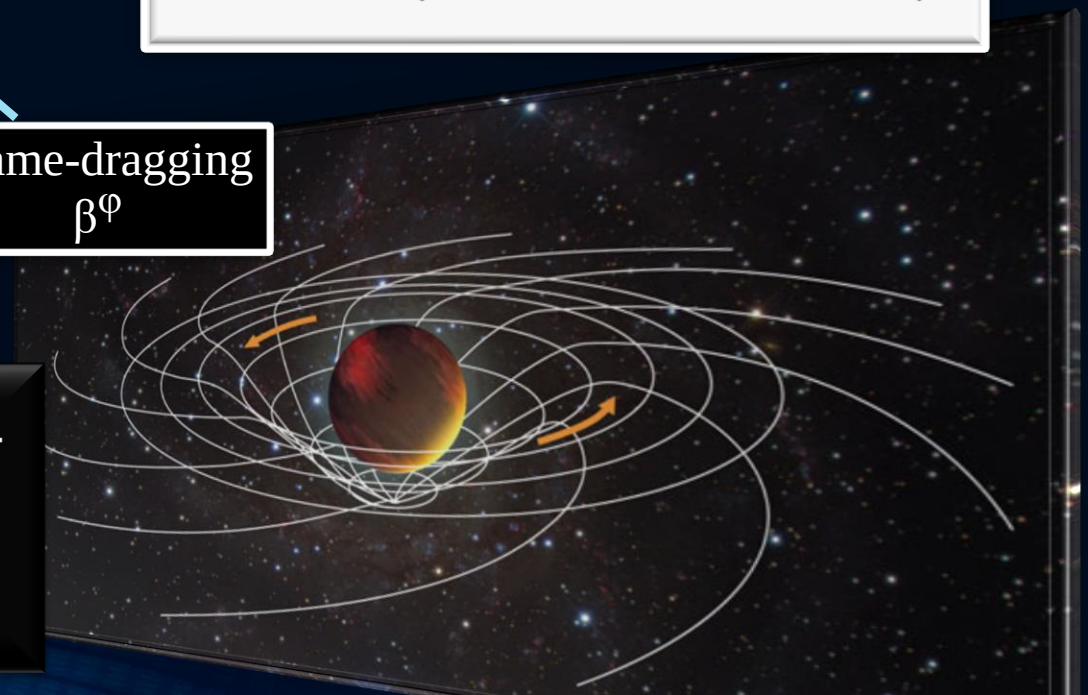

Focus: Inner core of the differentially rotating HMNS

M. Shibata, K. Taniguchi, and K. Uryu, Phys. Rev. D 71, 084021 (2005)
M. Shibata and K. Taniguchi, Phys. Rev. D 73, 064027 (2006)
F. Galeazzi, S. Yoshida and Y. Eriguchi, A&A 541, p. A156 (2012)
W. Kastaun and F. Galeazzi, Phys. Rev. D 91, p. 064027 (2015)

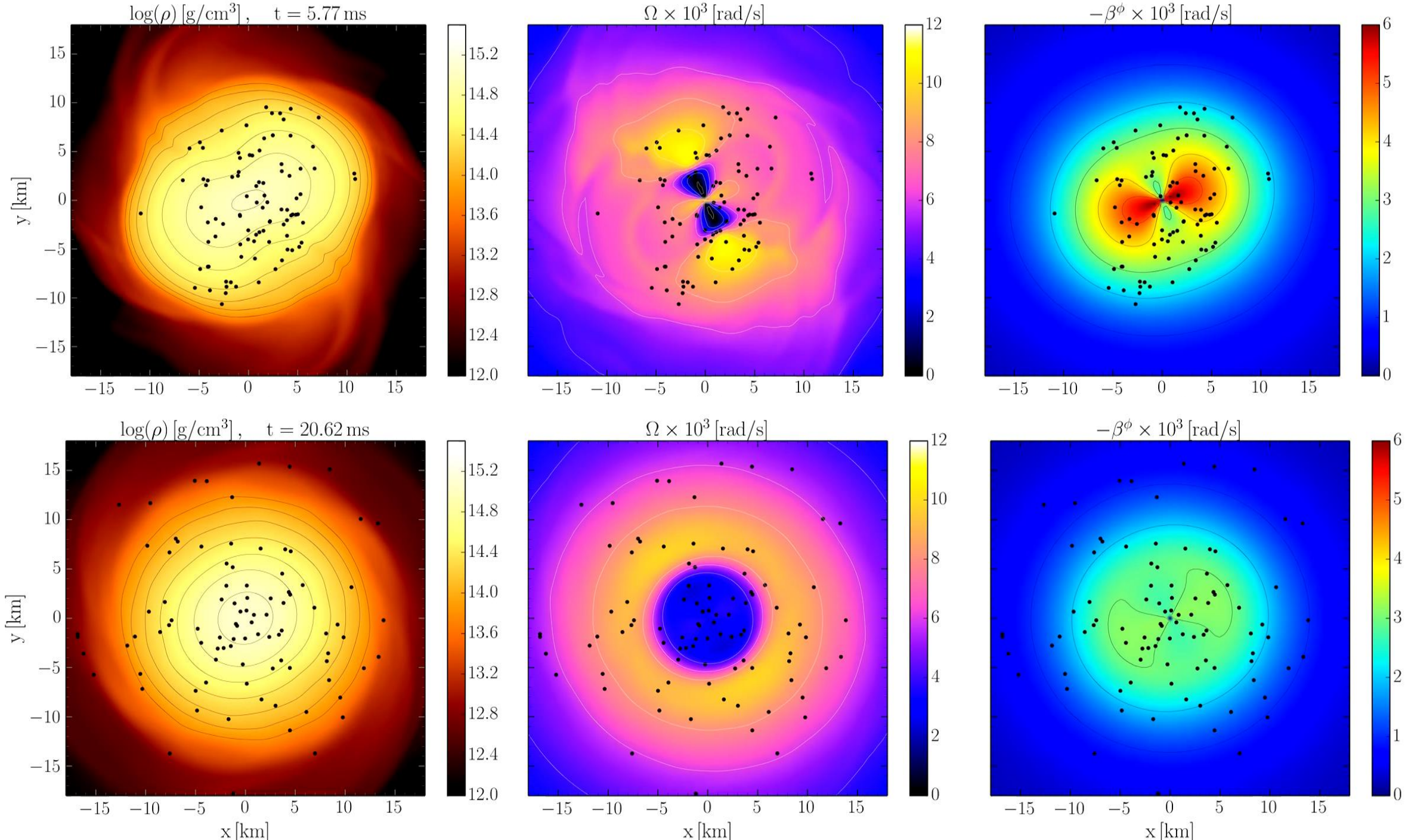
log(ρ) [g/cm³] , t = 5.77 ms
Ω × 10³ [rad/s]
−β^φ × 10³ [rad/s]
log(ρ) [g/cm³] , t = 20.62 ms
Ω × 10³ [rad/s]
−β^φ × 10³ [rad/s]
y [km]
x [km]

Time-averaged Rotation Profiles of the HMNSs

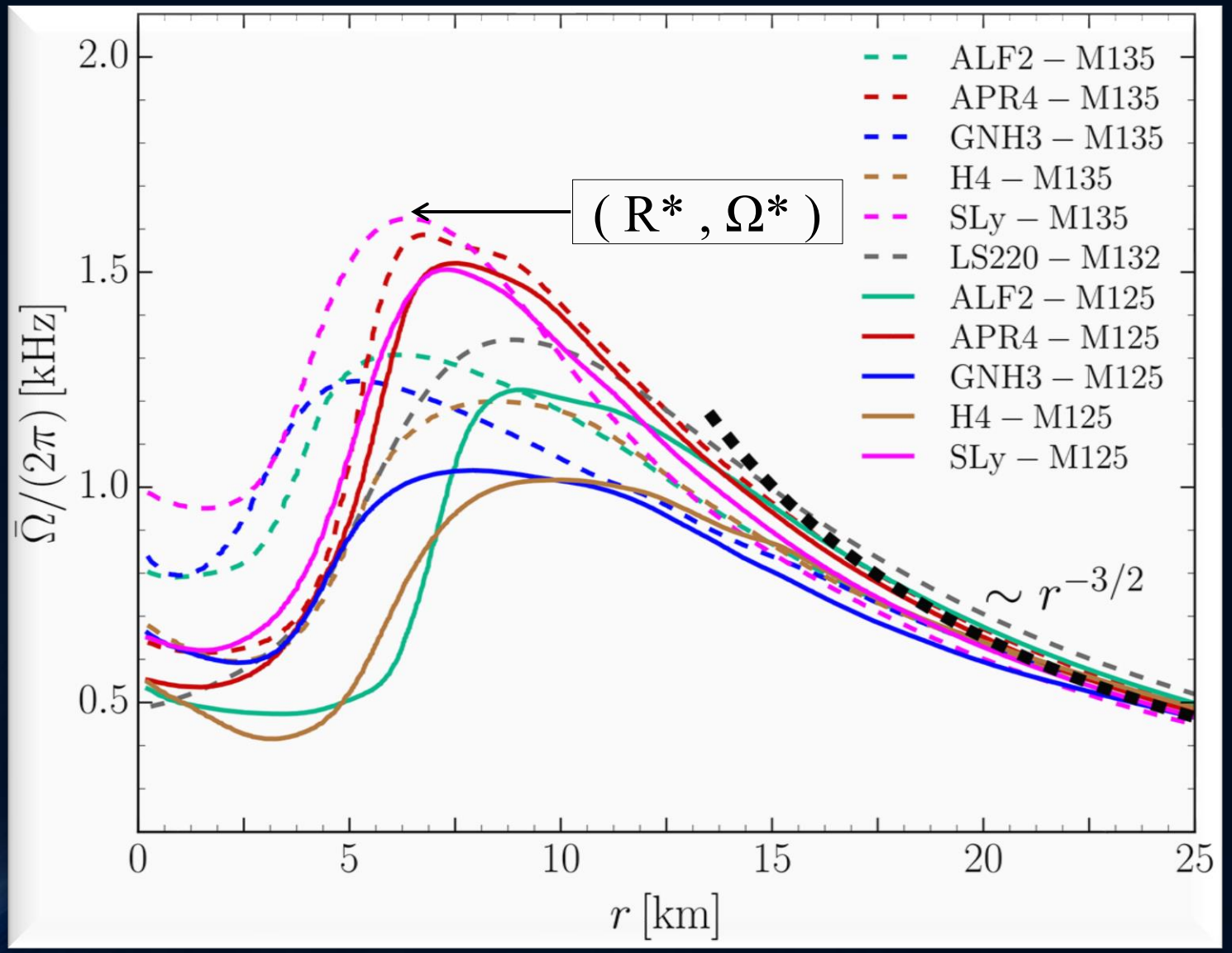

Soft EoSs:
Sly
APR4

Stiff EoSs:
GNH3
H4

Time-averaged rotation profiles for different EoS
Low mass runs (solid curves), high mass runs (dashed curves).

Hanauske, et.al. PRD, 96(4), 043004 (2017)

Temperature

Angular Velocity

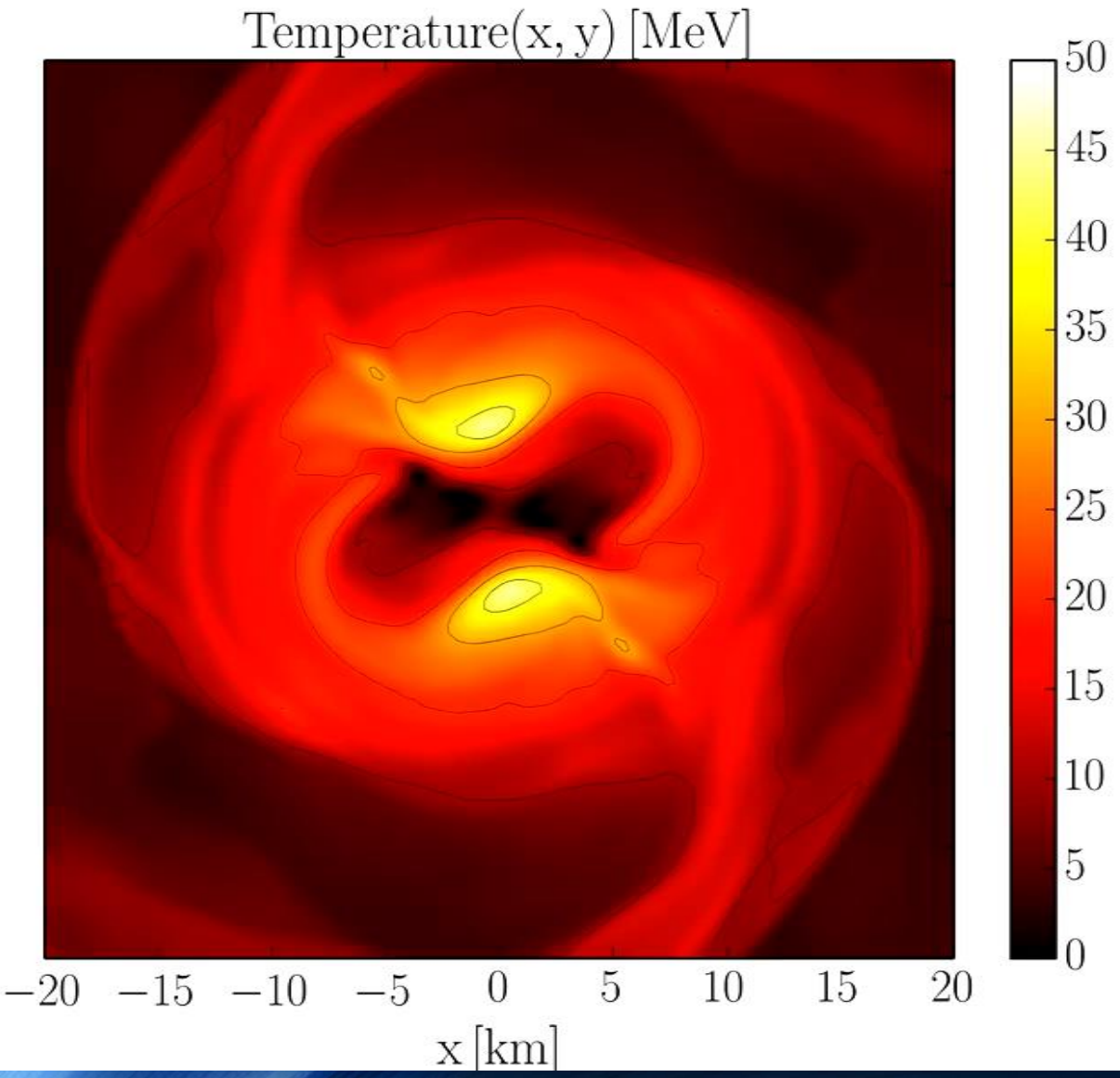

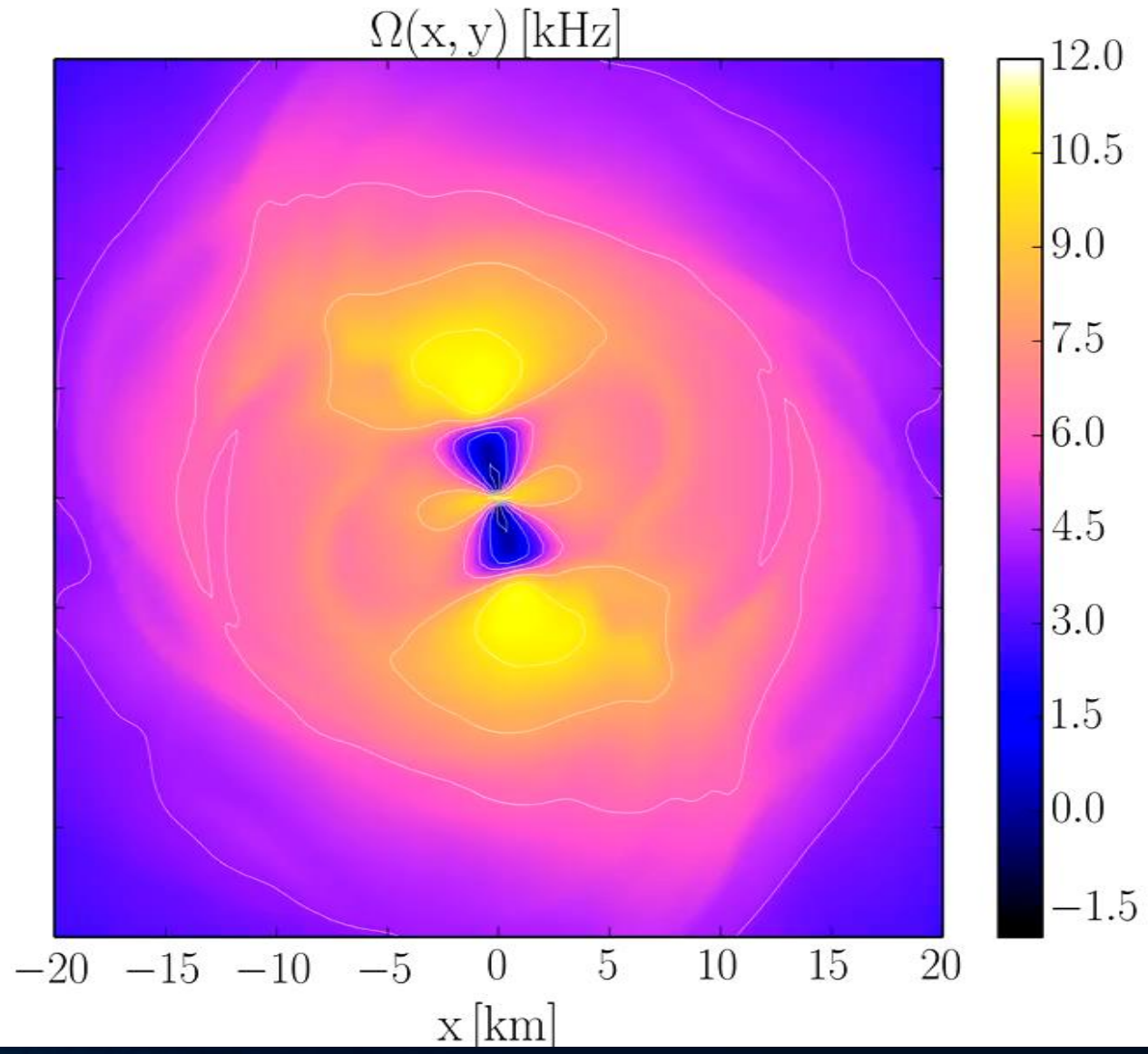

EOS: LS200 , Mass: 1.32 M_{solar} , simulation with Pi-symmetry

Postmerger gravitational-wave signatures of phase transitions in binary compact star mergers

- Introduction
- Numerical general relativity of compact star mergers
- The equation of state of compact star matter and the hadron-quark phase transition
- The different phases of a binary compact star merger event
- **Gravitational-wave signatures of the hadron-quark phase transition in binary compact star mergers**
  - The inspiral and merger phase (premerger signals)
  - Hypermassive hybrid stars (HMHS) within the prompt phase transition scenario (PPT)
  - HMHS within the delayed phase transition scenario (DPT)
  - HMHS within the phase transition triggered collapse scenario (PTTC)
- Summary and Outlook

Postmerger gravitational-wave signatures of phase transitions in binary compact star mergers

- Introduction
- Numerical general relativity of compact star mergers
- The equation of state of compact star matter and the hadron-quark phase transition
- The different phases of a binary compact star merger event
- Gravitational-wave signatures of the hadron-quark phase transition in binary compact star mergers
  - The inspiral and merger phase (premerger signals)
    - Hypermassive hybrid stars (HMHS) within the prompt phase transition scenario (PPT)
    - HMHS within the delayed phase transition scenario (DPT)
    - HMHS within the phase transition triggered collapse scenario (PTTC)
- Summary and Outlook

GW170817
Constraining the maximum mass and radius of neutron stars

L.Rezzolla, E.Most, L.Weih, "Using Gravitational Wave Observations and Quasi-Universal Relations to constrain the maximum Mass of Neutron Stars",The Astrophysical Journal Letters 852, L25 (2018): 2.01 +/-0.04 < M_{TOV} < 2.16 +/-0.17

Constraining M_{TOV} , see also: S.Lawrence et al. ,APJ808,186, 2015, Margalit & Metzger, The Astrophysical Journal Letters 850, L19 (2017): M_{TOV} < 2.17 (90%) Zhou, Zhou, Li, PRD 97, 083015 (2018) Ruiz, Shapiro, Tsokaros, PRD 97,021501 (2018)

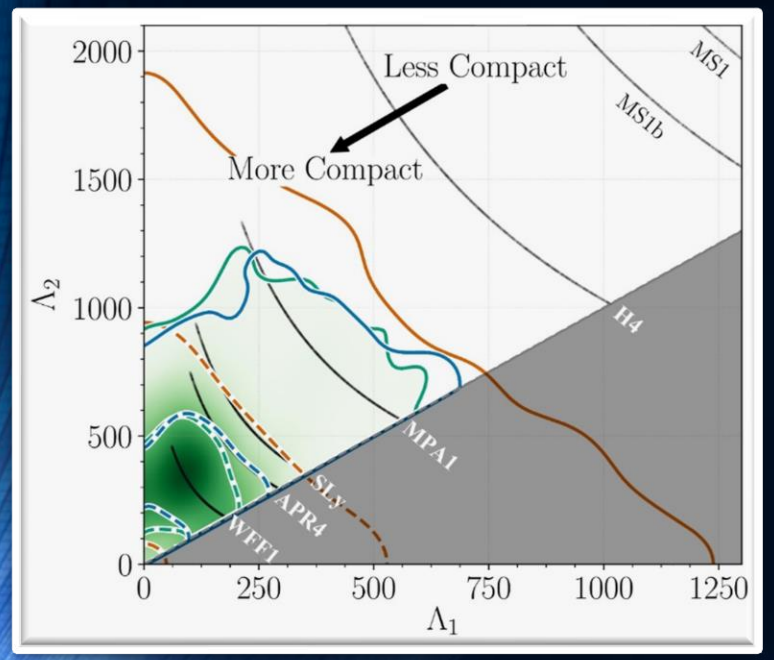

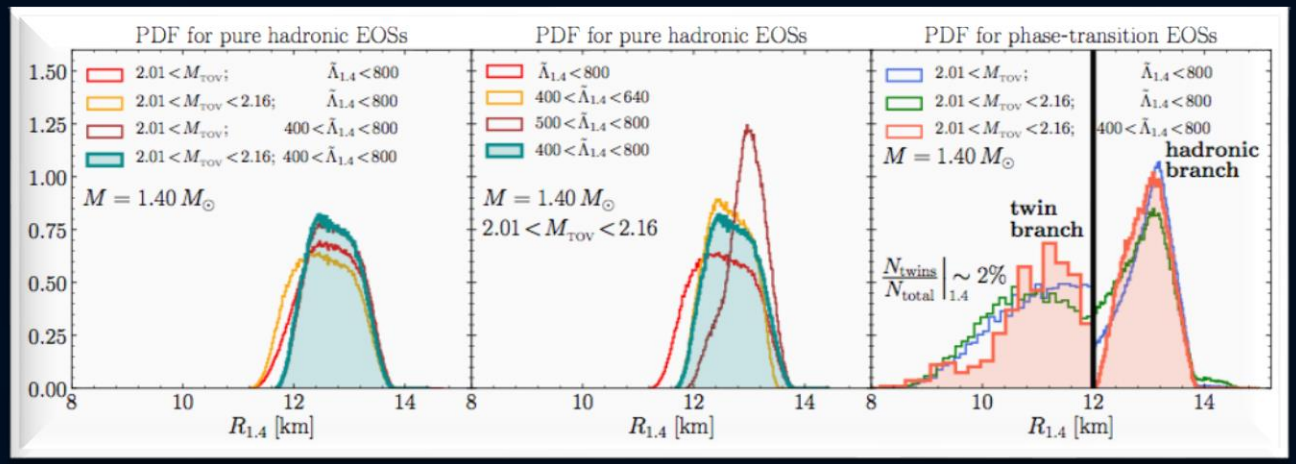

E.Most, L.Weih, L.Rezzolla, J. Schaffner-Bielich "New constraints on radii and tidal deformabilities of neutron stars from GW170817", PRL 120, 261103 (2018)

GW170817: Measurements of neutron star radii and equation of state, *The LIGO /Virgo Collaboration*, arXiv:1805.11581v1

See also: De, Finstad, Lattimer, Brown, Berger, Biwer, (2018), arXiv:1804.08583 ; Bauswein, Just, Janka, N. Stergioulas, APJL 850, L34 (2017) ; Fattoyev, Piekarewicz, Horowitz, PRL 120, 172702 (2018) ; Nandi & Char, Astrophys. J. 857, 12 (2018) ; Paschalidis, Yagi, Alvarez-Castillo, Blaschke, Sedrakian, PRD 97, 084038 ; Ruiz, Shapiro, Tsokaros, PRD 97, 021501 (2018) ; Annala, Gorda, Kurkela, Vuorinen, PRL 120, 172703 (2018) ; Raithel, Özel, Psaltis, (2018) arXiv:1803.07687

The Hadron-Quark Phase Transition and the Third Family of Compact Stars (Twin Stars)

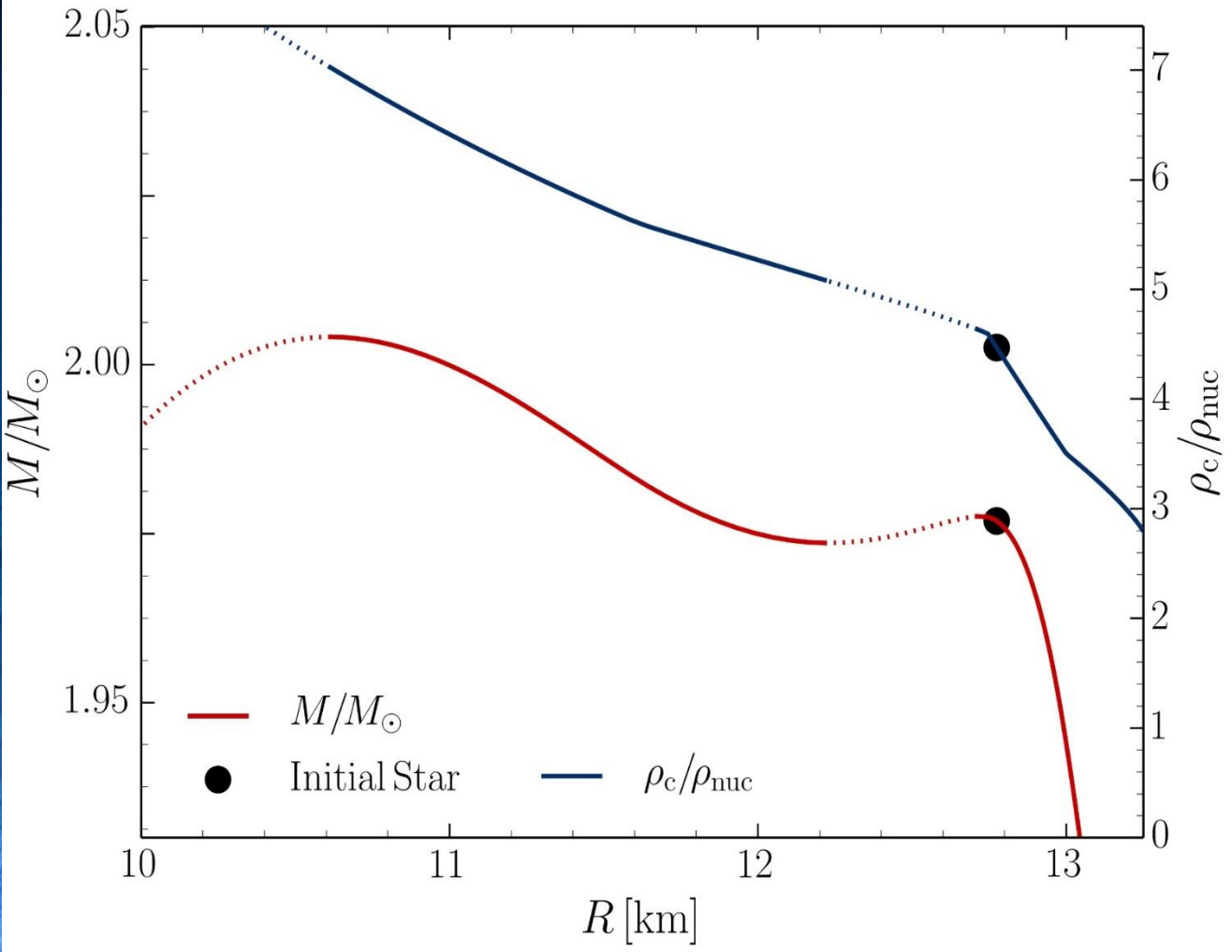

Glendenning, N. K., & Kettner, C. (1998). Nonidentical neutron star twins. Astron. Astrophys., 353(LBL-42080), L9.

Sarmistha Banik, Matthias Hanauske, Debades Bandyopadhyay and Walter Greiner, Rotating compact stars with exotic matter, Phys.Rev.D 70 (2004) p.12304

I.N. Mishustin, M. Hanauske, A. Bhattacharyya, L.M. Satarov, H. Stöcker, and W. Greiner, Catastrophic rearrangement of a compact star due to quark core formation, Physics Letters B 552 (2003) p.1-8

M.Alford and A. Sedrakian, Compact stars with sequential QCD phase transitions. Physical review letters, 119(16), 161104 (2017).

D.Alvarez-Castillo and D.Blaschke, High-mass twin stars with a multipolytrope equation of state. Physical Review C, 96(4), 045809 (2017) .

A. Ayriyan, N.-U. Bastian, D. Blaschke, H. Grigorian, K. Maslov, D. N. Voskresensky, How robust is a third family of compact stars against pasta phase effects?, arXiv:1711.03926 [nucl-th]

Constraining the hadron-quark phase transition with GW170817

Construction of the EOS with a hadron-quark phase transition

The Mass-Radius relation and the twin star property

Maxwell Construction Gibbs Construction

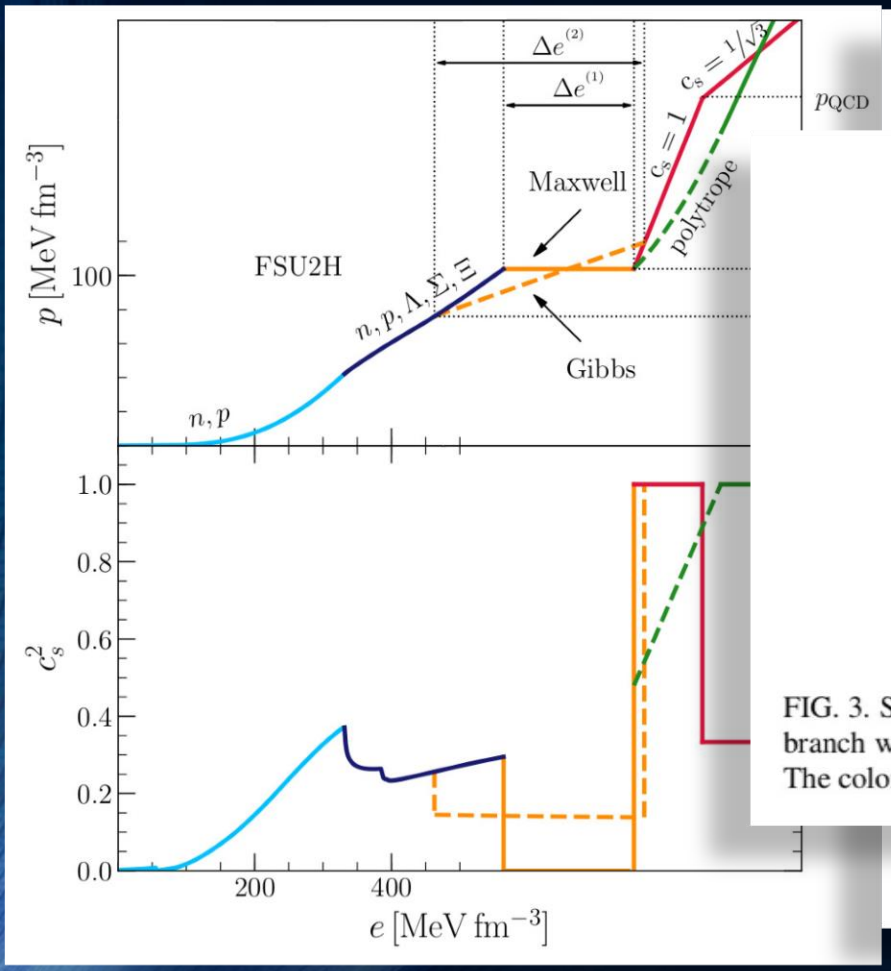

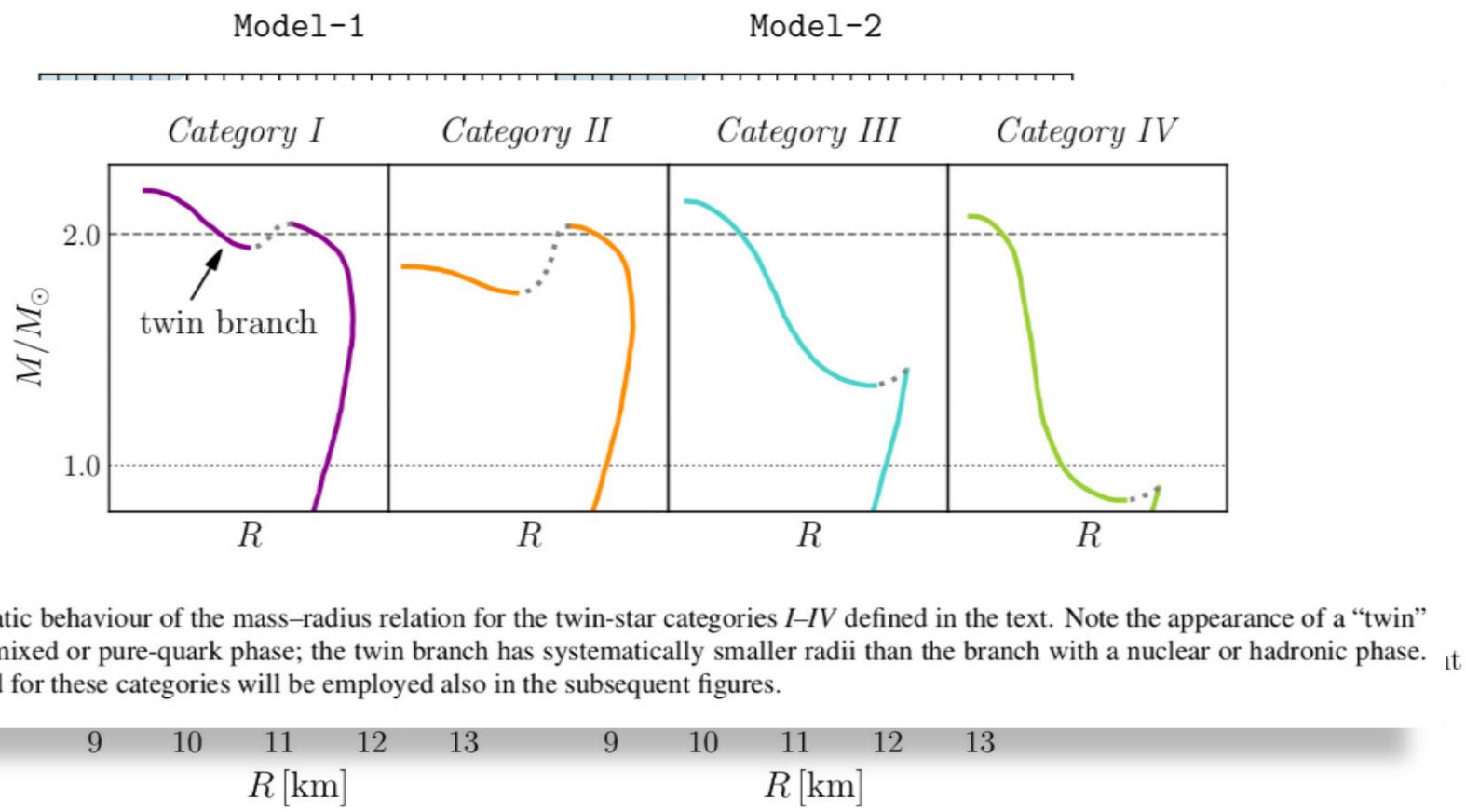

FIG. 3. Schematic behaviour of the mass–radius relation for the twin-star categories *I–IV* defined in the text. Note the appearance of a "twin" branch with a mixed or pure-quark phase; the twin branch has systematically smaller radii than the branch with a nuclear or hadronic phase. The colors used for these categories will be employed also in the subsequent figures.

G. Montana, L.Tolos, M.Hanauske and L.Rezzolla „Constraining twin stars with GW170817„, PRD 99(10), 2019

The inspiral and merger phase *Pre-merger signatures of the hadron-quark phase*

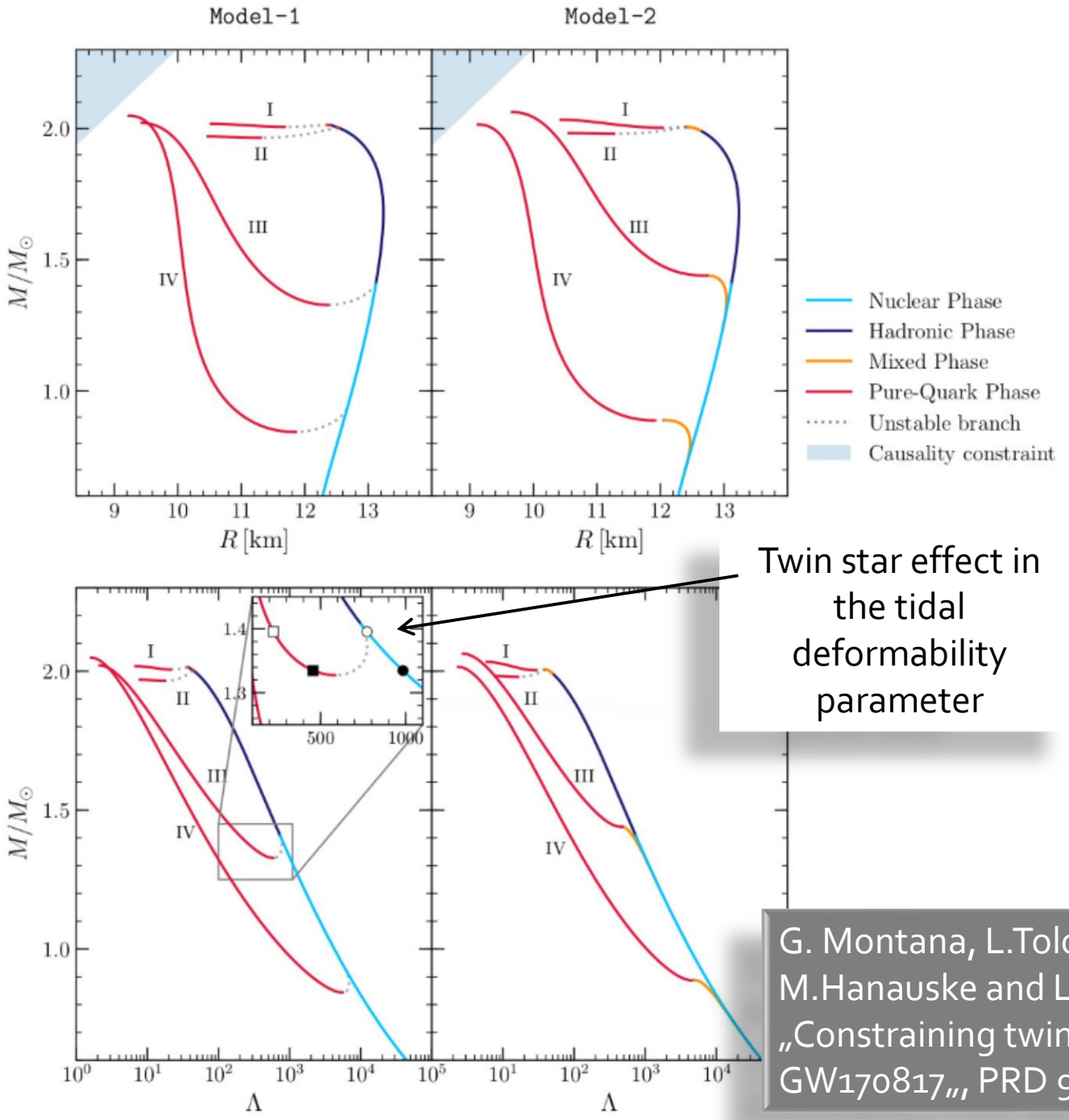

Twin star effect in the tidal deformability parameter

G. Montana, L.Tolos, M.Hanauske and L.Rezzolla „Constraining twin stars with GW170817„, PRD 99(10), 2019

Reference	R_i [km]
Without a phase transition	
Bauswein et al. [42]	$10.68^{+0.15}_{-0.03} \leq R_{1.6}$
Most et al. [51]	$12.00 \leq R_{1.4} \leq 13.45$
Burgio et al. [54]	$11.8 \leq R_{1.5} \leq 13.1$
Tews et al. [55]	$11.3 \leq R_{1.4} \leq 13.6$
De et al. [56]	$8.9 \leq R_{1.4} \leq 13.2$
LIGO/Virgo [57]	$10.5 \leq R_{1.4} \leq 13.3$
With a phase transition	
Annala et al. [46]	$R_{1.4} \leq 13.6$
Most et al. [51]	$8.53 \leq R_{1.4} \leq 13.74$
Burgio et al. [54]	$R_{1.5} = 10.7$
Tews et al. [55]	$9.0 \leq R_{1.4} \leq 13.6$
This work	
NS	$R_{1.4} = 13.11$
HS Model-2	$12.9 \leq R_{1.4} \leq 13.11$
HS Model-1	$10.1 \leq R_{1.4} \leq 12.9$
HS Model-2	$10.4 \leq R_{1.4} \leq 11.9$

Constraints on the radius of neutron stars from r models without a phase transition (top), works con- ossibility of a transition to quark matter (middle) and *ategory III* in the present work (bottom).

Postmerger gravitational-wave signatures of phase transitions in binary compact star mergers

- Introduction
- Numerical general relativity of compact star mergers
- The equation of state of compact star matter and the hadron-quark phase transition
- The different phases of a binary compact star merger event
- Gravitational-wave signatures of the hadron-quark phase transition in binary compact star mergers
  - The inspiral and merger phase (premerger signals)
  - Hypermassive hybrid stars (HMHS) within the prompt phase transition scenario (PPT)
  - HMHS within the delayed phase transition scenario (DPT)
  - HMHS within the phase transition triggered collapse scenario (PTTC)
- Summary and Outlook

Hybrid Star Mergers with T-dependent EOS *(PRL paper 2)*

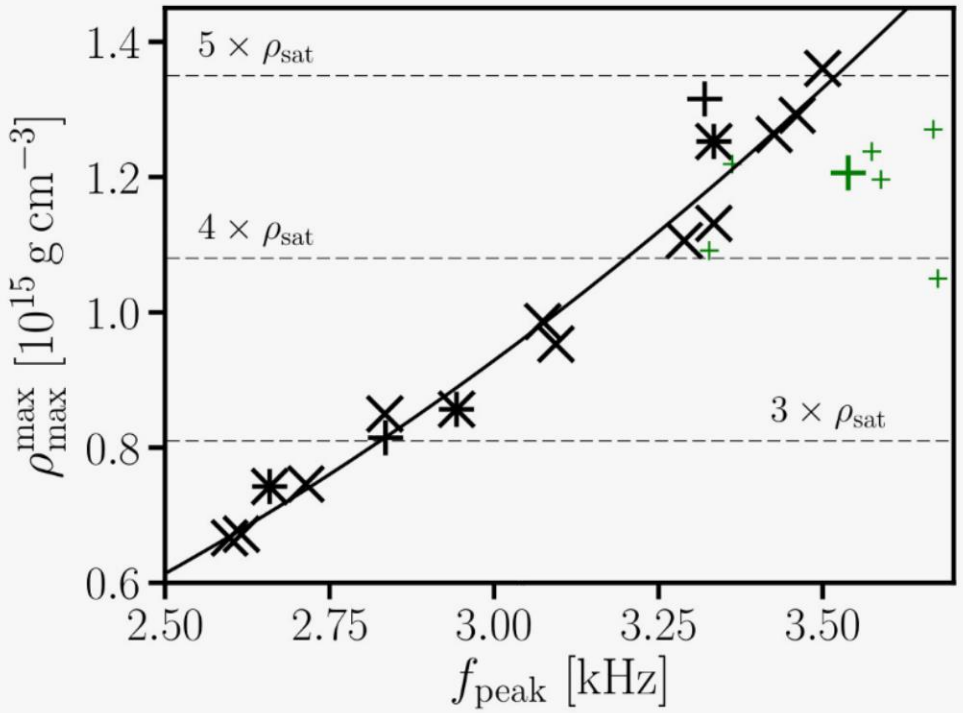

FIG. 4: Maximum rest-mass density $\rho_{\rm max}^{\rm max}$ during the first milliseconds of the postmerger phase as function of the dominant postmerger GW frequency $f_{\rm peak}$ for 1.35-1.35 $M_\odot$ mergers. Green symbols display results for DD2F-SF (big symbol for DD2F-SF-1). Asterisks indicate models with hyperons. Black plus signs display ALF2/4. Solid curve is a second order polynomial least square fit to the data excluding hybrid EOSs.

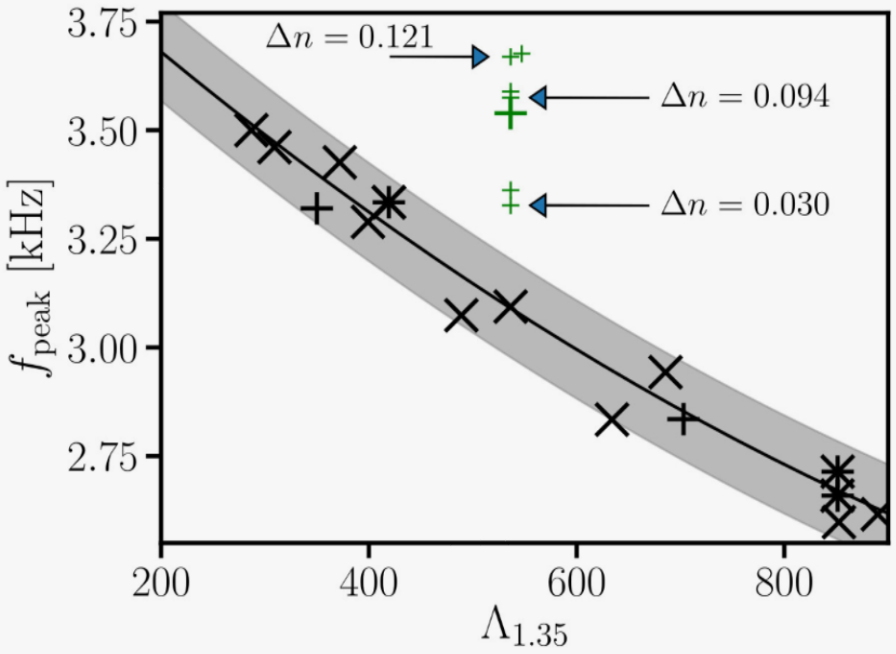

FIG. 3: Dominant postmerger GW frequency $f_{\rm peak}$ as function of tidal deformability Λ for 1.35-1.35 $M_\odot$ mergers. The DD2F-SF models with a phase transition to deconfined quark matter (green symbols) appear as clear outliers (big symbol for DD2F-SF-1). Solid curve displays the least square fit Eq. (1) for all purely hadronic EOSs (including three models with hyperons marked by asterisks). ALF2 and ALF4 are marked by black plus signs. EOSs incompatible with GW170817 are not shown. Arrows mark DD2F-SF models 3, 6 and 7, which feature differently strong density jumps Δn (in fm^{-3}) with roughly the same onset density and stiffness of quark matter.

Post-merger gravitational-wave signatures of phase transitions in binary compact star mergers

PRL 124, 171103 (2020)

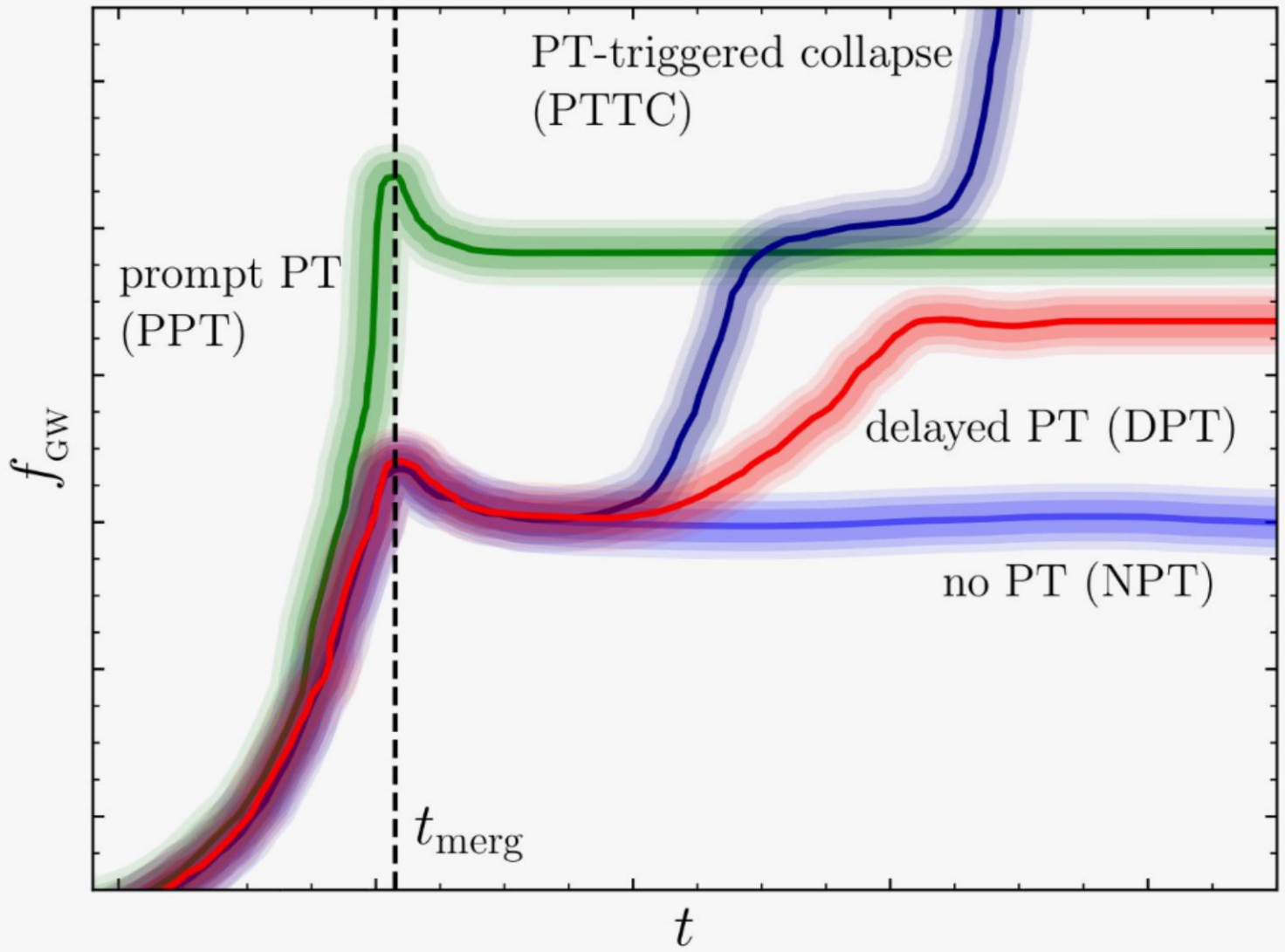

Schematic overview of the instantaneous gravitational wave frequency and how its evolution can be used to classify the different scenarios associated with a hadron-quark phase transition.

Post-merger gravit
of phase transitions in
PRL 124

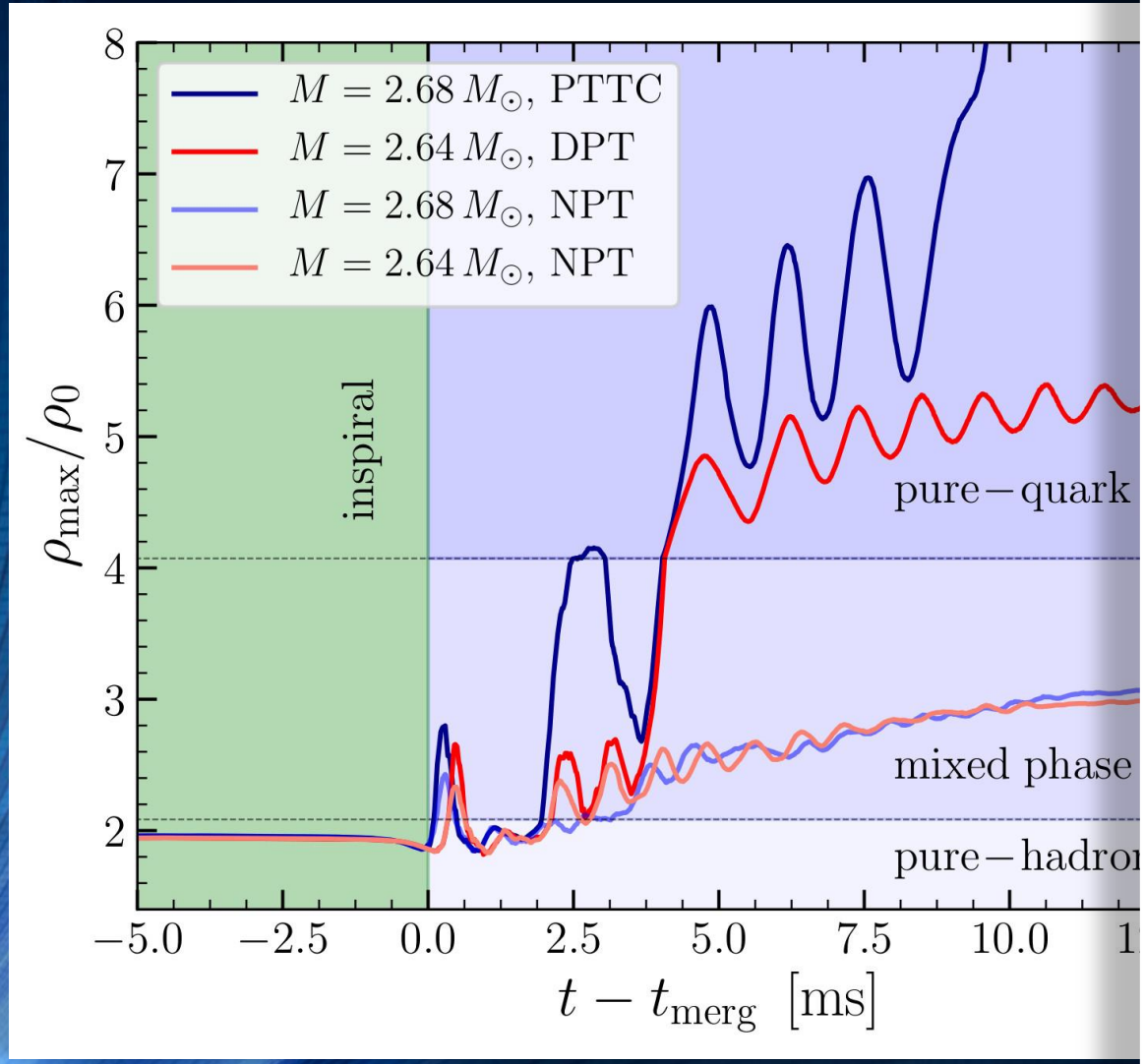

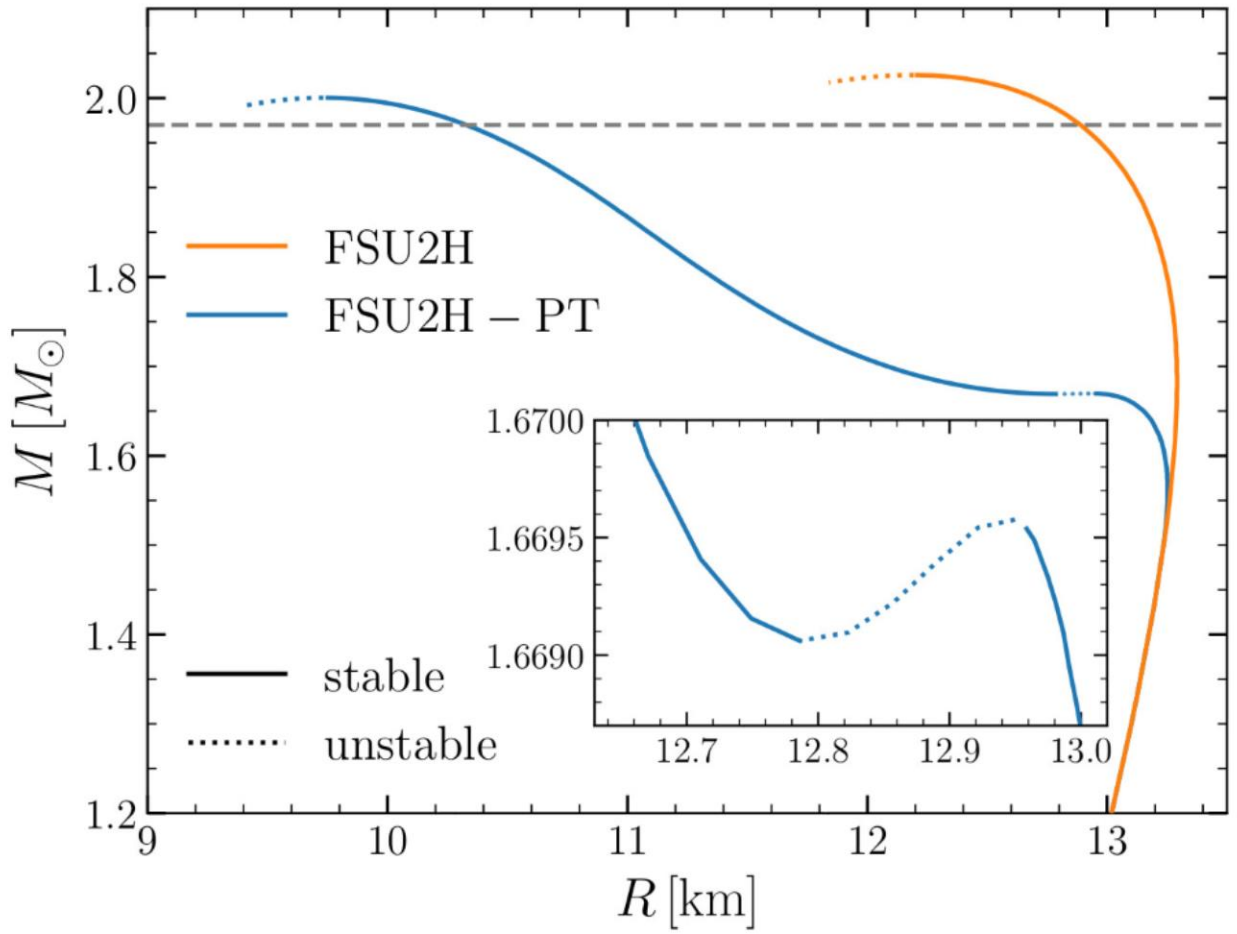

FIG. 1. Mass-radius relation for the purely hadronic EOS (FSU2H) and its modified version (FSU2H−PT). The latter shows a second stable (solid lines) branch after a small region of instability (dotted). The grey dashed line marks the limit of $1.97\,M_\odot$.

Postmerger gravitational-wave signatures of phase transitions in binary compact star mergers

- Introduction
- Numerical general relativity of compact star mergers
- The equation of state of compact star matter and the hadron-quark phase transition
- The different phases of a binary compact star merger event
- Gravitational-wave signatures of the hadron-quark phase transition in binary compact star mergers
  - The inspiral and merger phase (premerger signals)
  - Hypermassive hybrid stars (HMHS) within the prompt phase transition scenario (PPT)
  - HMHS within the delayed phase transition scenario (DPT)
  - HMHS within the phase transition triggered collapse scenario (PTTC)
- Summary and Outlook

Metastable hypermassive hybrid stars as neutron-star merger remnants

A case study

Matthias Hanauske[1,2,a], Lukas R. Weih[2], Horst Stöcker[1,2,3], and Luciano Rezzolla[2,4,5]

[1] Frankfurt Institute for Advanced Studies, Ruth-Moufang-Straße 1, 60438 Frankfurt, Germany
[2] Institut für Theoretische Physik, Max-von-Laue-Straße 1, 60438 Frankfurt, Germany
[3] GSI Helmholtzzentrum für Schwerionenforschung GmbH, 64291 Darmstadt, Germany
[4] School of Mathematics, Trinity College, Dublin 2, Ireland
[5] Helmholtz Research Academy Hesse for FAIR, Max-von-Lau

Abstract. Hypermassive hybrid stars (HMHS) are
jects that could be produced in the merger of a binar
In contrast to their purely hadronic counterparts, h
(HMNS), these highly differentially rotating objects

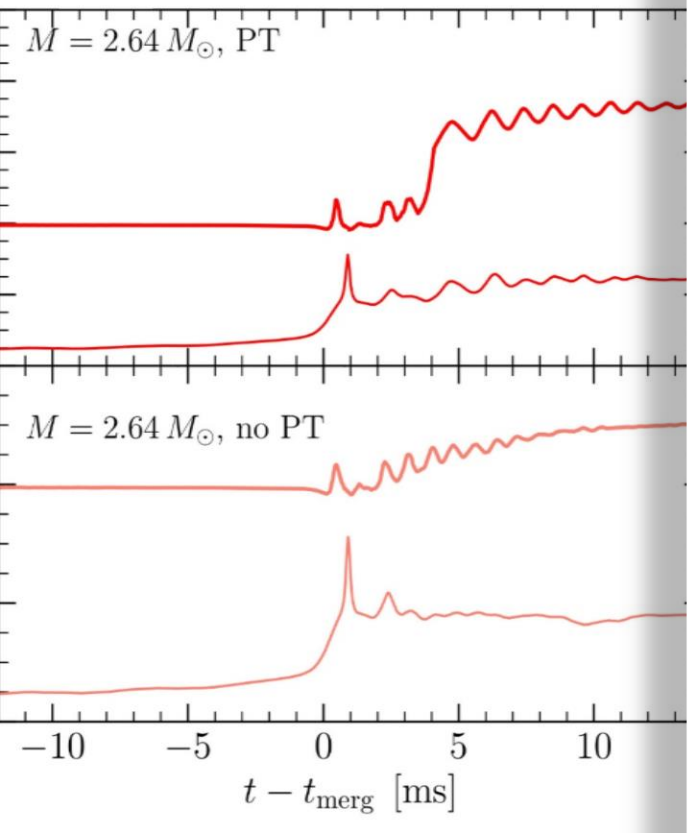

Article submitted
(under review)

EPJ Special Topics on
"Nuclear Astrophysics
in Our Time:
Supernovae, Neutron
Stars and Binary
Neutron Star Mergers"

The delayed phase transition scenario DPT

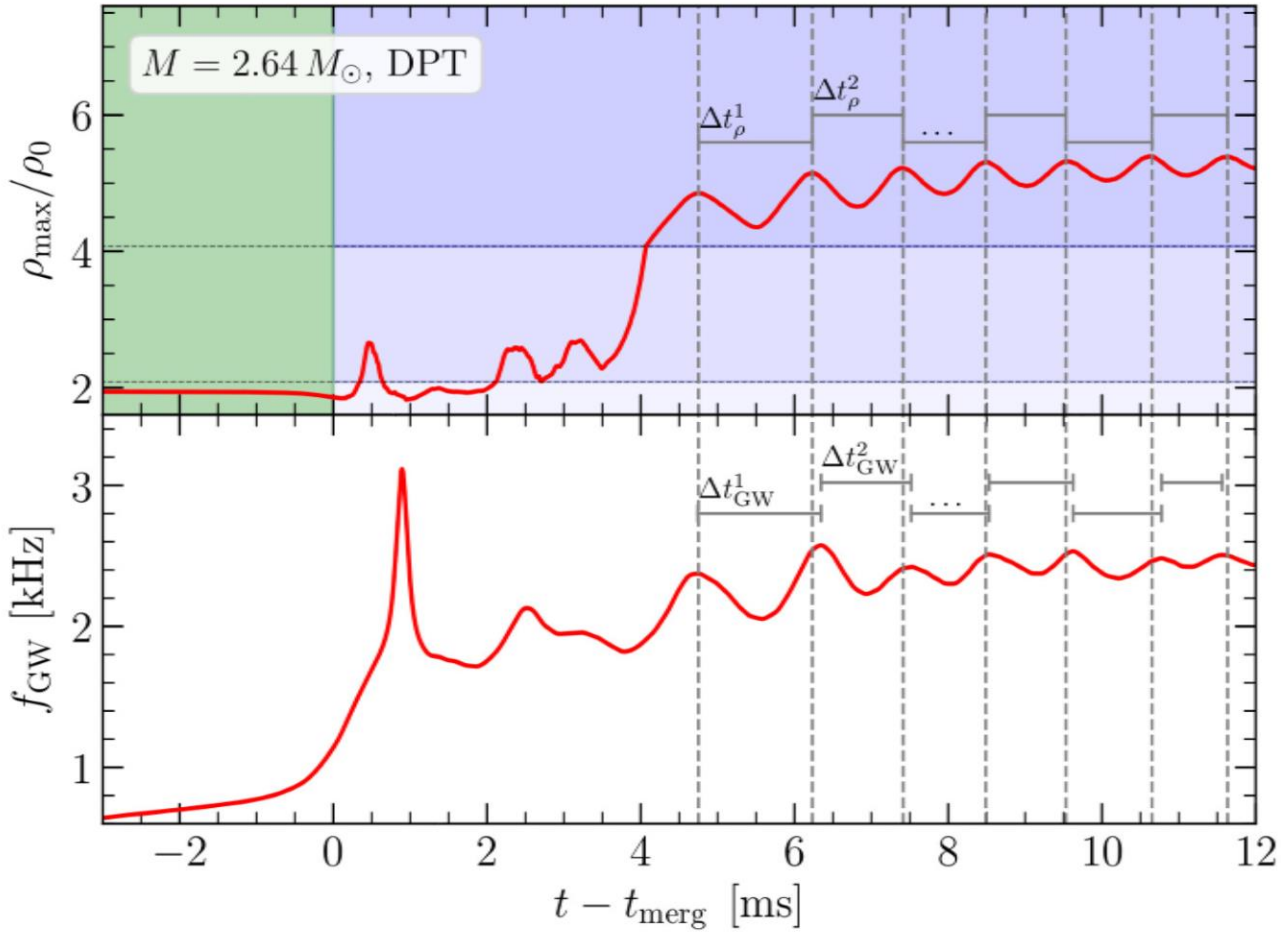

Fig. 3. *Top:* Same as Fig. 1. *Bottom:* Instantaneous GW frequency. The time intervals Δt_ρ^i and $\Delta t_{\rm GW}^i$ between consecutive peaks in the top and bottom panel, respectively, are marked by horizontal grey lines. The average difference between the two different types of peaks is less than 5%.

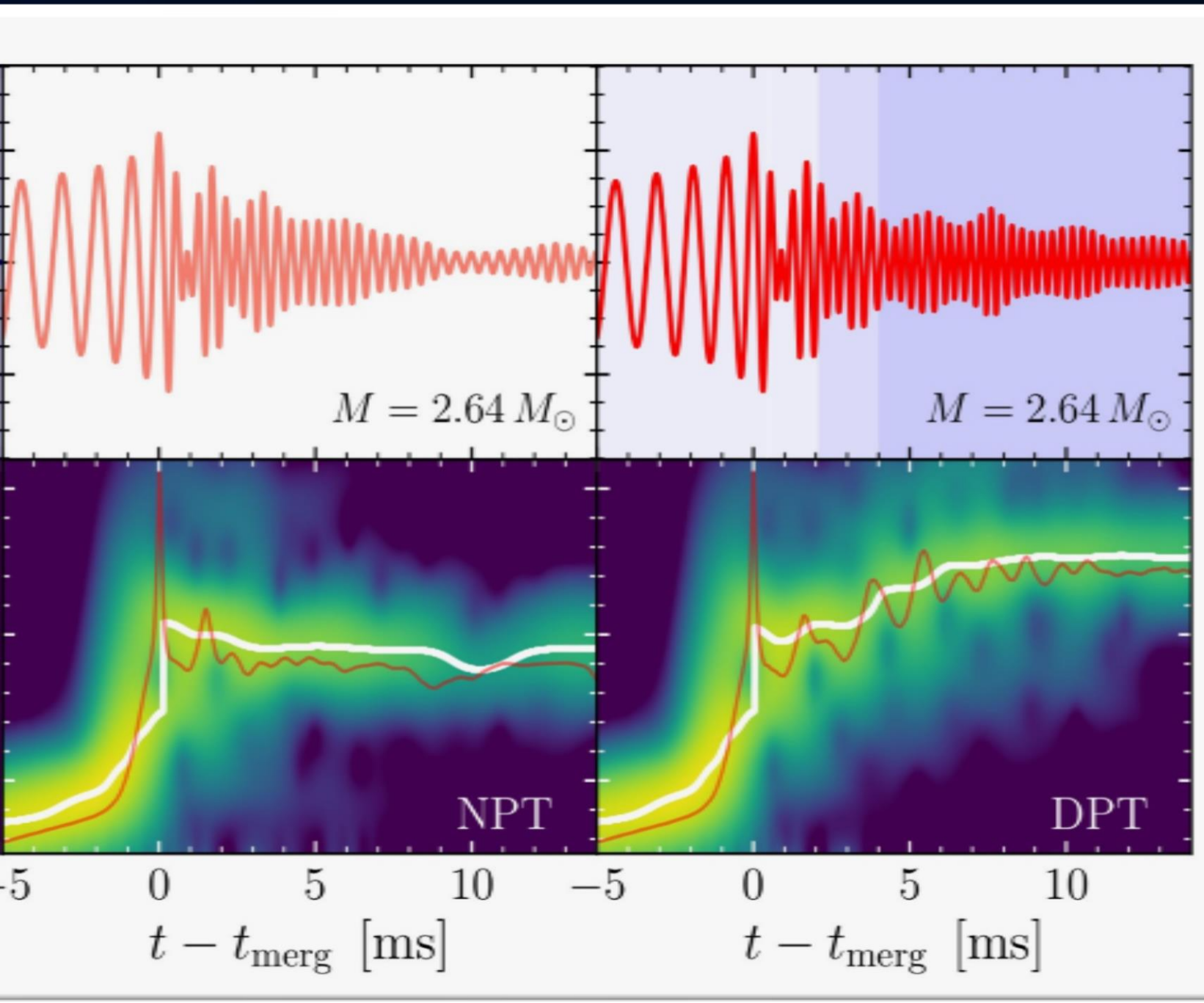

Strain h+ (top) and its spectrogram (bottom) for the binary neutron star simulation of the delayed phase transition scenario. In the top panel the different shadings mark the times when the HMNS core enters the mixed and pure quark phases.. In the bottom panels, the white lines trace the maximum of the spectrograms, while the red lines show the instantaneous gravitational-wave frequency.

Density and temperature evolution inside the HMHS

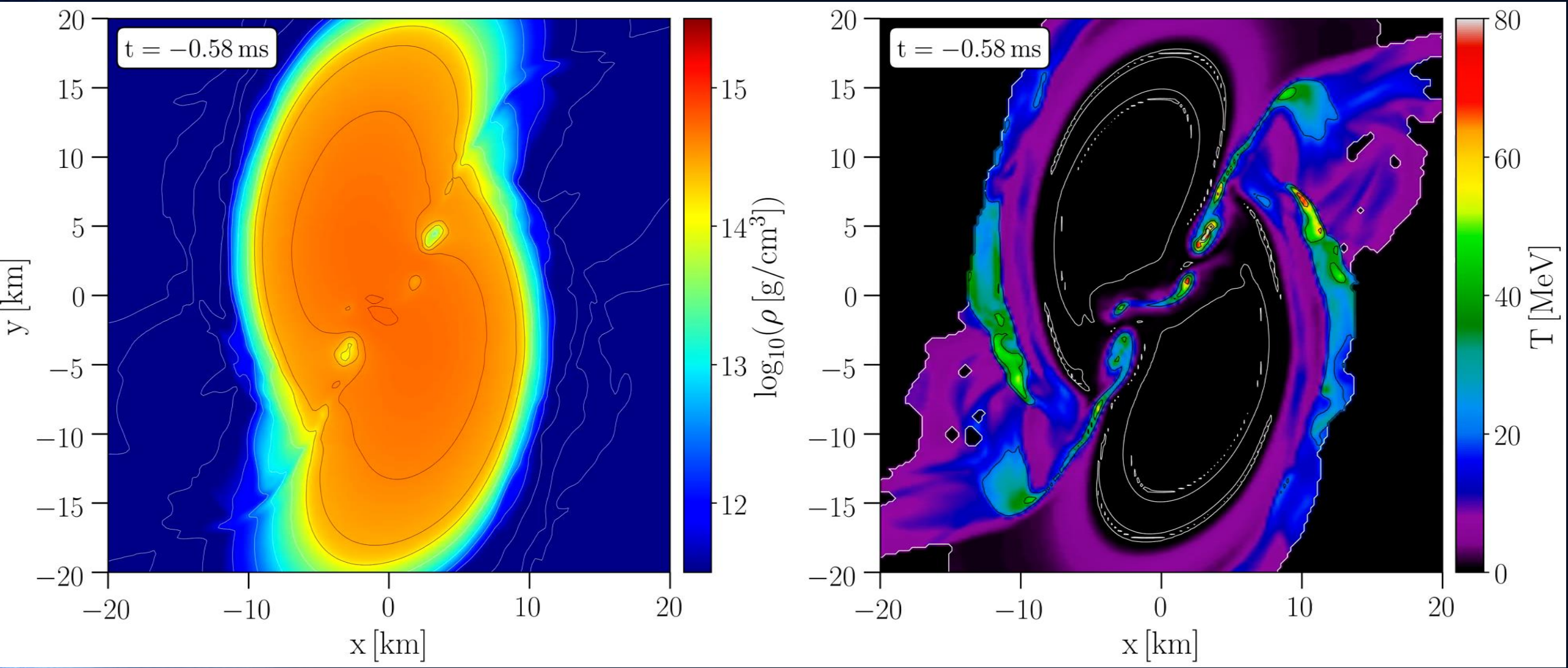

EOS: FSU2H-PT + thermal ideal fluid, Mass: 1.32 M_{solar}

Binary Neutron Star Mergers in the QCD Phase Diagram

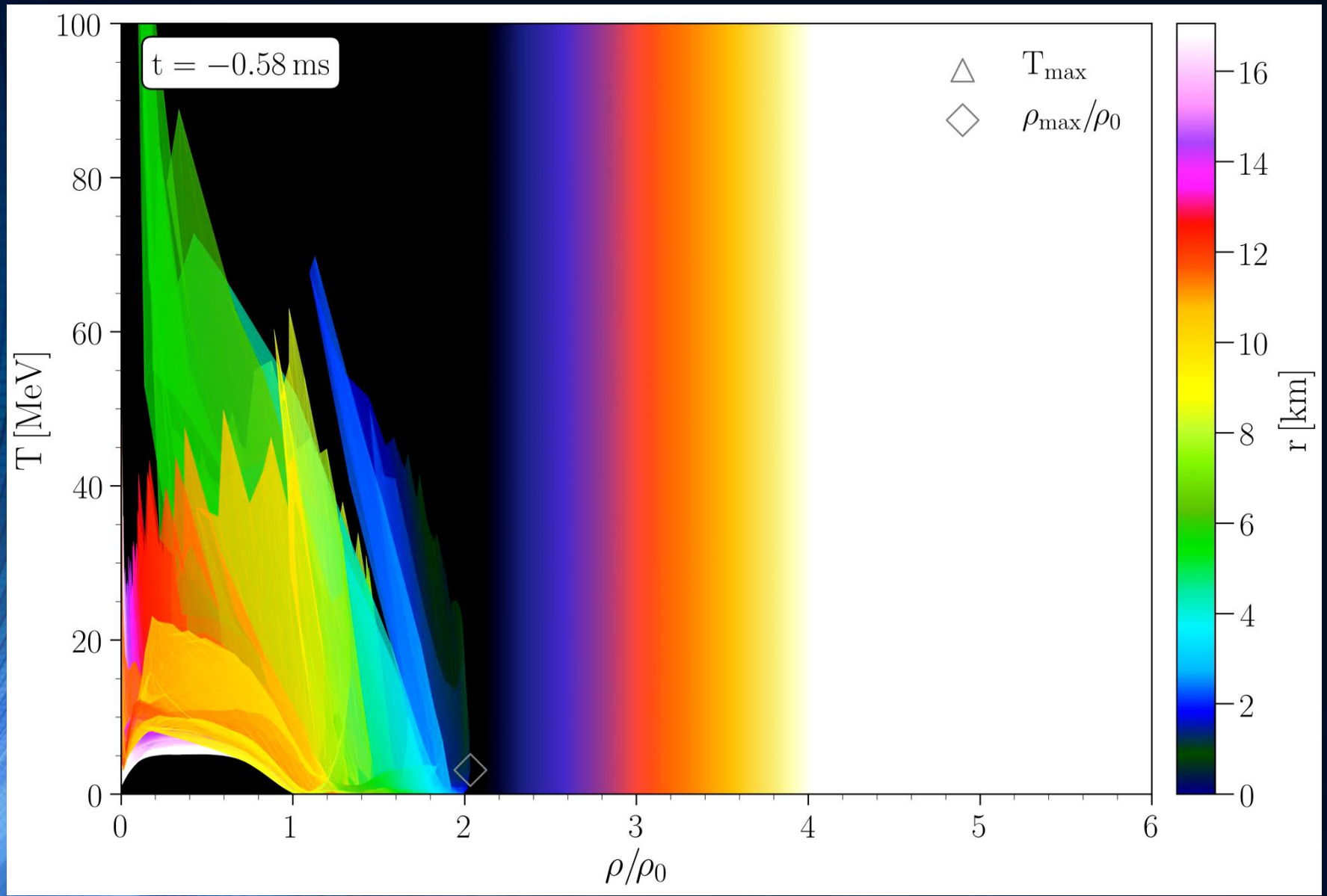

Evolution of hot and dense matter inside the inner area of a hypermassive hybrid star simulated within the (FSU2H-PT + thermal ideal fluid) EOS with a total mass of $M_{total}=2.64\ M_{solar}$ in the style of a (T- ρ) QCD phase diagram plot

The color-coding indicate the radial position r of the corresponding (T- ρ) fluid element measured from the origin of the simulation (x , y) = (o , o) on the equatorial plane at z = o.

The open triangle marks the maximum value of the temperature while the open diamond indicates the maximum of the density.

These figures show the configuration of the HMHS at a time right before the collapse to the more compact star. The small asymmetry in the density profile and especially the double-core structure is amplified by the collapse resulting in a large one-sided asymmetry (i.e., an m = 1 asymmetry in a spherical-harmonics decomposition), which triggers a sizeable h21 GW strain.

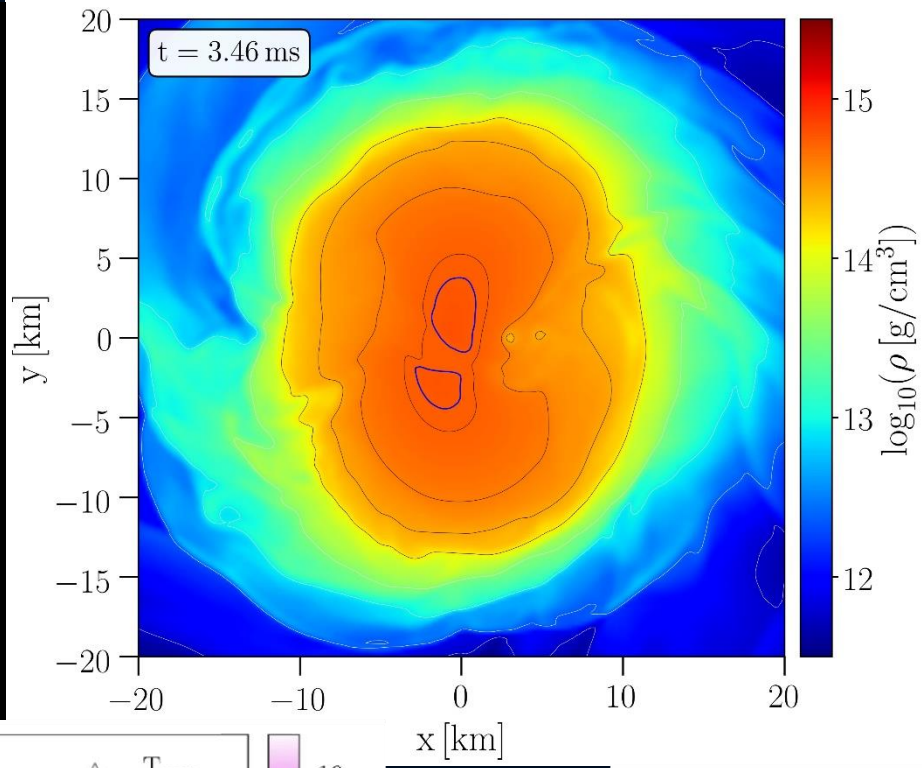

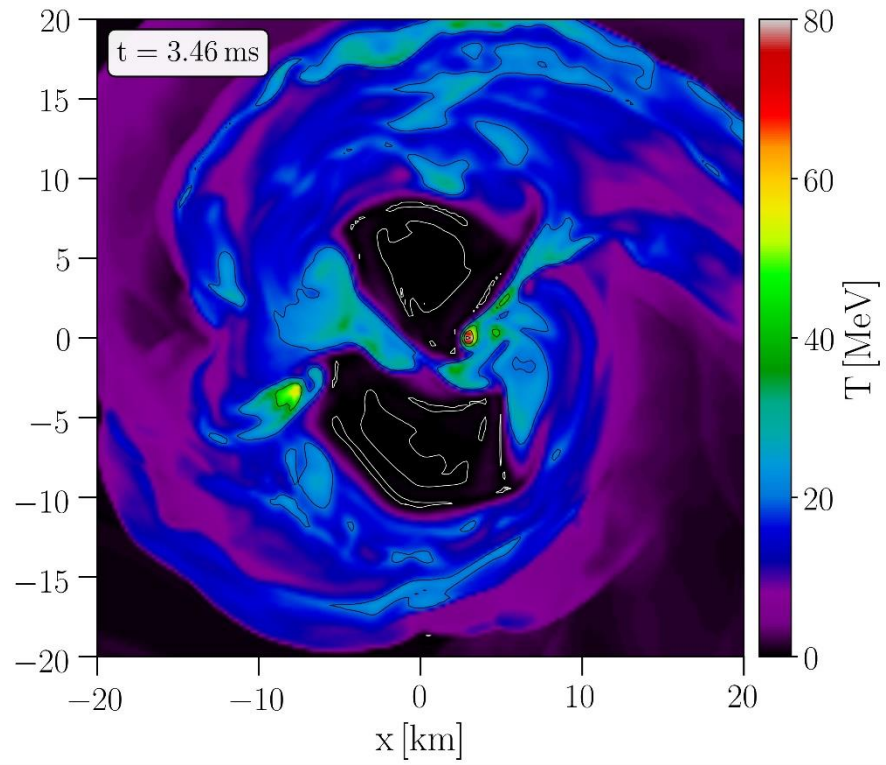

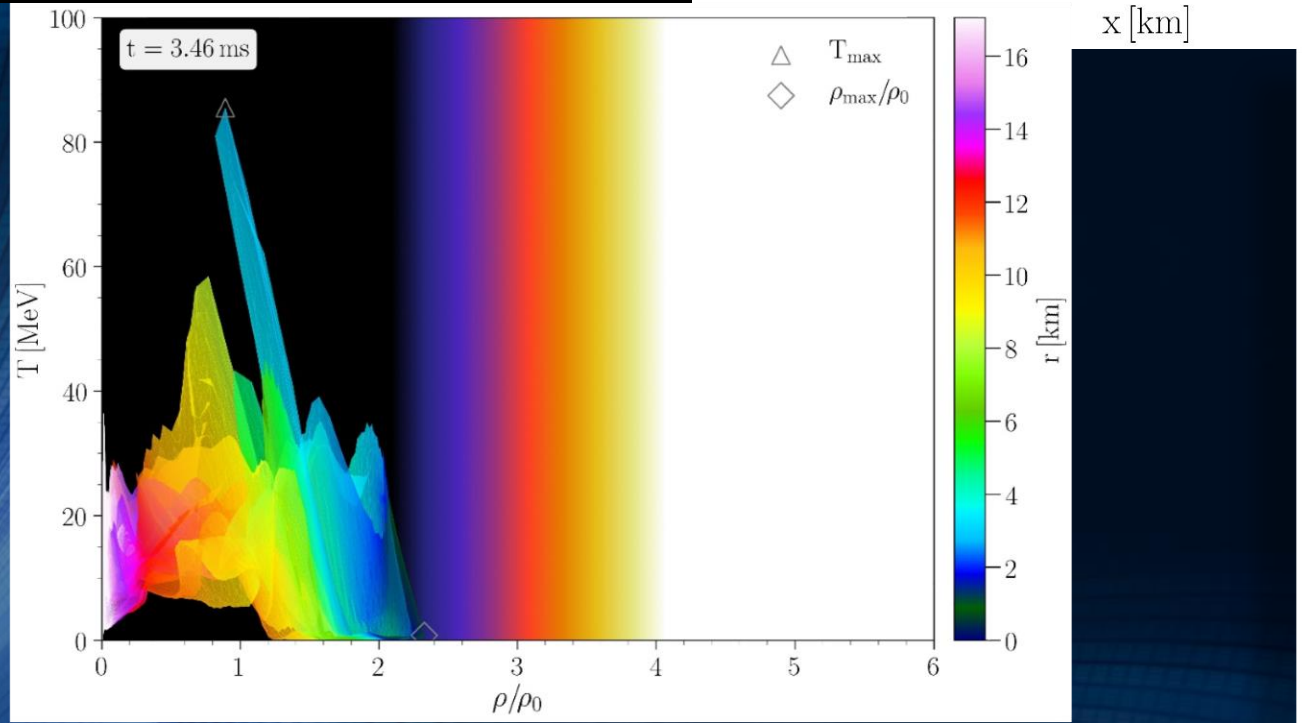

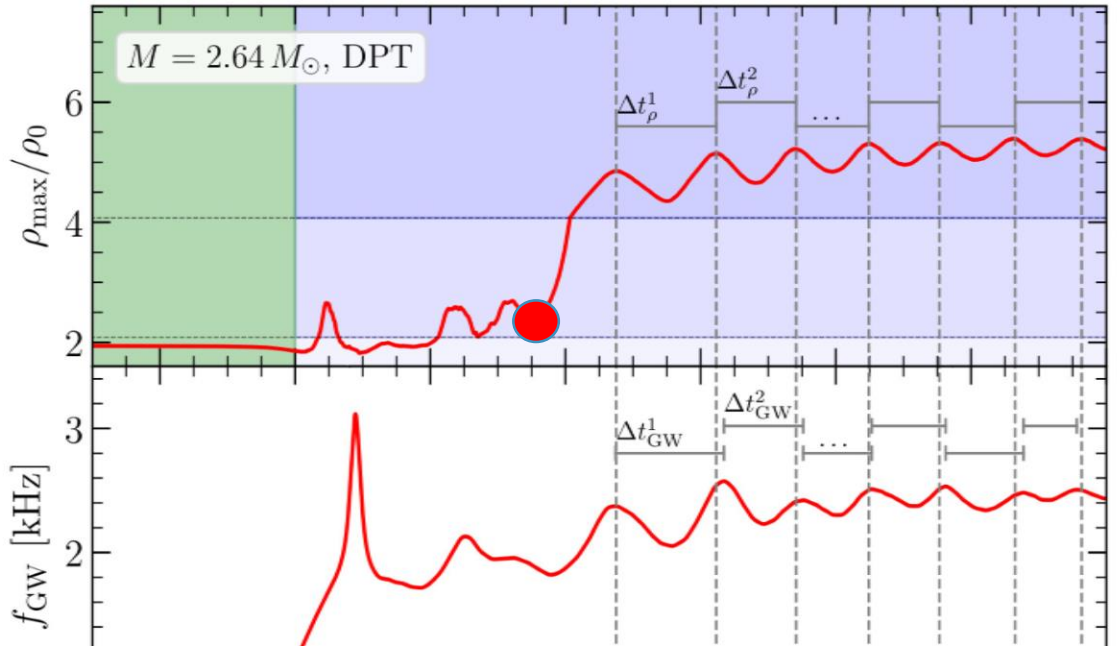

The figures correspond to a time near the first density maximum at t = 4.8ms (see red marker). The large m = 1 contribution can be seen by looking at the asymmetry of the spatial location of the quark core, which is marked with the second blue contour line. As a result of this asymmetry, the location of the two temperature are at different radial distances from the grid center.

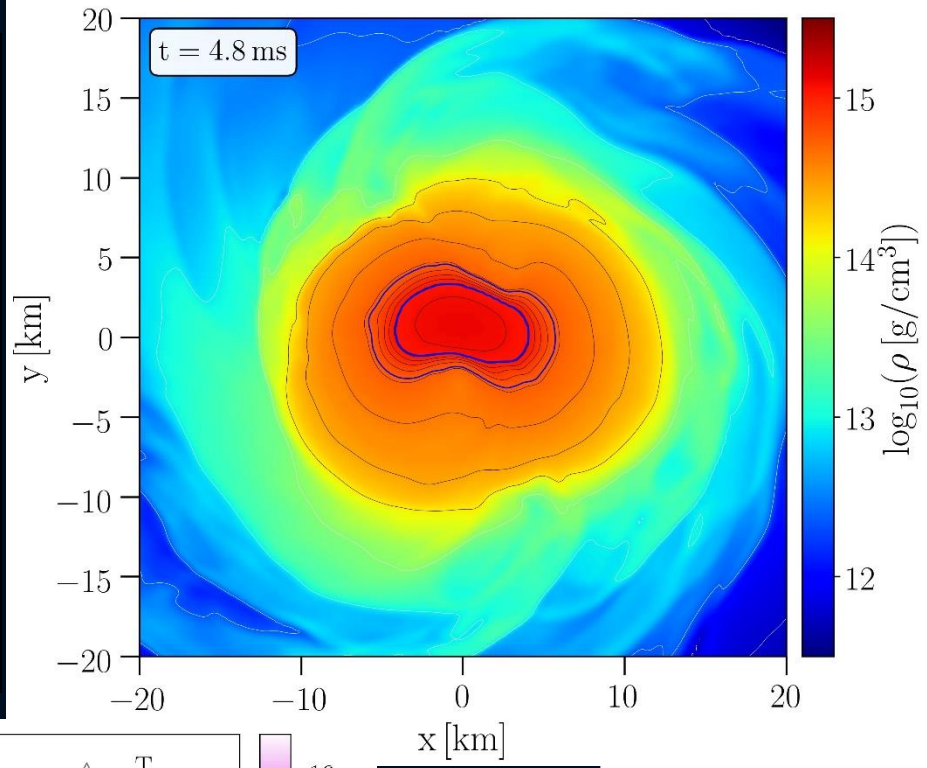

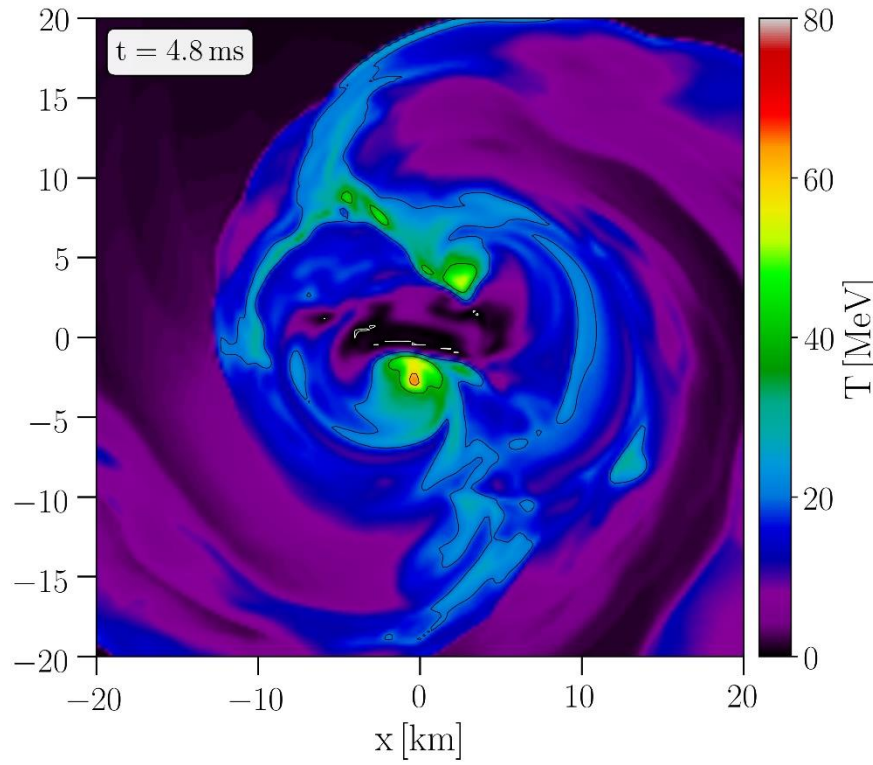

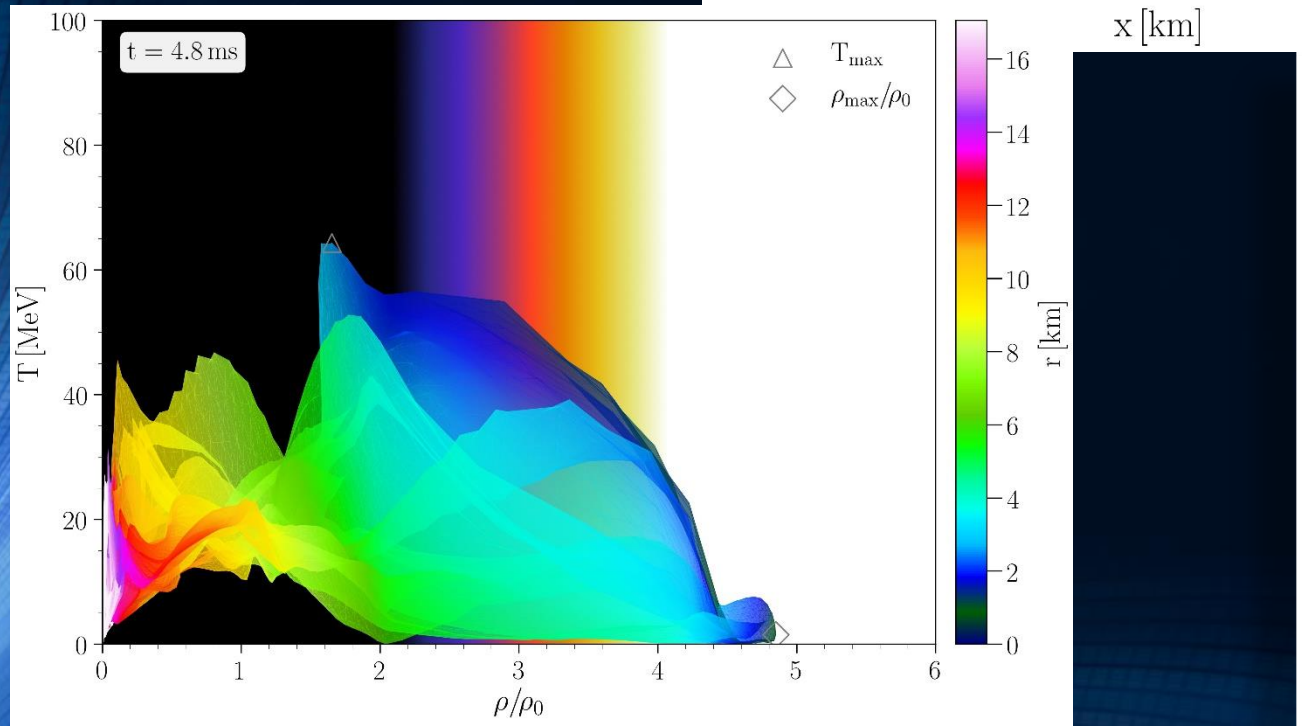

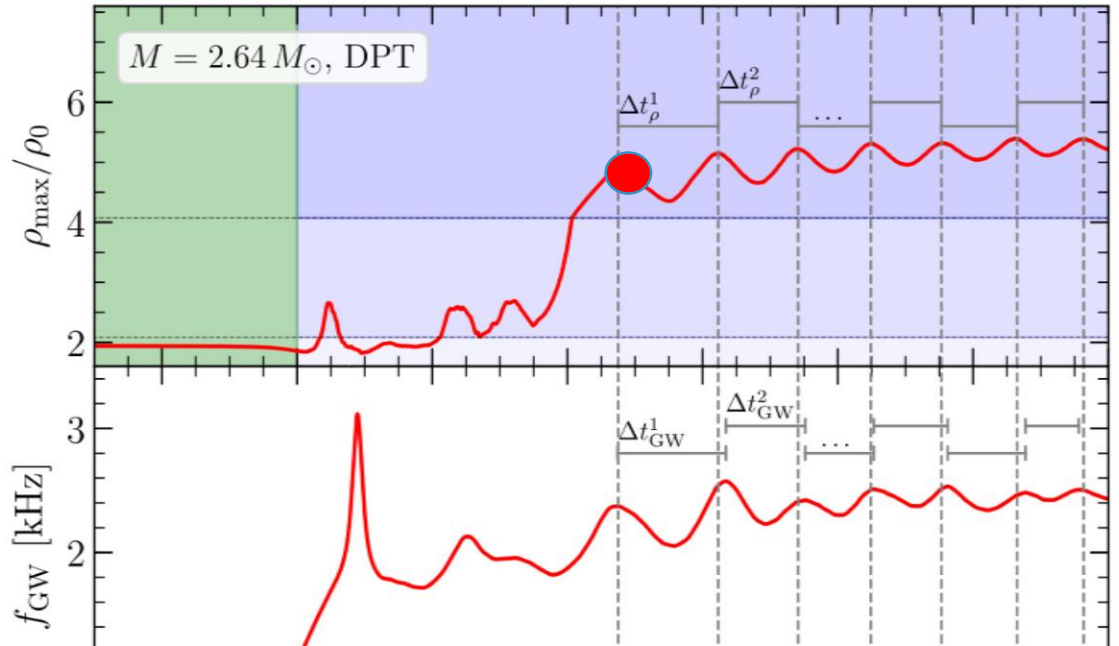

The figures correspond to a time near the first density minimum at t = 5.52ms (see red marker). The large m = 1 contribution can be seen by looking at the asymmetry of the spatial location of the quark core, which is marked with the second blue contour line. As a result of this asymmetry, the location of the two temperature are at different radial distances from the grid center.

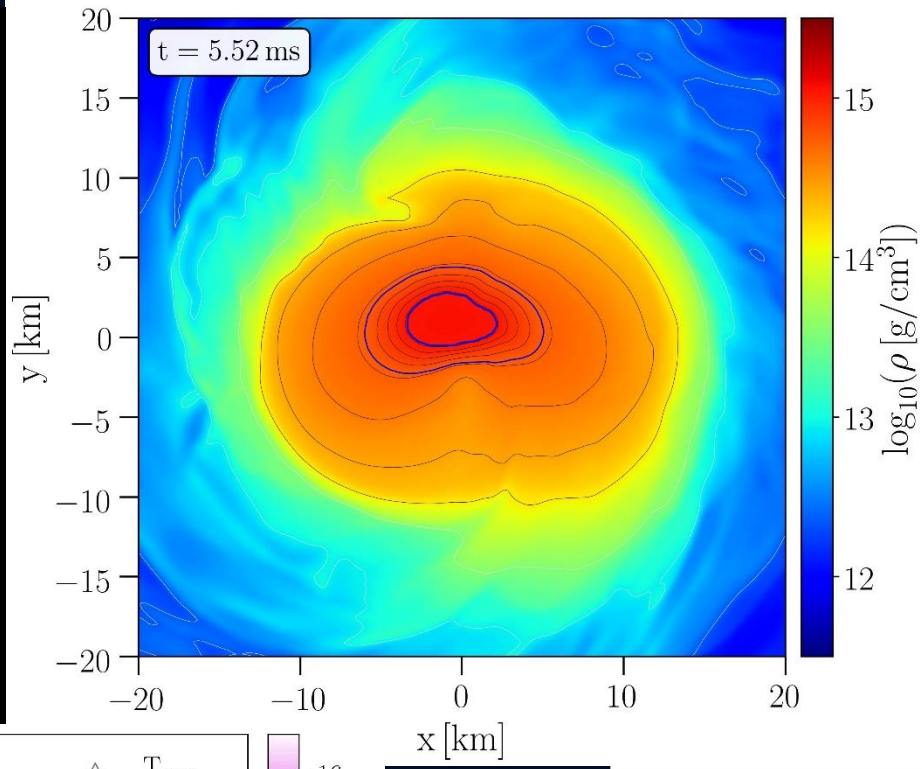

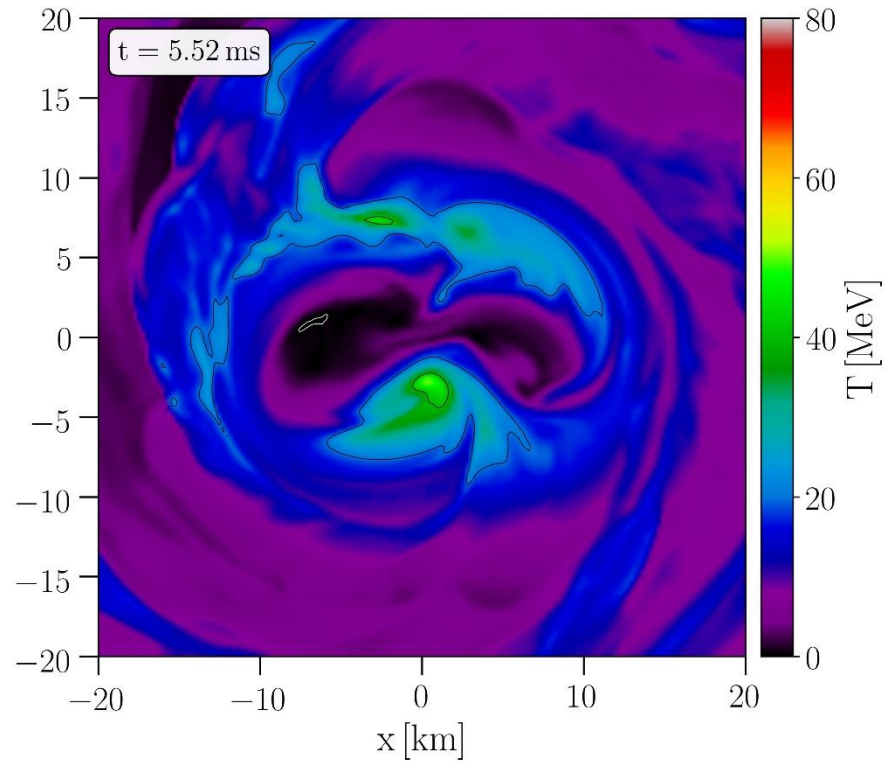

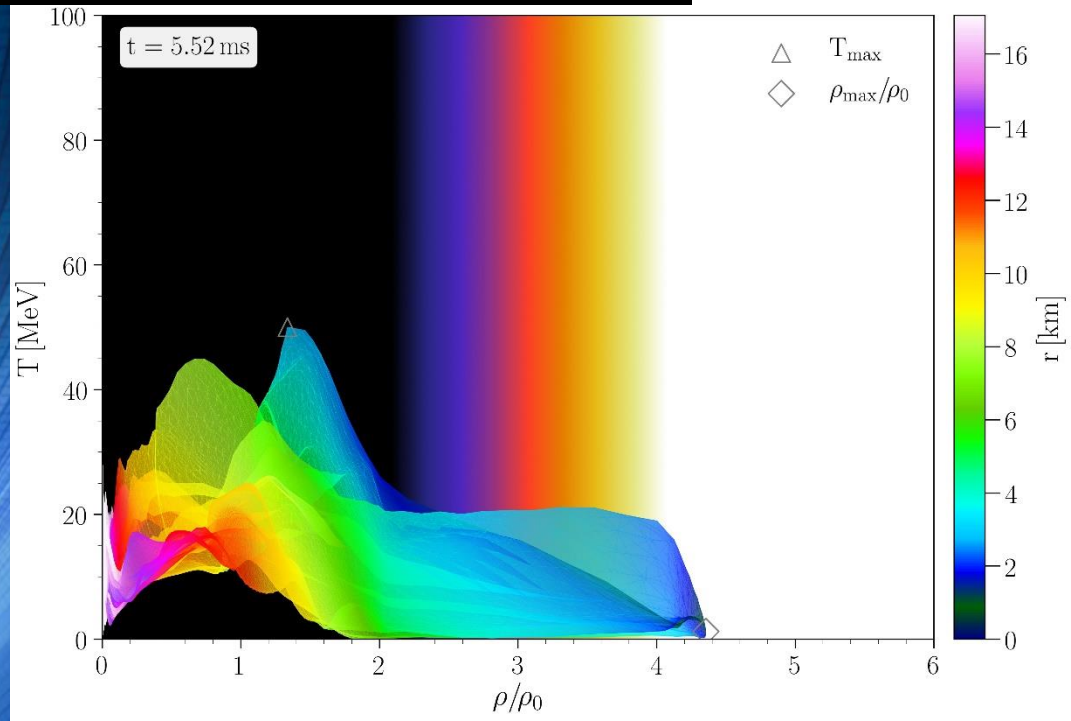

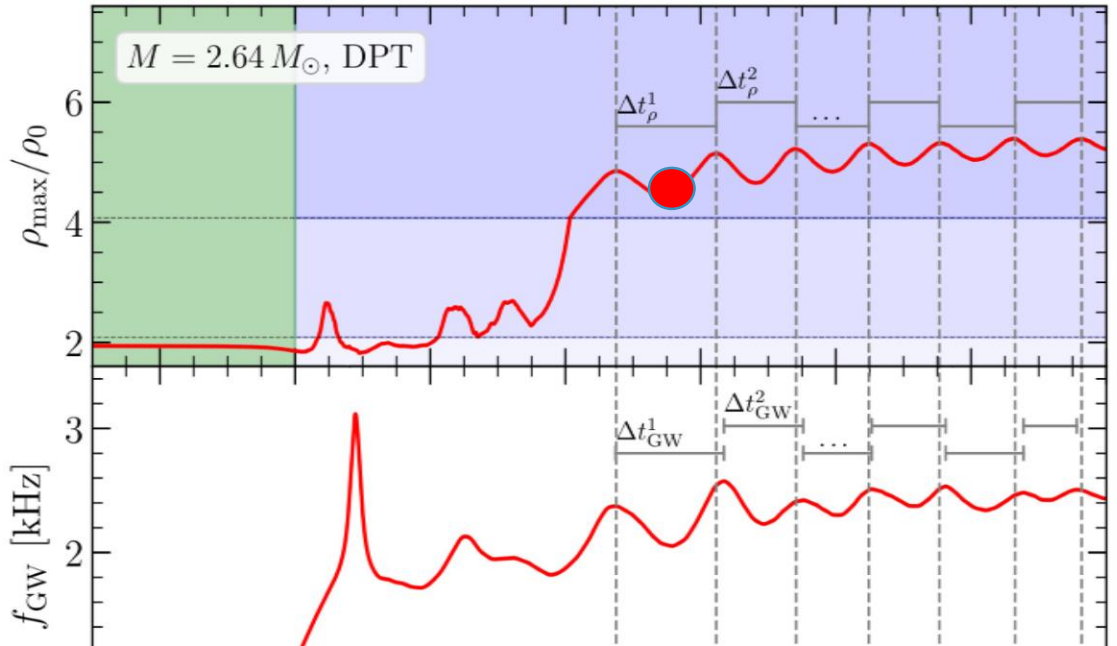

The collapse of the HMNS to the HMHS causes the system to vibrate. At the times when the maximum of the central density is reached, the pure quark core with its stiffer equation of state presses violently against the gravitational pressure and the star expands again and, as a result, its central density decreases.

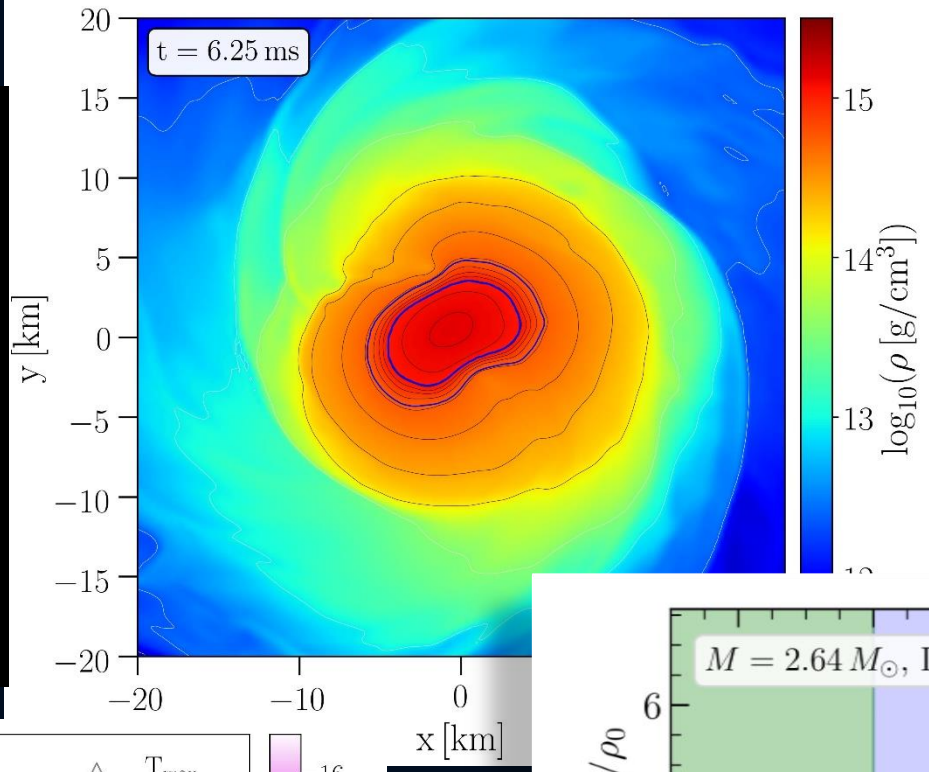

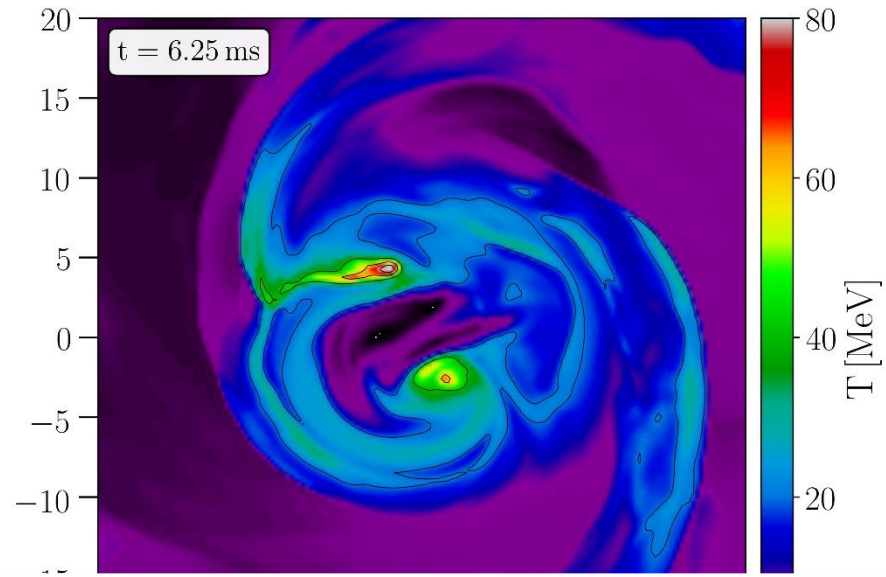

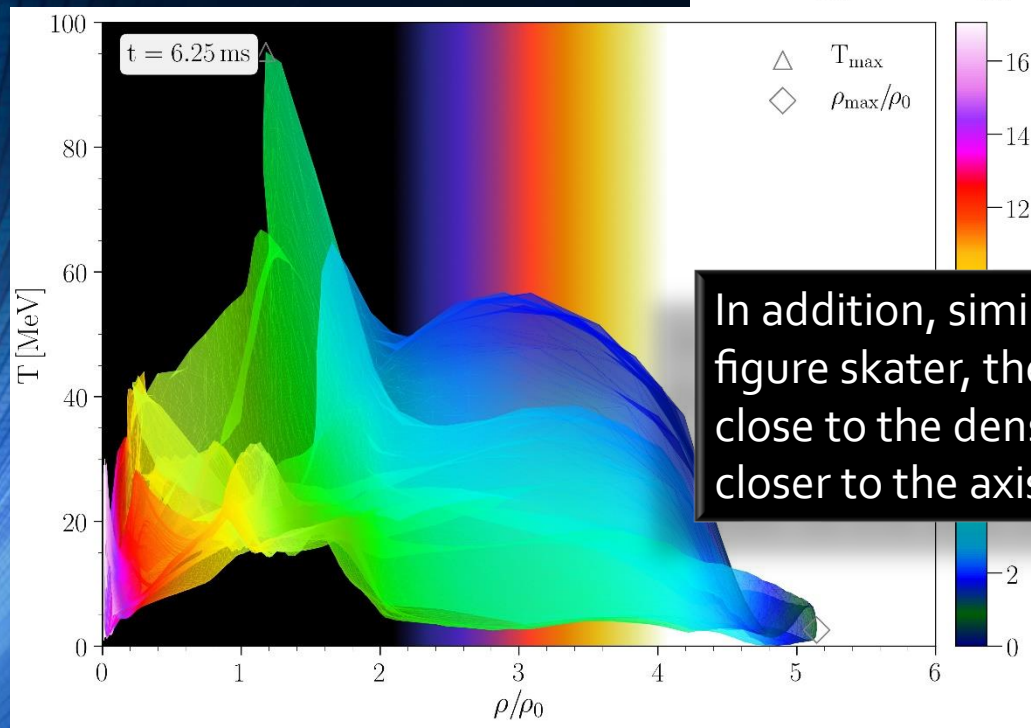

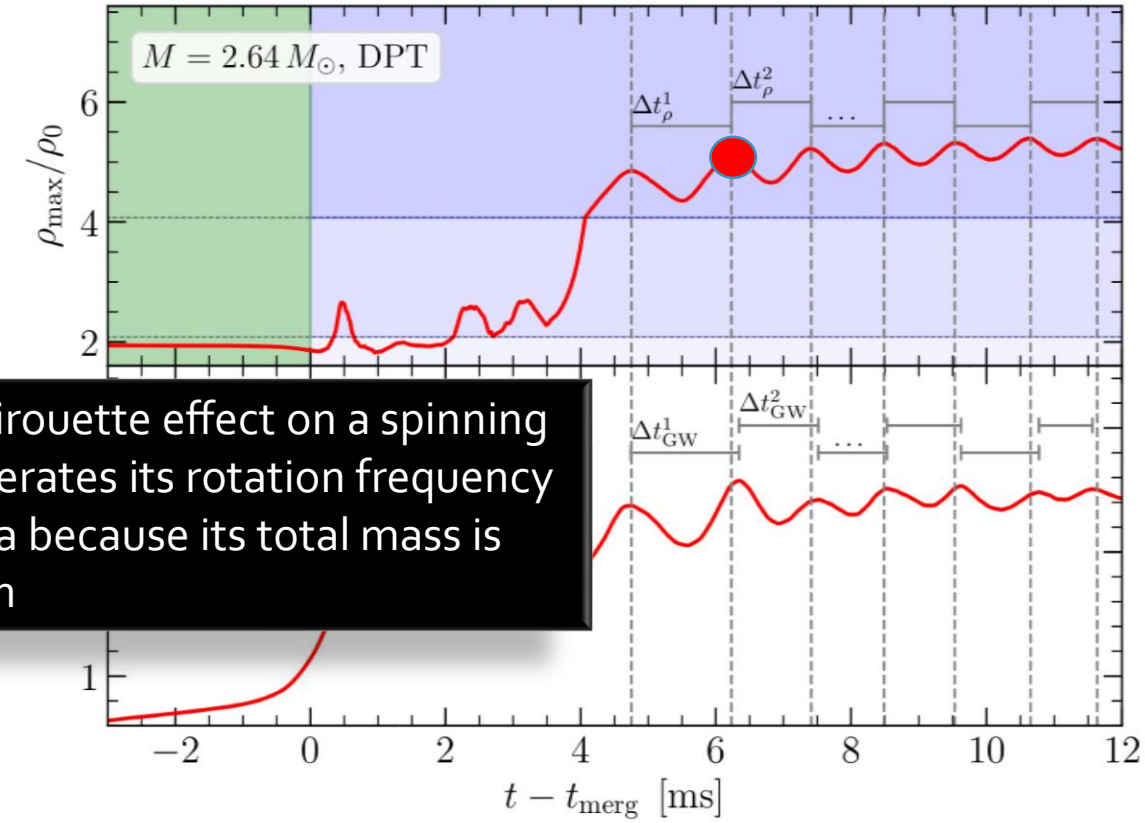

In addition, similar to the pirouette effect on a spinning figure skater, the star accelerates its rotation frequency close to the density maxima because its total mass is closer to the axis of rotation

These figures report the HMHS properties at t = 13.15ms and shows that in addition to the two temperature hot-spots, a new high temperature shell surrounding a cold core appears within the mixed phase region of the remnant . For subsequent post-merger times, the two temperature hot-spots will be smeared out to become a ring like structure on the equatorial plane

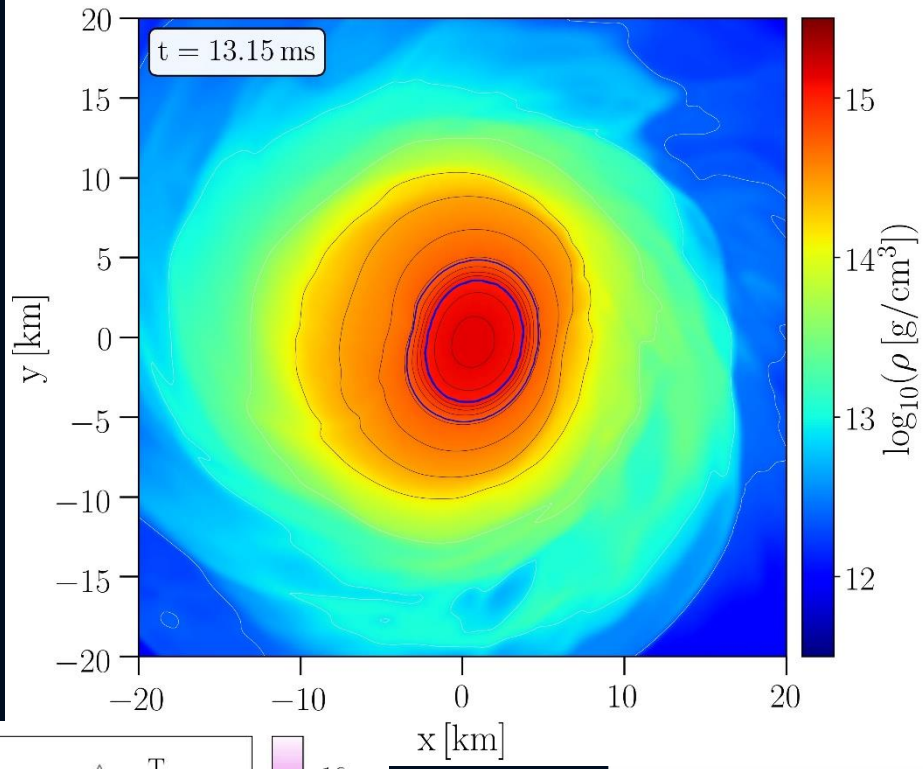

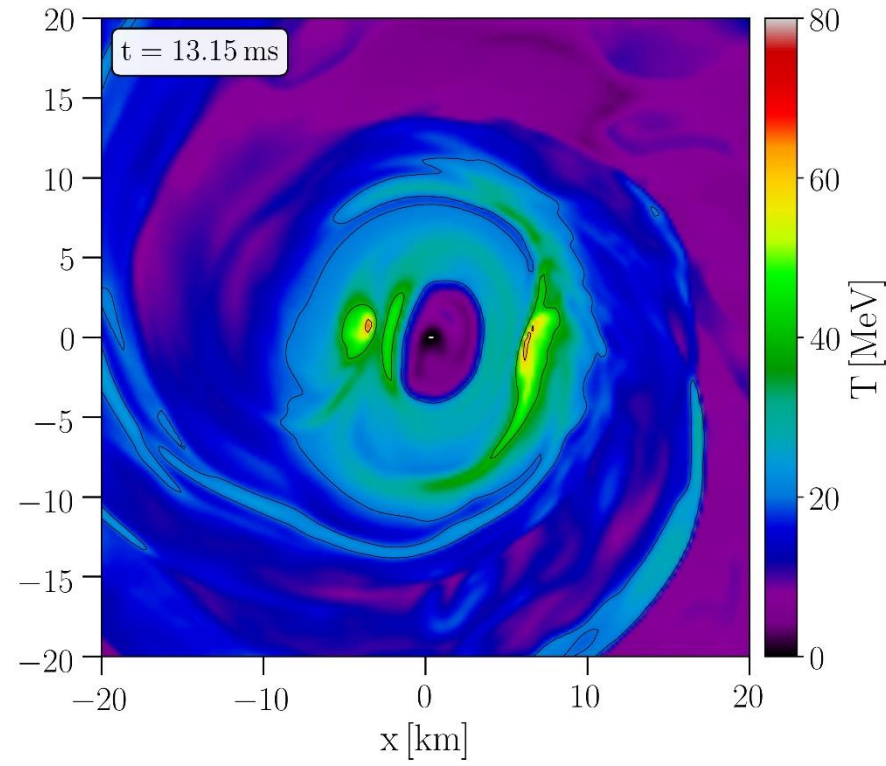

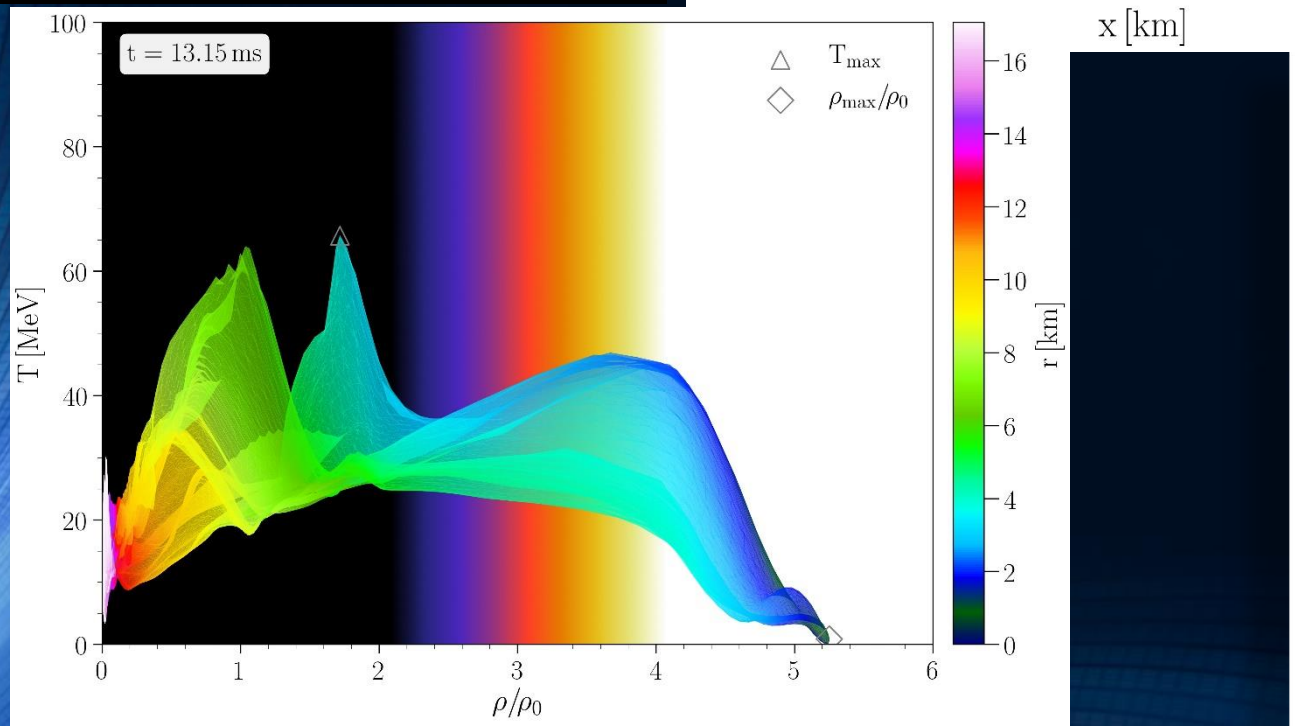

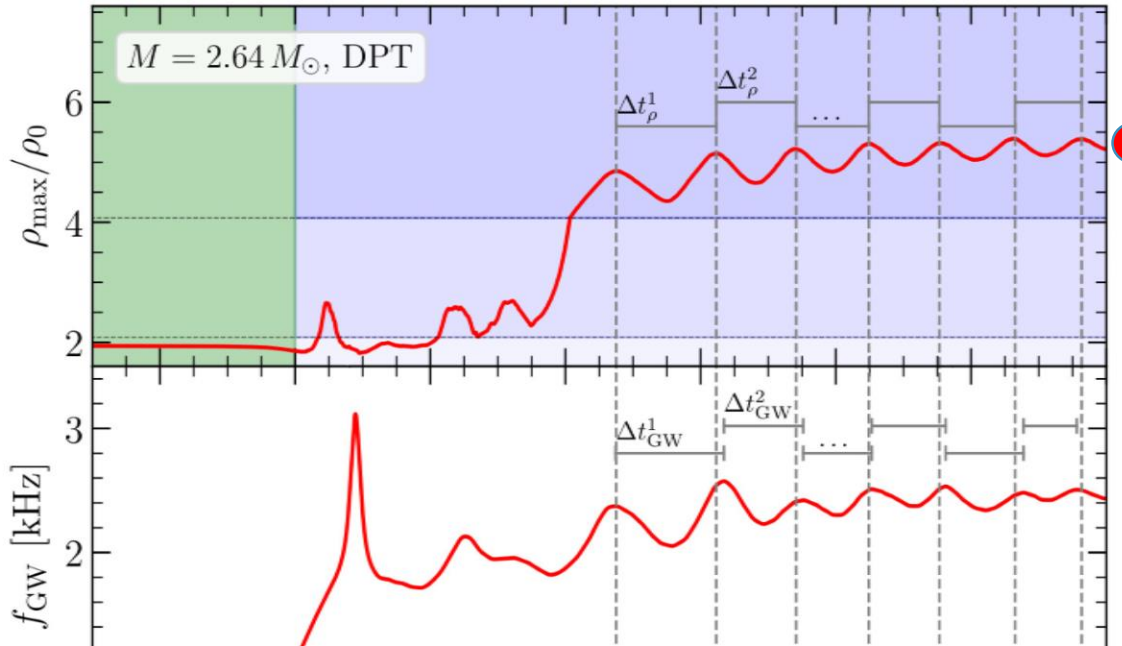

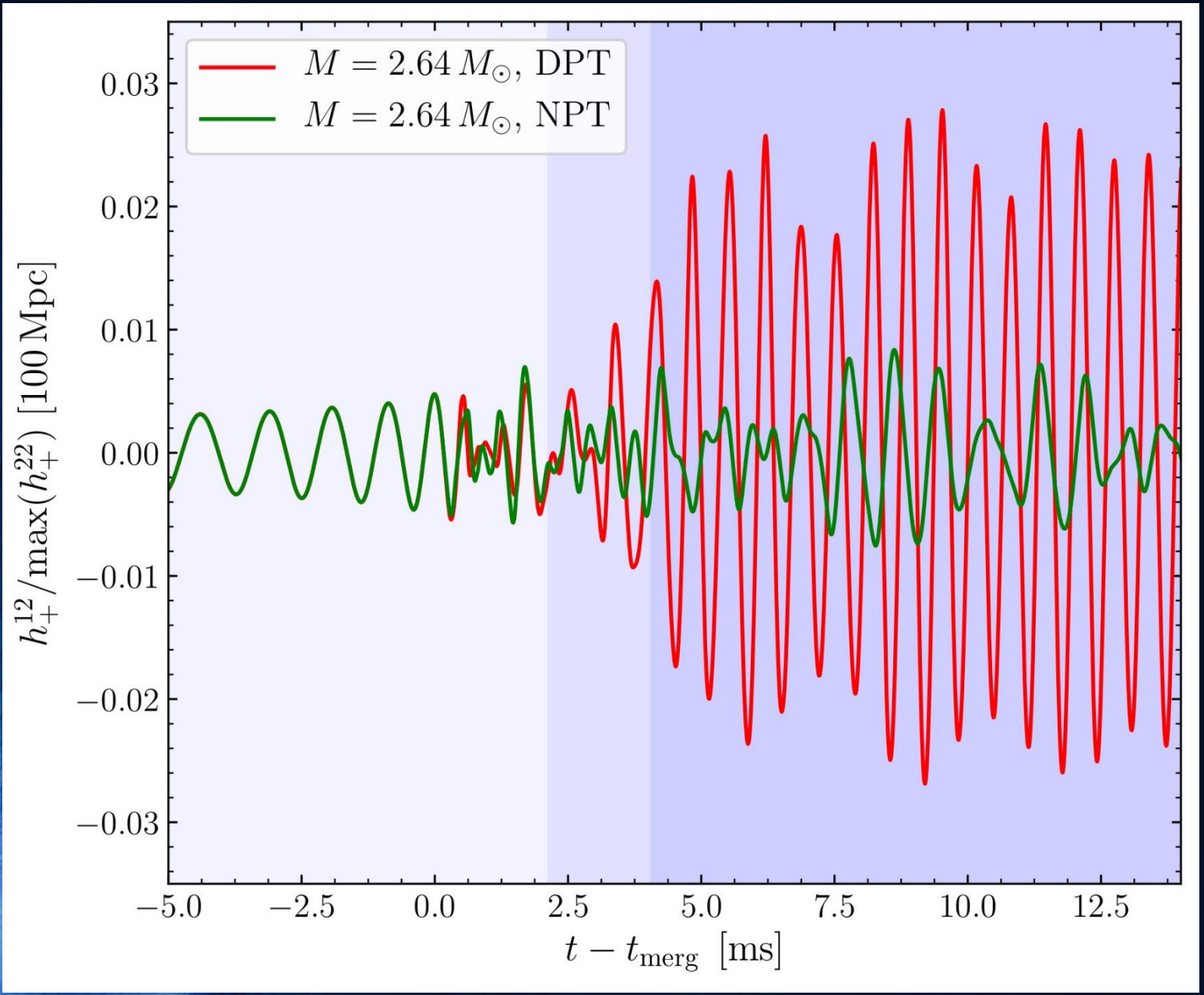

Due to the large m=1 mode of the emitted gravitational wave in the DPT case, a qualitative difference to the NPT scenario might be observable in future by focusing on the h12-gravitational wave mode during the post-merger evolution.

Article submitted (under review)

EPJ Special Topics on "Nuclear Astrophysics in Our Time: Supernovae, Neutron Stars and Binary Neutron Star Mergers"

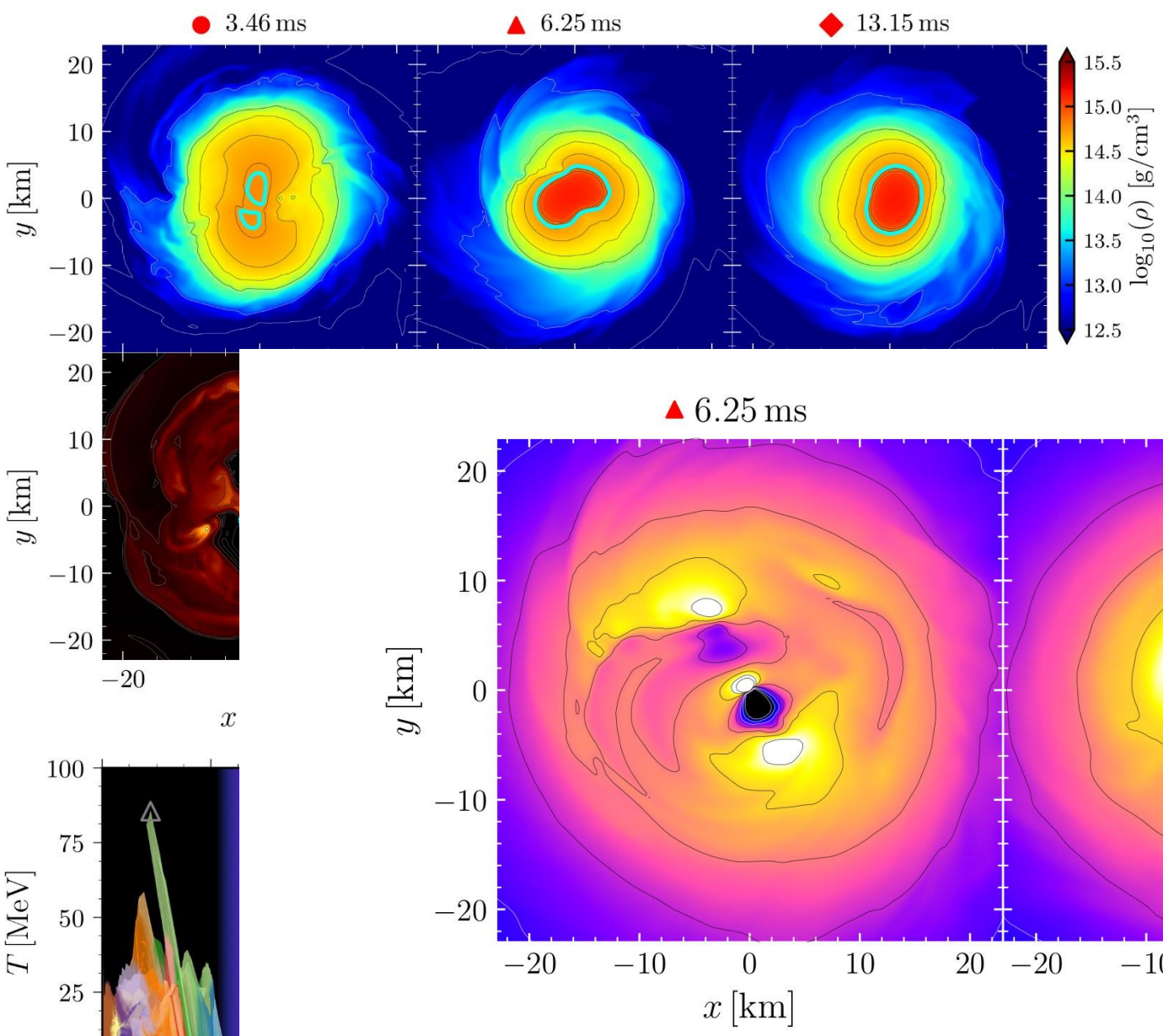

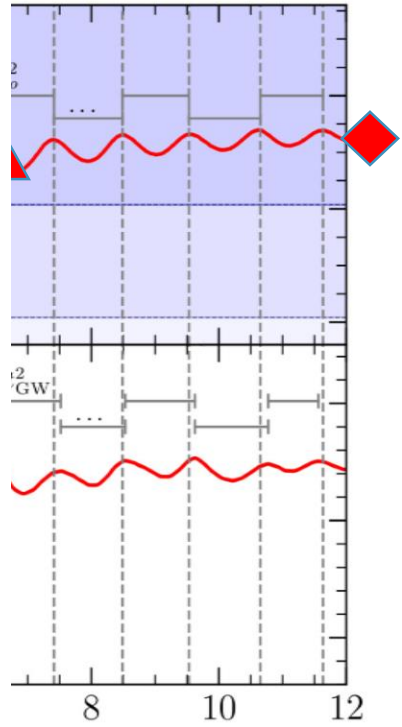

Fig. 4. Angular velocity for two representative times. Contours are drawn for $\Omega \in [0, 2, 4]$ kHz (white) and $\Omega \in [6, 8, 10, 12, 14]$ kHz (black).

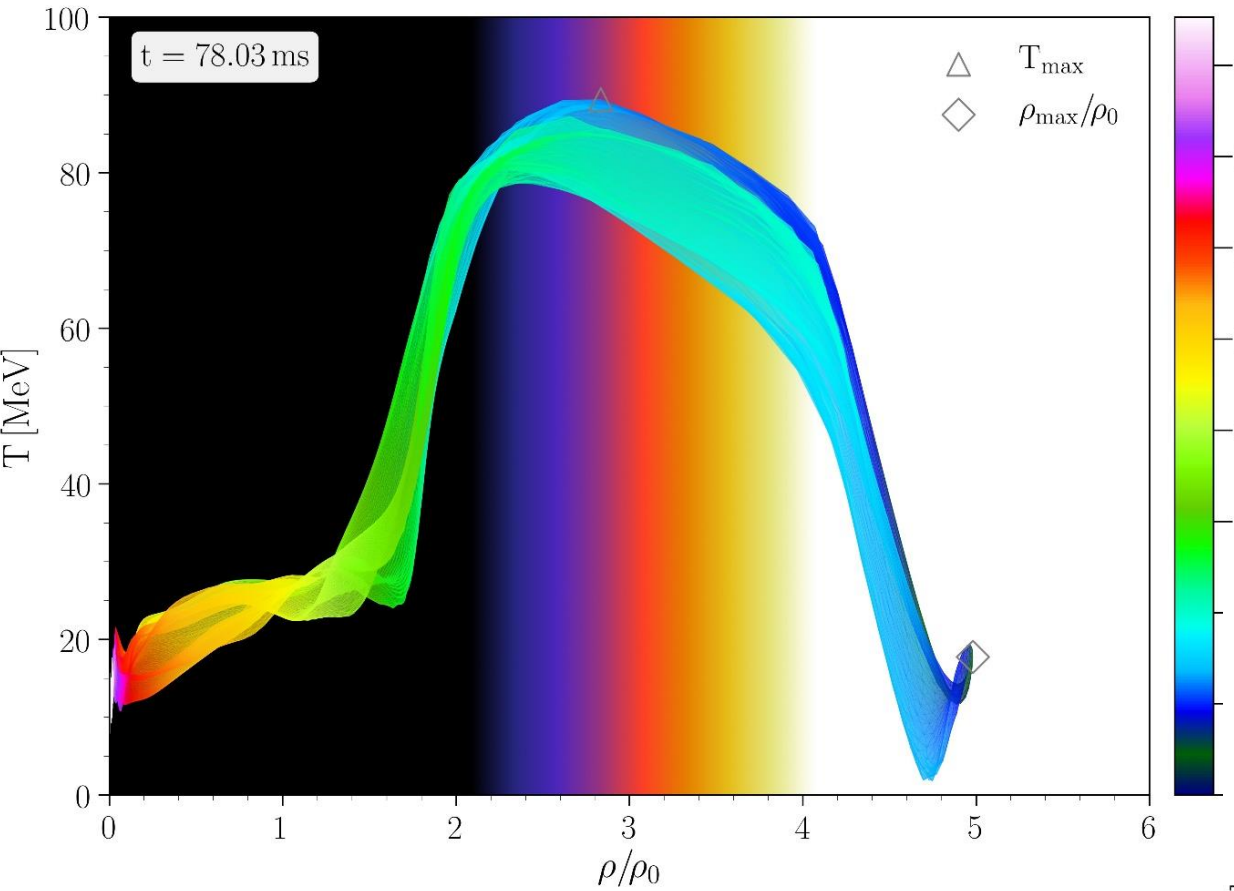
t = 78.03 ms
T_max
ρ_max/ρ_0
T [MeV]
ρ/ρ_0

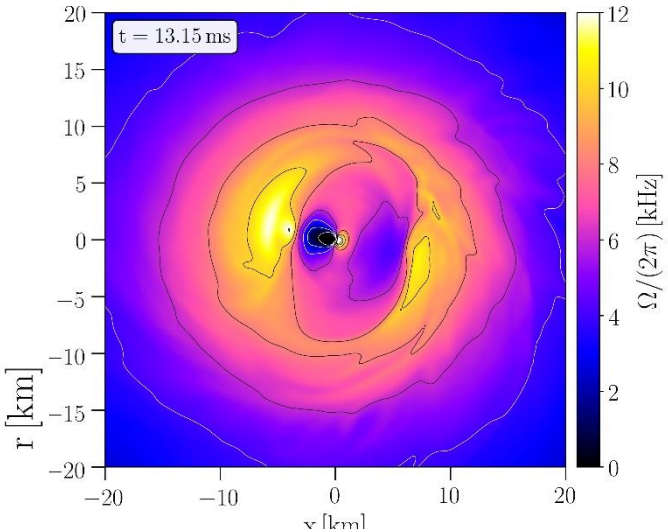
t = 13.15 ms
r [km]
x [km]
Ω/(2π) [kHz]

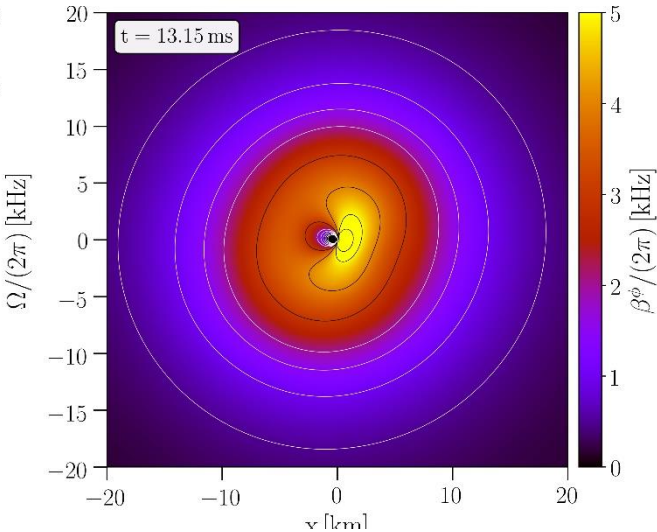
t = 13.15 ms
x [km]
β^φ/(2π) [kHz]

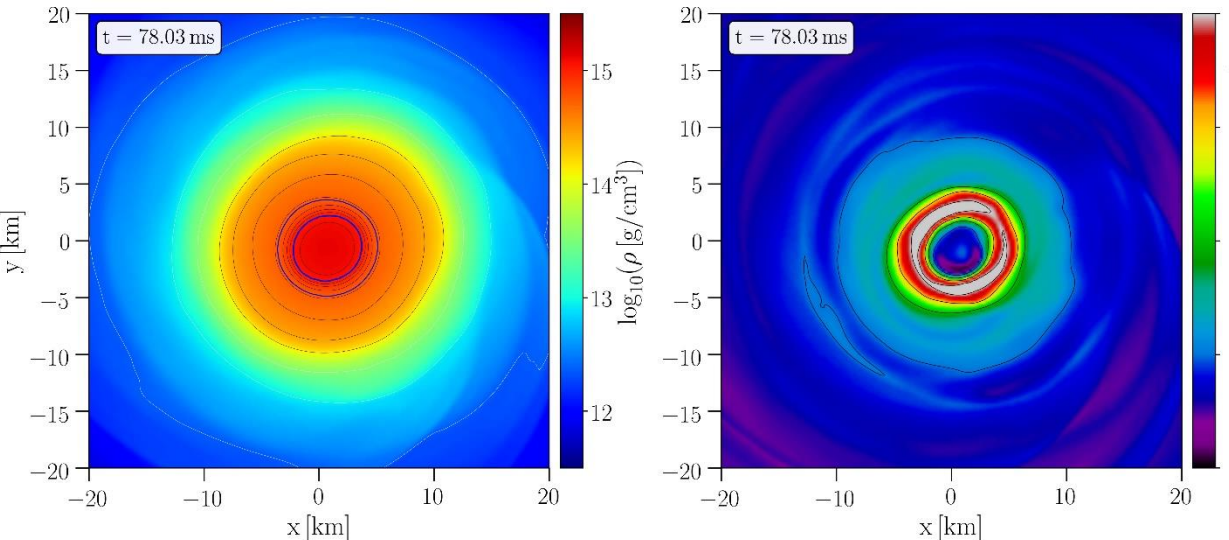
t = 78.03 ms
y [km]
x [km]
log10(ρ [g/cm^3])
t = 78.03 ms
x [km]

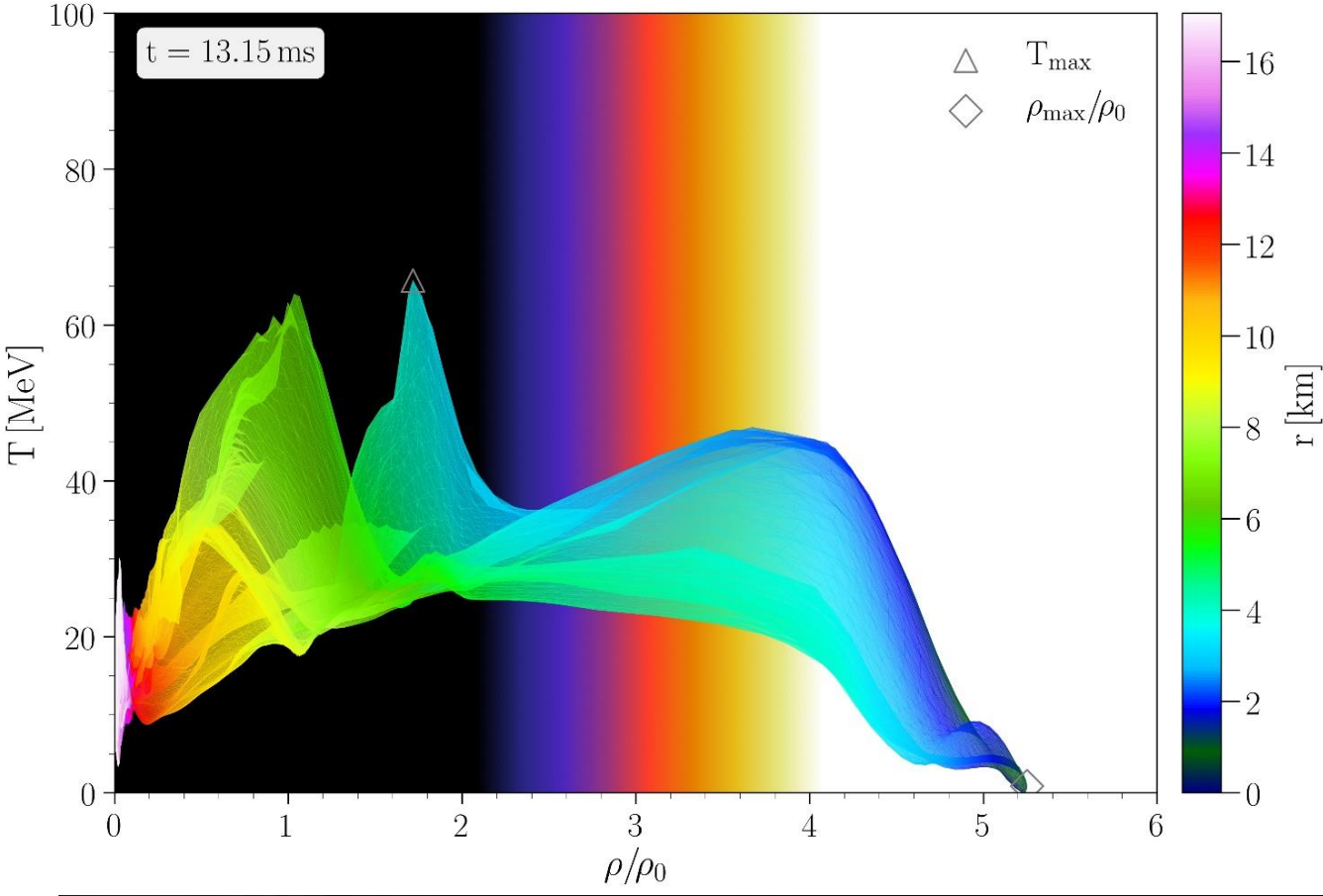
t = 13.15 ms
T_max
ρ_max/ρ_0
T [MeV]
ρ/ρ_0
r [km]

How to detect the hadron-quark phase transition with gravitational waves

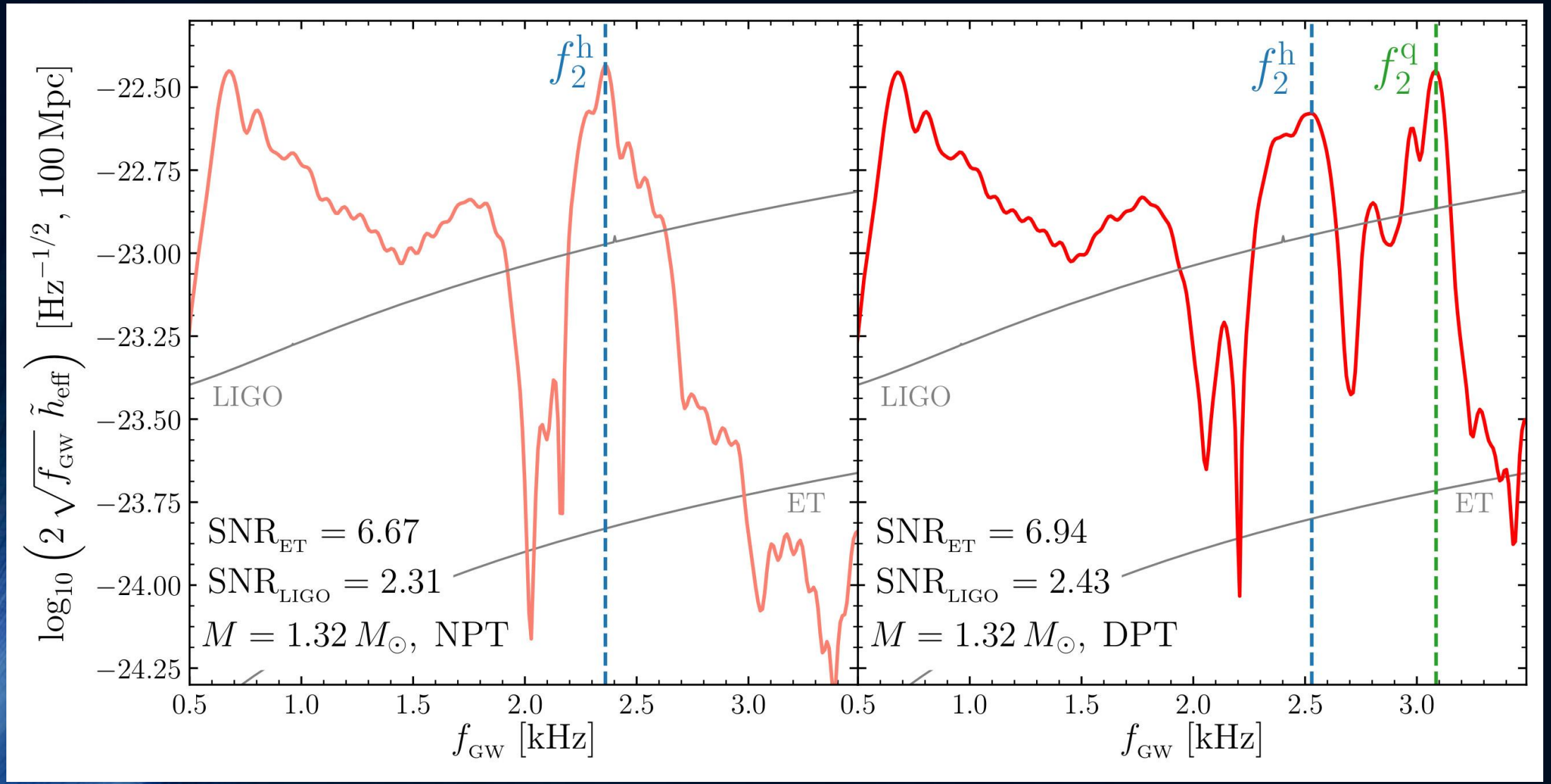

Total gravitational wave spectrum (left NPT, right DPT), PRL 124, 171103 (2020)

Postmerger gravitational-wave signatures of phase transitions in binary compact star mergers

- Introduction
- Numerical general relativity of compact star mergers
- The equation of state of compact star matter and the hadron-quark phase transition
- The different phases of a binary compact star merger event
- Gravitational-wave signatures of the hadron-quark phase transition in binary compact star mergers
  - The inspiral and merger phase (premerger signals)
  - Hypermassive hybrid stars (HMHS) within the prompt phase transition scenario (PPT)
  - HMHS within the delayed phase transition scenario (DPT)
  - HMHS within the phase transition triggered collapse scenario (PTTC)
- Summary and Outlook

HMHS within the PTTC scenario using a T-dependent EOS

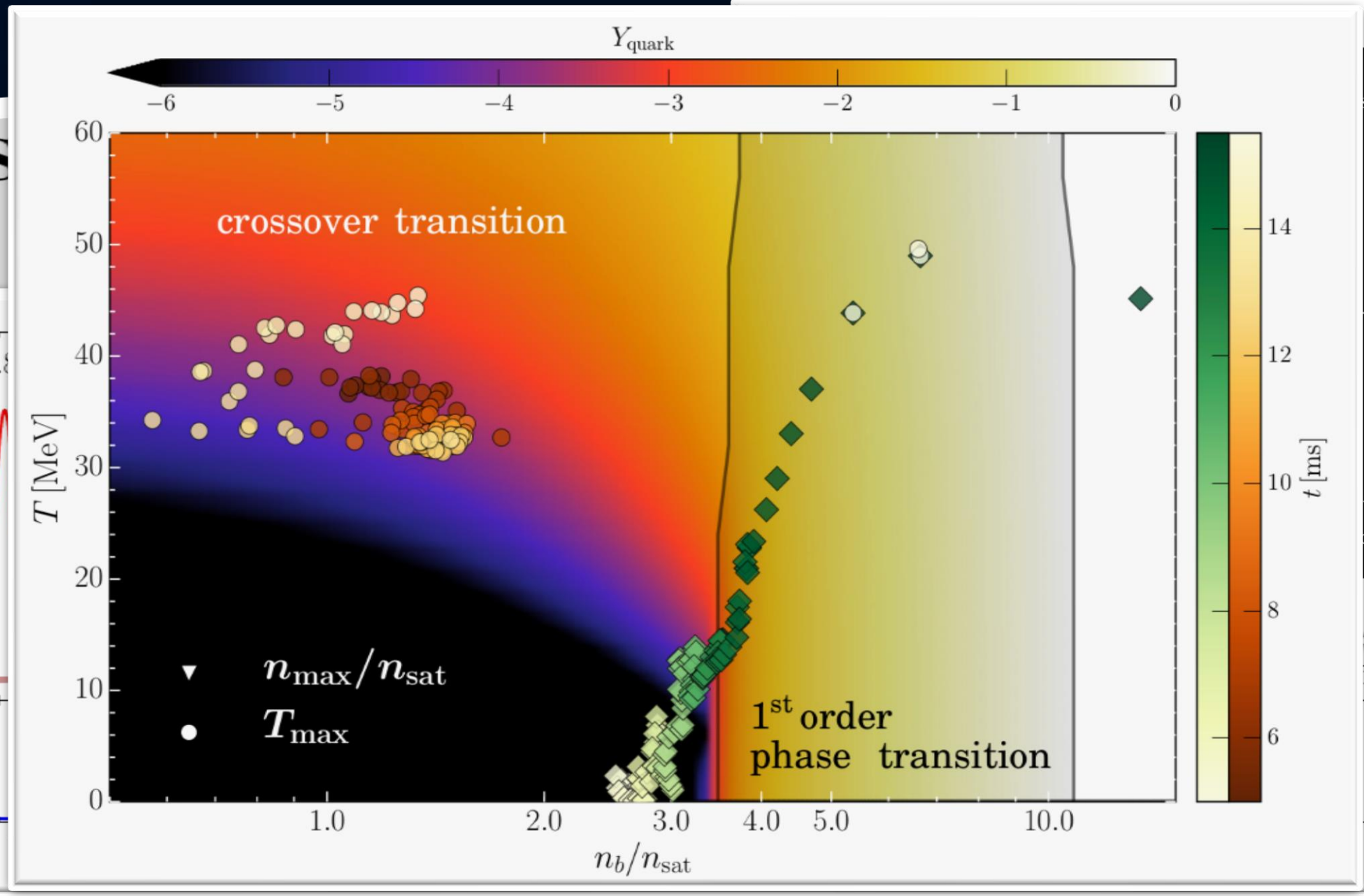

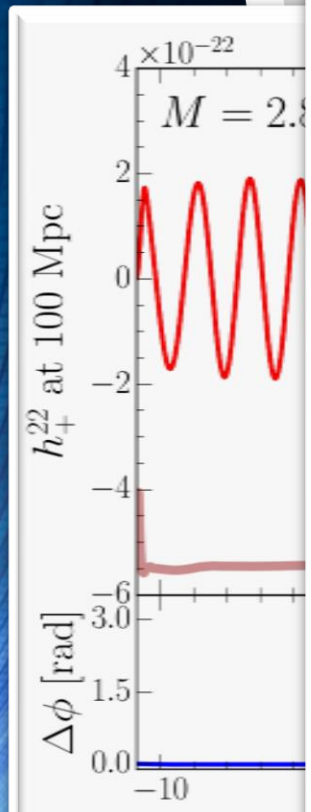

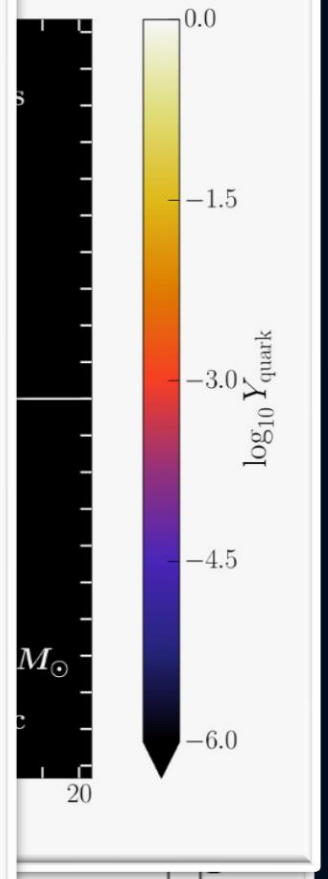

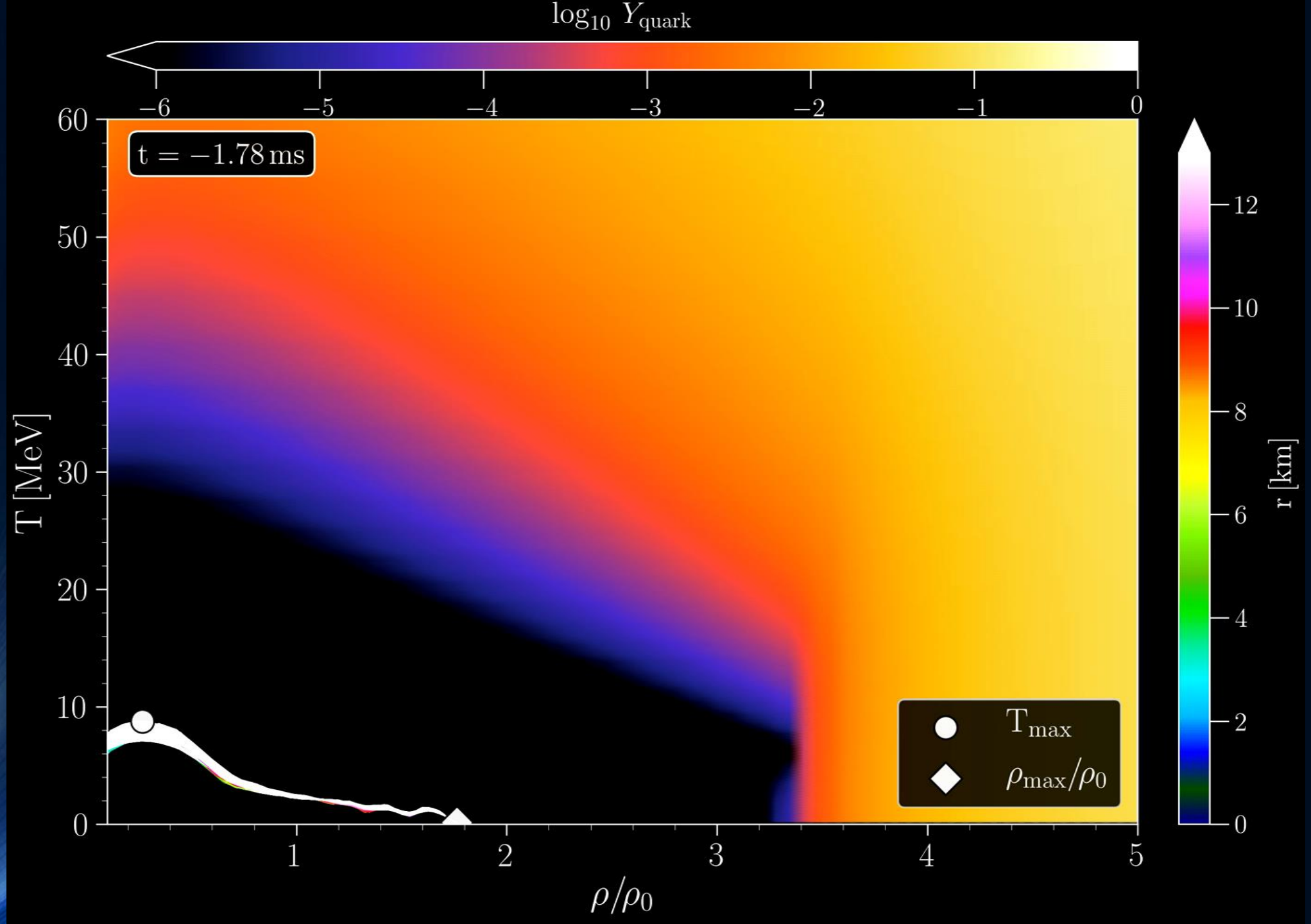
$\log_{10} Y_{\mathrm{quark}}$
−6
−5
−4
−3
−2
−1
0
t = −1.78 ms
T [MeV]
60
50
40
30
20
10
0
1
2
3
4
5
ρ/ρ_0
T_{max}
$\rho_{\mathrm{max}}/\rho_0$
r [km]
12
10
8
6
4
2
0

Merger Phase

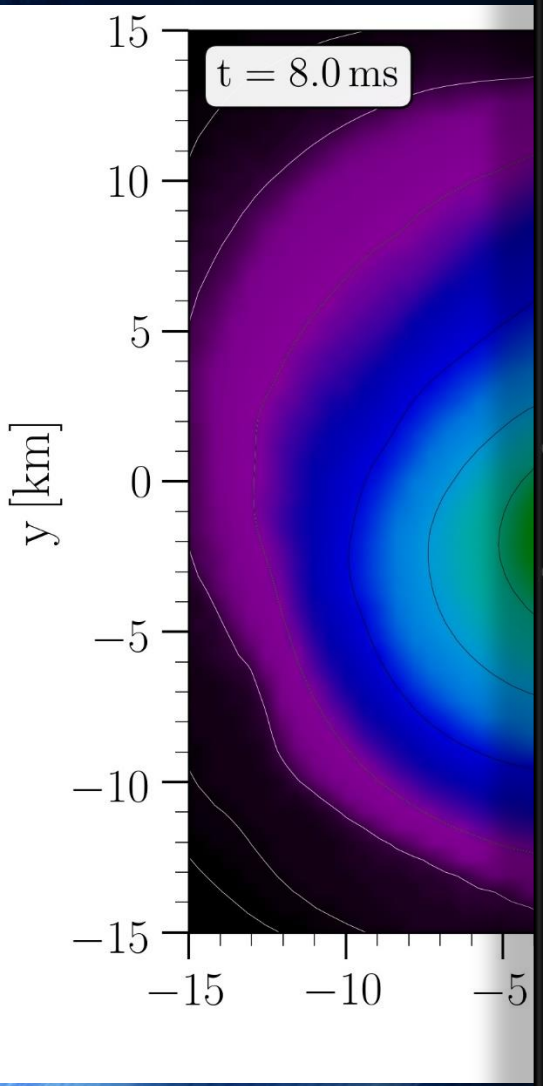

Rest mass density

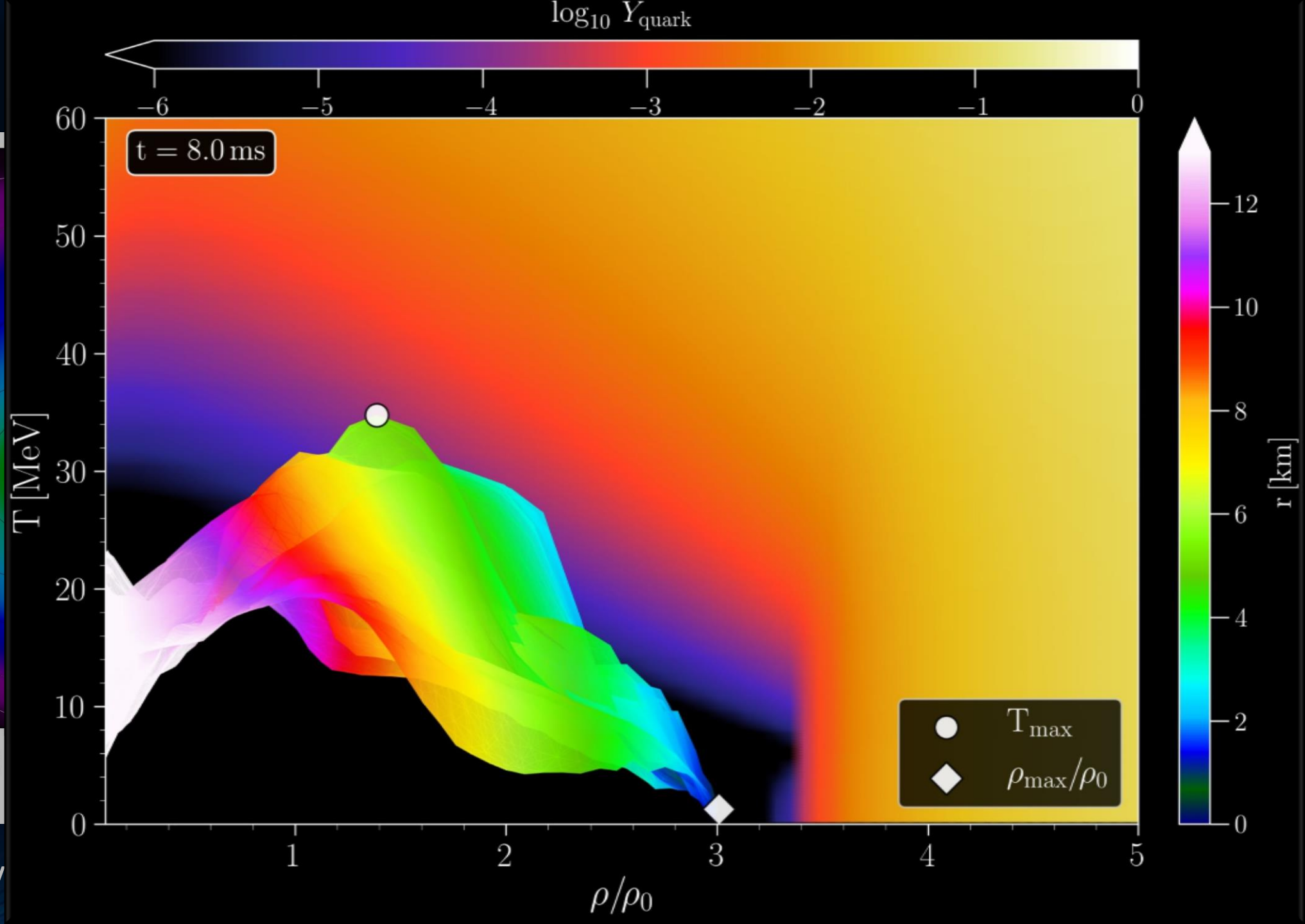

Merger Phase

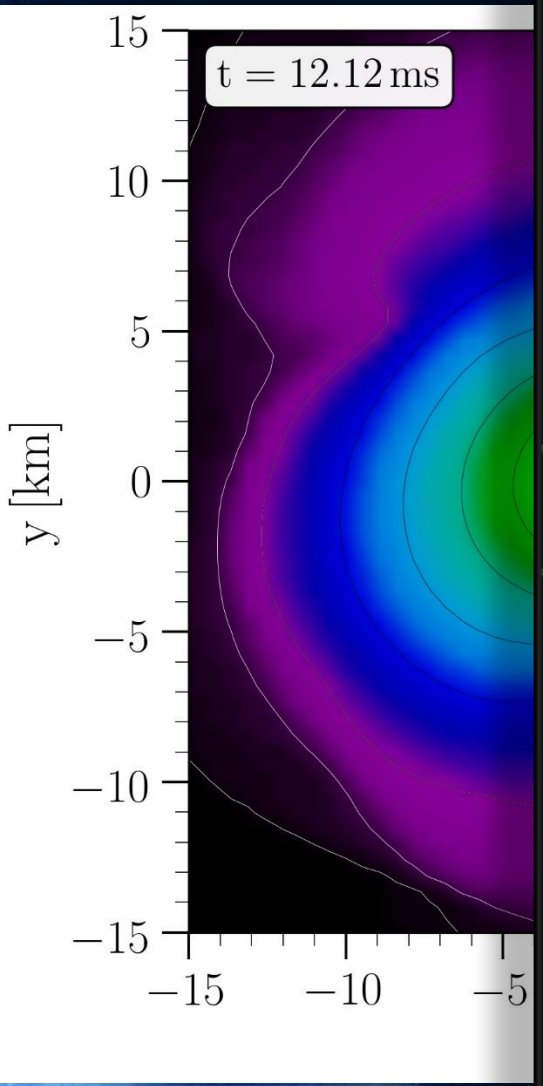

Rest mass density

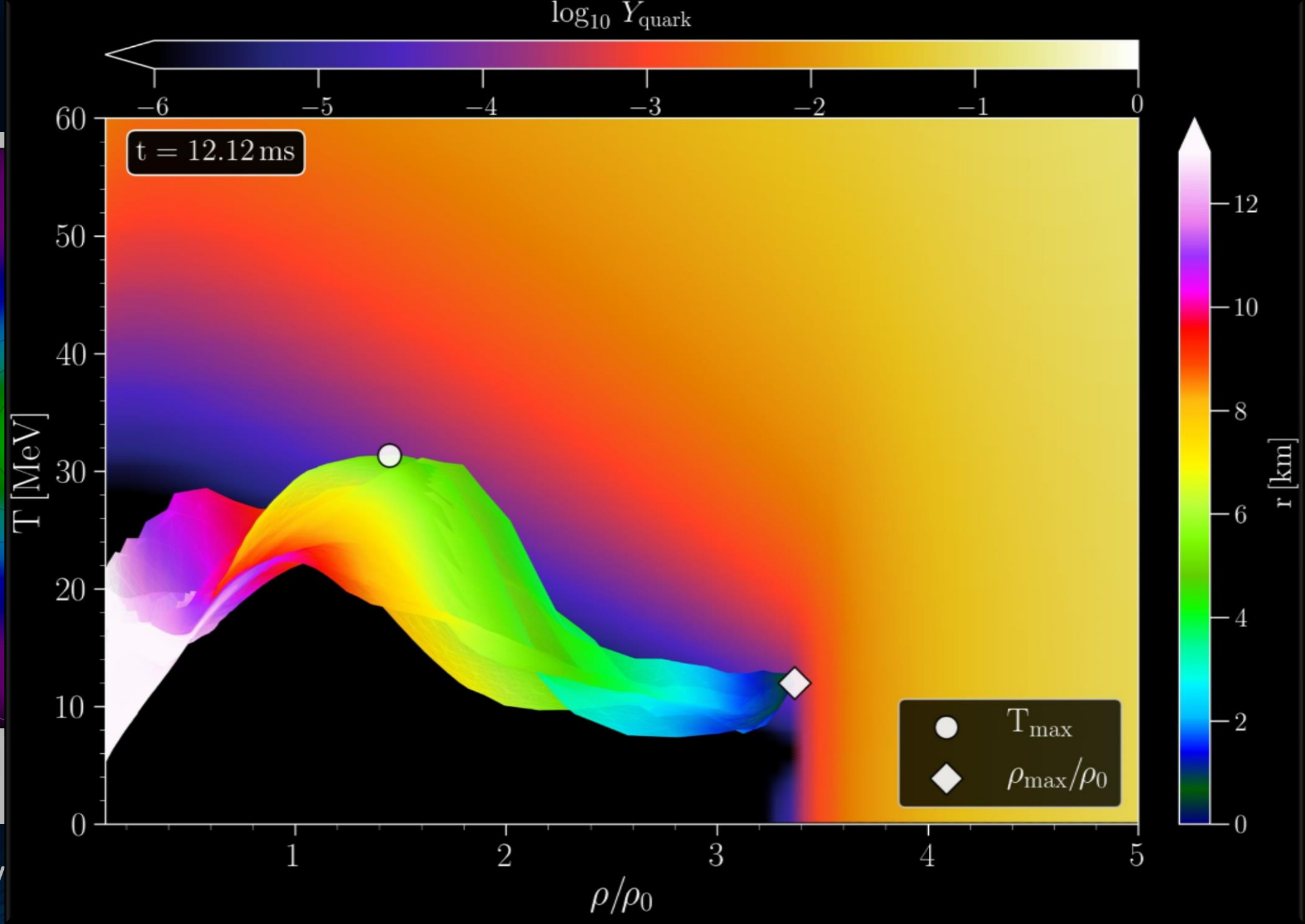

Merger Phase

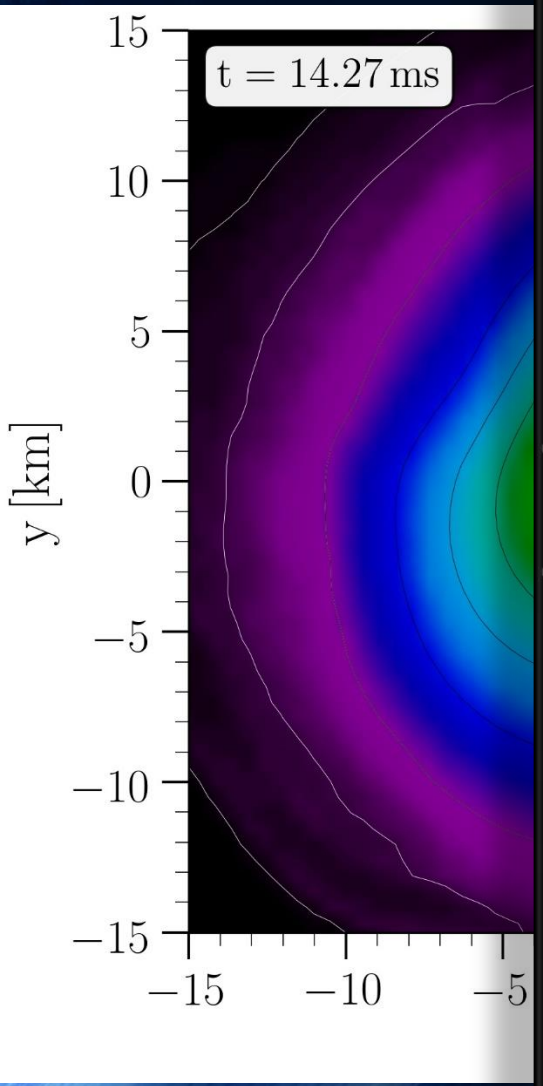

Rest mass density

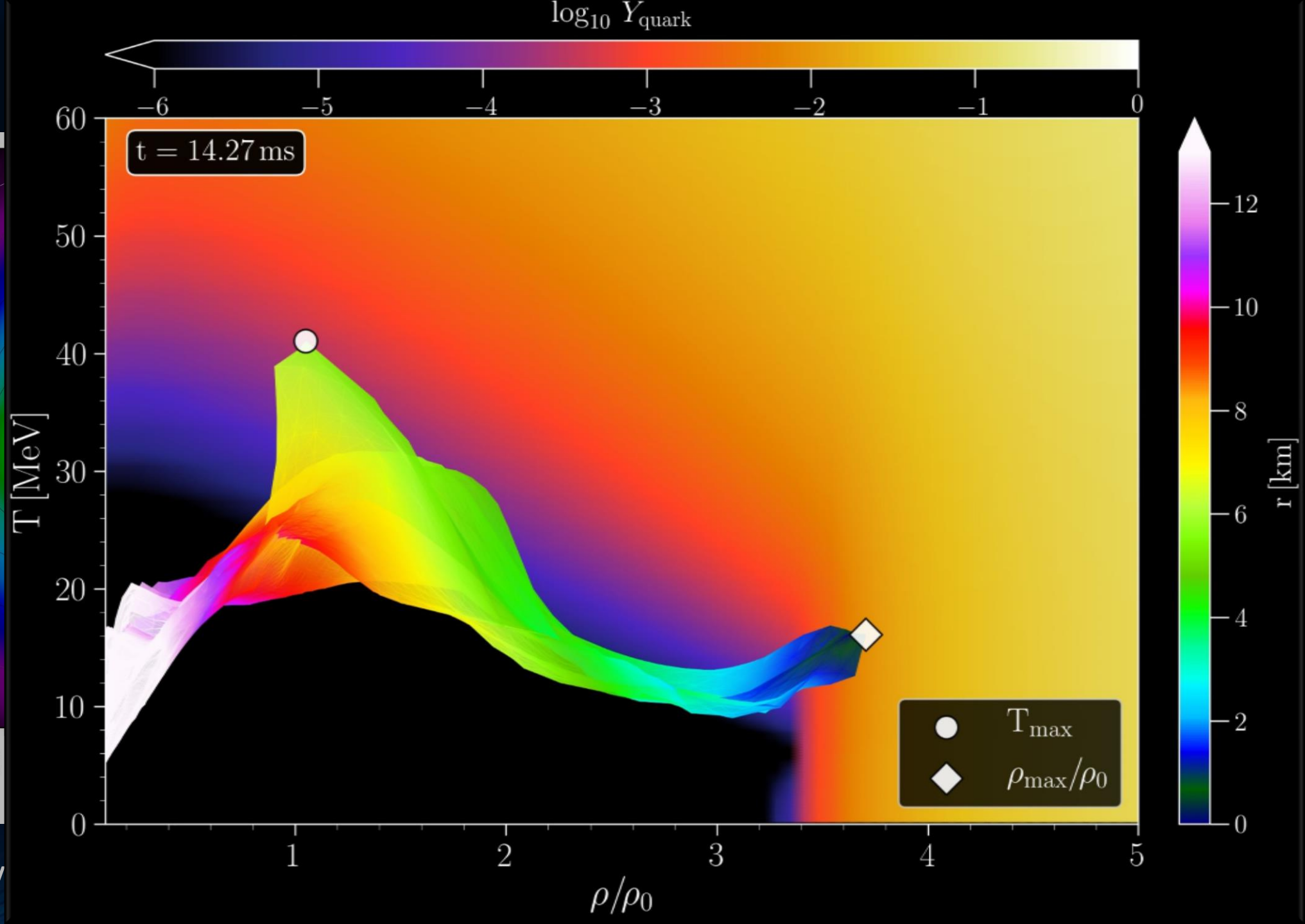

Merger Phase

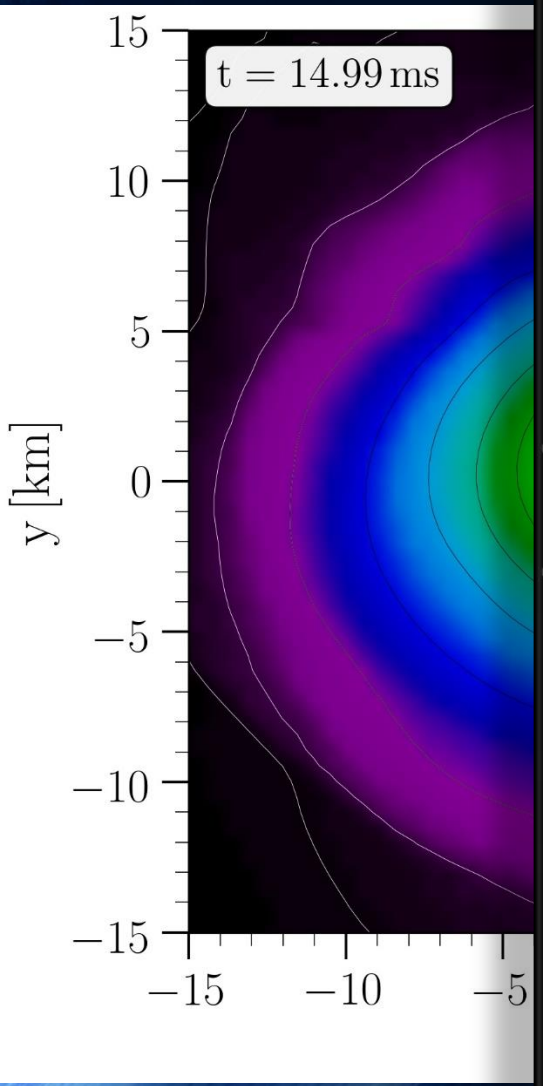

Rest mass density

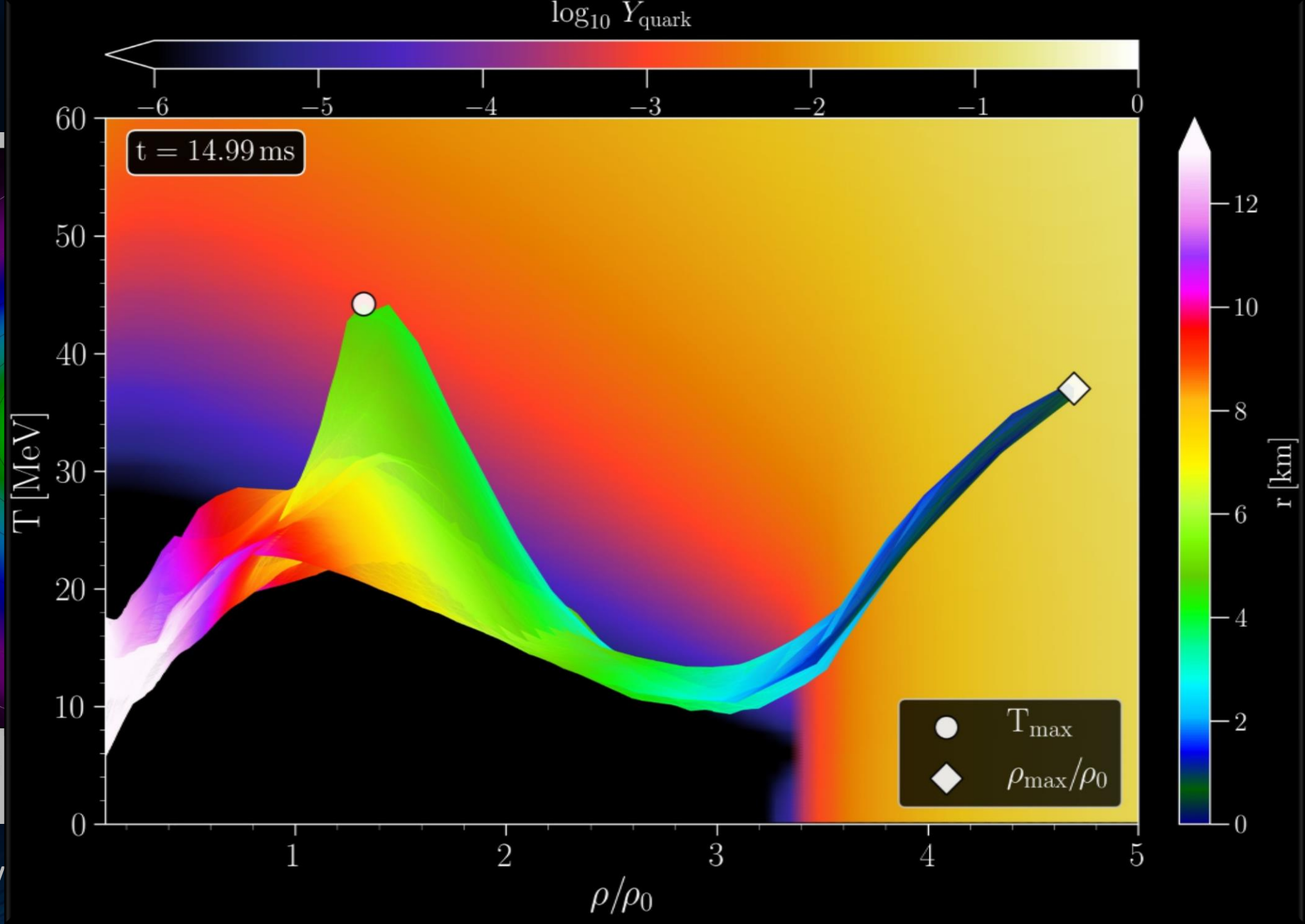

Merger Phase

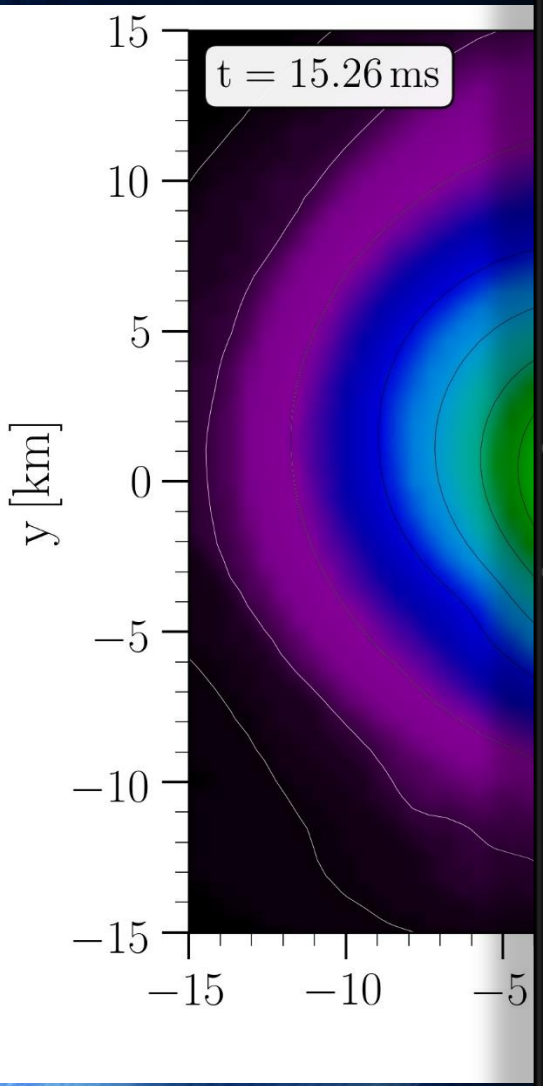

Rest mass density

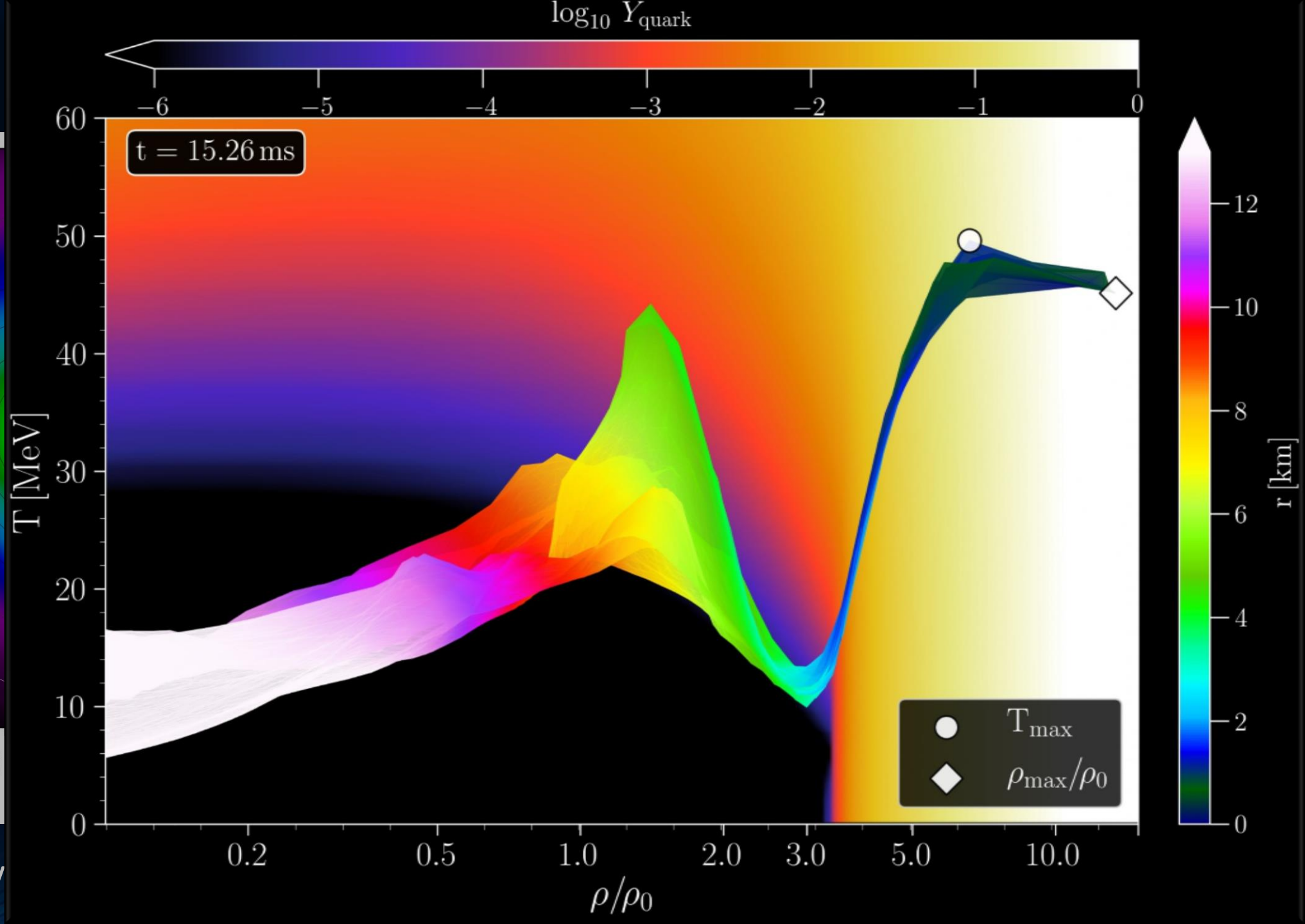

The Pelican Plot

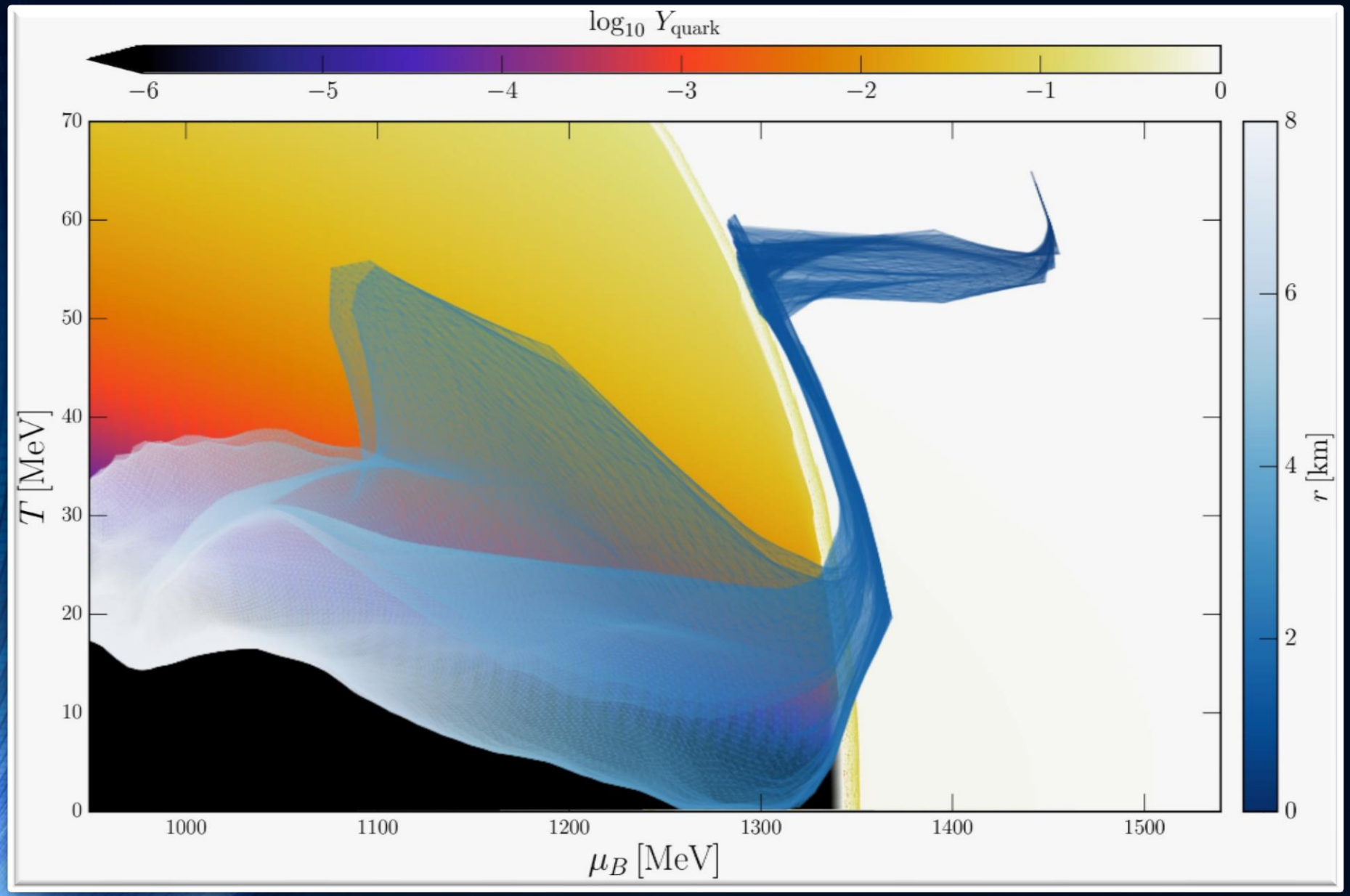

E.Most, J. Papenfort, V.Dexheimer, M.Hanauske, H.Stöcker and L.Rezzolla;
„On the deconfinement phase transition in neutron-star mergers„; arXiv:*1910.13893*

The shadowy blue image resembles the shape of a strange bird, e.g. a pelican, wherein the hot head of a pelican contains a high amount of strange quark matter, its thin neck follows the QCD phase boundary, while its hot wings (local temperature maxima) contain mostly hadronic matter at much lower densities.
The maximum tempearture and density points correspond to the head of the pelican where pure strange quark is present. Due to the stiffening of the EOS in the pure quark phase, the temperature stops rising and the high pressure in the central region pushes against the hudge gravitational force.

GW170817: Constraining the maximum mass of Neutron Stars

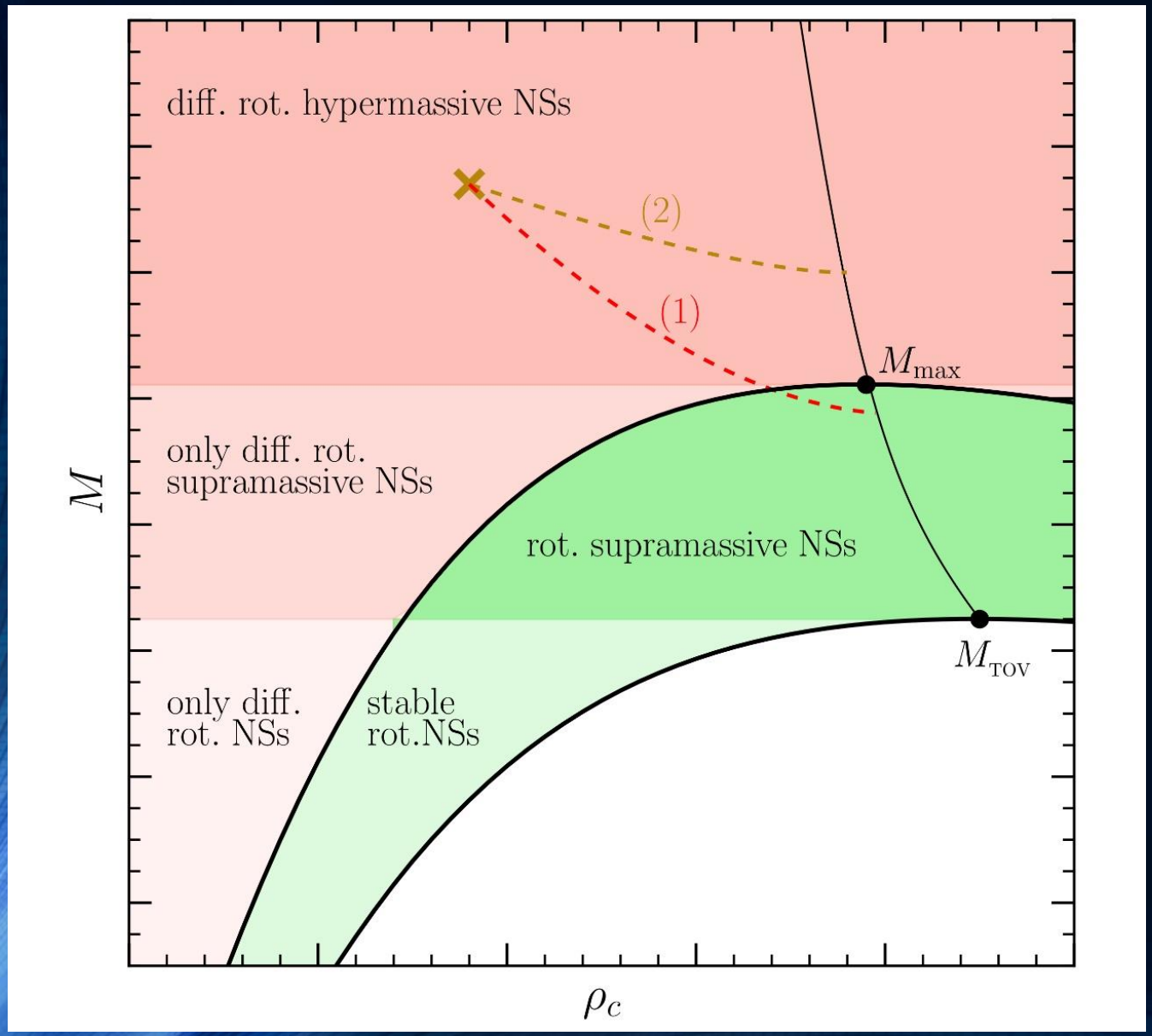

The highly differentially rotating hypermassive/supramassive neutron star will spin down and redistribute its angular momentum (e.g. due to viscosity effects, magnetic braking). After ~1 second it will cross the stability line as a uniformly rotating supramassive neutron star (close to M_{max}) and collapse to a black hole. Parts of the ejected matter will fall back into the black hole producing the gamma-ray burst.

L.Rezzolla, E.Most, L.Weih, "Using Gravitational Wave Observations and Quasi-Universal Relations to constrain the maximum Mass of Neutron Stars",The Astrophysical Journal Letters 852, L25 (2018):
2.01 +/-0.04 < M_{TOV} < 2.16 +/-0.17

See also: S.Lawrence et al. ,APJ808,186, 2015
Margalit & Metzger, The Astrophysical Journal Letters 850, L19 (2017): M_{TOV} < 2.17 (90%)
Zhou, Zhou, Li, PRD 97, 083015 (2018)
Ruiz, Shapiro, Tsokaros, PRD 97,021501 (2018)

GW170817: Tidal Deformability
Restrictions on the Equation of State (EOS)
(for high and low spin assumption)

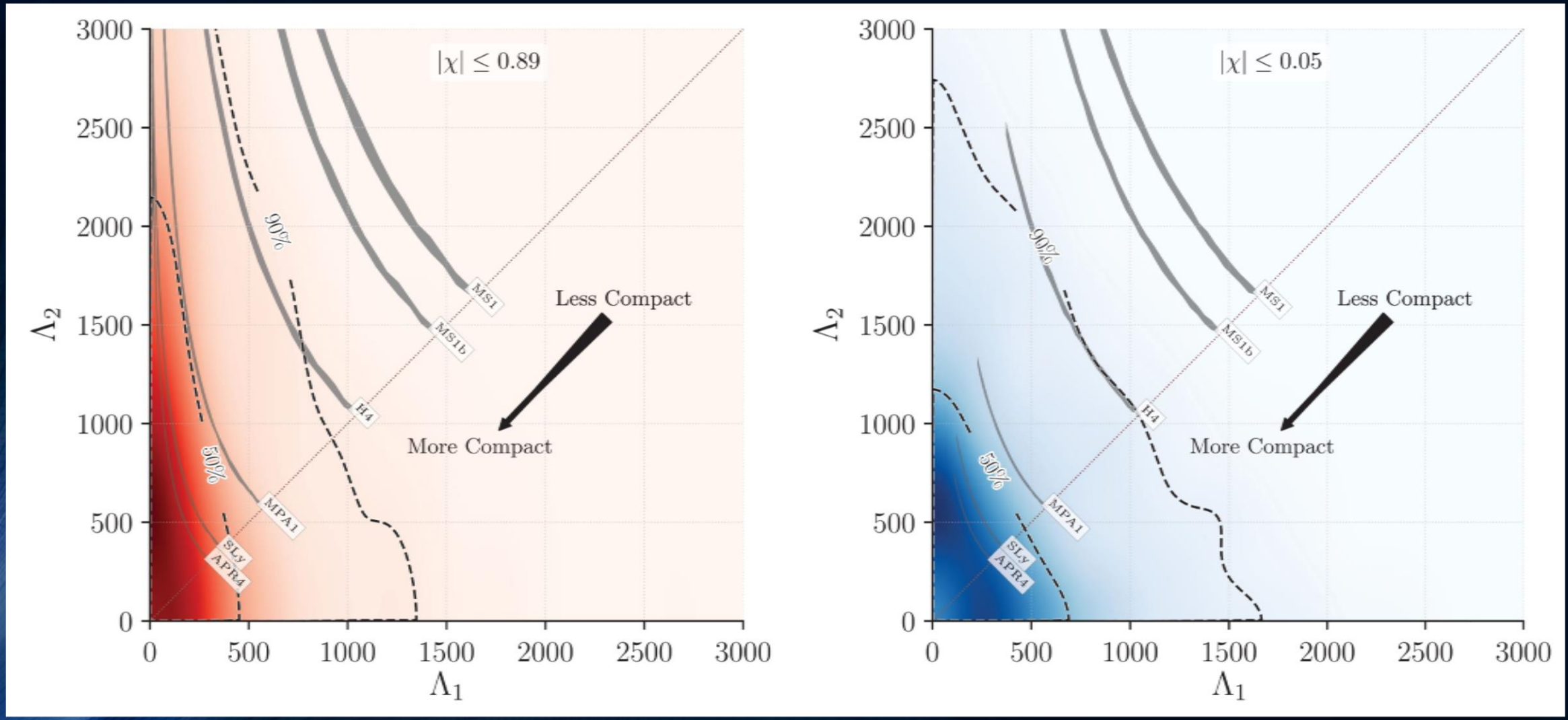

GW170817: Constraining the Neutron Star Radius and EOS

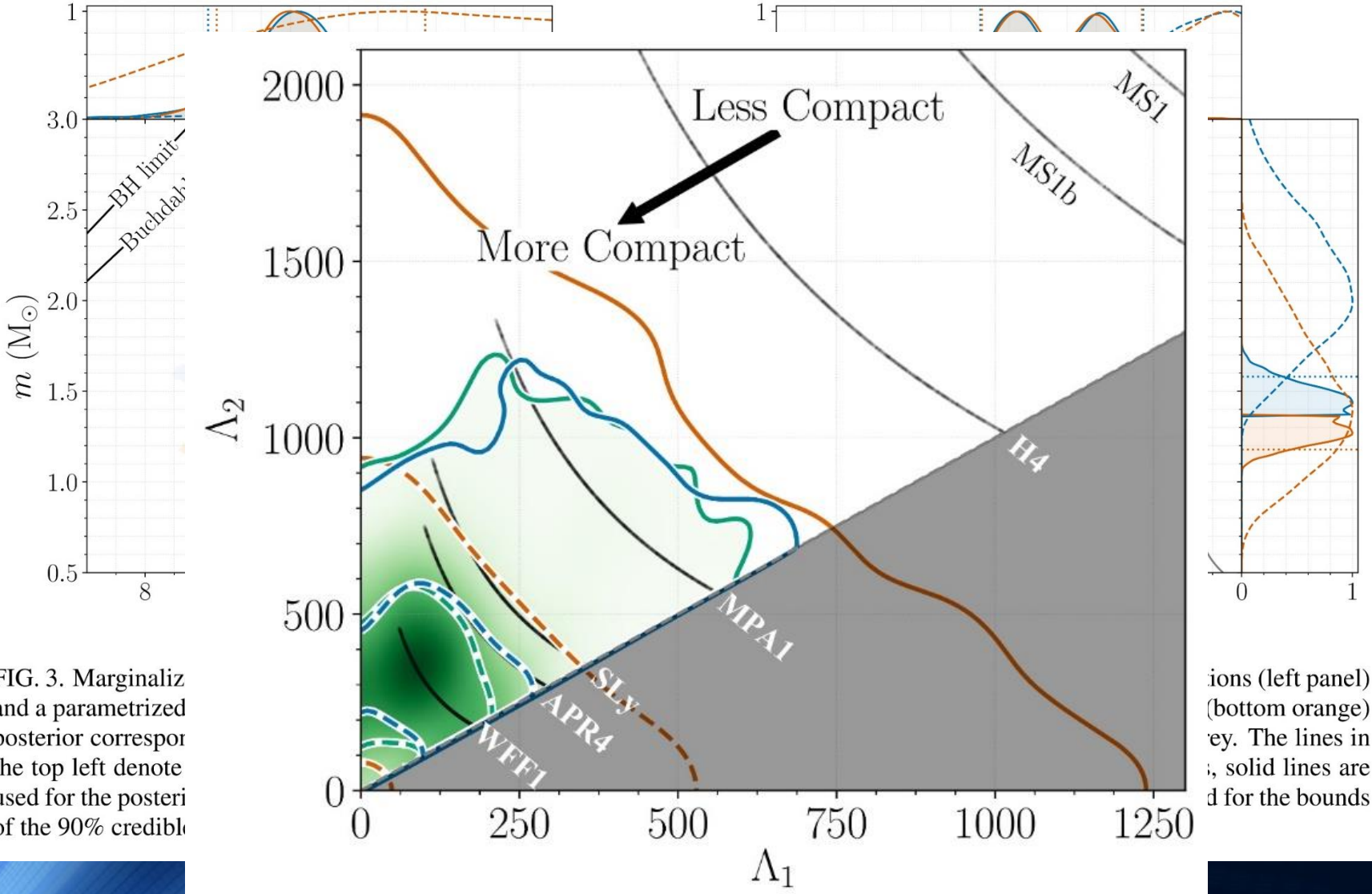

FIG. 3. Marginaliz
and a parametrized
posterior corresponding
the top left denote
used for the posteri
of the 90% credibl

ions (left panel)
(bottom orange)
ey. The lines in
, solid lines are
d for the bounds

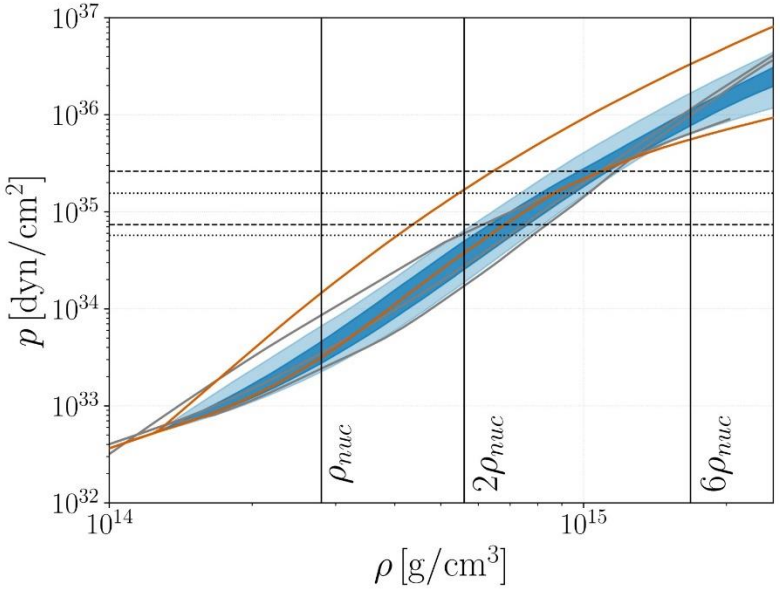

FIG. 2. Marginalized posterior (blue) and prior (orange) for the pressure p as a function of the rest-mass density ρ of the NS interior using the spectral EOS parametrization and imposing a lower limit on the maximum NS mass supported by the EOS of $1.97\,M_\odot$. The dark (light) blue shaded region corresponds to the 50% (90%) posterior credible level and the orange lines show the 90% prior credible interval. Horizontal lines denote the 90% credible interval for the central pressure of the heavier (dashed) and the lighter (dotted) binary components. Vertical lines correspond to once, twice, and six times the nuclear saturation density. Overplotted in grey are representative EOS models [121, 122, 124], using data taken from [19]; from top to bottom at $2\rho_{\rm nuc}$ we show H4, APR4, and WFF1.

GW170817: Measurements of neutron star radii and equation of state, *The LIGO /Virgo Collaboration*, arXiv:1805.11581v1

GW170817: ...us

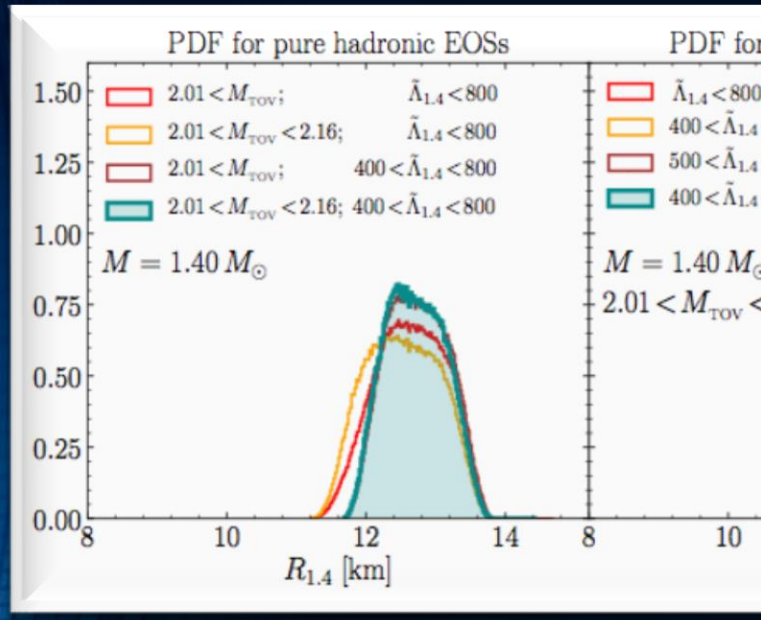

$$12.00 < R_{1.4}/\mathrm{km} < 13.45$$

$$8.53 < R_{1.4}/\mathrm{km} < 13.74 \qquad \bar{R}$$

Reference	R_i [km]
Without a phase transition	
Bauswein et al. [42]	$10.68^{+0.15}_{-0.03} \leq R_{1.6}$
Most et al. [51]	$12.00 \leq R_{1.4} \leq 13.45$
Burgio et al. [54]	$11.8 \leq R_{1.5} \leq 13.1$
Tews et al. [55]	$11.3 \leq R_{1.4} \leq 13.6$
De et al. [56]	$8.9 \leq R_{1.4} \leq 13.2$
LIGO/Virgo [57]	$10.5 \leq R_{1.4} \leq 13.3$
With a phase transition	
Annala et al. [46]	$R_{1.4} \leq 13.6$
Most et al. [51]	$8.53 \leq R_{1.4} \leq 13.74$
Burgio et al. [54]	$R_{1.5} = 10.7$
Tews et al. [55]	$9.0 \leq R_{1.4} \leq 13.6$
This work	
NS	$R_{1.4} = 13.11$
HS Model-2	$12.9 \leq R_{1.4} \leq 13.11$
HS_T Model-1	$10.1 \leq R_{1.4} \leq 12.9$
HS_T Model-2	$10.4 \leq R_{1.4} \leq 11.9$

TABLE II. Constraints on the radius of neutron stars from GW170817 for models without a phase transition (top), works considering the possibility of a transition to quark matter (middle) and for EOSs of *Category III* in the present work (bottom).

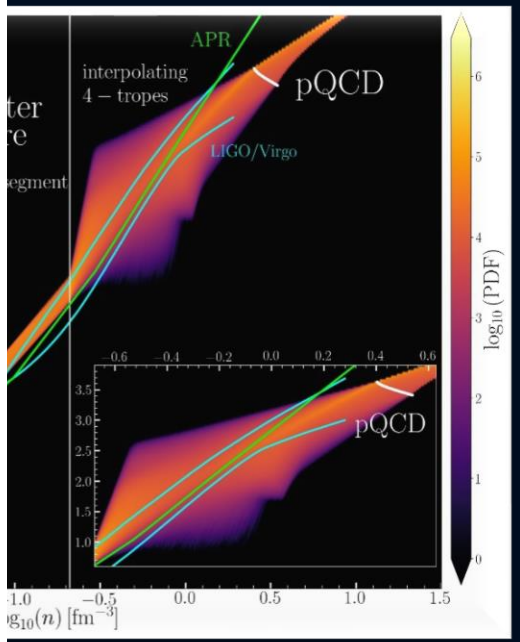

t, L.Weih, L.Rezzolla, J.
ner-Bielich "New
aints on radii and tidal
nabilities of neutron
rom GW170817",
1803.00549,
oted in PRL)

See also: De, Finstad, Lattimer, Brown, Berger, Biwe
172702 (2018) ; Nandi & Char, Astrophys. J. 857, 12 (201
Annala, Gorda, Kurkela, Vuorinen, PRL 120, 172703 (201

v, Piekarewicz, Horowitz, PRL 120,
ros, PRD 97, 021501 (2018) ;

The Hadron-Quark Phase Transition and the Third Family of Compact Stars (Twin Stars)

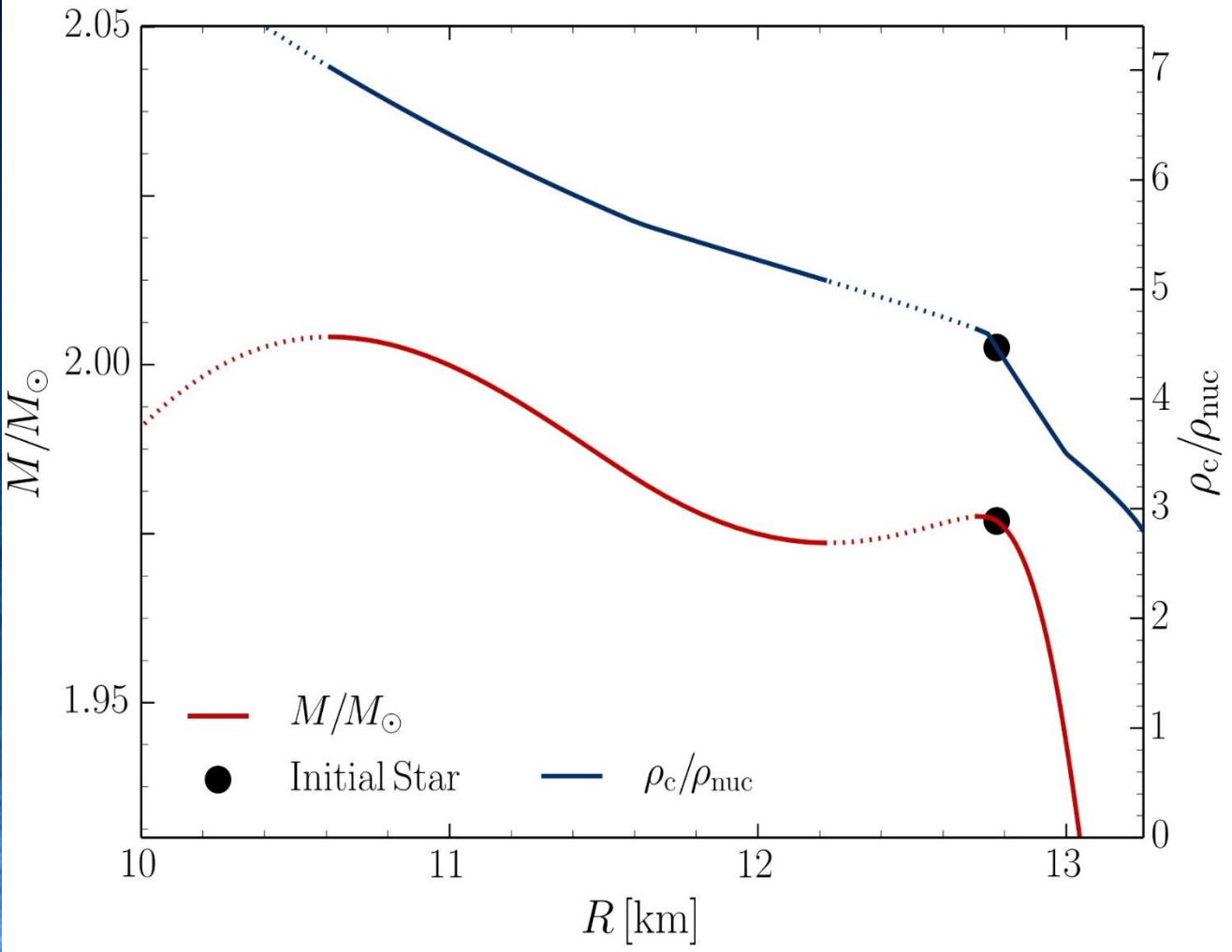

Glendenning, N. K., & Kettner, C. (1998). Nonidentical neutron star twins. Astron. Astrophys., 353(LBL-42080), L9.

Sarmistha Banik, Matthias Hanauske, Debades Bandyopadhyay and Walter Greiner, Rotating compact stars with exotic matter, Phys.Rev.D 70 (2004) p.12304

I.N. Mishustin, M. Hanauske, A. Bhattacharyya, L.M. Satarov, H. Stöcker, and W. Greiner, Catastrophic rearrangement of a compact star due to quark core formation, Physics Letters B 552 (2003) p.1-8

M.Alford and A. Sedrakian, Compact stars with sequential QCD phase transitions. Physical review letters, 119(16), 161104 (2017)..

D.Alvarez-Castillo and D.Blaschke, High-mass twin stars with a multipolytrope equation of state. Physical Review C, 96(4), 045809 (2017) .

A. Ayriyan, N.-U. Bastian, D. Blaschke, H. Grigorian, K. Maslov, D. N. Voskresensky, How robust is a third family of compact stars against pasta phase effects?, arXiv:1711.03926 [nucl-th]

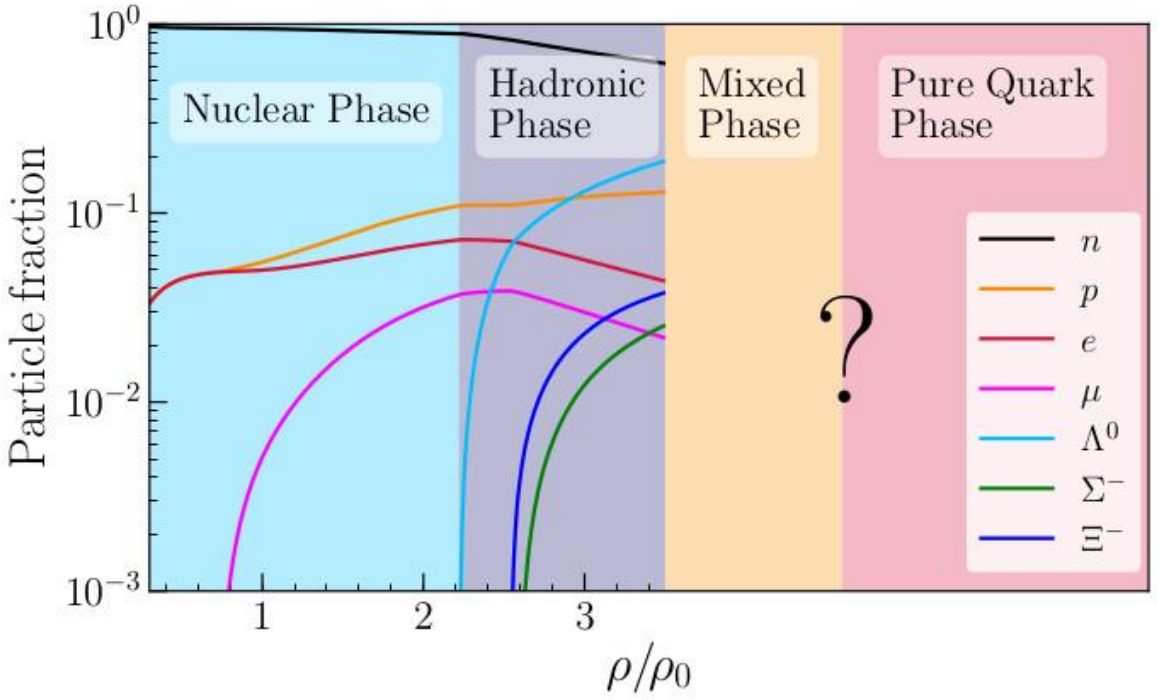

FIG. 1. Particle fractions as functions of the baryonic density for the FSU2H model [69, 70] up to the point where the HQPT is implemented, giving rise to a phase of deconfined quark matter which can be separated from the nuclear (or hadronic) phase by a mixed phase of hadrons and quarks. We note that the actual fractions of nucleons/hyperons and quarks u, d, s in the mixed and quark phases cannot be determined with the parametrizations used in this work.

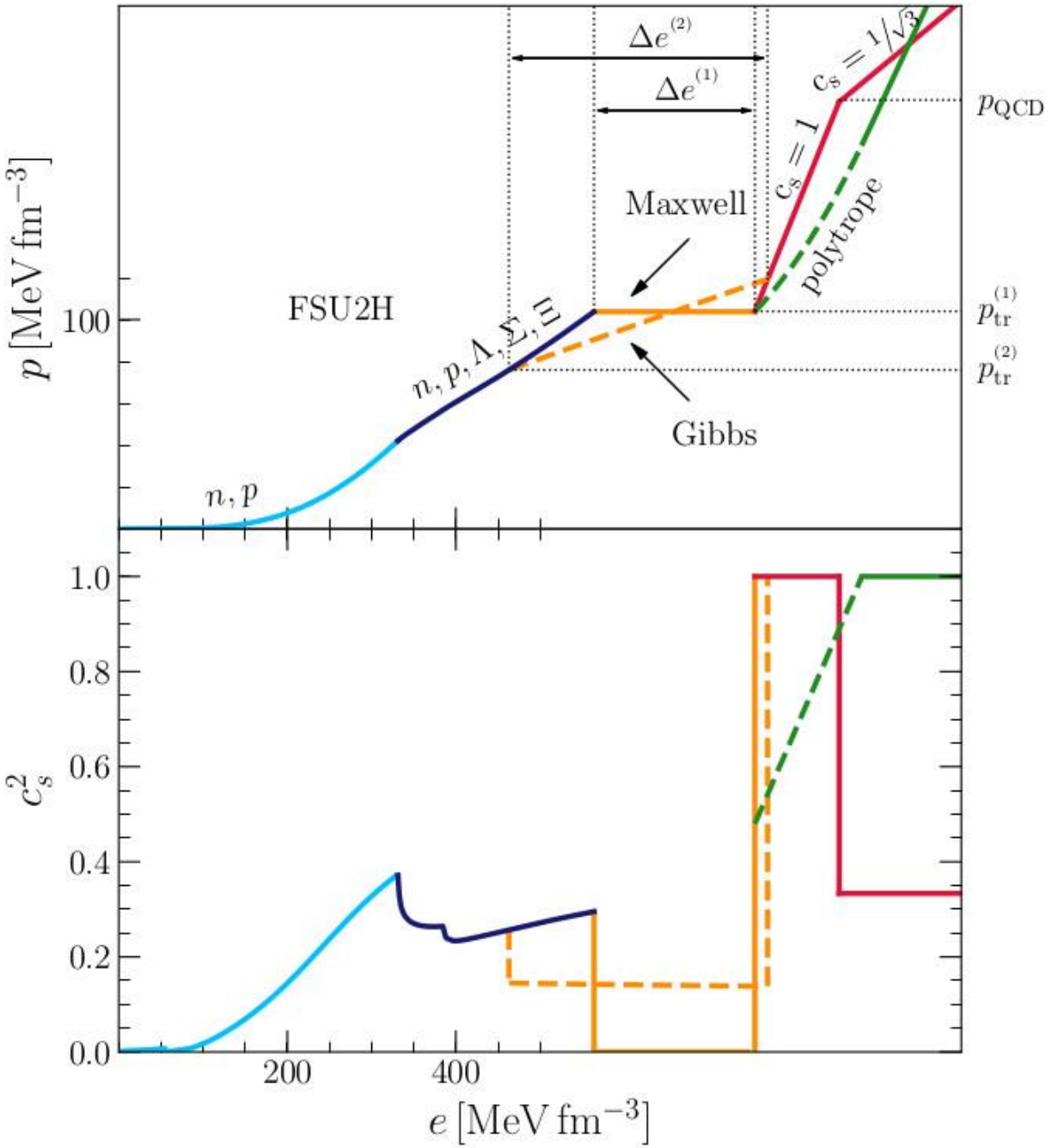

Mass-Radius Relations for Twin-Star EOSs

The mass and radius of a single, non-rotating and spherically symmetric neutron star can be easily calculated by solving the static TOV equation numerically for a given EOS.

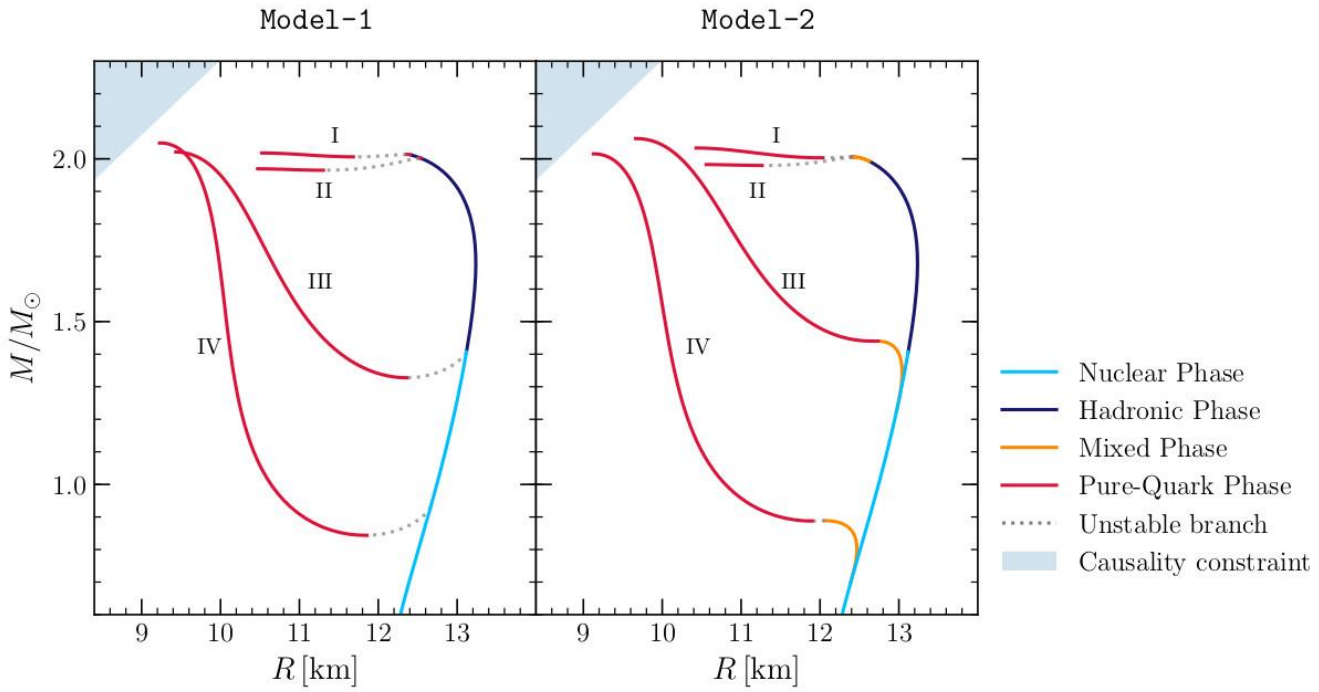

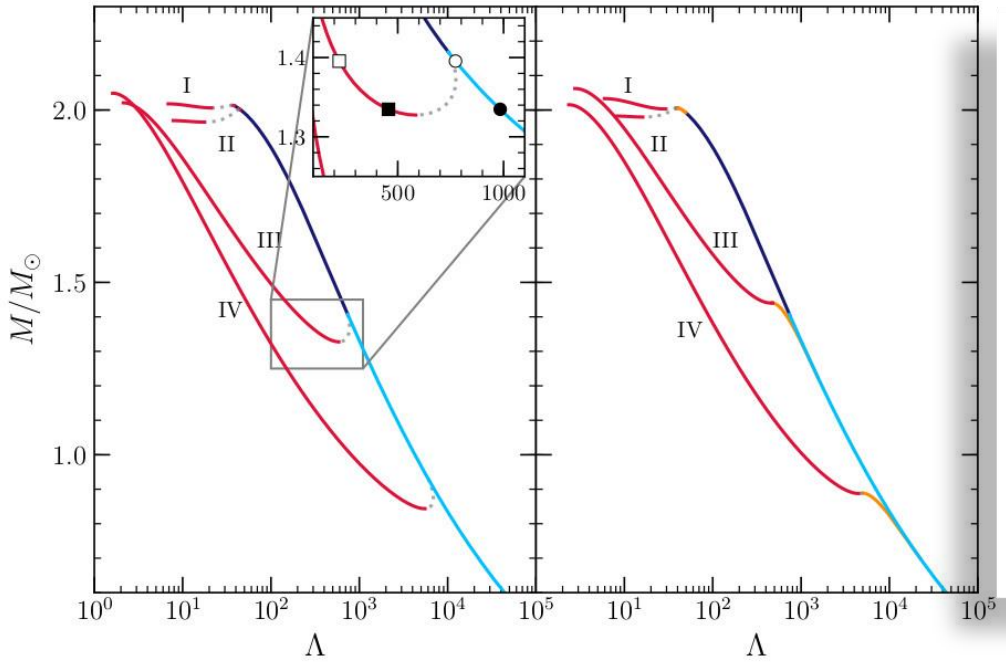

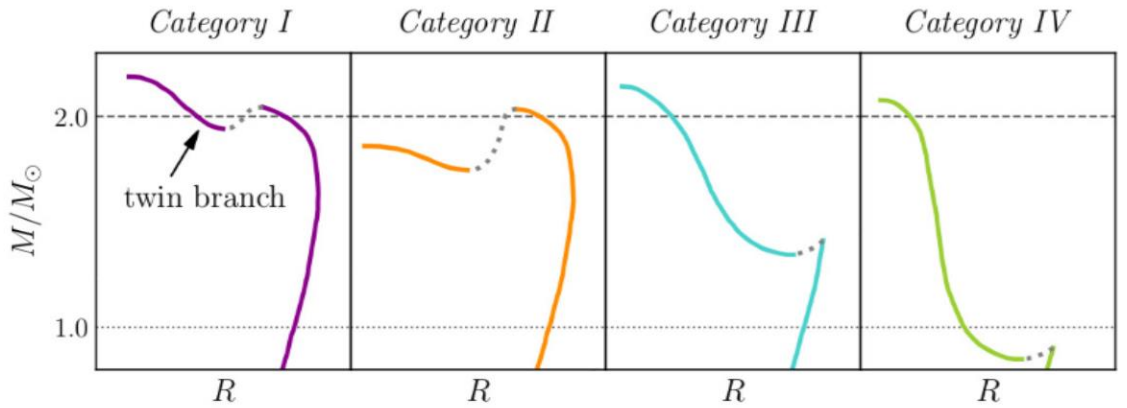

FIG. 3. Schematic behaviour of the mass–radius relation for the twin-star categories *I–IV* defined in the text. Note the appearance of a "twin" branch with a mixed or pure-quark phase; the twin branch has systematically smaller radii than the branch with a nuclear or hadronic phase. The colors used for these categories will be employed also in the subsequent figures.

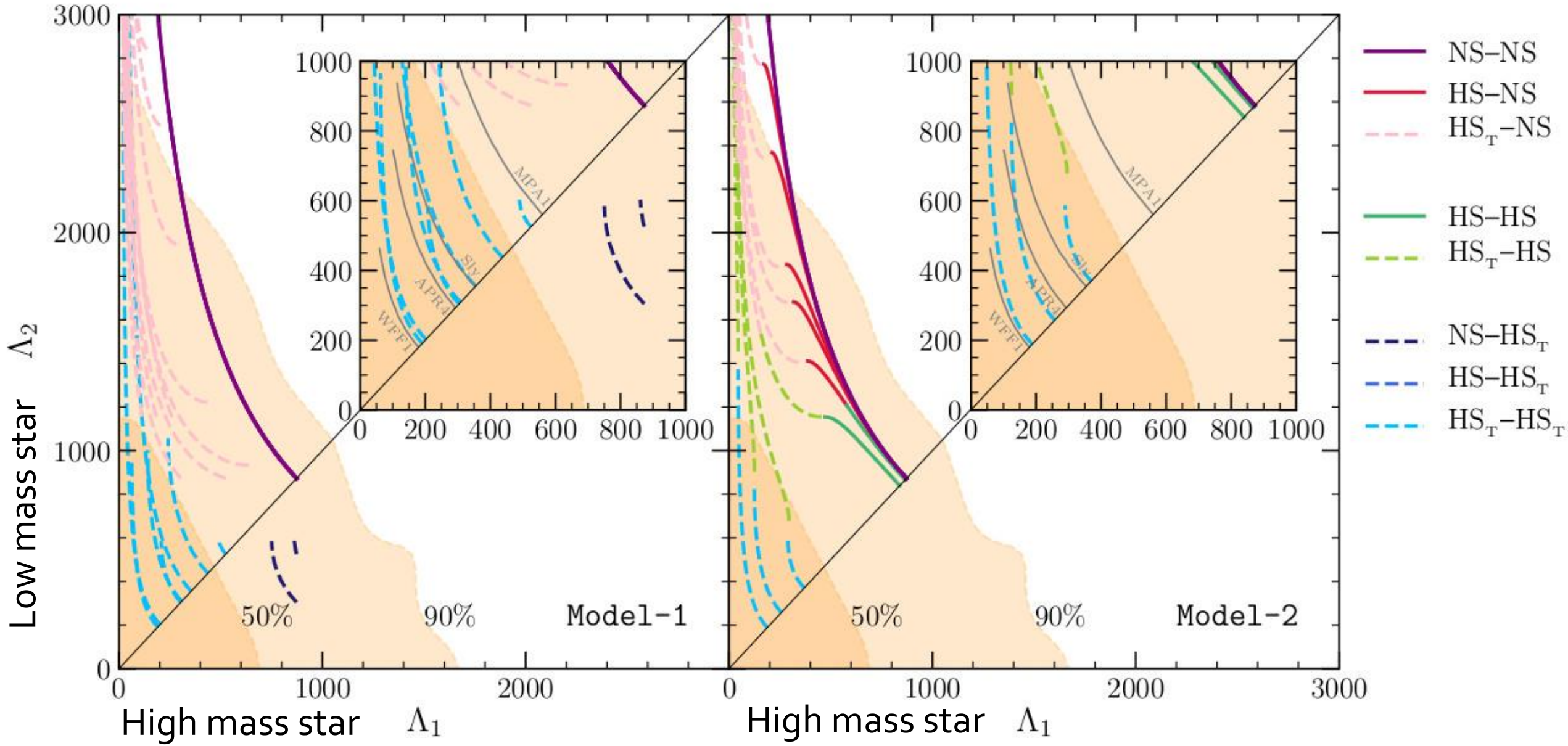

In a binary hybrid star merger the two masses of the individual stars can be different (q<1). As a result, the tidal deformability and the stars composition can be different. In this plot the total mass of the binary system has been fixed to the measured chirp mass of GW170817 (M=1.188 M_{solar}) and the different curve show results for EOSs of Category III.

Constraining the global parameters of the phase transition with GW170817

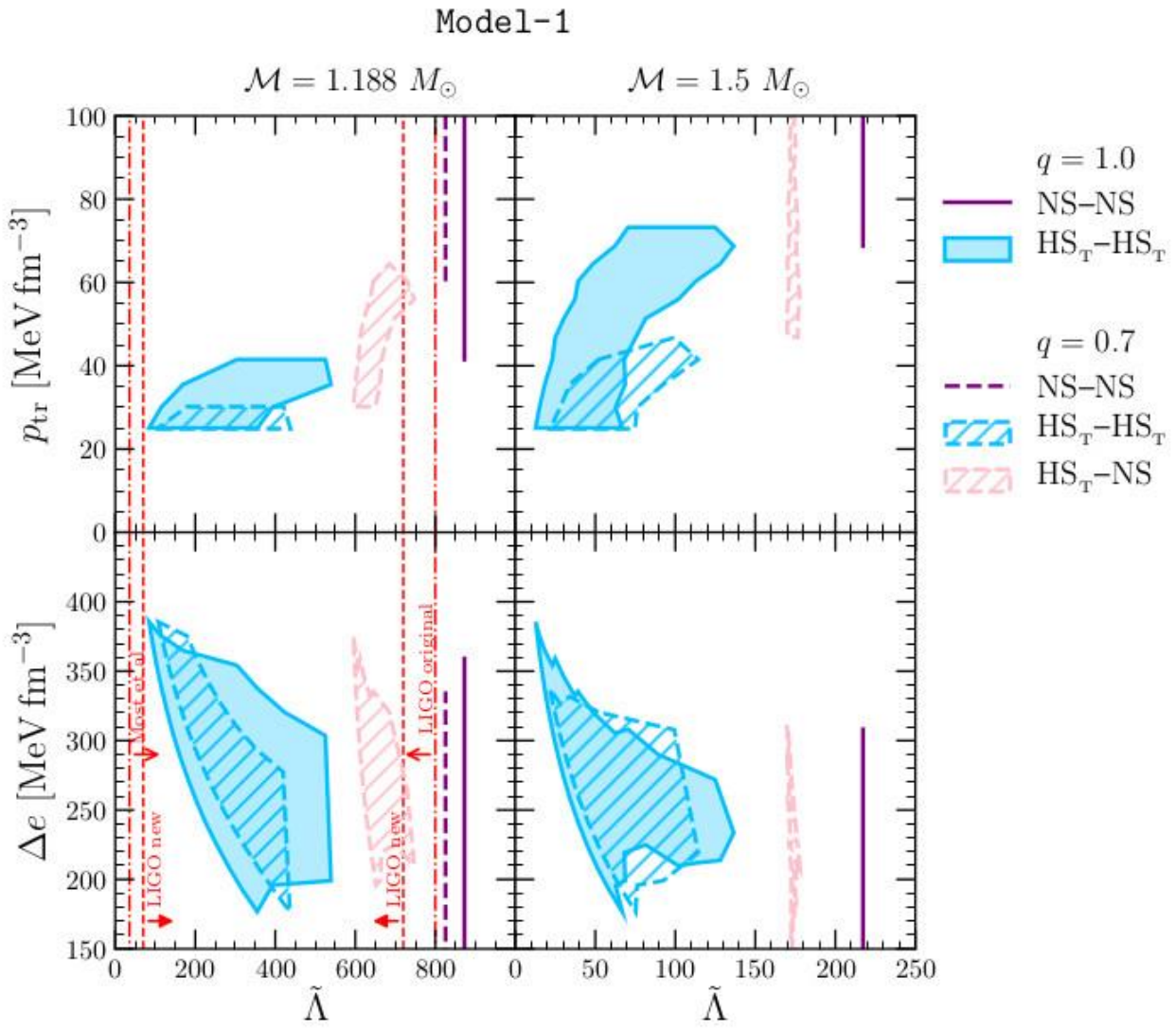

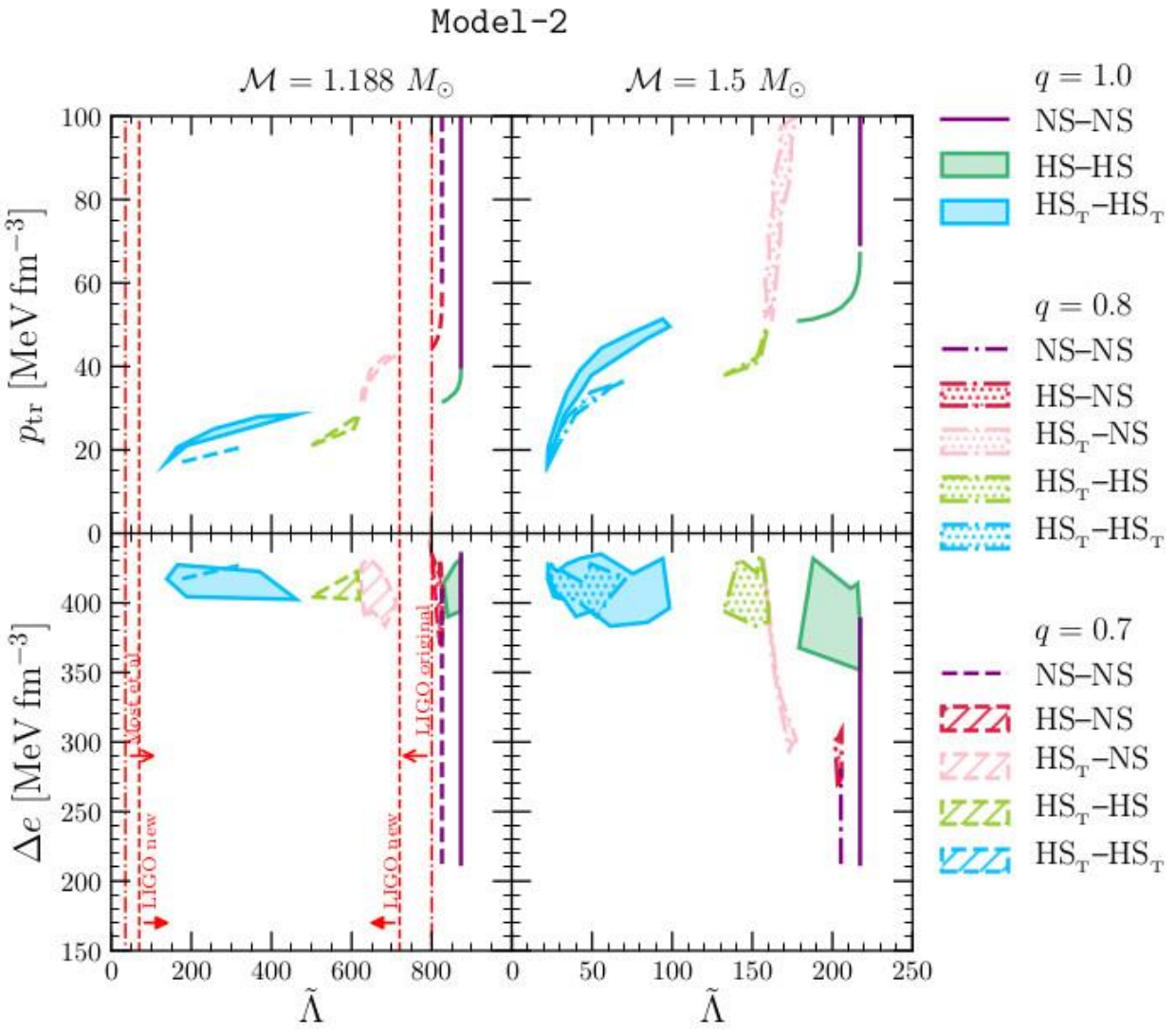

Binary Hybrid Star Mergers and the QCD Phase Diagram

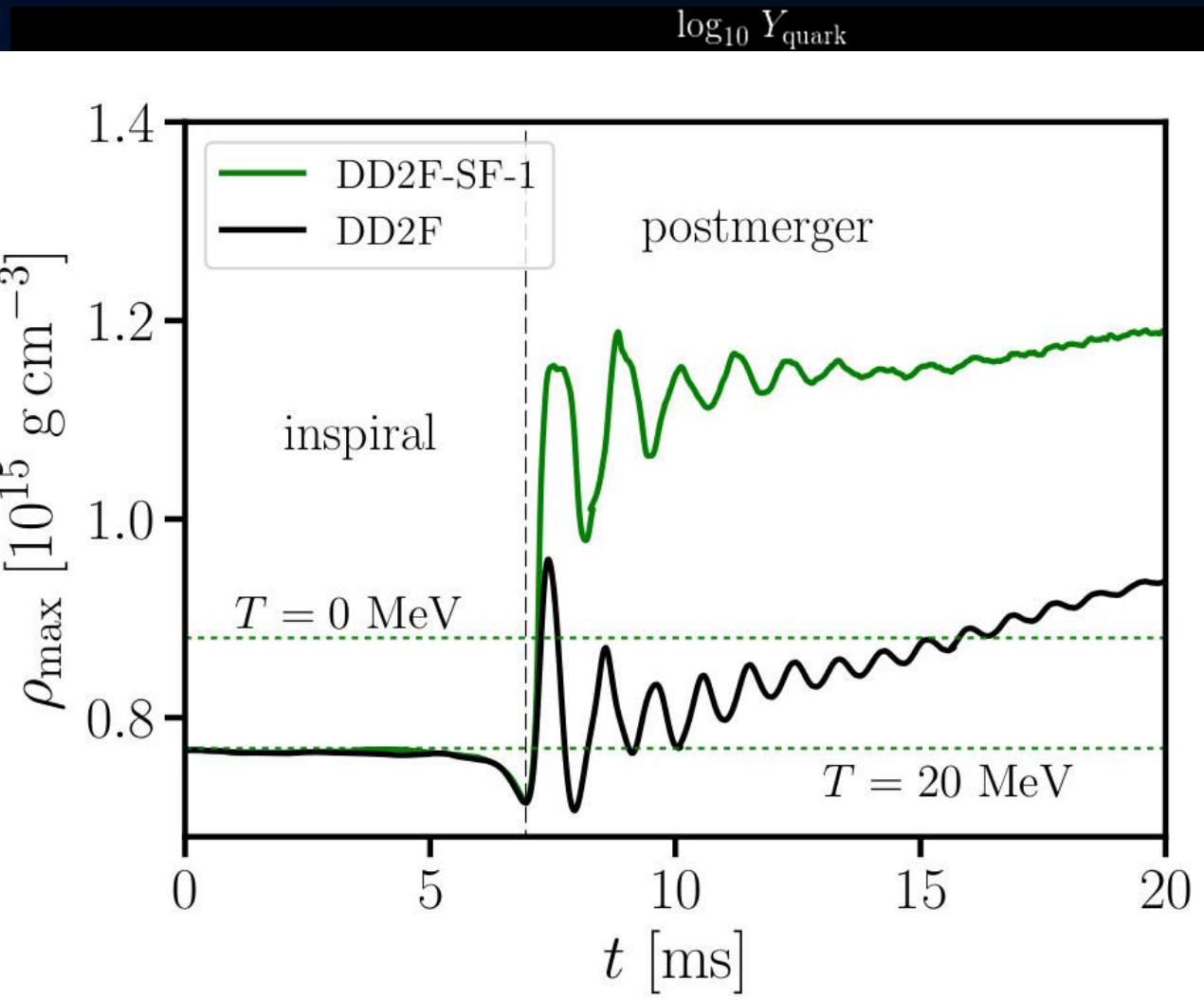

Hot and dense matter inside the inner area of a hypermassive

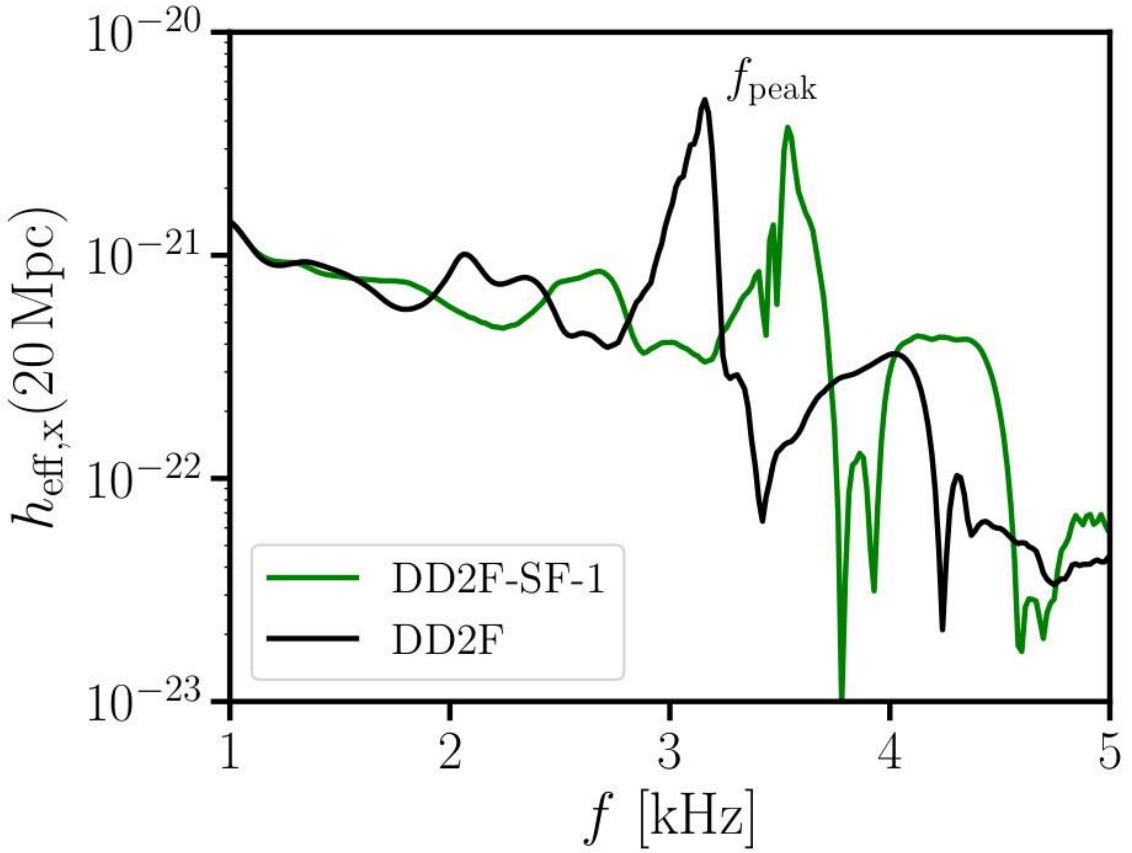

A.Bauswein, N.U.F. Bastian, D.B.Blaschke, K.Chatziioannou, J.A.Clark, T.Fischer and M.Oertel „Identifying a first-order transition in neutron star mergers through gravitational waves", PRL 2019

E.R.Most, L.J.Papenfort, V.Dexheimer, M.Hanauske, S.Schramm, H.Stöcker and L.Rezzolla „Signatures of quark-hadron phase transitions in general-relativistic neutron-star mergers„ PRL 2019

Post-merger gravitational-wave signatures of phase transitions in binary compact star mergers

PRL 124, 171103 (2020)

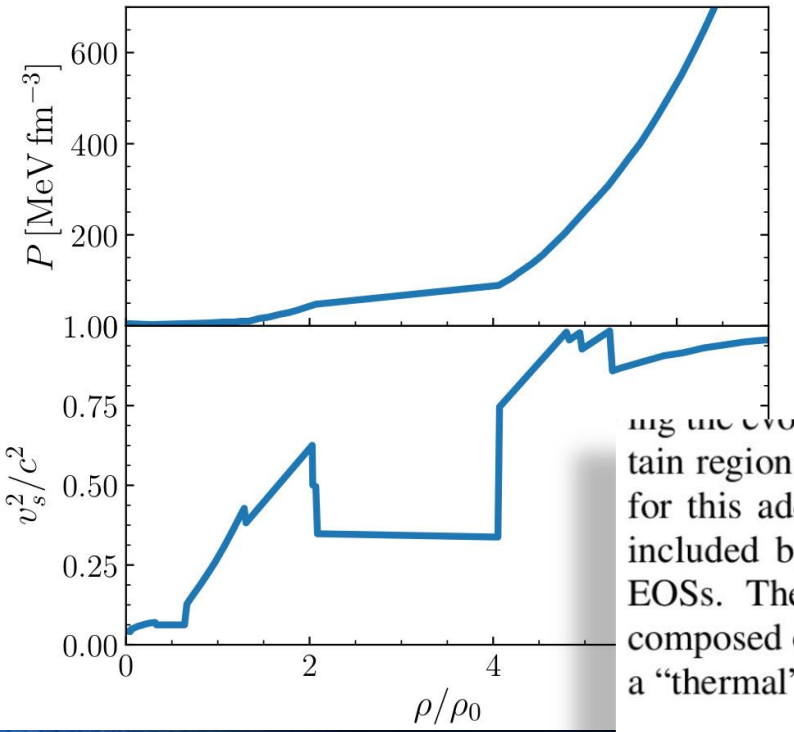

Cold EOS: FSU2H-PT

To account for additional shock heating during the merger and post-merger phase, thermal effects are included by adding a "thermal" ideal-fluid component ($p_{\rm th} = \rho\epsilon_{\rm th}\,(\Gamma_{\rm th} - 1)$) to the cold EOS where ρ is the rest-mass density, and $\Gamma_{\rm th} = 1.75$. The effective temperature obtained within this ideal-gas approach can be roughly approximated as $T = (m_{\rm n} p_{\rm th})/(k_{\rm B}\rho)$, where $m_{\rm n}$ is the nucleonic mass and $k_{\rm B}$ the Boltzmann constant. It should be stressed that the estimated temperature within this simple approximation only accounts for contributions of the ideal gas of neutrons and protons (mass differences have been neglected). Especially at the low-density regions of the outer crust of the hybrid star (which is composed of gas of leptons and nuclei at high values of electron fraction Y_e), the underlying temperature estimates deduced from the thermal pressure should be decreased by a factor $(1 + Y_e)$ and account

ing the evolution, shocks will increase the temperature in cer-
tain regions of the collapsing and oscillating star. To account
for this additional shock heating, the thermal effects where
included by adding an ideal-fluid component to the "cold"
EOSs. The pressure p and the specific internal energy ϵ are
composed of the "cold" part ($p_{\rm c}$) which includes a HQPT and
a "thermal" ideal-fluid component $p_{\rm th}$ [117]

pressure [see Eq. (2) in [26]]. Finally, the thermal
s not account for any contribution resulting from a
r transition and, as a result, the structure of the phase
om that resulting from fully temperature-dependent

$$p = p_{\rm c} + p_{\rm th}\,, \quad \epsilon = \epsilon_{\rm c} + \epsilon_{\rm th}\,, \quad p_{\rm th} = \frac{k_B}{m_N}\,\rho T\,, \qquad (3)$$

where p and ϵ are the pressure and specific internal energy, respectively. The "thermal" part of the EOS is given by

$$p_{\rm th} = \rho\,\epsilon_{\rm th}\,(\Gamma_{\rm th} - 1)\,, \qquad \epsilon_{\rm th} = \epsilon - \epsilon_{\rm c}\,, \qquad (4)$$

where $\Gamma_{\rm th} = 1.75$.

+ "thermal" ideal-fluid component

Hybrid Star Mergers with T-dependent EOS *(PRL paper 2)*

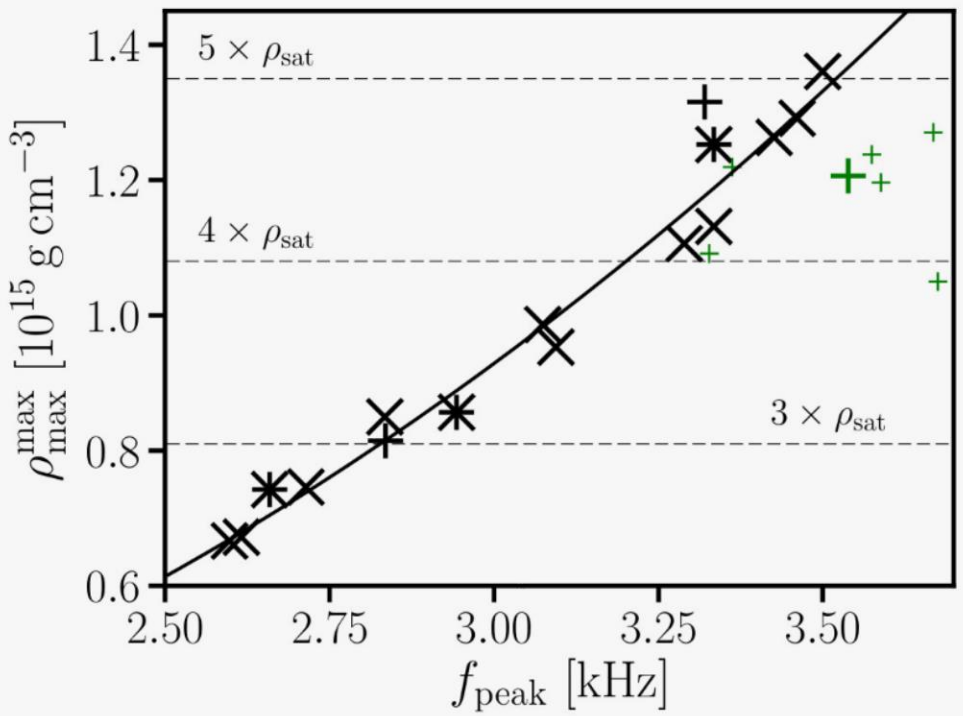

FIG. 4: Maximum rest-mass density $\rho_{\rm max}^{\rm max}$ during the first milliseconds of the postmerger phase as function of the dominant postmerger GW frequency $f_{\rm peak}$ for 1.35-1.35 $M_\odot$ mergers. Green symbols display results for DD2F-SF (big symbol for DD2F-SF-1). Asterisks indicate models with hyperons. Black plus signs display ALF2/4. Solid curve is a second order polynomial least square fit to the data excluding hybrid EOSs.

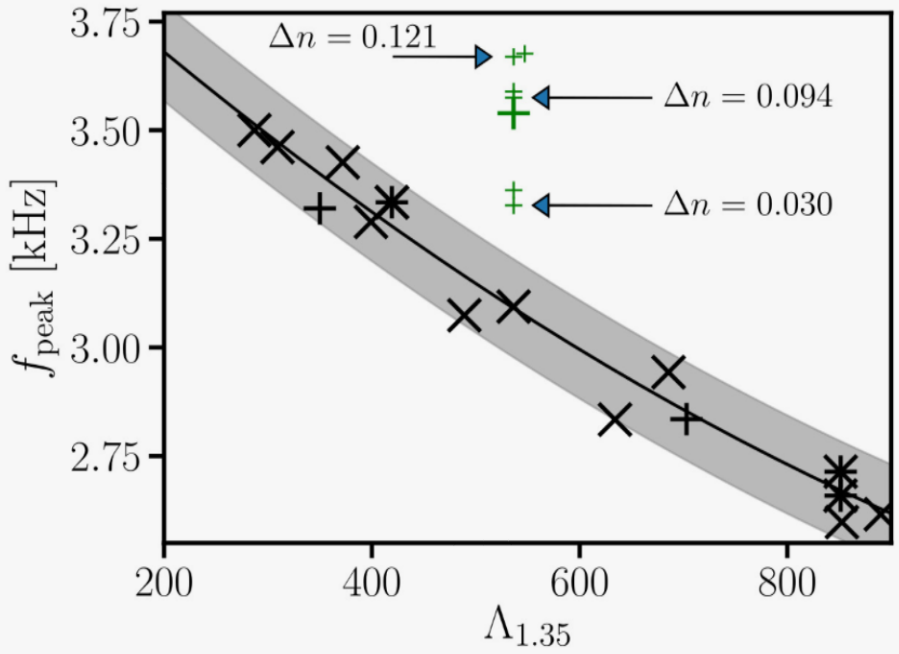

FIG. 3: Dominant postmerger GW frequency $f_{\rm peak}$ as function of tidal deformability Λ for 1.35-1.35 $M_\odot$ mergers. The DD2F-SF models with a phase transition to deconfined quark matter (green symbols) appear as clear outliers (big symbol for DD2F-SF-1). Solid curve displays the least square fit Eq. (1) for all purely hadronic EOSs (including three models with hyperons marked by asterisks). ALF2 and ALF4 are marked by black plus signs. EOSs incompatible with GW170817 are not shown. Arrows mark DD2F-SF models 3, 6 and 7, which feature differently strong density jumps Δn (in fm^{-3}) with roughly the same onset density and stiffness of quark matter.

GW170817: Constraining the Neutron Star Radius and EOS

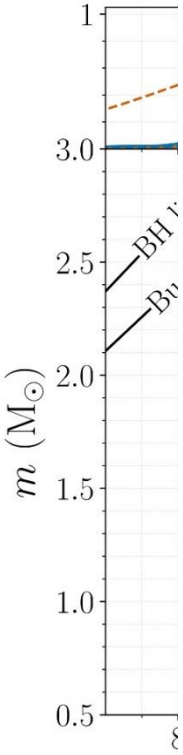

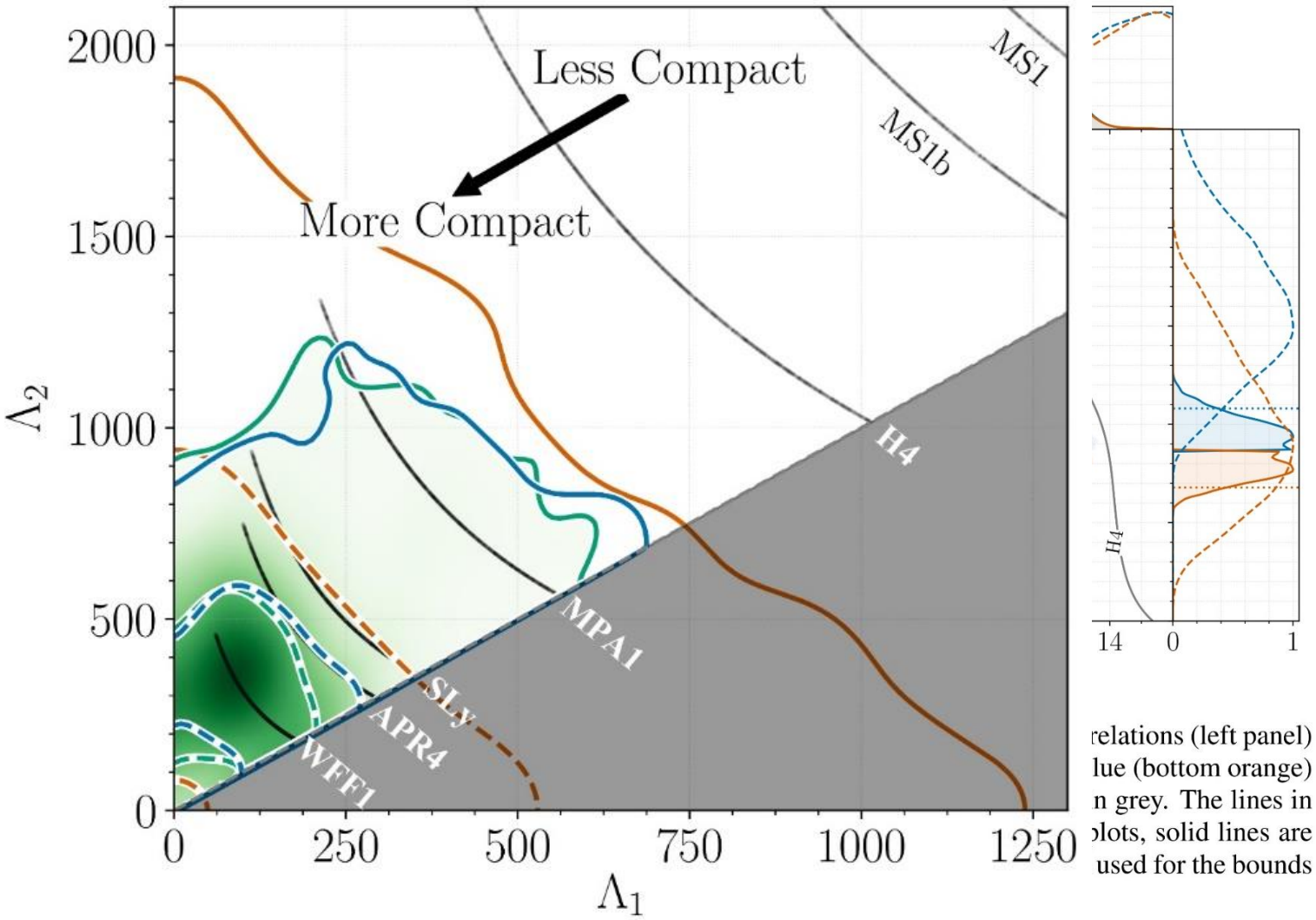

FIG. 3. Margin
and a parametr
posterior corre
the top left der
used for the po
of the 90% cre

relations (left panel)
lue (bottom orange)
n grey. The lines in
lots, solid lines are
used for the bounds

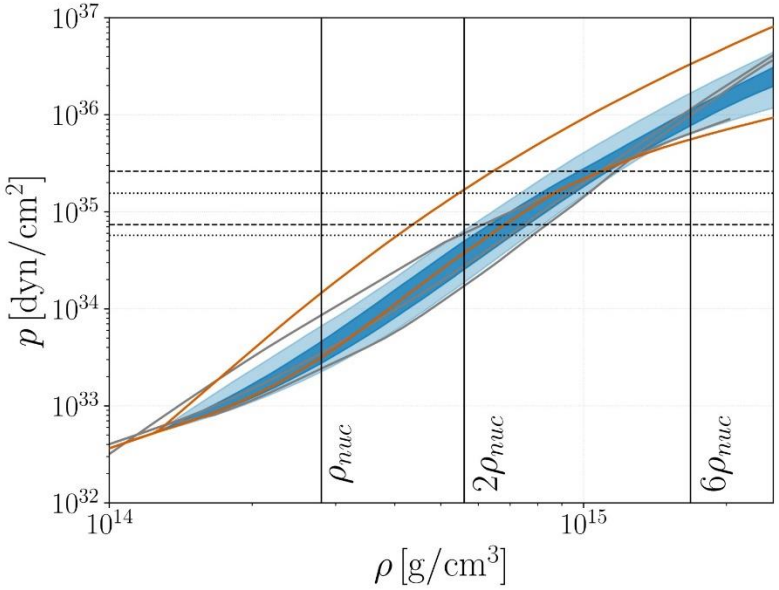

FIG. 2. Marginalized posterior (blue) and prior (orange) for the pressure p as a function of the rest-mass density ρ of the NS interior using the spectral EOS parametrization and imposing a lower limit on the maximum NS mass supported by the EOS of $1.97\,\mathrm{M}_\odot$. The dark (light) blue shaded region corresponds to the 50% (90%) posterior credible level and the orange lines show the 90% prior credible interval. Horizontal lines denote the 90% credible interval for the central pressure of the heavier (dashed) and the lighter (dotted) binary components. Vertical lines correspond to once, twice, and six times the nuclear saturation density. Overplotted in grey are representative EOS models [121, 122, 124], using data taken from [19]; from top to bottom at $2\rho_{\mathrm{nuc}}$ we show H4, APR4, and WFF1.

GW170817: Measurements of neutron star radii and equation of state, *The LIGO /Virgo Collaboration*, arXiv:1805.11581v1

GW170817: ...us

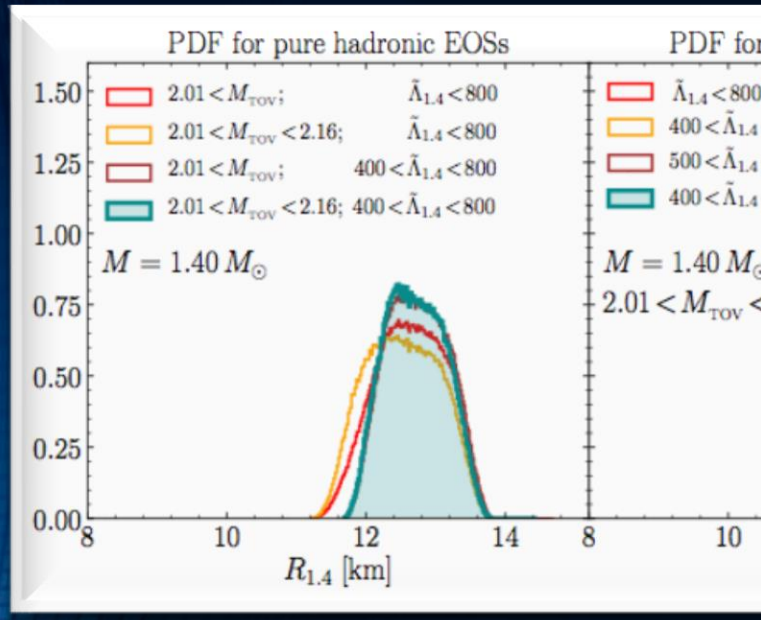

$$12.00 < R_{1.4}/\mathrm{km} < 13.45$$

$$8.53 < R_{1.4}/\mathrm{km} < 13.74 \qquad \bar{R}$$

Reference	R_i [km]
Without a phase transition	
Bauswein et al. [42]	$10.68^{+0.15}_{-0.03} \leq R_{1.6}$
Most et al. [51]	$12.00 \leq R_{1.4} \leq 13.45$
Burgio et al. [54]	$11.8 \leq R_{1.5} \leq 13.1$
Tews et al. [55]	$11.3 \leq R_{1.4} \leq 13.6$
De et al. [56]	$8.9 \leq R_{1.4} \leq 13.2$
LIGO/Virgo [57]	$10.5 \leq R_{1.4} \leq 13.3$
With a phase transition	
Annala et al. [46]	$R_{1.4} \leq 13.6$
Most et al. [51]	$8.53 \leq R_{1.4} \leq 13.74$
Burgio et al. [54]	$R_{1.5} = 10.7$
Tews et al. [55]	$9.0 \leq R_{1.4} \leq 13.6$
This work	
NS	$R_{1.4} = 13.11$
HS Model-2	$12.9 \leq R_{1.4} \leq 13.11$
HS_T Model-1	$10.1 \leq R_{1.4} \leq 12.9$
HS_T Model-2	$10.4 \leq R_{1.4} \leq 11.9$

TABLE II. Constraints on the radius of neutron stars from GW170817 for models without a phase transition (top), works considering the possibility of a transition to quark matter (middle) and for EOSs of *Category III* in the present work (bottom).

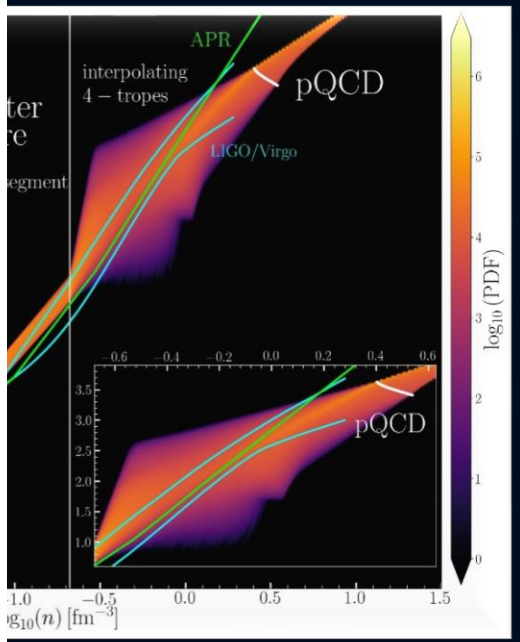

t, L.Weih, L.Rezzolla, J.
ner-Bielich "New
aints on radii and tidal
nabilities of neutron
rom GW170817",
1803.00549,
oted in PRL)

See also: De, Finstad, Lattimer, Brown, Berger, Biwe
172702 (2018) ; Nandi & Char, Astrophys. J. 857, 12 (201
Annala, Gorda, Kurkela, Vuorinen, PRL 120, 172703 (201

v, Piekarewicz, Horowitz, PRL 120,
ros, PRD 97, 021501 (2018) ;

Constraining the mass and radius with GW170817

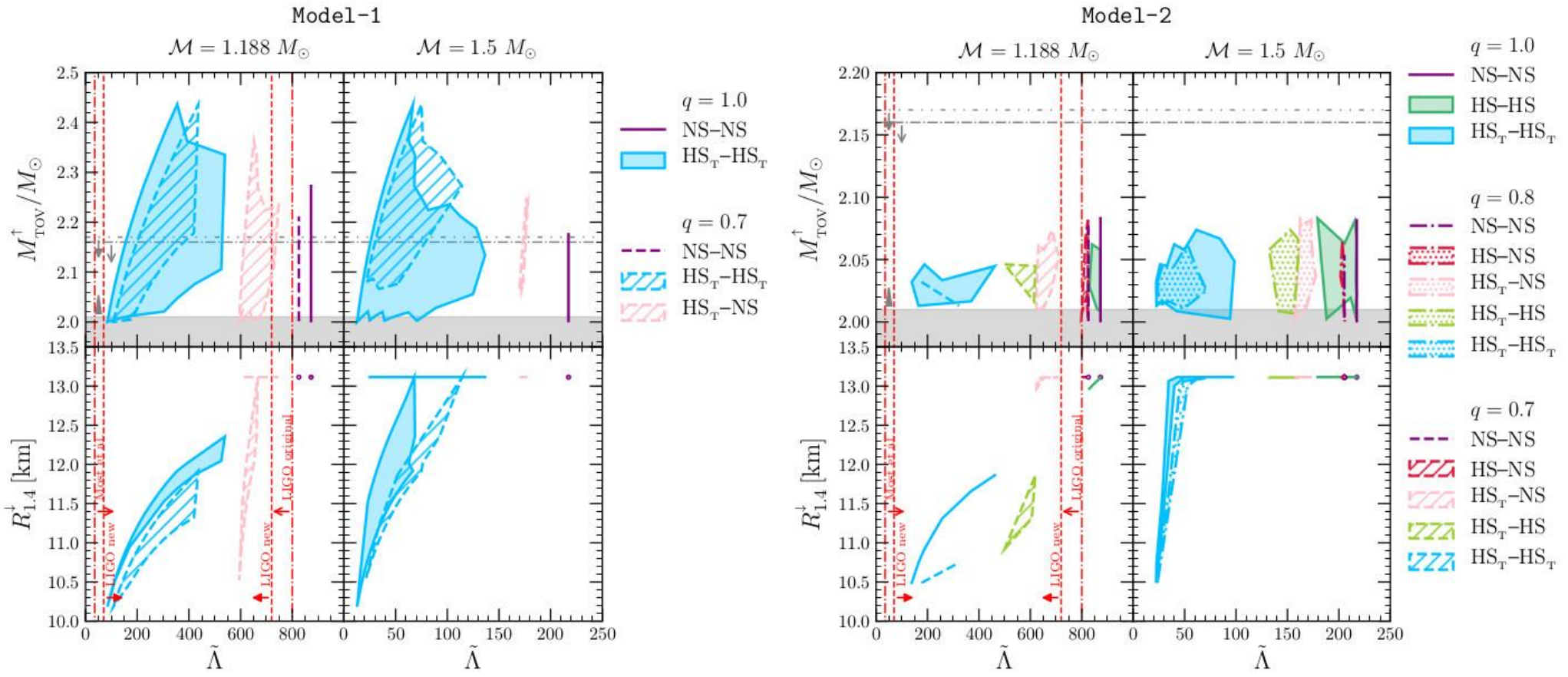

FIG. 10. Left plot: Maximum mass (upper panels) and radius of a 1.4 $M_\odot$ star (lower panels) as a function of the weighted $\tilde{\Lambda}$ for the same cases as in the left plot of Fig. 9. Right plot: Maximum mass (upper panels) and radius of a 1.4 $M_\odot$ star (lower panels) as a function of the weighted $\tilde{\Lambda}$ for the same cases as in the right plot of Fig. 9. In these plots, together with the constraints on tidal deformability, we display a lower horizontal band coming from the lower limit of 2 $M_\odot$ observations [19, 20] as well as recent constraints on the maximum mass of $\sim$ 2.16–2.17 $M_\odot$ from multi-messenger observations of GW170817 [41, 44].

The long-awaited event GW170817

	Low-spin priors ($\lvert\chi\rvert \leq 0.05$)	High-spin priors ($\lvert\chi\rvert \leq 0.89$)
Primary mass m_1	1.36–1.60 $M_\odot$	1.36–2.26 $M_\odot$
Secondary mass m_2	1.17–1.36 $M_\odot$	0.86–1.36 $M_\odot$
Chirp mass $\mathcal{M}$	$1.188^{+0.004}_{-0.002} M_\odot$	$1.188^{+0.004}_{-0.002} M_\odot$
Mass ratio m_2/m_1	0.7–1.0	0.4–1.0
Total mass $m_{\rm tot}$	$2.74^{+0.04}_{-0.01} M_\odot$	$2.82^{+0.47}_{-0.09} M_\odot$
Radiated energy $E_{\rm rad}$	$> 0.025 M_\odot c^2$	$> 0.025 M_\odot c^2$
Luminosity distance $D_{\rm L}$	40^{+8}_{-14} Mpc	40^{+8}_{-14} Mpc
Viewing angle Θ	$\leq 55°$	$\leq 56°$
Using NGC 4993 location	$\leq 28°$	$\leq 28°$
Combined dimensionless tidal deformability $\tilde{\Lambda}$	≤ 800	≤ 700
Dimensionless tidal deformability $\Lambda(1.4 M_\odot)$	≤ 800	≤ 1400

Gravitational Wave GW170817 and Gamma-Ray Emission GRB170817A

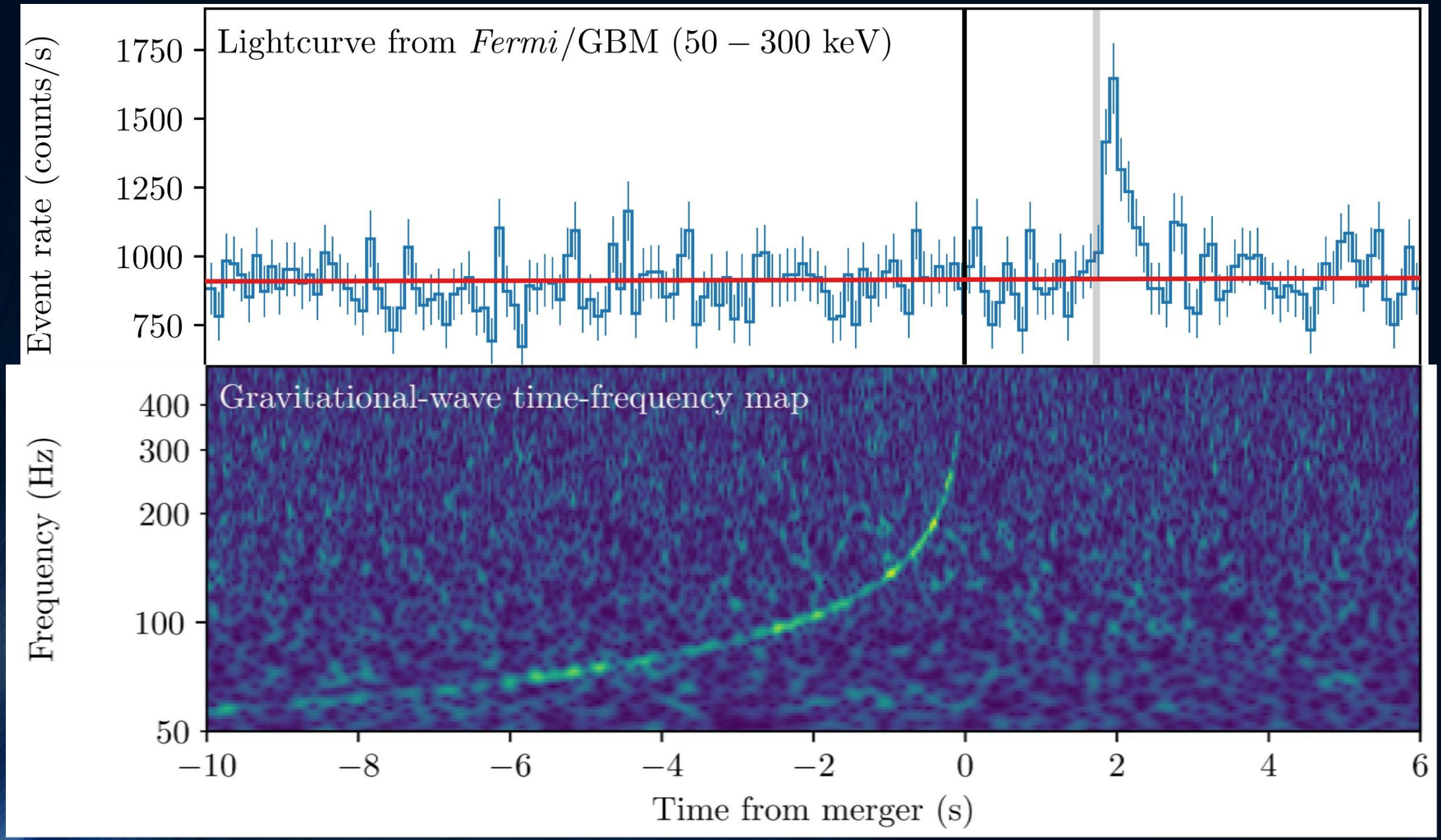

GW170817

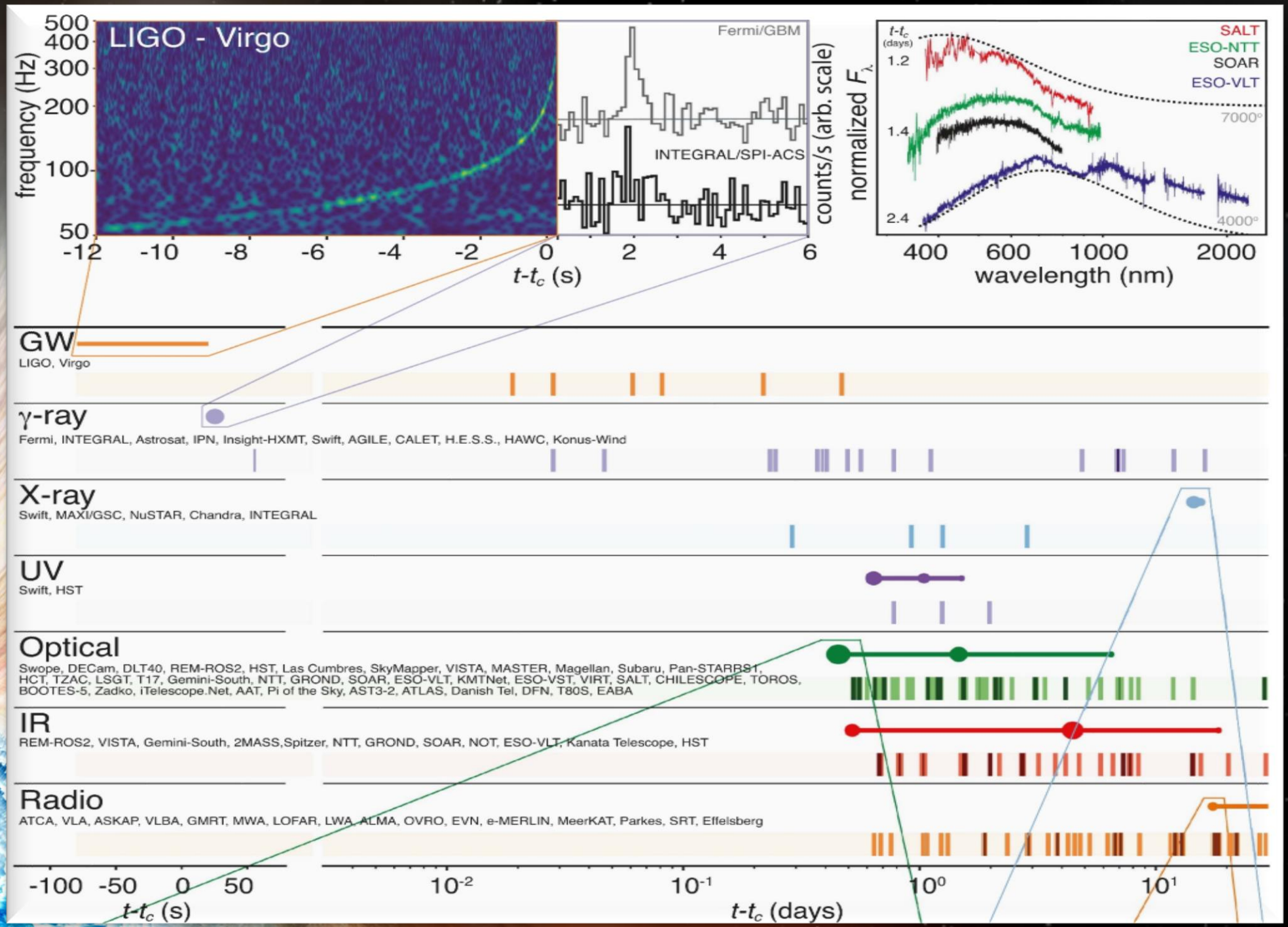
LIGO - Virgo
frequency (Hz)
500
400
300
200
100
50
-12
-10
-8
-6
-4
-2
0
2
4
6
t-t_c (s)
Fermi/GBM
INTEGRAL/SPI-ACS
counts/s (arb. scale)
t-t_c (days)
1.2
1.4
2.4
normalized F_λ
SALT
ESO-NTT
SOAR
ESO-VLT
7000°
4000°
400
600
1000
2000
wavelength (nm)
GW
LIGO, Virgo
γ-ray
Fermi, INTEGRAL, Astrosat, IPN, Insight-HXMT, Swift, AGILE, CALET, H.E.S.S., HAWC, Konus-Wind
X-ray
Swift, MAXI/GSC, NuSTAR, Chandra, INTEGRAL
UV
Swift, HST
Optical
Swope, DECam, DLT40, REM-ROS2, HST, Las Cumbres, SkyMapper, VISTA, MASTER, Magellan, Subaru, Pan-STARRS1, HCT, TZAC, LSGT, T17, Gemini-South, NTT, GROND, SOAR, ESO-VLT, KMTNet, ESO-VST, VIRT, SALT, CHILESCOPE, TOROS, BOOTES-5, Zadko, iTelescope.Net, AAT, Pi of the Sky, AST3-2, ATLAS, Danish Tel, DFN, T80S, EABA
IR
REM-ROS2, VISTA, Gemini-South, 2MASS,Spitzer, NTT, GROND, SOAR, NOT, ESO-VLT, Kanata Telescope, HST
Radio
ATCA, VLA, ASKAP, VLBA, GMRT, MWA, LOFAR, LWA, ALMA, OVRO, EVN, e-MERLIN, MeerKAT, Parkes, SRT, Effelsberg
-100
-50
0
50
t-t_c (s)
10^{-2}
10^{-1}
10^{0}
10^{1}
t-t_c (days)

The second event: GW190425

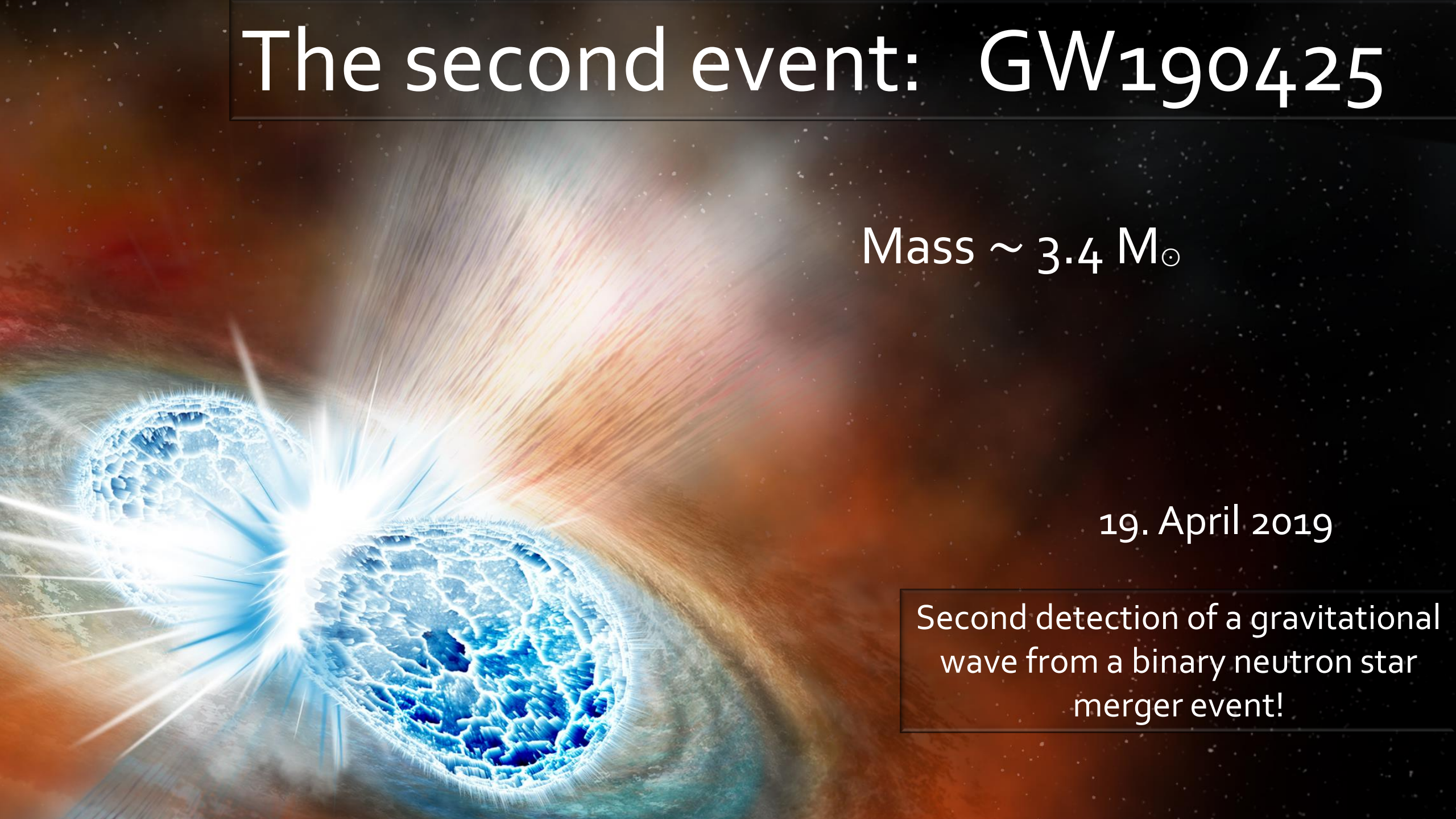

Mass ~ 3.4 $M_\odot$

19. April 2019

Second detection of a gravitational wave from a binary neutron star merger event!

The third event ? GW190814

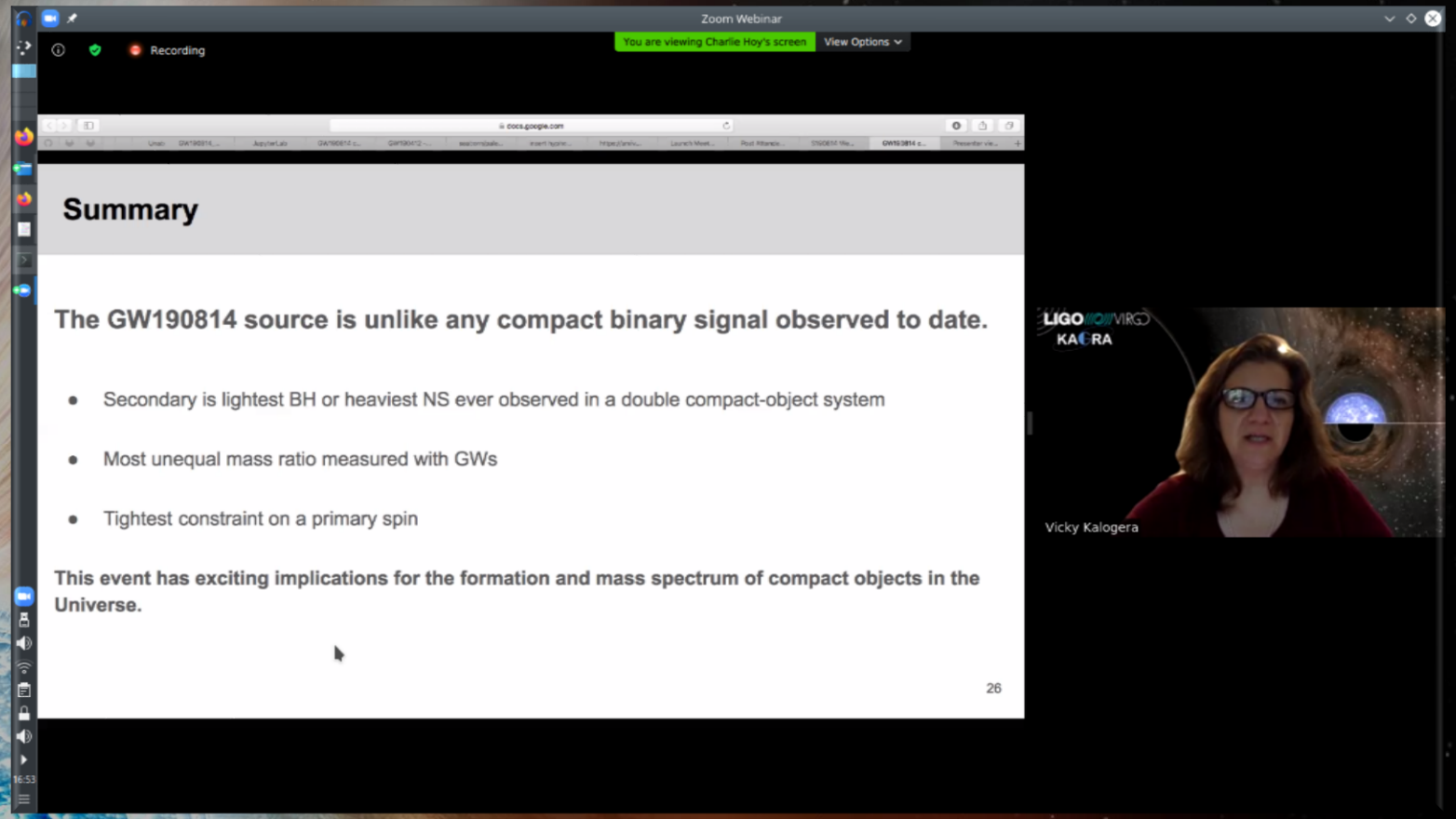

Where are we?

From O1 and O2:

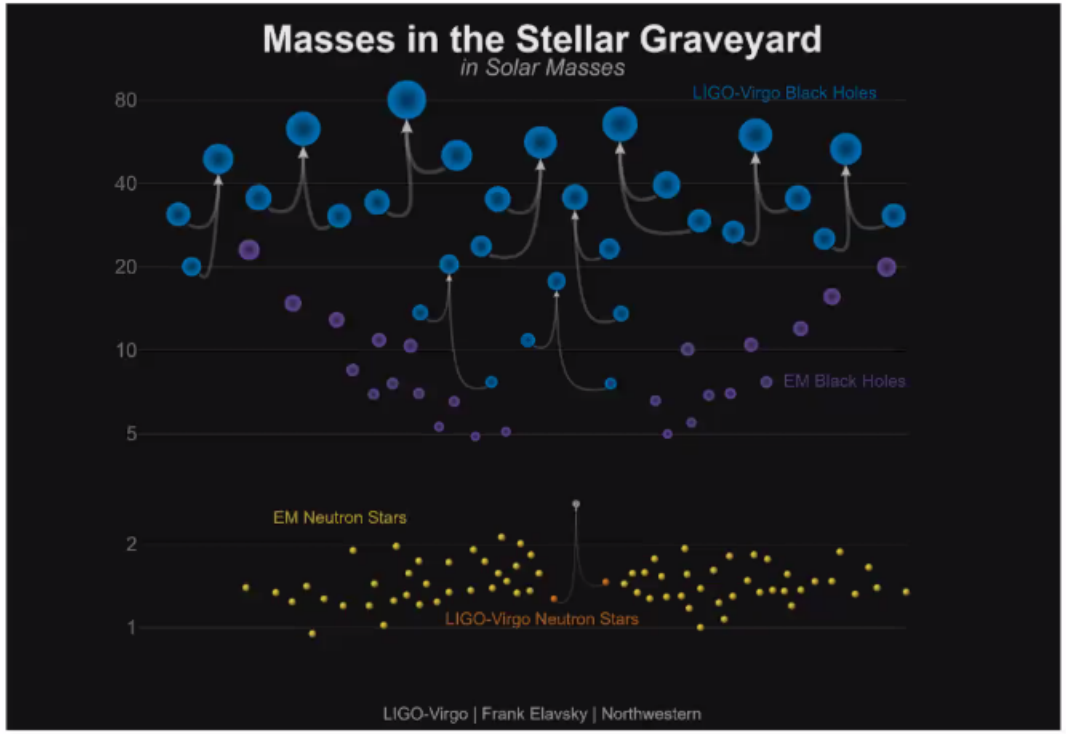

O3 (Apr 2019 - Mar 2020):

GW190425: Likely BNS with component masses between: 1.12-2.52 $M_\odot$

GW190412: BBH with component masses ~30 $M_\odot$ and ~8$M_\odot$

~50 candidate events from the O3 public alerts

4

At the time of GW190814...

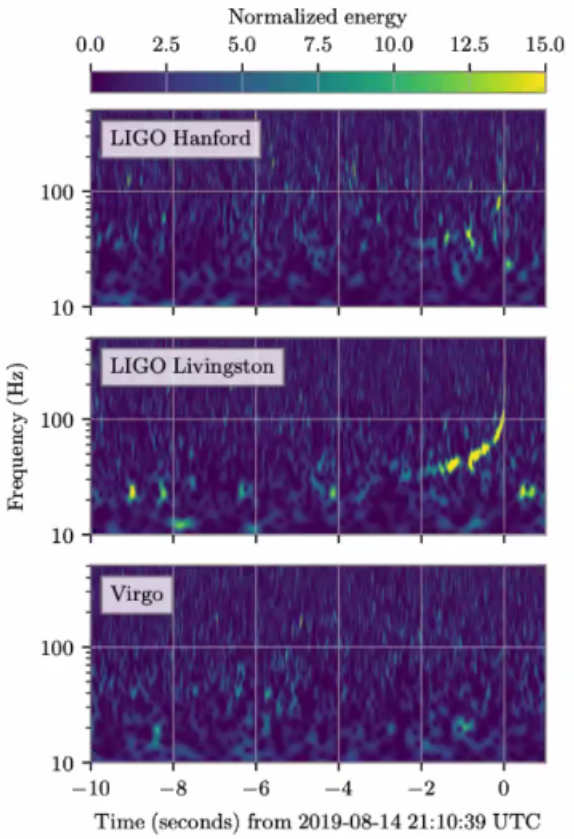

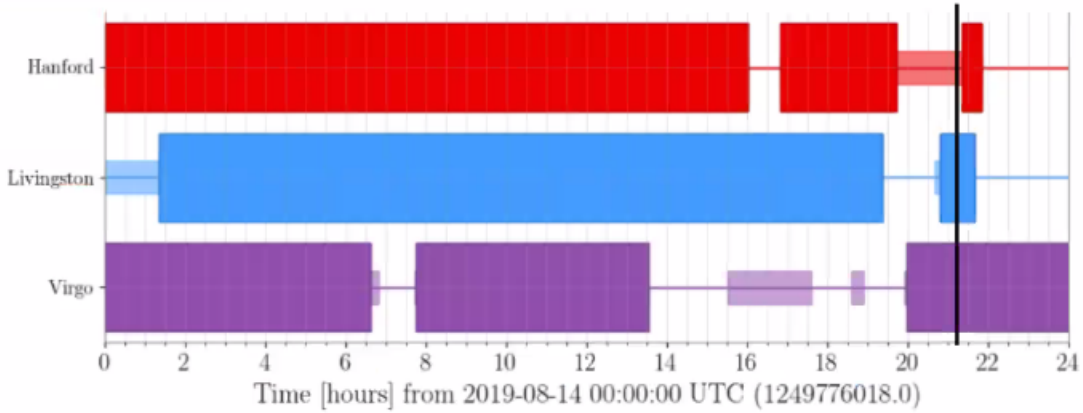

- +/- 5 minutes around GW190814 no commissioning activities were taking place at Hanford
- We find no evidence instrumental or environmental disturbances could account for GW190814
- Note: there is some low-frequency transient noise due to scattered light in Livingston caused by thunderstorms

5

docs.google.com

GW190814 colloquium

File Edit View Insert Format Slide Arrange Tools Add-ons Help Last edit was made 23 minu...

Present Share

Background Layout Theme Transition

Detecting GW190814

14th Aug 2019 21:11 UTC	Loud 2-detector event by low latency GstLAL
~21:30 UTC	GCN issued: - Blue skymap - Classification = Mass Gap
~23:30 UTC	- GstLAL & PyCBC reanalysed data with 3 detectors - SNR: Hanford 10.6, Livingston 21.6, Virgo 4.5 - GCN circular issued: - orange skymap (38 deg^2)
15th Aug 2019 ~10:41 UTC	GCN circular: - Green skymap (23 deg^2) - Classification = NSBH

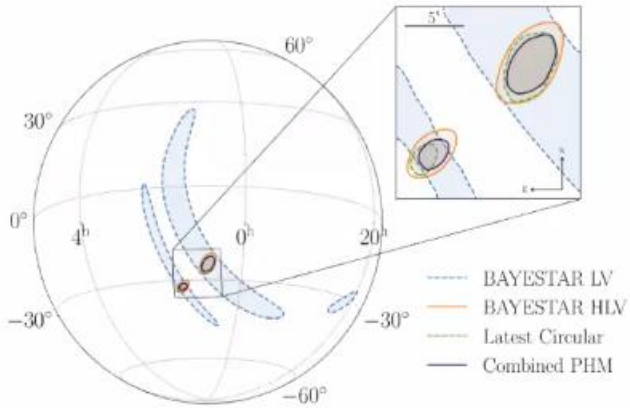

No electromagnetic or neutrino counterpart has been reported

6

Click to add speaker notes

Laura Nuttall

GW190814 - Source frame masses

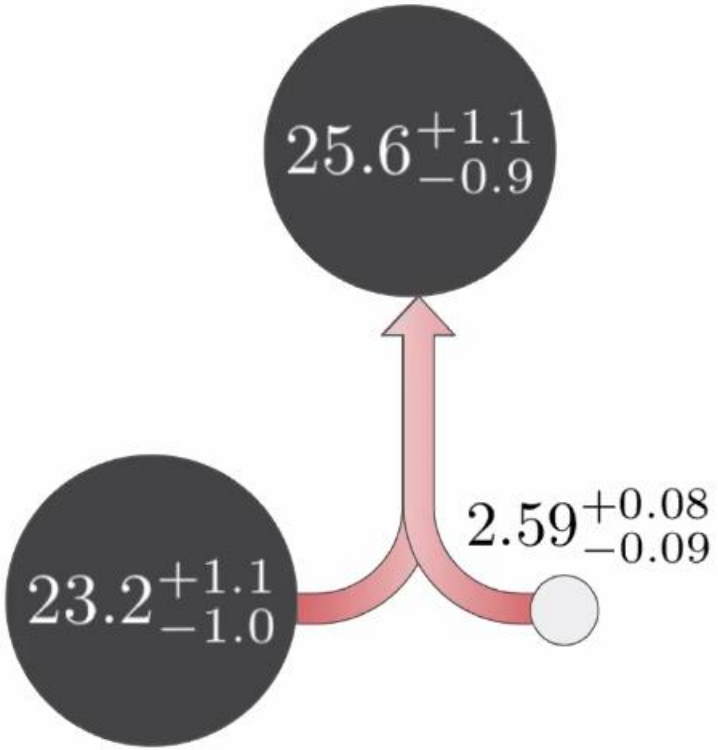

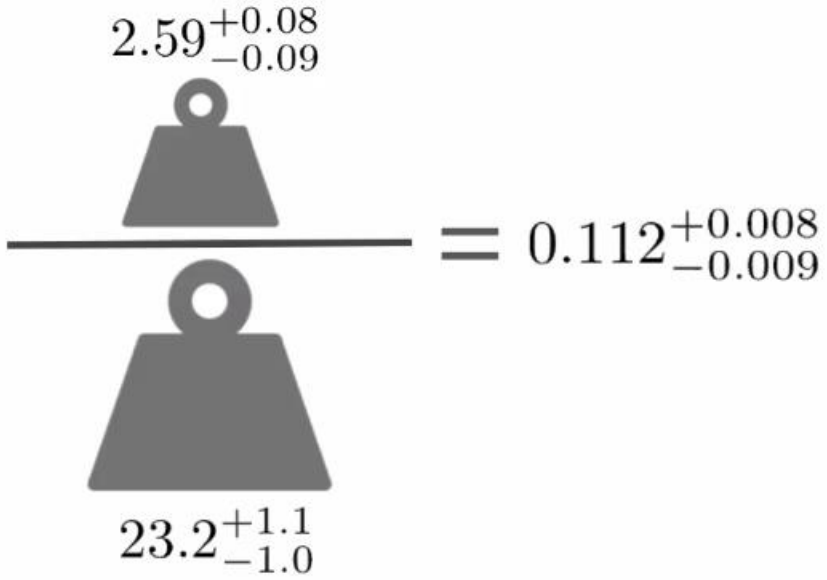

8

docs.google.com

GW190814 - Source frame masses

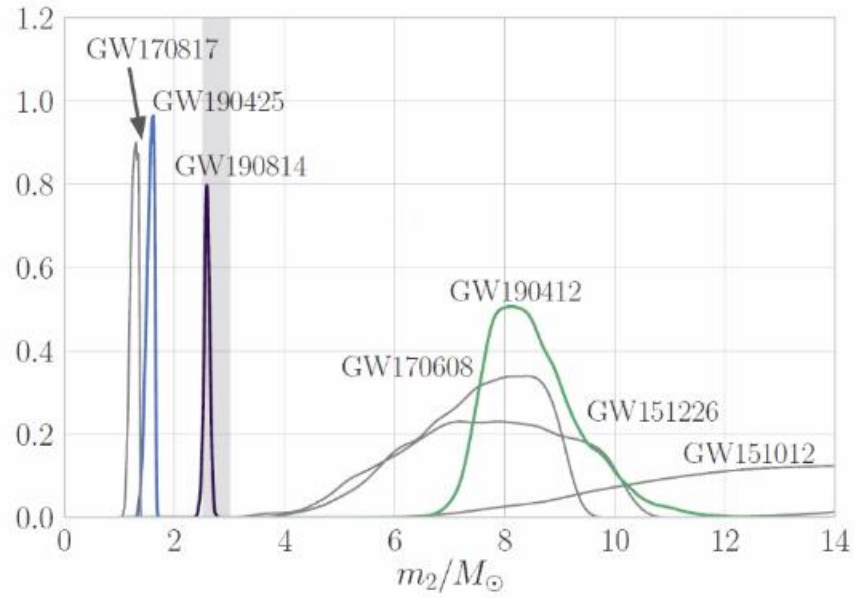

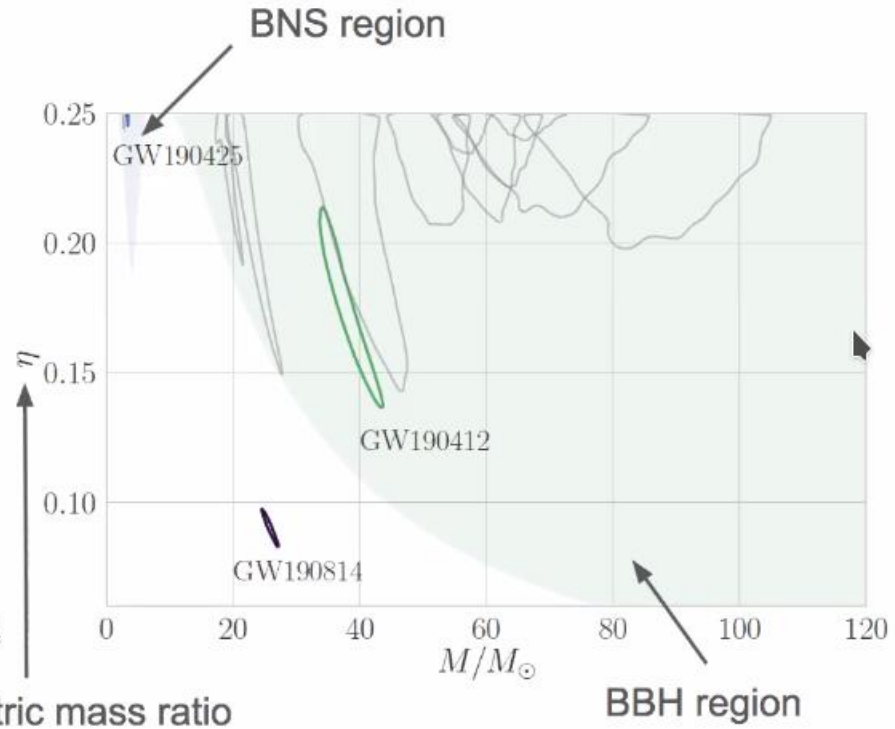

GWTC-1: LIGO Scientific Collaboration, and Virgo Collaboration (2019)
GW190425: LIGO Scientific Collaboration, and Virgo Collaboration (2020)
GW190412: LIGO Scientific Collaboration, and Virgo Collaboration (2020)

docs.google.com

GW190814 - Searching for tidal signatures

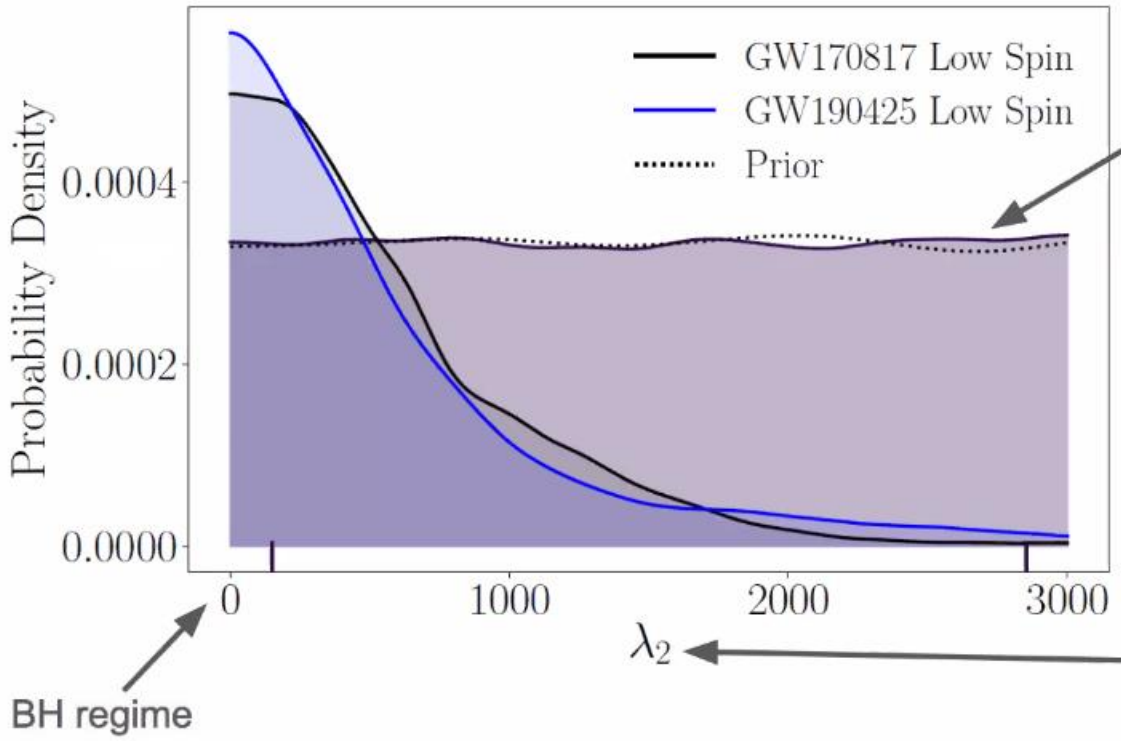

For GW190814, we recover no information about the tidal deformability of the secondary object.

Tidal deformability of the secondary object

docs.google.com

GW190814 - Spins

Upper bound on primary spin magnitude χ_1 : 0.07

Effective inspiral spin parameter $\chi_{\rm eff}$: $-0.002^{+0.060}_{-0.061}$

Upper bound on effective precession parameter $\chi_{\rm p}$: 0.07

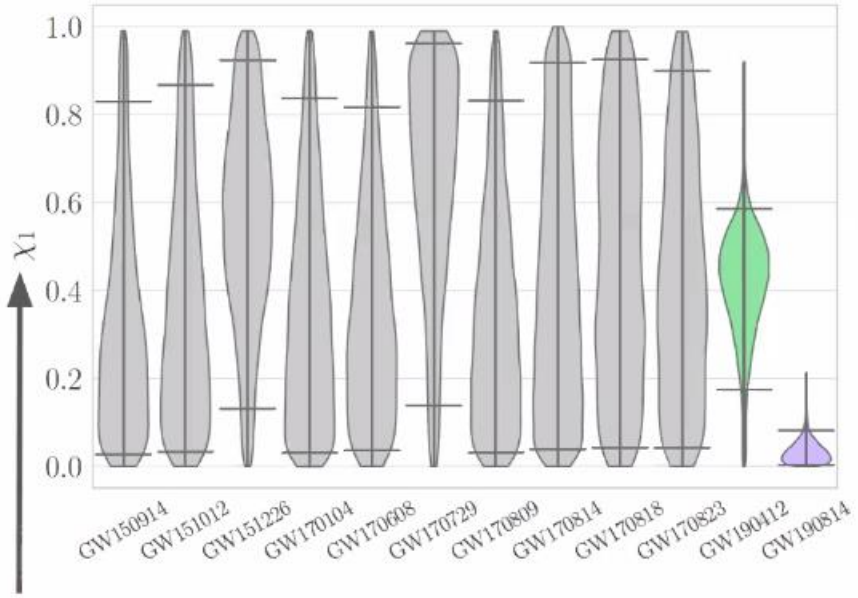

Primary spin magnitude

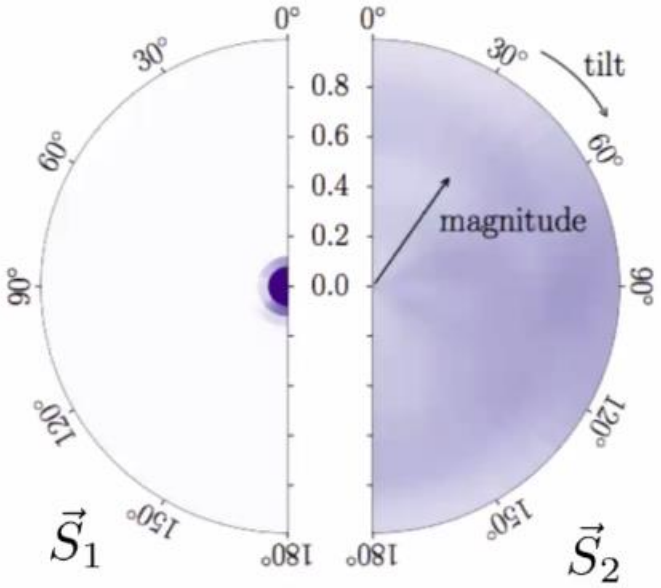

11

16:29

Higher order multipoles

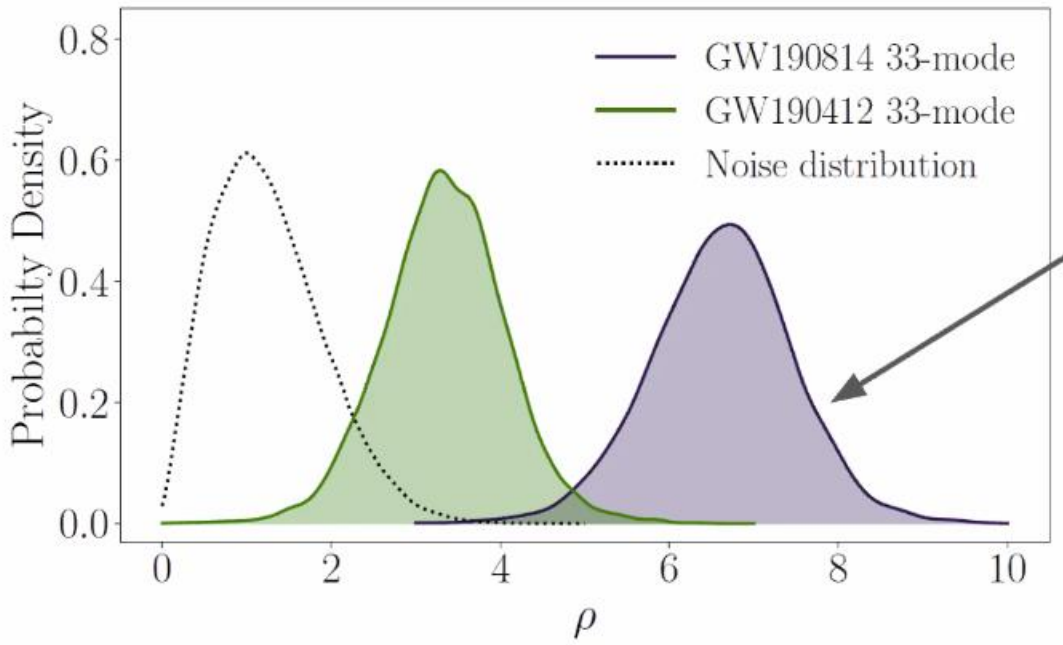

GW190814 has the strongest evidence for Higher order multiples that we have ever detected.

SNR in 33 multipole nearly as high as the total SNR of GW151012

docs.google.com

Compact object from the mass gap

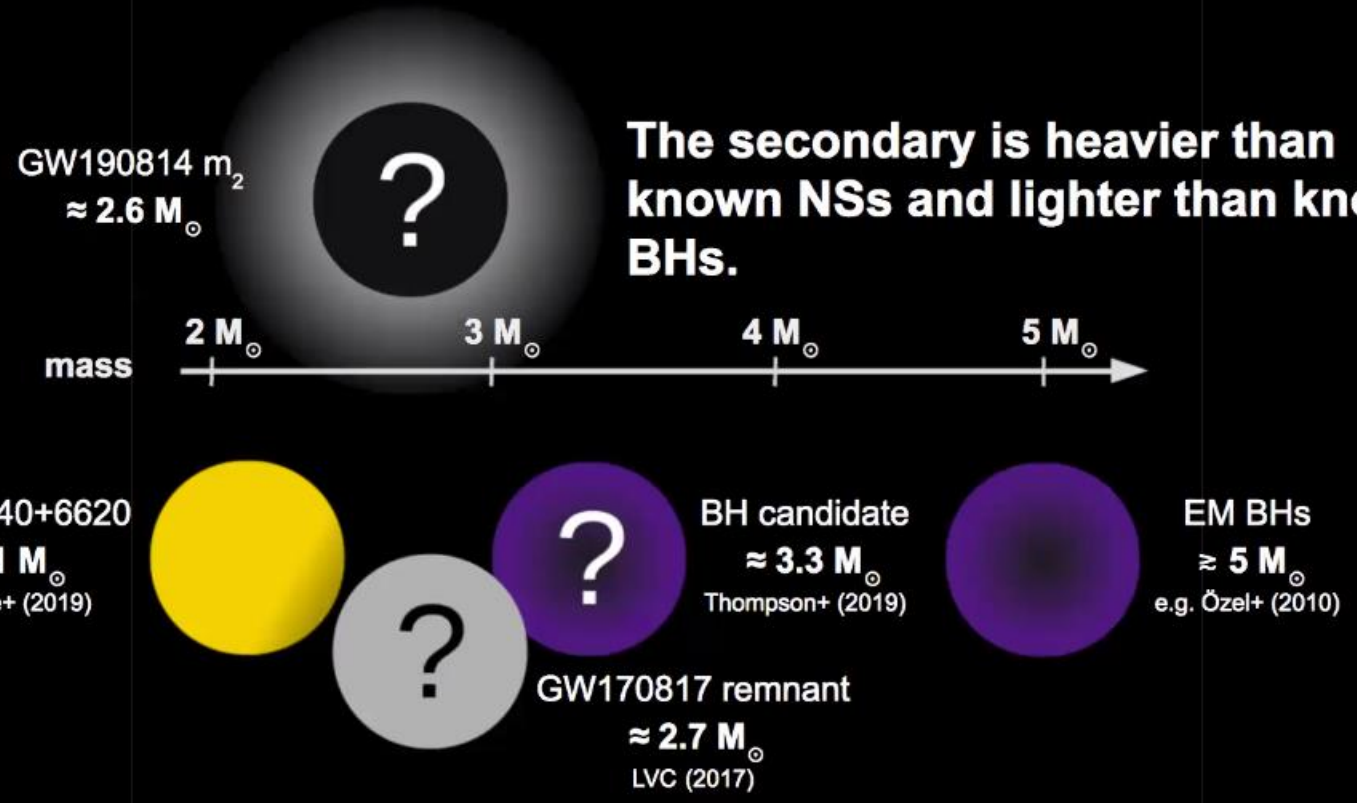

14

Philippe Landry

docs.google.com

Heavy neutron star or light black hole?

The secondary mass is above typical estimates of the maximum NS mass.

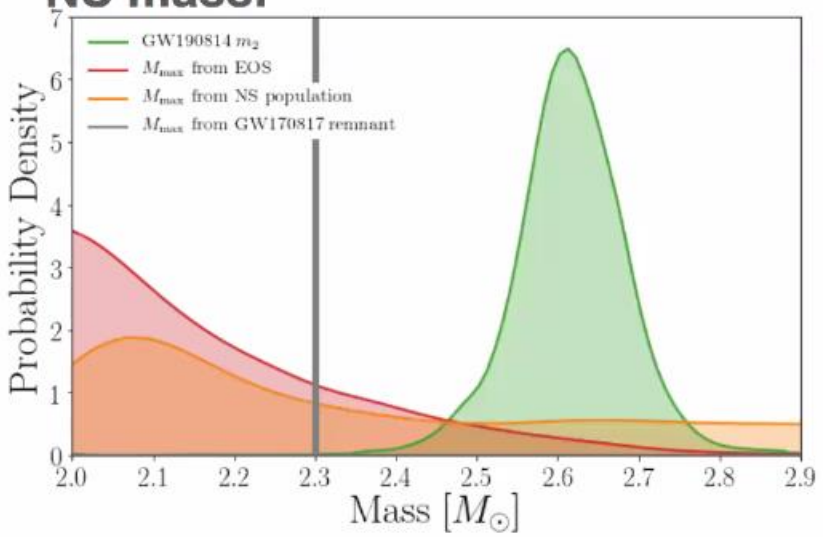

M_{max} from EOS (LVC 2018): spectral EOS analysis of GW170817, $M_{max} \lesssim 2.4\ M_\odot$ (90% CL)

$$P(m_2 \leq M_{max}) \approx 3\%$$

M_{max} from NS pop (Farr+Chatziioannou 2020): fit to Galactic NS population, $M_{max} \lesssim 3.1\ M_\odot$ (90% CL)

$$P(m_2 \leq M_{max}) \approx 29\%$$

M_{max} from GW170817 remnant (e.g. LVC 2020): map threshold for collapse of rotating remnant to nonrotating maximum mass, $M_{max} \lesssim 2.3\ M_\odot$

$$P(m_2 \leq M_{max}) \ll 1\%$$

Zoom Webinar

You are viewing Charlie Hoy's screen | View Options

Recording

docs.google.com

Heavy neutron star or light black hole?

The secondary mass is above typical estimates of the maximum NS mass.

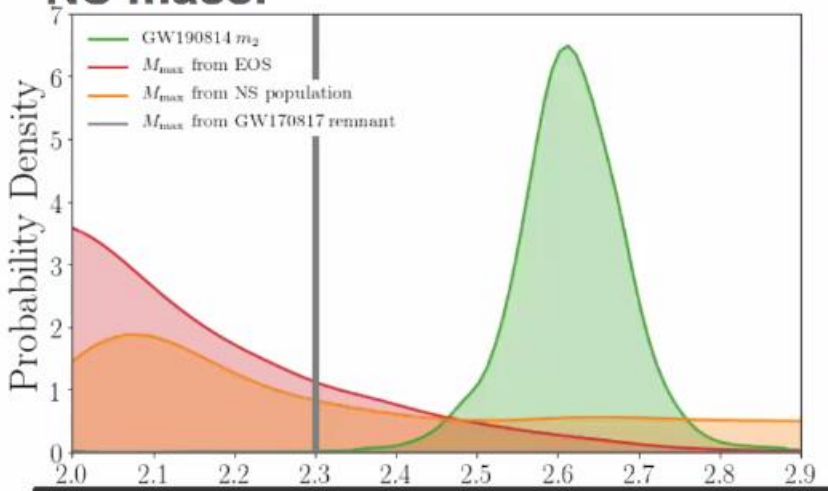

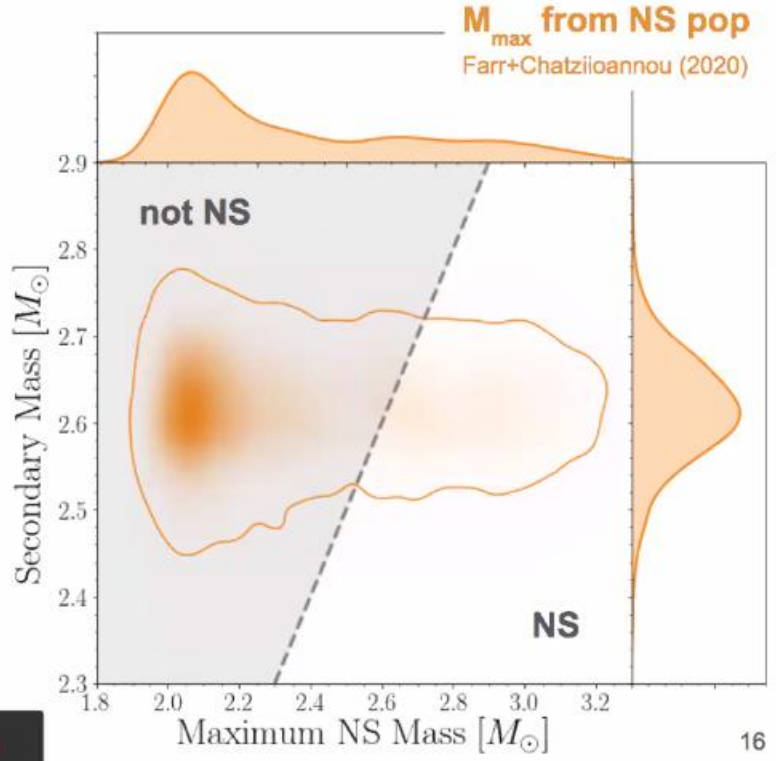

Slide 16 | Q&A | Notes | Pointer | Tips | EXIT

16

Philippe Landry

16:40

docs.google.com

Rate of GW190814-like mergers

GW190814 represents a new class of compact binary mergers.

Astrophysical merger rate density estimated as

1 - 23 Gpc^{-3} yr^{-1}

based on

- One detection so far
- Surveyed spacetime volume V × T

BNS
110 - 3840 Gpc^{-3} yr^{-1}
LVC GWTC-1 (2019)

BBH
10 - 101 Gpc^{-3} yr^{-1}
LVC GWTC-1 (2019)

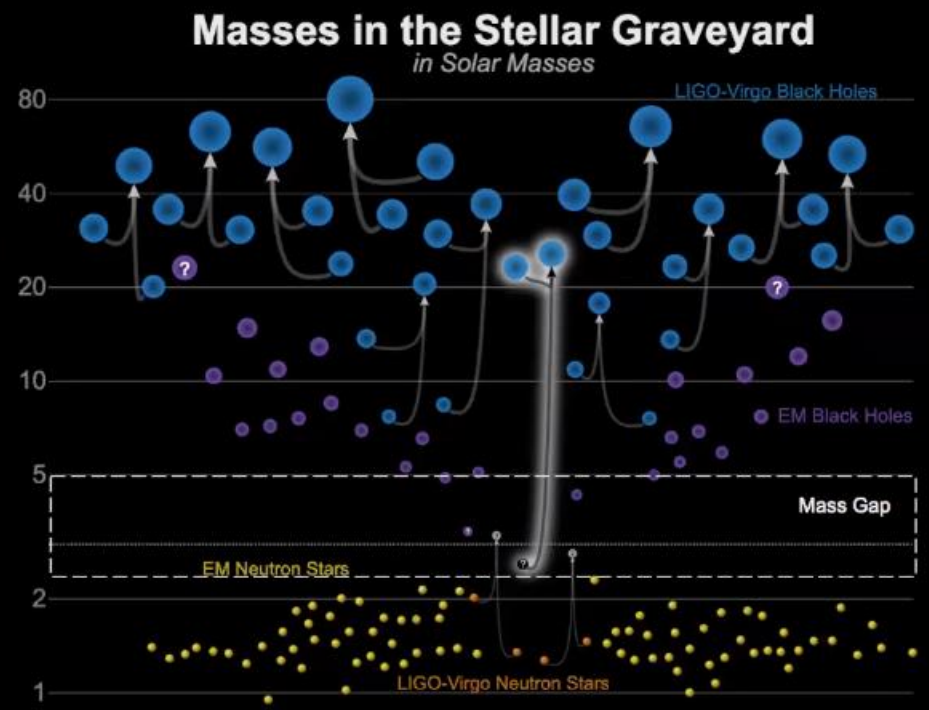

Slide 17 Q & A Notes Pointer Tips EXIT

Updated 2020-05-16
LIGO-Virgo | Frank Elavsky, Aaron Geller | Northwestern

17

16:41

Astrophysical implications and formation channels

Robust mass measurement

$$2.59^{+0.08}_{-0.09}\,M_\odot$$

Implications on

- Supernova explosion mechanism
- Existence of the lower mass gap

Adapted from Abbott B.~P., et al., 2019, ApJL, 882, L24

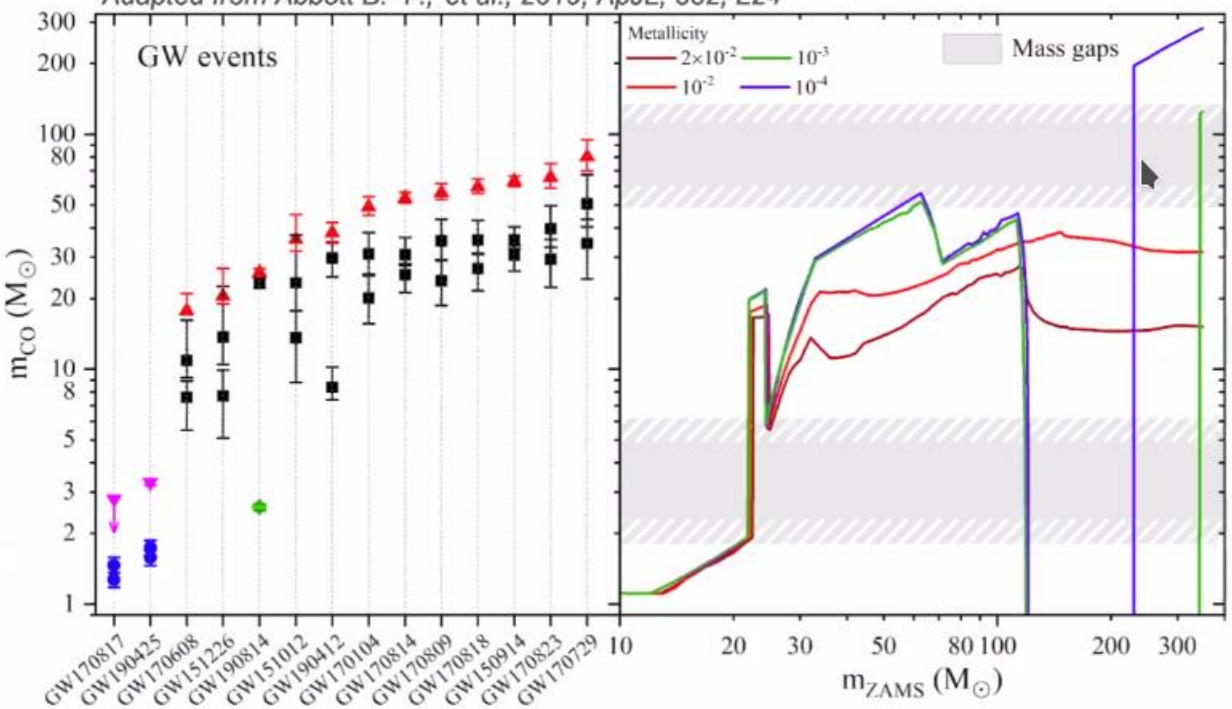

19

docs.google.com

Summary

The GW190814 source is unlike any compact binary signal observed to date.

- Secondary is lightest BH or heaviest NS ever observed in a double compact-object system
- Most unequal mass ratio measured with GWs
- Tightest constraint on a primary spin

This event has exciting implications for the formation and mass spectrum of compact objects in the Universe.

Vicky Kalogera

docs.google.com

Summary

The GW190814 source is unlike any compact binary signal observed to date.

- Secondary is lightest BH or heaviest NS ever observed in a double compact-object system
- Most unequal mass ratio measured with GWs
- Tightest constraint on a primary spin

This event has exciting implications for the formation and mass spectrum of compact objects in the Universe.

docs.google.com

Summary

The GW190814 source is unlike any compact binary signal observed to date.

- Secondary is lightest BH or heaviest NS ever observed in a double compact-object system
- Most unequal mass ratio measured with GWs
- Tightest constraint on a primary spin

This event has exciting implications for the formation and mass spectrum of compact objects in the Universe.